QUANTUM MECHANICAL STUDY OF MODELLED/BIOMIMETIC HEME AND NON-HEME TYPE METALLOENZYMES

THESIS SUBMITTED FOR THE AWARD OF THE DEGREE

of

Doctor of Philosophy

in

Applied Physics

Submitted By

Rolly Yadav

Enrollment No.: 062/14

Under the Supervision of

Prof. Devesh Kumar

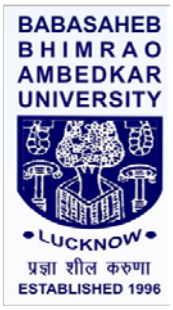

Department of Applied Physics
School for Physical Sciences
Babasaheb Bhimrao Ambedkar University
Lucknow (U.P.), India – 226025

2021

THIS THESIS IS DEDICATED

TO

MY

LOVING PARENTS

DECLARATION

I declare that the thesis entitled **"Quantum Mechanical Study of Modelled/Biomimetic Heme and Non-Heme type Metalloenzymes"** has been prepared by me under the supervision of **Prof. Devesh Kumar**, Department of Applied Physics, School for Physical Sciences, Babasaheb Bhimrao Ambedkar University, Lucknow. No part of this thesis has formed the basis for the award of any degree, diploma or fellowship previously. Further, I declare that the material embodied in the present work is based on original research work and the indebtedness to others has been duly acknowledged at relevant places. This is also declared that the thesis is essentially free from all kinds of plagiarism.

Date: 21/12/2021

Place: Lucknow

Rolly Yadav

(Rolly Yadav)
Enrollment no. 062/14
Department of Applied Physics
School for Physical Sciences
Babasaheb Bhimrao Ambedkar University
Vidya Vihar, Rae Bareli Road
Lucknow, (U.P.), India-226025

CERTIFICATE

This is to certify that the thesis titled **"Quantum Mechanical Study of Modelled/Biomimetic Heme and Non-Heme type Metalloenzymes"** submitted by **Ms. Rolly Yadav** is an original research work and has not been previously submitted in part or full for the award of any other degree or diploma to this or any other university or institutions. The thesis submitted to the Babasaheb Bhimrao Ambedkar University, Lucknow, satisfies all the requirements as stipulated in the ***Doctor of Philosophy (Ph.D.) regulations -1999 as amended in 2013*** and it is fit for submission and evaluation for the award of Doctor of Philosophy of the University.

Date: 21/12/2021

Supervisor

Head of the Department

ACKNOWLEDGEMENT

I am thankful to the almighty for his constant blessing bestowed on me and I took this herculean task in my hands, completed it and compiled it in the form of the thesis. Dear God! Thank you for this Day.

I feel obliged to take this opportunity to express heartfelt reverences towards my supervisor and mentor **Prof.** (**Dr.) Devesh Kumar**. He guided me throughout, till the completion of my thesis work. Without him, this thesis would not have taken this apt form. Besides teaching with the research process, work and ethics of the research, he also taught me to remain patient in the research. He was always there watching cautiously for any barrier that could hinder the progress or rather completion of this Ph.D. work. I am failing out of word to express my profound gratitude towards him; he is my mentor as well as father figure to me. Thank you sir, for showing faith in me and my capabilities.

I am highly grateful for the help and support provided by the faculties of the department: Dr. B. C. Yadav, Dr. Ramesh Chandra, Dr. A. K. Yadav, Dr. K. B. Thapa and Dr. Ajeet Maurya for helping me to complete this task. They were always available for fruitful discussions culminating into successful results. I feel extremely enlightened by the company of their thought provoking deliberations.

No words in the entire universe can express my feelings and gratitude towards my family. But I would keep it simple, thank you mummy and papa, you have been constant torch bearers for me, constantly encouraging and providing all necessary guidance, support and inspiration towards acquiring new skills.

I am also thankful to my colleagues **Miss Anamika Shukla**, **Miss Nidhi Awasthi**, **Miss Bhawna Pal**, **Miss Varsha Gautam**, **Mr. Mritunjai Mishra**, **Mr. Sumit**

Tiwari and **Mr. Manish Kumar** for their consistent support in every situation and for providing friendly environment. I would specially like to thank my colleague and friend **Dr. Anwesh Pandey** and **Miss Shivani Chaudhary** for research discussions and support.

I am also grateful to my seniors Dr. Jeevitesh Kumar Rajpoot, Dr. Amarjeet Yadav, Dr. Suresh Kumar, Dr. Asheesh Kumar and Dr. Jitendra Kumar for being with me as well as for helping and supporting me in every possible manner.

A special thanks to **Prof. C. V. Sastri** (IIT-Guwahati) for providing me the computational facilities during my research. I gratefully acknowledge the financial support from Department of science and technology (DST- India) in form of **INSPIRE/IF-170546** fellowship.

I deeply acknowledge the help of office staff of the department who was always ready to support me at every stage of my research work. Further, I would like to thank the facilities of Central Library and the Computer Center of the University, Lucknow which were useful at every stage of the research work.

Last but not least, I would like to thank one and all, who directly or indirectly helped me during my studies leading to this thesis.

Rollyyadav

Rolly Yadav

ABSTRACT

Enzymes are green “catalysts”, ever since their potential is recognized; researchers have wondered and argued about how they work. Metalloenzymes have metal as cofactor bound to proteins. The metal ions at active site of enzymes allow it to perform redox reactions. Metals were used in most developed civilizations since ages in therapeutic purposes but the mechanism was not known properly. With advent of computer, the theoreticians could compute structures and reaction pathways within reasonable time. The quantum mechanical methods have been of great help in devising competing methods for explaining involved phenomena. With advancement in technology, these theoretical results were validated by experimentalists as well. Hence both began working in close collaboration. Their concerted efforts have helped develop highly benchmarked computational methods that produce reliable results. Now modeled structures have grown in size and complexity. Better understanding of the mechanism by which they work and performs biological transformation reactions. This will lead to advances in the area of designing new drugs (as many drugs are inhibitors, which will eventually bind to enzymes and prevent them from further functioning), designing new and better biomimetic or engineered catalysts, analysis of effect of mutations will help in predicting the metabolism of pharmaceuticals. Thus, there is a great demand of development of protein catalyst for practical applications in the field of pharmaceutical, chemical and biotechnology industries. Computational modeling has a major role in understanding these enzymatic processes due to unstable species such as reaction intermediates and transition state which cannot be studied directly via experiments in these complex systems. In this work, iron (IV)-oxo species have been studied in great detail. Reaction pathways have been proposed that closely

match with experimental results. Our calculations have established catalytic mechanisms for aliphatic and aromatic hydroxylation, epoxidation, sulfoxidation and dehydrogenation reactions by iron(IV)-oxo heme cation radical oxidants, which identified the rate determining step in the mechanism and the electronic features of oxidant, substrate and enzyme environment that drive the reaction. In another work better synthetic oxidant was tried to be designed and modeled which matches well with the experimental results which is one of its kind. Therefore, the studies have provided a deep understanding on chemical catalysis by high valent metal-oxo oxidants and have set the scene for future studies in the field.

PREFACE

The thesis entitled **"Quantum Mechanical Study of Modelled/Biomimetic Heme and Non-Heme type Metalloenzymes"** encapsulate the results of theoretical investigations carried out in the Department of Applied Physics, Babasaheb Bhimrao Ambedkar University in between 2016-2021 under the supervision of Prof. (Dr.) Devesh Kumar, Applied Physics, Babasaheb Bhimrao Ambedkar University, Lucknow.

Metalloenzymes are utilized by the nature for diverse function. Primarily they are used as catalyst in crucial biological processes such as metabolism and biosynthesis. Nearly one third of the proteins present require a metal atom centre for their functioning. This makes the study of metalloenzyme catalysis important from the point of chemical biology and biomedical sciences. Iron being most abundant in earth's crust is also found in prominence in most enzymes. Iron containing enzymes are classified as heme and non-heme enzymes. These enzymes sometimes also contain other transition or non-transition metals with homo/hetero-nuclear metal centre.

Nowadays computational techniques have matured to a level that one has various sets of extensively tested and benchmarked methods and procedures that produce reliable results that predate experimental data by many years. There are many instances when experimentalists have reproduced and validated theoretical results once technological advancements allowed them to do so. In study of transition metal complexes, the basic hindrance in experiment is their short life time. Computational study helps in

studying the properties of short lived intermediates and transition state complexes and help in determining reaction pathways or in fine-tuning a known reaction mechanism.

This thesis will focus on reaction mechanism of metalloenzymes having transition metal (iron) into their active sites. There will also be a focus on how synthetic substituted catalysts may be used to imitate their reaction mechanisms. The thesis is divided in six chapters.

Chapter 1 reviews the theoretical work done so far on heme and non-heme type metal enzyme and also discusses the suitability of various computational quantum mechanical methods available in terms of accuracy etc.

Chapter 2, discusses development and mathematical details of quantum mechanical methods has been discussed.

Chapter 3 deals with the results obtained from the calculation for aliphatic hydroxylation mechanism of estragole modeled by Cytochrome P450.

Chapter 4 is focused on the results obtained from the study of the aromatic hydroxylation and epoxidation mechanism of BPA and its analogs via Cytochrome P450 enzyme. A comparison of reactivity mechanism based on quantum mechanically obtained energy profile was also made in this chapter.

Chapter 5 investigates the search of the better non-heme synthetic ligand frame work for the iron(IV)-oxo species (originally on the N4PY), so that rate of the reaction can be enhanced, understood and hence controlled.

The general conclusions of the thesis are drawn in **Chapter 6**.

Conceivably, better understanding of the mechanism of these natural catalysts as well as biomimetics should lead to more efficient and effective work of computational chemistry in future.

LIST OF ABBREVIATION

S.No.	Abbrv.	Full form
1.	B1	Basis set 1 - LACVP or LANL2DZ basis set
2.	B2	Basis set 2 - LACVP** basis set which adds polarisation functions to first row atoms and hydrogen
3.	BS	Basis Set
4.	BA	Benzyl Alcohol
5.	CID	Collision Induced Dissociation
6.	CHD	Cyclohexadiene
7.	CT	Charge-Transfer
8.	CI	Configuration-Interaction
9.	Cpd0	Compound 0, Iron-Hydroperoxo Intermediate
10.	CpdI	Compound I, Iron-oxo Ferryl Species
11.	CpdII	Compound II, One-Electron reduced form of CpdI
12.	CPO	Chloroperoxidase
13.	CDO	Cysteine Dioxygenase
14.	CYP	Cytochrome P450
15.	D	Doubly-reduced pentacoordinated complex of P450
16.	DNA	Deoxyribonucleic acid
17.	DHA	Dihydroanthracene
18.	DMS	Dimethylsulfide
19.	DFT	Density Functional Theory
20.	EA	Electron Affinity

21.	EE	Electrostatic Embedding
22.	ECP	Effective Core Potential
23.	EPR	Electron Paramagnetic Resonance
24.	FT-ICR	Fourier Transform-Ion Cyclotron Resonance
25.	GTO	Gaussian type orbital
26.	HAT	Hydrogen Atom Abstraction
27.	HAT	Hartree-Fock
28.	HOMO	Highest Occupied Molecular Orbital
29.	HTP	Heme-Thiolate Proteins
30.	IE	Ionization Energy
31.	KIE	Kinetic Isotope Effect
32.	LCAO	Linear Combination of Atomic Orbital
33.	LUMO	Lowest Unoccupied Molecular Orbital
34.	MM	Molecular Mechanics
35.	MD	Molecular Dynamics
36.	MS	Mass Spectrometry
37.	MNHID	Mononuclear Nonheme Iron Dioxygenases
38.	OAT	Oxygen Atom Transfer
39.	PDB	Protein Data Bank
40.	PES	Potential Energy Surface
41.	P450	Cytochrome P450 enzyme
43.	P450cam	Cytochrome P450 from Pseudomonas putida, hydroxylase of Camphor
46.	QM	Quantum Mechanics
47.	RHF	Restricted Hartree-Fock

49.	SCF	Self Consistent Field
50.	STO	Slater Type Orbital
51.	Tp	Trispyrazolylborato
52.	TS	Transition State
53.	UHF	Unrestricted Hartree-Fock
54.	ZPE	Zero Point Energy

LIST OF AMINO ACID ABBREVIATIONS

S. No.	Amino Acid	Three letter code
1.	Alanine	Ala
2.	Arginine	Arg
3.	Asparagine	Asn
4.	Aspartic acid	Asp
5.	Cysteine	Cys
6.	Glutamine	Gln
7.	Glutamic acid	Glu
8.	Glycine	Gly
9.	Histidine	His
10.	Isoleucine	Ile
11.	Leucine	Leu
12.	Lysine	Lys
13.	Methionine	Met
14.	Phenylalanine	Phe
15.	Proline	Pro
16.	Serine	Ser
17.	Valine	Val
18.	Threonine	Thr
19.	Tryptophan	Trp
20.	Tyrosine	Tyr

LIST OF TABLES

LIST OF FIGURES

TABLE OF CONTENTS

CHAPTER 1

INTRODUCTION

CHAPTER-1

INTRODUCTION

1.1: Metalloenzymes

Enzymes are known as biological catalysts which are responsible for performing chemical reactions inside living beings. The enzymes that involve metal at their active site are termed as metalloenzymes or metalloproteins. Metal ions can easily bind to the protein as they easily lose electron to become ions and enzymes are electron rich species. Transition metals exhibit multiple oxidation states hence they can assist in electron/ proton transfer reactions, and thus are present in large number of enzymes at active centre. Metals are regarded inevitable through enzymes as without them reactions catalyzed will be rather slow. Metalloenzymes account for nearly half of enzymes in nature [1].

Various metabolic functions play key role in all living forms, e.g., methane hydroxylation used in methanophiles (bacteria), desaturation of fatty acids (plants), DNA and RNA repairs, β-lactam antibiotics biosynthesis (animals). In these metabolic functions, controlled oxidation of organic substrates takes place by the activation of dioxygen (O_2) and it is mediated by transition metals [2-6]. This attribute of enzyme finds important applications in industry, to be efficiently used in oxidation reactions [7-9]. Thus, researchers are interested in understanding mechanism of dioxygen activation in different heme and non-heme metalloenzymes [3, 10-24]. There are diverse types of active sites in

enzymes like mononuclear, dinuclear, hetro-dinuclear regardless of this a common mechanistic hypothesis may also be fruitful in understanding dioxygen activation.

Nature utilizes enzymes to speed up the biochemical transformations in regioselective and stereospecific manner. Iron availability in earth crust is maximum hence most of the enzymes comprise iron at their active site [2,3,25-39]. Besides iron there are numerous other metal containing enzymes (transition as well as non-transition) like copper-,[40-42] vanadium-, [43,44] and molybdenum [45,46]. Also, in few of the metalloenzymes two or more metals are present at their active centers, for example ribonucleotide reductase is a diiron enzyme [47-49] or in photosystem II there is a multi-center cluster [50-53].

On the basis of mode of binding of the metal to the rest of the protein, enzymes can be classified as heme [26-33] and non-heme [2,3,34-40]. Two most well studied examples of each of these categories are: cytochrome P450 and taurine/α-ketoglutarate dioxygenase [54, 55]. Their structures are depicted in Figure 1.1. The P450 crystal structure coordinates are of human cytochrome P450 2A13 as shown in Figure 1.1 (a) which is found in liver and there it is responsible for detoxification of endogenous compounds. The heme group is connected to the rest of the protein via thiolate group of cyteinate residue (Cys439). This axial ligand is found responsible in fine-tuning the electronic properties of the enzyme (oxidant) and also in attributing its functional properties to behave as monooxygenase [56]. Peroxidases and catalases are two other varieties of heme enzymes which mainly differ due to type of axial ligand. In peroxidases hystidine is the axial ligand while in catalases tyrosinate group [57-59]. The crystal structure of taurine/α-ketoglutarate dioxygenase is shown in Figure 1.1 (b). Here iron metal is bound through a facial triad consisting of, two histidine (His) and an aspartate amino acid (Asp).

This enzyme is a non-heme enzyme and is involved in the biodegradation of taurine and also acts as a sulphur source. The intermediates involved during the reaction mechanism are highly short-lived and hence are difficult to be detected and characterized. This necessitates theoretical studies to be used in investigation of the mechanism and further validation of the experimental findings.

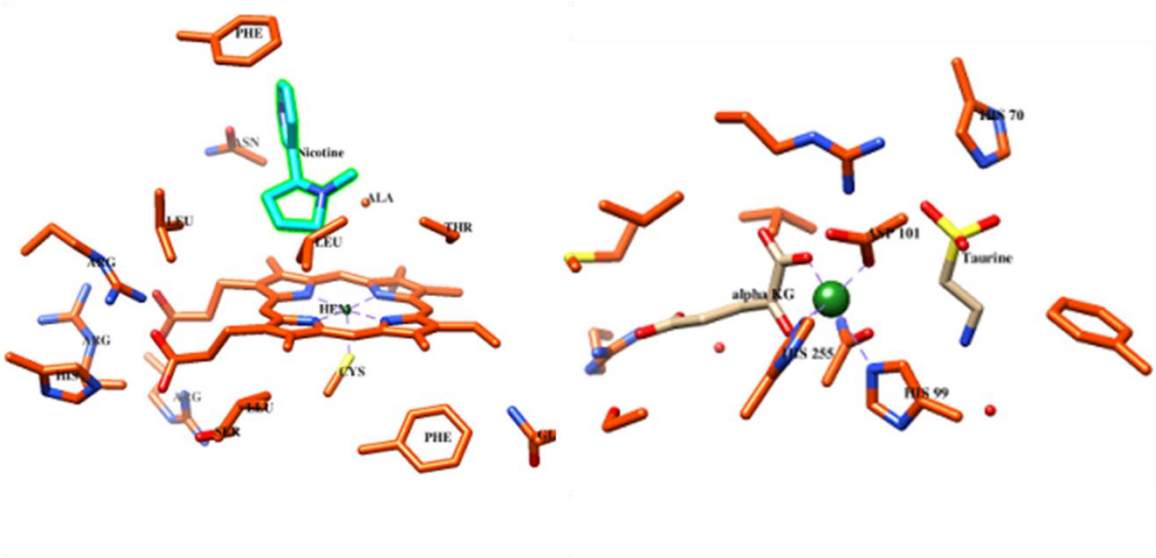

(a) **(b)**

Figure 1.1: Active site structures of typical mononuclear iron enzymes: (a) cytochrome P450 (PDB: 4EJG), (b) taurine/α-ketoglutarate dioxygenase (PDB: 1OS7).

A few decades ago, theoretical modeling played a minor role in understanding redox-active reactions of metalloenzymes. The theoretical methods were underdeveloped, due to this, either result was not accurate enough or the processing time was too long. But in today's scenario, the situation is changed with the development of methods and as well as insights from the applications. Development of density functional theory (DFT) has reached at the stage where their accuracy is not far from most accurate. The breakthrough was due to incorporation of density gradient terms for the exchange part and of fractions

of exact exchange [60]. During first year of its applications in transition-metal complexes, it was clear that results were quite accurate [61,62]. Decades of experience gained from the study of small models of transition metal containing complexes, gave ideas for further improvements in method to be used and how to address mechanism studies of large organometallic complexes, as surprisingly, small model methods were quite helpful in gaining insights in the action of mechanism of biomolecules. Transition-state structures as well as individual reaction steps turned not to be entirely dependent of the size of the model for understanding of reaction mechanism.

There are two originally different approaches in the study of enzymatic systems. First is the cluster model approach which uses small or truncated model system. This small model approach had a potential to elucidate main features of mechanism. First study using this model was done in 1997 on methane monoogygenase enzyme (MMO) [63]. Second approach was based on treating small core active site of the enzyme with extensive quantum mechanical (QM) methods using DFT, while rest of the system is described by molecular mechanics (MM); hence this approach is called as QM/MM model by Warshel and Levitt in 1976 [64]. The first application of QM/MM on the mechanism of galactose oxidase was made in 2000 [65]. Both approaches have been developed over the years from their original form. Nowadays, with improvements in computer technology, QM cluster models can handle quite big models i.e. with more than 200 atoms, and even larger QM core can be used in the QM/MM approach.

Now-a-days theoretical model calculation can be regarded of equal importance in determining mechanism of metalloenzymes. Experimental methods have the advantage that they are being studied on the actual system, but spectroscopically guarding of short-

lived species, electron transfer and interpretation of results is quite troublesome. In both approaches accuracy of the results is the key factor [66]. In theoretical modeling, accuracy of the results depends on the accurate choice of the method and real system under consideration. More than two decades of experience in this area has made the understanding of limitations and applicability on different models to reach a mature stage.

Computational modeling has emerged to be very useful in assisting experimentalist by analyzing various fundamental properties and effects of ligand substitution on the reactivity and catalytic features of enzymes [67-70]. As an example, theory predicted that high-valent iron(IV)-oxo heme cation radical is the active site of the enzyme [71-73], 10 years before the first characterization of active species of P450 i.e., Compound I (Cpd I) by Rittle *et al.* using electron paramagnetic resonance (EPR), absorption and Mössbauer spectroscopy [74]. Computational modeling was also helpful in comparison between properties of heme and non-heme iron enzymes and origin of ability of hydrogen-atom abstraction [75-79]. For both heme and non-heme iron complexes extensive studies on the ligand effects both axially and equatorially are done and reviewed as well [80, 81] In various heme and non-heme enzymatic systems, high-valent metal-oxo type intermediates are involved in oxidation reactions [3,29,33,82-90] An iron (IV)-oxo porphyrin π- cation radical species is the active oxidant of P450 which is utilized in various metabolic conversions [29,84-86]. High valent manganese-oxo radicals are present in photosystem II (PSII) [91-94]. Non-heme enzymes such as taurine α-ketoglutarate dioxygenase (TauD), prolyl-4-hydroxylase, and halogenase CytC3 also utilize iron(IV)-oxo intermediates as their oxidant [95-99]. Besides iron (IV)-oxo species,

iron(III)-superoxo, iron(III)-peroxo and iron(III)-hydroperoxo complexes are also detected as the active intermediates in different heme and non-heme enzymes. Synthetic analogues or biomimetic model of key intermediates of these enzymes have improved our understanding through studies on their structural and spectroscopic properties along with the reactivities [100-110]. One of the first biomimetic models of mononuclear non-heme iron(IV)-oxo was complex of tetraazamacrocyclic TMC ligand (TMC, 1,4,8,11-tetramethyl-1,4,8,11-tetraazacyclotetradecane). The iron(IV)-oxo species was penned and structurally characterized and since then have been studied extensively to strengthen understanding on its physical properties, axial ligand effects and its reactivities with substrates [108]. In contrast with the intermediates present in the catalytic cycle of P450 there were considerable differences in reactivity pattern due to ligand influences. Hence various models were characterized and developed over recent years for other ligated heme and non-heme enzymes.

Combined experimental and computational techniques have made it possible to gain substantial insights into the intrinsic properties of heme and non-heme metal-oxygen complexes. Short lived intermediates species such as iron (III)-superoxo, iron(III)-peroxo, iron(III)-hydroperoxo and iron(IV)-oxo have been synthesized and characterized through non-heme ligated systems. Additionally, remarkable differences between heme and non-heme systems were discovered after their comparative studies. Like in the case of porphyrin, biomimetic complex of P450 enzyme, Cpd I was found to be the most prominent active oxidant, such studies have approved presence of the single oxidant in heme enzymes (e.g. P450). Whereas considerable differences were found in non-heme analogues where superoxo and hydroperoxo complexes revealed higher reactivity than

the iron(IV)-oxo complexes [103]. Thus, it seems obvious that theory assists experimental studies in biocatalysis and biotransformation by giving insights into the reaction mechanism and underlying pathways.

1.2: Heme Enzymes

In heme based enzymatic systems, the poryphyrin ring contains a metal ion (usually iron) at its centre. Iron (Fe) is basically responsible to serve three main roles: (1) transfer and storage of molecular oxygen, (2) catalysis and (3) transfer of electrons. Heme group due to its tendency to easily switch between Fe (II) and Fe (III) oxidation states makes them used by nature as electron transfer cofactors. They usually transfer electron in specific electron transfer proteins, known as cytochromes, or as in transportation of electron inside the same enzyme to an active site [111].

Many enzymes have heme group as its part of active site where it performs plethora of chemical reactions. Heme enzymatic system can catalyze both oxidative and reductive chemistry [112-114]. Oxidants involved in heme enzymes are broadly classified into two categories: oxygenases and peroxidases. Oxygenases use O_2 to oxidize, most of the times to oxygenate substrates, whereas peroxidases use H_2O_2 to oxidize, but not necessarily to oxygenate substrates. Out of the two oxidants, molecular oxygen is the unusual one because thermodynamically oxidation of nearly all biological molecules is possible but oxygen is non-reactive molecule. Due to O_2 being paramagnetic there are large kinetic barriers to these reactions. Biological molecules that have paired spins, hence it is a spin forbidden process. To execute these reactions with relative ease nature has appointed transition metals and heme in enzyme active sites. P450s (superfamily) are class of heme enzymes, which have characteristic heme group at its active site. Till date this enzyme

has been extensively studied computationally and experimentally due to its applicability in biomedical industry and drug designing [30]. Similarly heme –copper oxidase and peroxidases are superfamily of enzymes where heme cofactor at its active site plays a crucial role. Nitric oxide reductase, cyctochrome c oxidase enzymes have a binuclear active site and contain a non-heme metal either iron or copper.

1.2.1: Cytochrome: P450

Throughout the biosphere, P450s are widely distributed in all life forms and constitute the largest superfamily of enzymes [115]. P450s are well-known for their function in detoxification (removal) of toxic compounds from the body. Inside the liver, drug and other xenobiotics gets hydroxylated through various P450s (mostly CYP3A4) which make these compounds more susceptible for easier elimination. Other than catabolic functions, P450s also perform reactions necessary for the biosynthesis of essential compounds like steroids synthesis. This enzyme is a monooxygenase i.e., it inserts single oxygen atom into substrate. The structure of active site of P450 is shown in Figure 1.4, PDB ID (4L40) taken from the protein data bank. Cytochrome P450's unique name originated when it showed strong absorption band (Soret band) at 450 nm in the UV-Vis spectrum after getting exposed with carbon monoxide (CO); in its reduced from (Fe^{2+}). The poryphyrin is an electron rich moiety and its peak at 450 nm arises due to π- π^* electronic dipole transition [116]. In cytochrome P450 generally one oxygen atom is transferred to the product formation and the other is reduced to form a water molecule. The two electrons and protons in this process comes from a reducing partner NADH or NADPH via reductases such as cytochrome B5, ferredoxins, cytochrome P450 reductases [117].

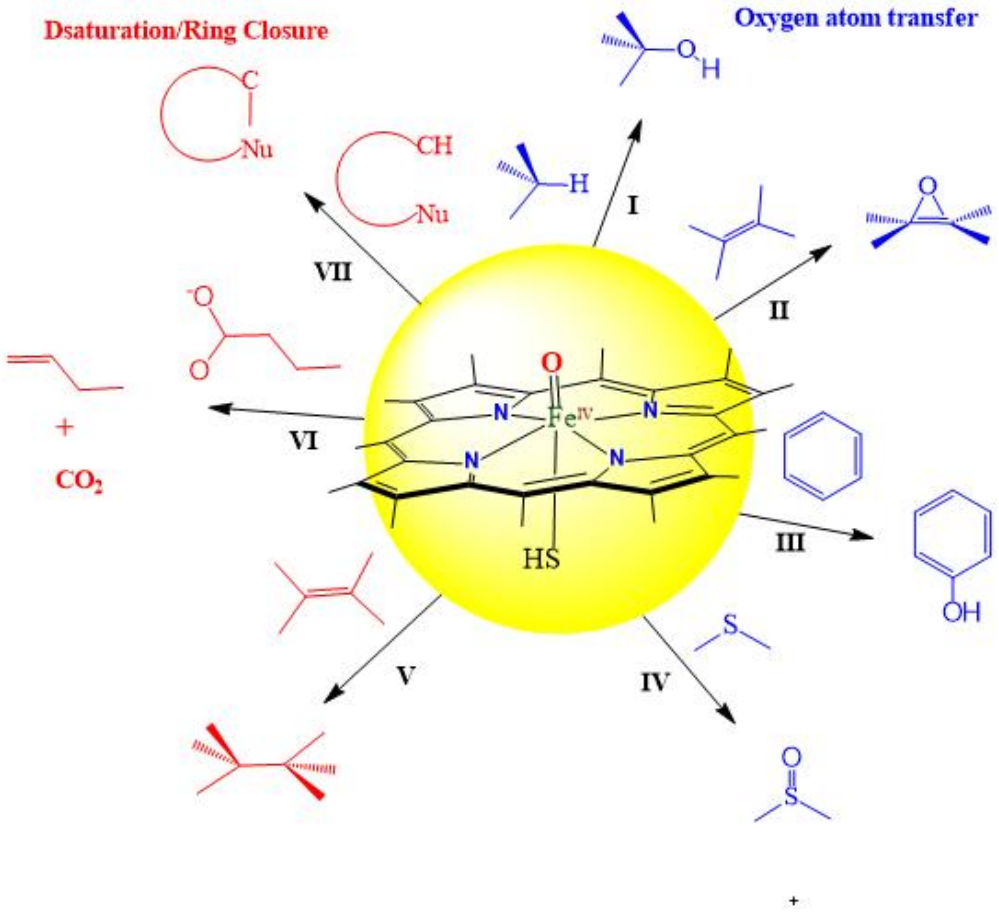

Figure 1.2: Reaction mechanism catalyzed by P450 Compound I.

There are also some self –sufficient bacterial and fungal P450s in nature which uses the required reducing equivalents from hydrogen peroxide (H_2O_2) for the insertion of an oxygen atom [118-120]. P450 displays wide variety of substrate activation reactions hence this enzyme is important with perspective in field of biotechnology and medicine. The range of reactions formed by P450 isoenzymes on the substrates are shown in Figure 1.2. The active oxidant responsible for the oxidation or catalysis is believed to be iron (IV) oxo species having poryphyrin cation radical [Fe (IV)=O] $(por)^{+\cdot}$, popularly known as compound I (Cpd I) [121-123]. The oxidant occurs in two closely lying spin states due

to ferromagnetic or antiferromagnetic coupling of three unpaired electrons. Due to their remarkable functions and diverse genome these enzymes have gathered special attention in decades; both computationally and experimentally [124]. Here we will discuss few of these computational studies based on DFT and before that we should understand its catalytic cycle for the formation of Compound I which is the main hero in modeling studies of enzymatic processes governed by P450s.

1.2.1.1: Catalytic Cycle of P450: Compound I formation

Cytochrome P450s are regarded as nano-machine which performs the catalysis based on the catalytic cycle depicted in Figure 1.3. The cycle starts with the resting state **(1)** where water molecule is ligated onto the distal side of the ferric iron. This is a hexacoordinated complex with five electrons in the d-block of iron atom. The entrance of substrate such as; alkane AlkH triggers the catalytic process by displacing the water molecule leaving the complex to be in pentacoordinated ferric state **(2)**. Due to pentacoordiantion, iron which was earlier in plane of heme having low-spin doublet electronic arrangement comes below the heme and now attains high-spin sextet electronic configuration. Ferric complex **(2)**, being a good electron acceptor takes an electron from reductase protein and converts itself to ferrous high-spin complex **(3)**. Ferrous dioxygen complex **(4)** is formed with the binding of molecular oxygen, which is a good electron acceptor and has a singlet spin state. This initiates the second reduction step and it gets reduced to form ferric-peroxo anion species **(5)**. This reduction step is thought to be rate determining step in the entire catalytic cycle, but not always.

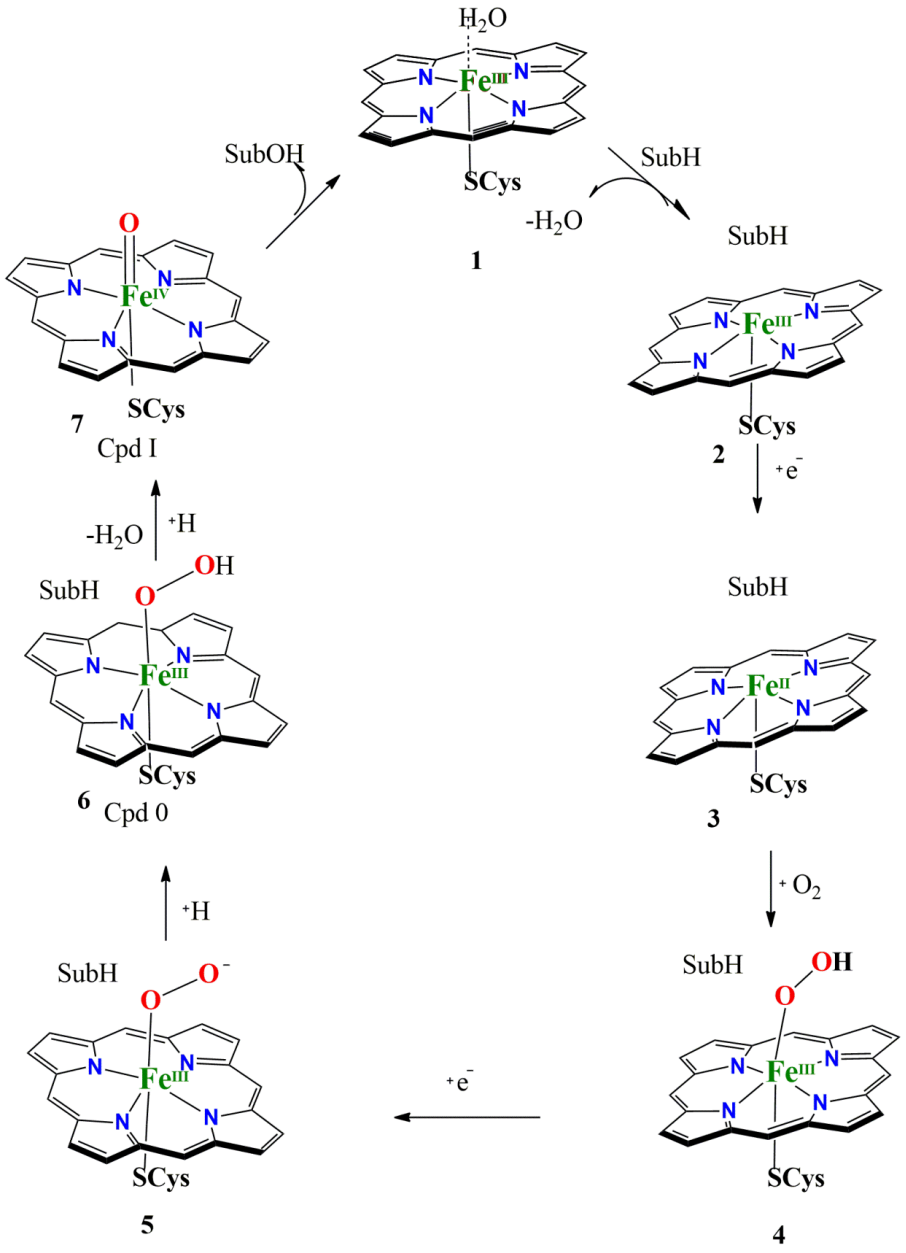

Figure 1.3: Catalytic cycle of P450 after entry of substrate SubH.

Ferric-peroxo anion complex **(5)** is a good Lewis base, it readily gets protonated and converts to ferric-hydroperoxide species **(6)**, which is also known as Compound 0 (Cpd 0). Cpd 0 is also a good Lewis base, it further abstracts proton to form Compound I (Cpd I). This species is responsible for the transfer of an oxygen atom to different substrates to form products like, alcohol, epoxides, sulphoxides etc. Product formed leaves the binding

pocket, water molecule gets attached to distal side and resting state is restored, ready for another cycle. This mechanism predicted by theory was elusive until Rittle and Green [74] characterized Cpd I and confirmed its validity to substrate oxidation.

1.2.1.2: Role Density Functional Modelled Calculations of P450 in solving controversies

1.2.1.2.1: Ethene Epoxidation by Cpd 0 and Cpd I

To test the validity of two oxidants present in the catalytic cycle of P450, comparative studies for epoxidation via both oxidant Cpd 0 and Cpd I were performed by two groups Shaik [125] and Yoshizawa [126]. They both tested epoxidation of ethene with truncated model of enzyme active site that involves protoporphyrin IX macrocycle without side chains. Shaik et al. studied the reaction profile with cysteniate ligand being replaced by thiolate, the epoxidation barriers for ferric(III) hydroperoxy species (Cpd 0) and iron(IV) oxo (Cpd I) species were compared [125]. It was found and can be seen in Figure 1.4, the barrier for Cpd 0 was very high (37- 44 kcal/mol) as compared to Cpd I with a barrier height of (13.0 kcal/mol). The Cpd I performs the epoxidation reaction on two spin states due to degeneracy. It follows a non-synchronous epoxidation mechanism; high spin (HS) state involves cationic intermediate and can lose stereochemistry whereas the low spin state (LS) proceeds via the concerted mechanism. On the other hand, Cpd 0 catalytic activity involves a single spin state. The results of Yoshizawa et al. were in agreement with the present study with slight variation in energy values due to differences in the choice of axial ligand (methylmercaptane in place of thiolate) [126]. Later experimentally conclusion was drawn that the ferric-hydroperoxo complex is a sluggish oxidant as compared to Cpd I for epoxidation reactions [127].

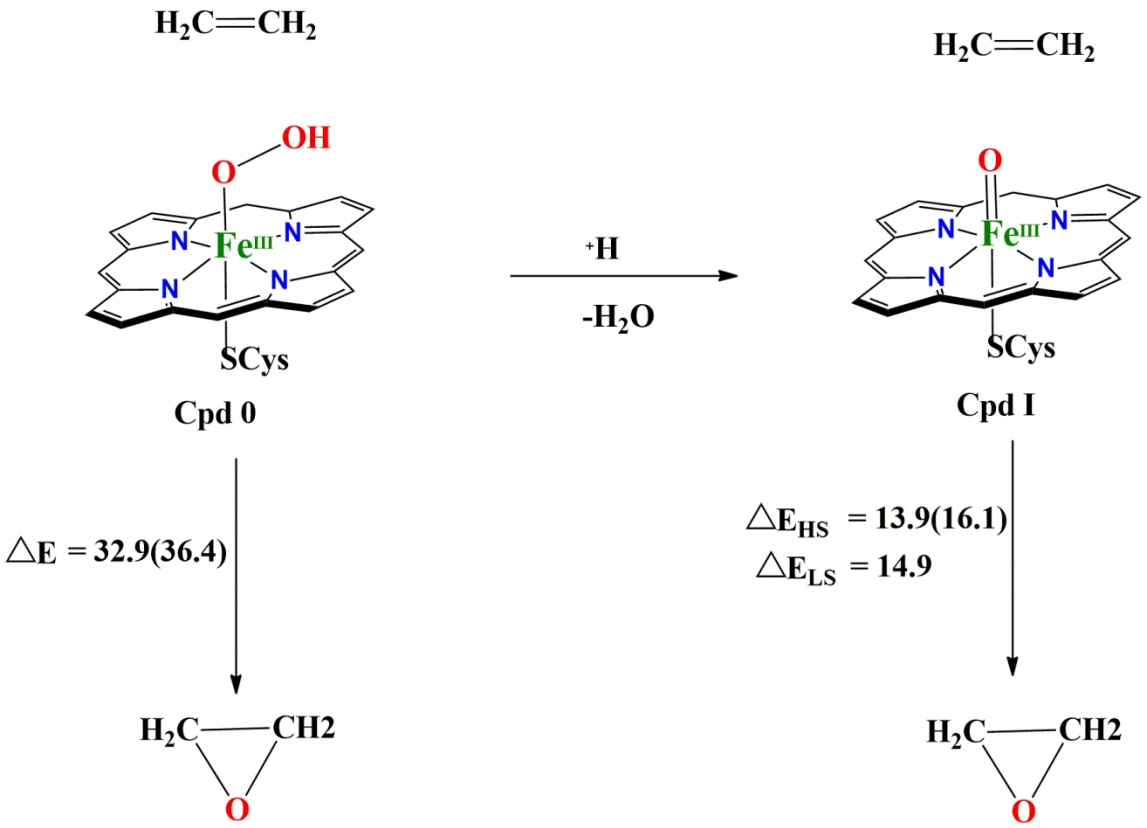

Figure 1.4: Epoxidation of ethene by Cpd 0 and Cpd I with energies in kcal/mol.

1.2.1.2.2: Sulfoxidation by Cpd 0 and Cpd I

Sulphoxidation reactions were also studied by several groups in the search for potent oxidant. Using truncated P450 model complexes, quantum mechanical calculations were employed in both Cpd 0 and Cpd I using dimethylsulphide (DMS) as their active substrate [128-132]. Figure 1.5 depicts the potential energy curves of DMS with Cpd 0 and Cpd I. Sulphoxidation reaction with Cpd I involved single transition states unlike C=C epoxidation and C-H hydroxylation reactions. Here, two electrons are transferred from DMS to heme for S-O bond formation. The reaction is stepwise and involves two spin states. However, the difference between $^{4}\mathbf{TS}_{SO}$ and $^{2}\mathbf{TS}_{SO}$ is considerable so one can say sulphoxidation proceeds via SSR (single state reactivity). The barrier heights are

different for quartet and doublet due to the electron transfer in different orbitals. In doublet spin state the electron transfer process occurs by filling of a_{2u} and π^*_{xz} and quartet spin state involves electron transfer in a_{2u} and $\sigma^*_z{}^2$ orbital. The orientation of the substrate to oxidant in rate determining transition state depends on the orbital in which electron is been transferred. Like in case of electron transfer in π^*_{xz}, the substrate attacks from sideways whereas in quartet spin state $\sigma^*_z{}^2$ involved the substrate attacks from the top. Now, when Cpd 0 is used as an oxidant, the barrier height for S-O bond formation was quite high, this gain suggested that Cpd 0 is a sluggish oxidant in comparison to Cpd I.

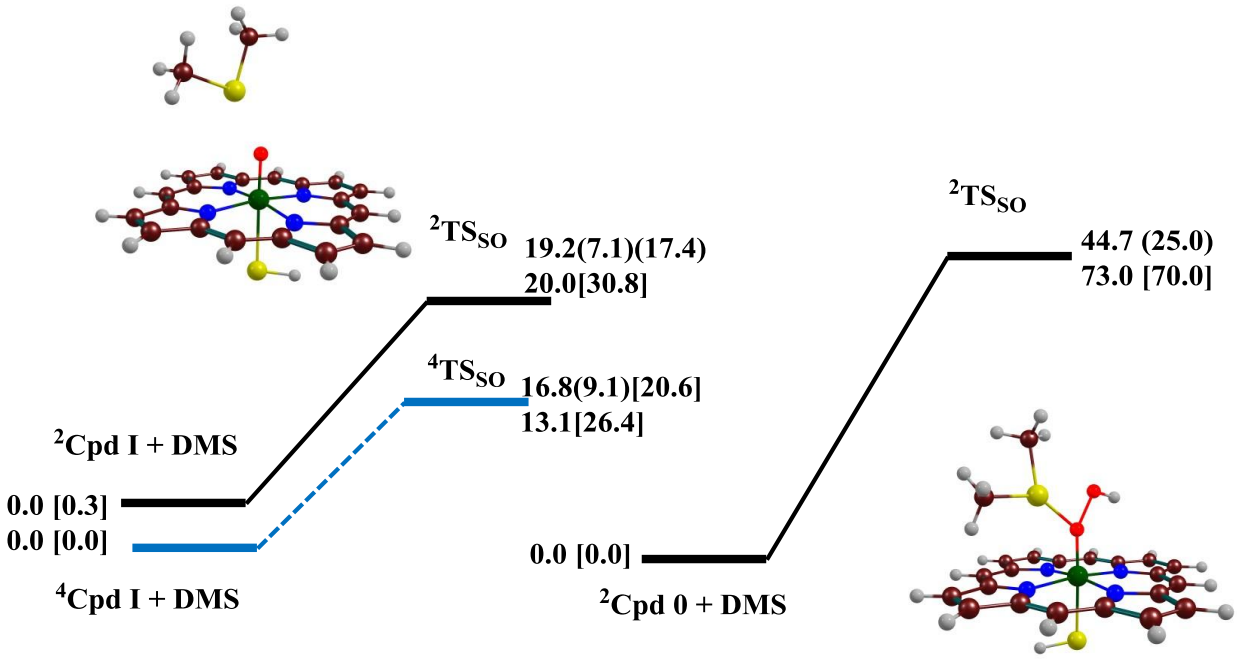

Figure 1.5: Potential energy profile of sulphoxidation of DMS by Cpd I and Cpd 0.

1.2.1.2.3: Rebound Controversy and Resolution by TSR Scenarios

The mechanism for C-H hydroxylation by Cpd I as active oxidant was given by Grooves et al. [133] Scheme 1.6 (a). It was first coined "rebound mechanism", its initial step

involves hydrogen abstraction from the alkane (Alk-H) by Cpd I. Subsequently, the alkyl radical ($Alk^{\cdot}$) can either instantaneously rebound to ferric hydroxy intermediate to give unarranged (**U**) alcohol product complex keeping original stereochemistry of the alkane preserved or can undergo skeletal arrangement first and thereafter rebound to form a rearranged (**R**) alcohol product. The rebound mechanism justifies key experimental data of partial loss of stereochemistry and geometrical rearrangement, [134] large intrinsic Kinetic Isotope Effects (KIEs) when hydrogen in transition is replaced by deuterium [133,136-141]. The apparent radical lifetime (τ_{aap}) calculation study was first done by Ortiz de Montellano Scheme 1.6 (b) using bicycle [2.1.0] pentene. They basically calculated the ratio of unarranged (**U**) to rearranged (**R**) product yield [**U**/**R**], divided by rate constant for rearranged free radical clock (K_R). The lifetime of radical intermediate was found to be short-lived but finite (τ=50ps).

The rebound mechanism was well accepted and looked solid until Newcomb and colleagues [142,143] started investigation through ultrafast radical and carbocationic clocks. The determination of quantity [U/R] with one of the probe substrates depicted in Scheme 1.6 (b) led to the conclusion that if radical intermediates are involved in the catalytic cycle of P450s, then these will have a lifetime of 100 fs [142,143] or less which means that real intermediate species is not possible. In P450 mutant species where Cpd I is assumed to be absent, the ratio [**R**/**U**] was larger than wild type enzyme [134]. This ought to the conclusion that rearranged product originates from the non-radical intermediates which get generated due to presence of another oxidant species which becomes active in mutants. Substrates that can distinguish between radical and carbocationic rearrangement patterns were subjected to validate this hypothesis and

results from this suggested that intermediate is a carbocation, not a radical in the hydroxylation reaction of alkane. Newcomb hence proposed that alkane hydroxylation proceeds via two oxidants present in enzyme Cpd I and its precursor Cpd 0 without the involvement of radical intermediate Scheme 1.6 (c). Cpd I allows concerted mechanism with insertion of [O] in C-H. On the other hand, Cpd 0 involves insertion of hydronium ion (OH+) in C-H bond and generates a protonated alcohol that undergoes rearrangement par carbocationic species. From the discussion in the above section, one can say that Cpd 0 is a sluggish oxidant and can only play a role where Cpd I is suppressed or not present. Thus, the two-oxidant mechanism is not reconcilable from experiment or theory from the reactivity study of Cpd 0 and Cpd I. But, indeed Newcomb studies lead doors open to intrude further into action of mechanism as "*experimental results pointed in the direction of products that behaved as they are originated from two different sources*".

The role of theory comes into the picture and it has already offered a reasonable resolution [125,144-146] of the main mechanistic problems depicted by experiment with the help of Two State Reaction (TSR) mechanism [144-146]. Let us first give a brief revision to our knowledge of Cpd I from theory and experiment and throw some basic light on the origin of the idea of two state reaction (TSR) mechanisms [145,147]. The very idea of "Two-State-Reactivity" is based on the fact that Cpd I has two closely lying (nearly degenerate) spin surfaces due to its molecular orbital arrangement [147].

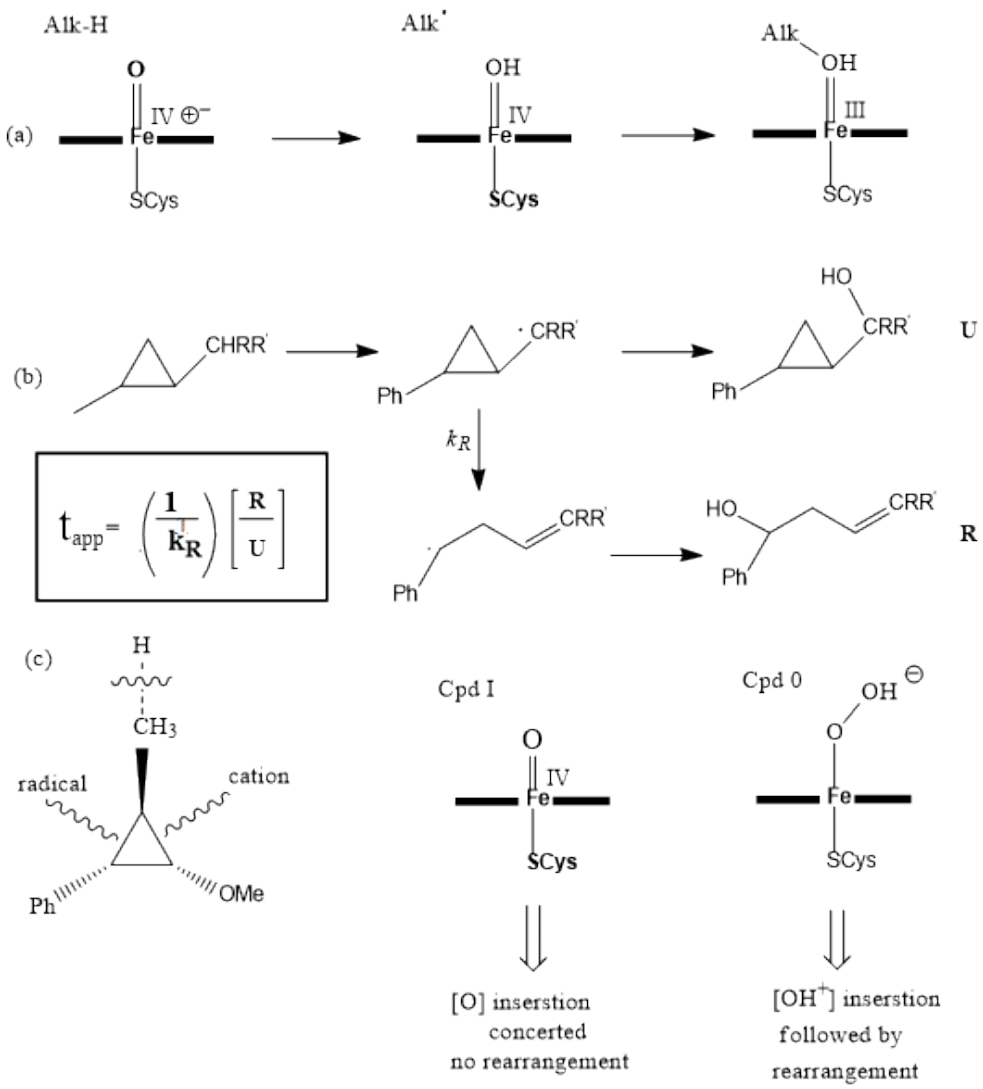

Scheme 1.6: (a) Rebound mechanism suggested by Grooves and McClusky. (b) Apparent lifetime (τ_{ap}) of a putative radical intermediate from the ratio of rearranged (***R***) to unrearranged (***U***) alcohol products produced from P450 hydroxylation of a substrate probe, here bicycle [2.1.0] pentene. (c) Probe that can distinguish between radical and carbocationic rearrangements, and the mechanistic proposal of C-H hydroxylation via two oxidants, Cpd I and Cpd 0.

The five 3d orbitals of metal split into the characteristic $3t_{2g}$-2_{eg} pattern. The $3t_{2g}$ further disassembles itself into one non-bonding (δ_{x}^{2}-$_{y}^{2}$) and two anti-bonding metal and distal oxygen orbital (π^*_{xz}, π^*_{yz}). The σ^*_{xy} and $\sigma^*_{z}{}^{2}$ are two high lying anti-bonding virtual orbitals. σ^*_{xy} originates from the mixing of σ orbitals on nitrogen and orbital of metal centre and $\sigma^*_{z}{}^{2}$ is the outcome of mixing of orbital along O-Fe-S axis i.e., mixing of $3d_z^2$ of Fe, $2p_z$ orbital on oxygen and lone pair of thiolate axial ligand.

The orbital occupation of metal looks like $\delta^2{}_{x}^{2}{}_{-y}^{2}$, $\pi^*_{xz}{}^{1}$, $\pi^*_{yz}{}^{1}$ hence the oxidation state of iron is IV Fe (IV). Apart from these metal orbitals there are two high lying orbitals of poryphyrin a_{1u} and a_{2u}. These two orbitals are degenerate in pure heme macrocycle but in the case of P450 enzymes, there is mixing of a_{2u} and σ orbital of axial sulphur ligand which results in increase in energy of a_{2u} with respect to $a_{1u.}$ Thus, due to lower energy a_{1u} is doubly occupied in ground state and a_{2u} is singly occupied and overall ground state electronic configuration of Cpd I becomes $\delta_{x2\text{-}y2}{}^{2}$, $a_{1u}{}^{2}$, $a_{2u}{}^{1}$, $\pi^*_{xz}{}^{1}$, $\pi^*_{yz}{}^{1}$. These three unpaired electrons ferromagnetically and antiferromagnetically couples to give what we called quartet and doublet spin states respectively with same orbital occupation. All the orbital and their occupation can be seen from Figure 1.7. The extensive Density Functional Theory (DFT) calculations reveal that energy difference between quartet and doublet spin states are within 1 kcal/mol. The ordering and the energy of these states depend on the axial ligand effects and perturbations in protein environment [77,148-150]. Cpd I have two closely lying spin states, quartet and doublet, which are referred as high spin (HS) and low spin (LS) states respectively. These states follow rebound mechanism [147]. It can be seen from Figure 1.8, reaction pathway involves C-H activation phase that involves barrier. Nature of this transition state is hydrogen atom abstraction type.

After this step, alkyl moiety attains a radical character and this moiety is loosely coordinated to ferric iron-hydroxo intermediate by C….HO hydrogen bond, followed by reorientation process in which radical "reorients" itself away from OH bond in a manner so that it can have a direct C…O bond formation.

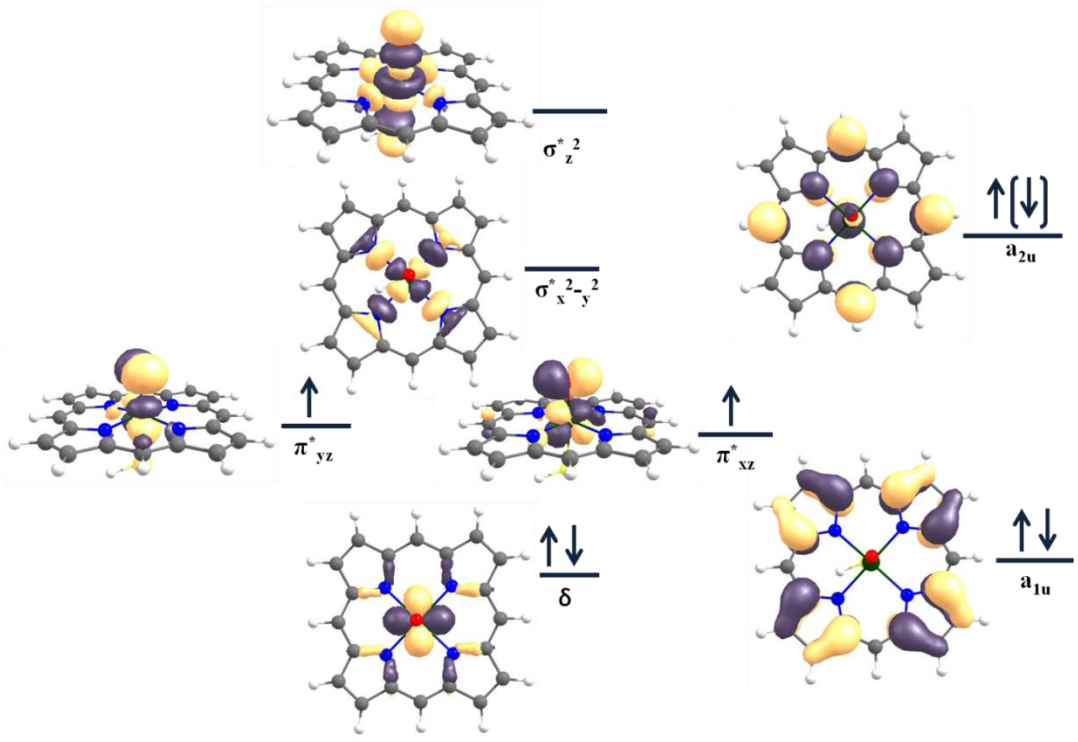

Figure 1.7: Molecular orbitals of Cpd I which are involved in oxygenation reactions.

The last step of the process is a rebound phase which allows C-O bond formation to give away the alcohol product. The HS and LS profile stays close in energy till PorFeOH/Alk˙ and then both states bifurcate. The LS manifold follows effectively concerted ones, the radical snaps out of the C…HO interaction from iron-hydroxo species [144-146] pathways leading to a product formation, while HS surface offers considerable barrier what we call rebound transition state. The reason behind the rebound barrier in HS surface is due to the promotion of an electron from the substrate to high lying virtual

orbital $\sigma^{*}_{z}{}^{2}$ and on LS state the promotion of this substrate electron takes place to a much low lying orbital π^{*}_{xz}. Hence, it can be inferred that radicals on the HS profile will have a significantly longer lifetime. In contrast to HS, LS will have an intermediate with a shorter lifetime and its upper limit will depend on the frequency of rotational modes, which establish a rebound position. Thus, TSR provides two-state information on the lifetime of the radical containing both "ultrashort" radical and "normal" radical [151].

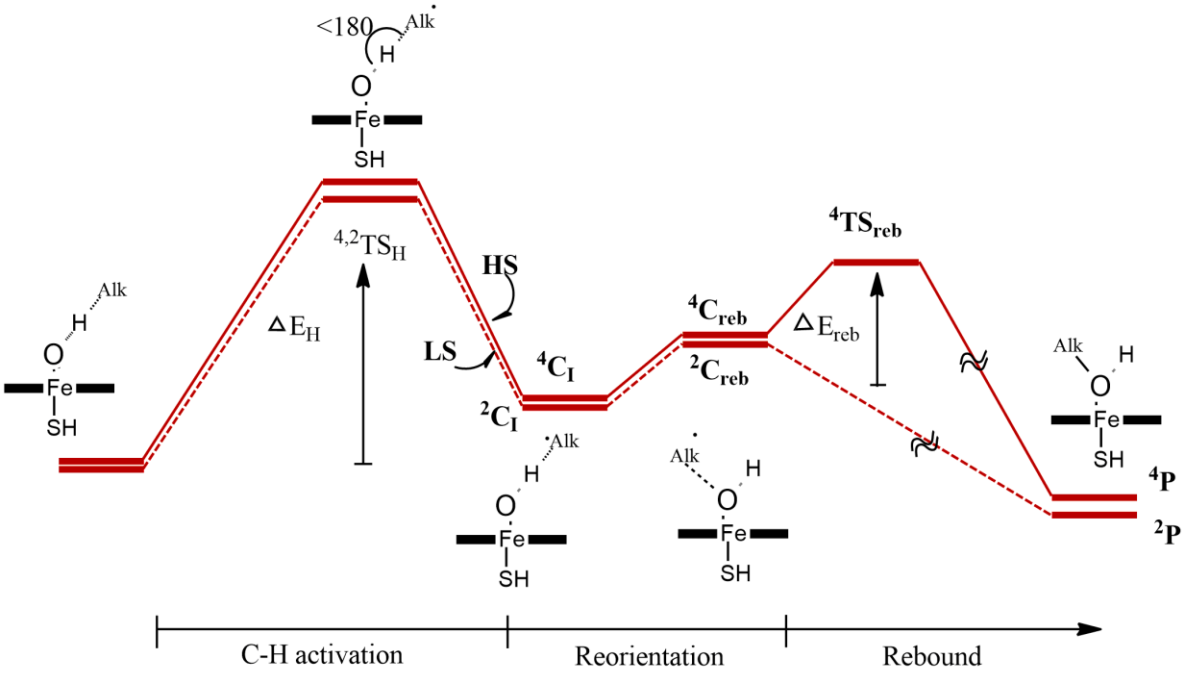

Figure 1.8: Typical reaction profile for C-H hydroxylation (Alk-H is the substrate) showing two-state reactivity (TSR) due to the closeness of the two spin-state profiles.

Now, this picture was extended to explain the radical clock experiment result from Scheme-1.6 which says that amount of rearranged product **R** mainly arrives from HS manifold and the unarranged product **U** is the outcome of both HS and LS manifold, or most of the time LS state. Apparent lifetime which is derived from the ratio [**U**/**R**] cannot

be regarded as a true lifetime since it is also taking relative yields of HS and LS in account. Taking example of C-H hydroxylation, the yield of product due to HS surface i.e., rearranged product will be small and majority of product will be unarranged product type which is outcome of LS manifold and this will lead to unrealistically short apparent lifetime calculation. But, the matter of the fact is that radicals exist on HS surface and have a normal lifetime, apparent lifetime manifestation is a result of the assumption that both the products arise from single radical intermediate. TSR mechanism can accommodate both the KIE results [152] which shows that the transition state is hydrogen- abstraction type in bond activation step and also it was able to explain that two-state rebound step too can lead to controversial lifetime if [$\boldsymbol{U}/\boldsymbol{R}$] is justified by single radical intermediate which can give partition between immediate rebound and first rearrangement followed by rebound [153].

1.2.2: Horseradish Peroxidase (HRP)

Horseradish peroxidase isoenzymes are heme class of enzyme. They come under the class III category of plant peroxidases superfamily, which mainly include peroxidases of fungal, bacterial, and plant origin [154]. It has been studied by researchers over the years. It serves many physiological roles such as lignifications, crosslinking of cell wall polymers, indole-3-acetic, suberin formation and resistance to infection. HRP consists of two different metal centre, iron (III) inserted in protoporphyrin IX (commonly referred as 'heme group') and two calcium atoms Figure 1.9. The enzyme structure majorly contains α-helix and small regions contain β-sheets also. It has two domains, the proximal and the distal and between these two domains heme group (plane) is situated, the structure is shown in Figure 1.9. The proximal side of the heme group in HRP is connected with the

histedine residue His170 through coordinate bond between Nitrogen of the histidine side-chain and Iron of the heme. The distal side of the heme is empty to be available to bind with hydrogen peroxide H_2O_2 at time of enzyme turnover or small gas molecules like cyanide, fluoride, carbon monoxide and azide. This makes iron atom hexa-coordinated. Two calcium atoms are placed at the distal and proximal side of the heme plane; they are linked in place with the hydrogen-bonding network. These calcium atoms are seven-coordinated from donar ligands of oxygen provided by nearby amino-acid side chains. Carboxylates of Asp, hydroxyl group of Ser, Thr, water molecule and carbonyls present in backbone [155]. After loss of calcium decrease in both the thermal stability and enzyme activity is obserevd.

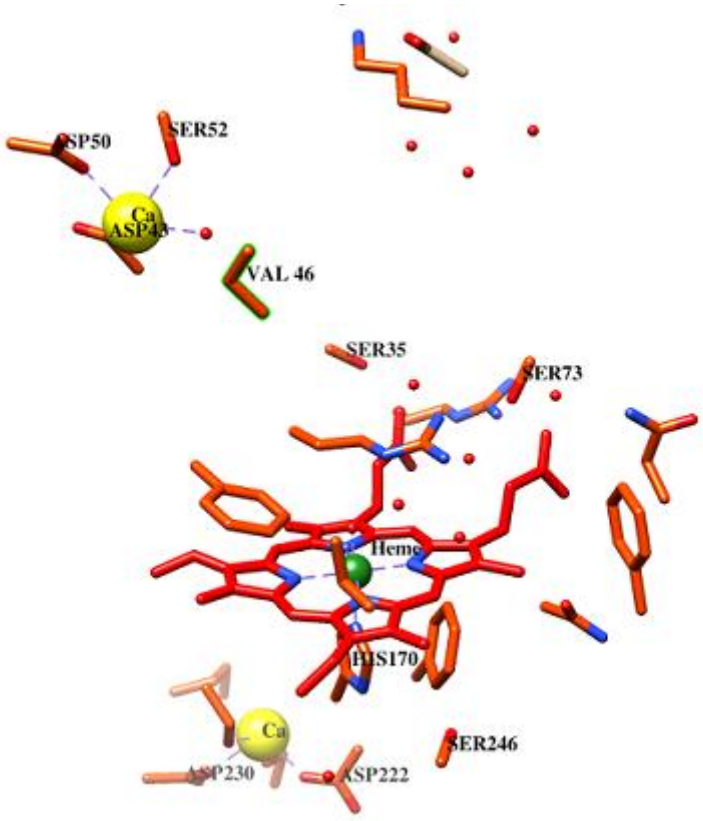

Figure 1.9: Active site of Horseradish Peroxidase (HRP) (1W4W pdb file).

1.2.3: Cytochrome c Oxidase (CcO)

Located in the bacterial and mitochondrial membrane Cytochrome c oxidase is the terminal enzyme of the respiratory chain. The active site structure of CcO is shown in Figure 1.10. It has binuclear centre which consists of heme group and copper atom ligated with the histidine as part of its active site. One of the histidine is cross-linked with the tyrosine residue that reduces molecular oxygen to water by a four electrons process. Two cofactors are responsible for the delivery of electron to the binuclear centre, one is the copper complex and another is heme group in the periphery of the binuclear center. Protons for the compensation of charges are provided by the membrane [156]. Cytochrome c oxidase is divided into subfamilies depending on the different numbers of channels for proton transfer and number of protons pumped per electron.

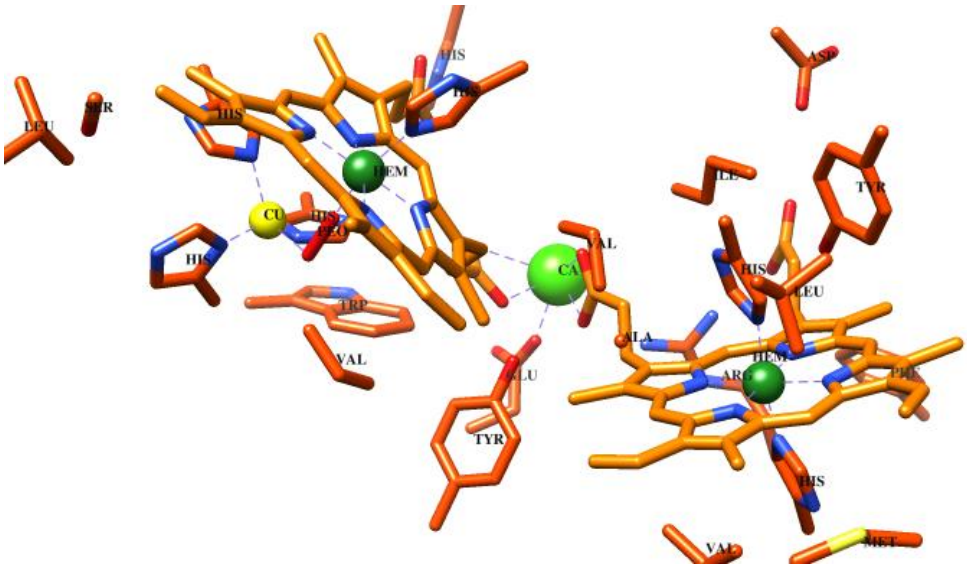

Figure 1.10: Active site of Cytochrome c Oxidase (5DJQ pdb file).

1.3: Non-Heme Enzymes

Over the years, activation of oxygen on the range of substrates by non-heme iron enzymes has progressed significantly [3,102,157,158]. Visualization of metalloenzymes active site is now possible by protein crystallography both in isolated form and various other states.

Generally, non-heme iron enzymes consist of two types of active sites (a) the first has mononuclear iron center that is coordinated with two histidines and a carboxylate group that fill one of the face of octahedron, (b) the second active site consists of a diiron center having two histidines and four carboxylates group and is usually associated with toluene and methane monooxygenases, ribonucleotide reductase and fatty acid desaturases [158]. As shown in the Figure 1.11 (a) this arrangement is popularly known as 2-His-1-as carboxylate facial triad.

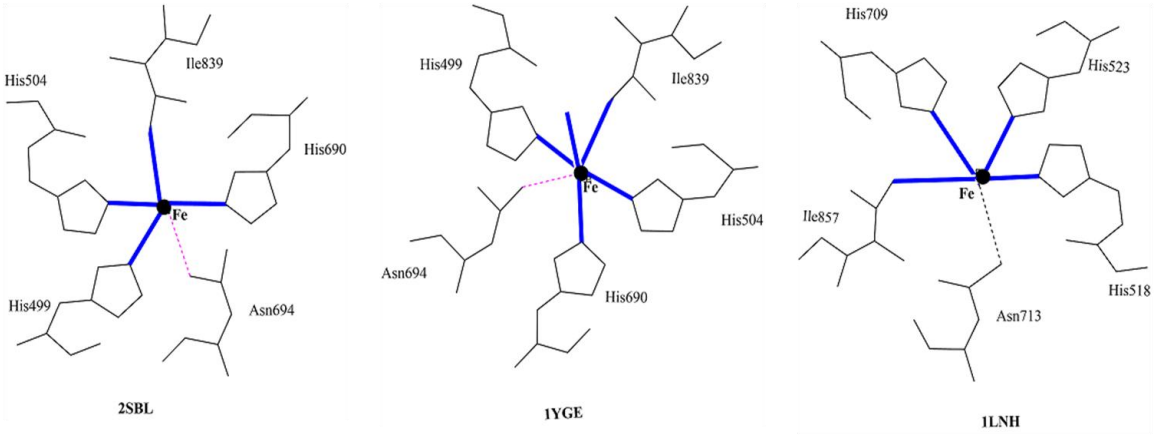

(a) **(b)** **(c)**

Figure 1.11: Structures of active site of ferrous LO: (a) SLO-1 (PDB: 2SBL) (b) SLO-1 (PDB: 1YGE) (c) 15-RLO (PDB: 1LNH).

This is the common structural motif of numerous mononuclear non-heme iron enzymes, [160]. This motif allows mechanistic flexibility by leaving three coordination sites of the metal center so that binding of exogenous ligands is possible such as cofactor, substrate, and/or O_2; on the other hand, in (b) at least one coordination site is available for exogenous ligand binding on each iron atom and mostly it is seen that O_2 binds with both the iron centers during the catalysis.

1.3.1: Mononuclear Non-heme iron

Mononuclear non-heme iron enzyme consisting of single iron at the active centre, forms a large group of enzymes which inserts single or both the oxygen atom of dioxygen (O_2) inside the substrates. Few of these mononuclear non-heme enzymes are discussed.

1.3.1.1: α-Ketoglutarate-Dependent and related enzymes

The α-ketoglutarate (α-KG or 2-oxoglutarate) is used as a cosubstrate in various class of mononuclear non-heme iron enzymes [161-163]. They are present inside microorganisms, plants and animals and play essential roles in large number of primary and secondary metabolic processes. The α-ketoglutarate dependent enzymes like lysyl hydroxylase, Prolyl 3-hydroxylase and prolyl 4-hydroxylase are responsible for the post-translational processing of collagen in animals [164]. Prolyl 4-hydroxylase catalyzes the synthesis of hydroxyproline-rich glycoproteins in plants, which helps in the regulation of cell wall extensibility and digestibility [165]. First step for the biosynthesis of antibiotic cephalosporin to deacetoxycephalosporin C is catalyzed by Deacetoxycephalosporin C synthase (DAOCS). All α-KG-dependent iron enzymes essentially need ferrous ion, O_2 and α-KG for their reactivity but have individual quarternary structures [161]. The

enzymes usually catalyze the reaction where α-KG decarboxylation is uncoupled from the substrate oxidation, either in the absence of substrate or in the presence of a substrate analogue [166-170].

Valegard *et al.* have reported the first crystal structure of DAOCS [171] Figure 1.12 shows apo (i.e., metal removed) DAOCS (PDB ID: 1DCS) and the DAOCS complex with Fe^{II} (PDB ID: 1RXF).

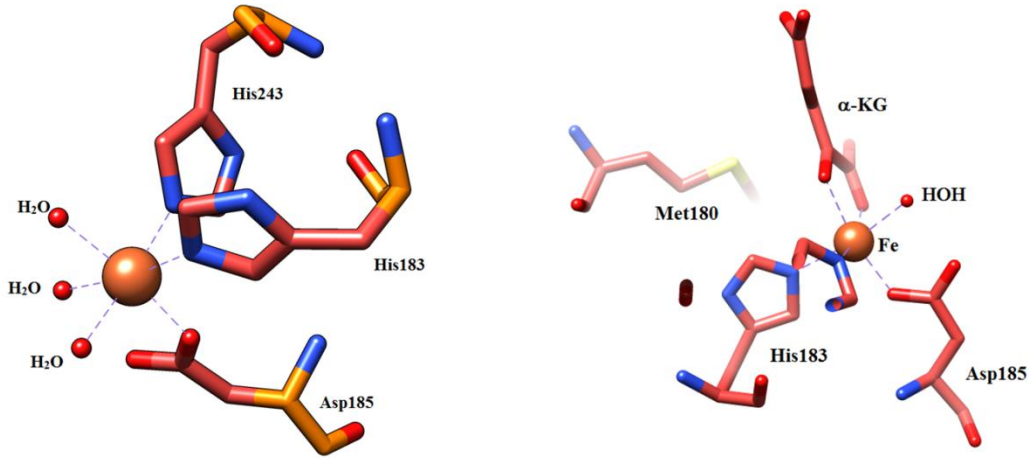

(a) (b)

Figure 1.12: Structure of the active site in DAOCS: (a) the apoenzymes, (PDB: 1DCS) (b) the complex of DAOCS/FeII, (PDB: 1RXF).

1.3.1.2: Rieske-Type Dioxygenases

The Rieske iron-sulfur comprises of two iron and two sulfur atoms ([2Fe-2S]) shown in Figure 1.13. First iron contains 2His and second iron contains 2Cys in its coordination environment, rather than 4Cys found in plant ferredoxins. It mainly assists in electron transport pathways of cytochrome complexes and also in some dioxygenases [172]. The latter type incorporate two protein components viz reductase that contains flavin and a

ferredoxin, [2Fe-2S] and a terminal oxygenase comprises of Rieske [2Fe-2S] cluster and iron non-heme active site[173]. Majority of Rieske-type oxygenases consists of mononuclear iron as its active site where dioxygen activation and substrate oxygenation takes place [173,174].

Alkene monooxygenase have binuclear iron site in its terminal oxygenase as studied by F. J. Small and S. A. Ensign in 1997. The majority of the Rieske-type mononuclear enzyme is aromatic dioxygenase. They perform cis-dihydroxylation catalysis of aromatic ring in regio- and stereospecific manner utilizing ring using dioxygen and NAD (P) H. The enzymes that perform aerobic degradation of aromatic compounds in soil bacteria are benzene dioxygenase (BDO), [175] phthalate dioxygenase (PDO), [176] toluene dioxygenase,[177] and naphthalene 1,2-dioxygenase (NDO) [178]. They are thus used in bioremediation. Apart from bacterial dioxygenases, other type of mononuclear Rieske oxygenases are anthranilate 1,2-dioxygenase,[179] that carry out substrate deamination and decarboxylation and produces catechol; chlorophenylacetate 3,4-dioxygenase [180].

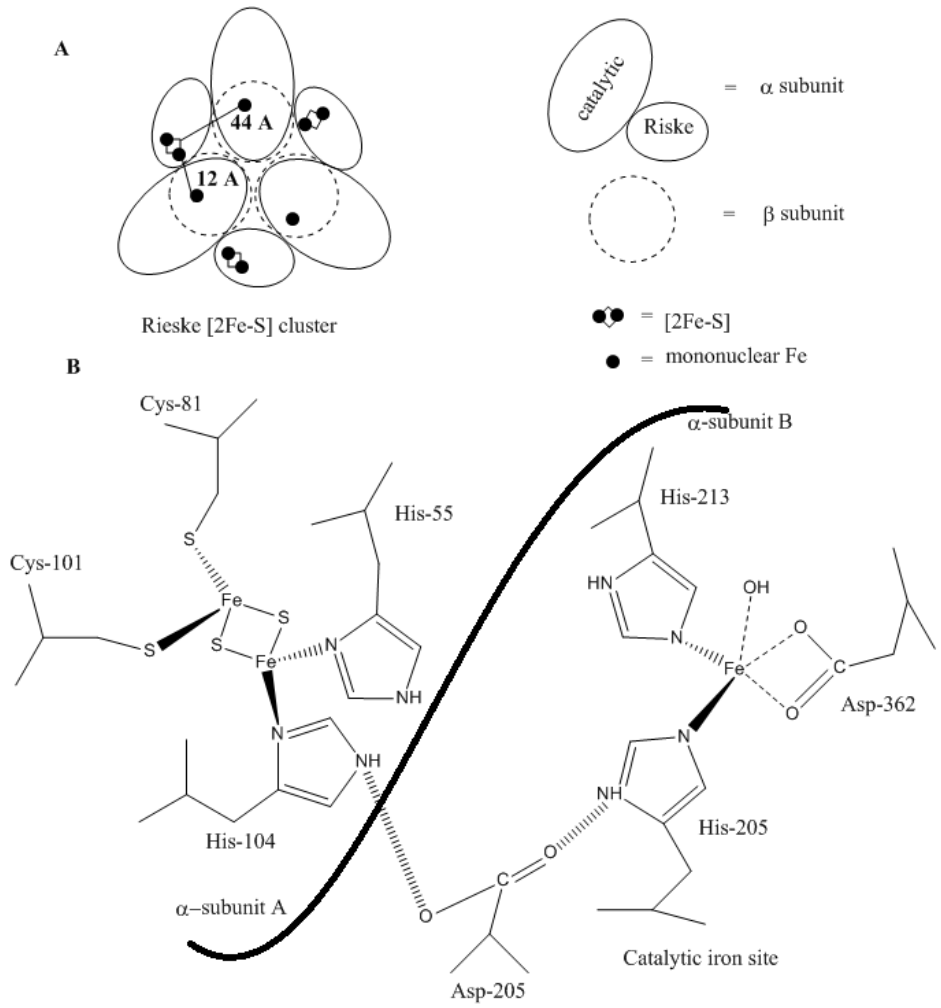

Figure 1.13: (a) Schematic overall protein structure of NDO showing α and β subunits and the inter- and intra-subunit distance between the Rieske site and the non-heme iron site. (b) Schematic structure of the Rieske site, the nonheme iron site and the proposed route of ET between them in NDO (Adapted from work by Kauppi *et al.* (1998) and Kurtz *et al.* (1999).

1.3.2 Binuclear Non-heme iron

Bridged oxygen binuclear non-heme iron cluster have been identified in dioxygen activation (O_2) and some of the members of this family have been characterized throughly.

1.3.2.1 Methane Monooxygenase

Methane monooxygenase (MMO) catalyzes extraordinarily stable C–H bond of methane (bond dissociation energy 104 kcal mol^{-1}) to produce methanol. They carry out oxygen insertion in the presence of NADH [181-183]. Afterwards; methanol is converted into formaldehyde by methane dehydrogenase, which later gets converted into formate catalyzed by formaldehyde dehydrogenase cooperatively with NAD+ reduction. Ultimately, formate dehydrogenase oxidizes formate CO_2 with help of NAD^+ as an oxidant. Methanotrophs are solely dependent on this pathway for their source and energy (to grow) through methane absorbtion [182,184,185]. Methanotrophs are broadly classified on the basis of metabolic pathway utilized, their morphology, and types of MMO expressed as type I, II, or X [184,185]. Active site of MMO shown in Figure 1.14, it has dimer of iron which is linked through oxygen derived ligands. It consists of two histidines and four glutamates [186]. The structure of active site is like diamond core, that has two briged oxo groups having Fe^2 (IV, IV) oxidation state, this is regarded as one of the highest oxidized species present in nature.

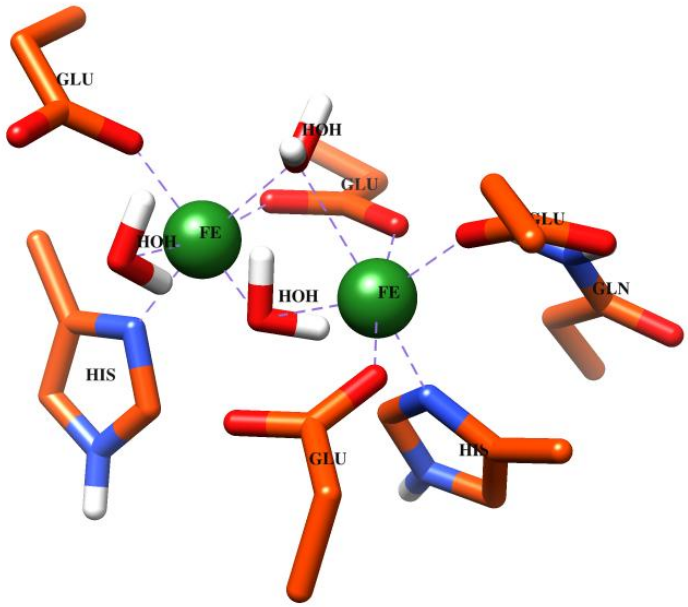

Figure 1.14: Representation of the crystallographically determined binuclear active sites of MMOH. (a) Diferric MMOH with (PDB: 1MTY).

1.3.2.2 Δ^9 Desturase

The 3-D structure of reduced Δ^9D extracted from the castor seeds has been determined by X-ray crystallography, at a resolution of 2.4 Å (PDB ID 1AFR) [187]. The acyl-ACP desaturases which are acyl-bound acyl carrier protein helps in dioxygen activation in desaturation reaction for insertion of a cis (or Z) double bond. In the biosynthesis of fatty acid desaturation it is an important step. In eukaryotes, desaturation is a post synthetic modification catalyzed by NADPH- and dioxygen-dependent binuclear non-heme iron enzymes. Identification of membrane bound and soluble bound both been done, apart from lot of isoforms found that differ in regiospecificity and substrate specificity [188-190]. Positioning of double bond and their number, show profound effect on physiological properties of fatty acids. Structure of the active site of enzyme is shown in Figure 1.15.

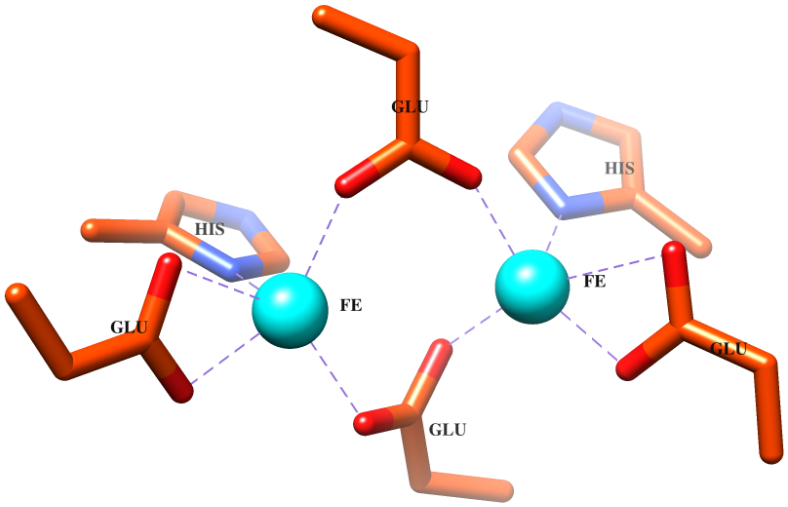

Figure 1.15: Representation of the crystallographically determined binuclear $Fe^{II}Fe^{II}$ active site of stearoyl-acyl carrier protein Δ^9 desaturase from caster seed (PDB:1AFR).

REFERENCES

[1] J. J. R. F. D. Silva, R. J. P. Williams, *The Biological Chemistry of the Elements*, Clarendon Press, Oxford (1991).

[2] E. I. Solomon, T. C. Brunold, M. I. Davis, J. N. Kemsley, S.-K. Lee, N. Lehnert, F. Neese, A. J. Skulan, Y. S. Yang, J. Zhou, *Chem. Rev.*, **100**, 235 (2000).

[3] M. Costas, M. P. Mehn, M. P. Jensen, L. Que Jr., *Chem. Rev.*, **104**, 939 (2004).

[4] R. P. Hausinger, *Crit. Rev. Biochem. Mol. Biol.*, **39**, 21 (2004).

[5] E. G. Kovaleva, J. D. Lipscomb, *Nat. Chem. Biol.*, **4**, 186 (2008).

[6] C. Loenarz, C. J. Schofield, *Nat. Chem. Biol.*, **4**, 152 (2008).

[7] H. Arakawa, M. Aresta, J. N. Armor, M. A. Barteau, E. J. Beckman, A. T. Bell, J. E. Bercaw, C. Creutz,E. Dinjus, D. A. Dixon, K. Domen, D. L. DuBois, J. Eckert, E. Fujita,D. H. Gibson,W. A. Goddard,D. W. Goodman, J. Keller, G. J. Kubas,H. H. Kung, J. E. Lyons,L. E. Manzer,T. J. Marks, K. Morokuma,K. M. Nicholas, R. Periana, L. Que, J. Rostrup-Nielson,W. M. Sachtler, L. D. Schmidt,A. Sen,G. A. Somorjai, P. C. Stair, B. R. Stults, W.Tumas, *Chem. Rev.*, **101**, 953 (2001).

[8] A. E. Shilov,G. B. Shul, G. B. Shul'pin, *Chem. Rev.*, **97**, 2879 (1997).

[9] B. L. Conley, W. J. Tenn, K. J. H. Young, S. Ganesh, S. Meier,V. Ziatdinov, O. Mironov, J. Oxgaard, J. Gonzales, W. A. Goddard, R. A. Periana, in *Activation of Small Molecules: Organometallic and Bioinorganic Perspectives*; W. B. Tolman (Ed.), Wiley-VCH: Weinheim, Germany, 235

(2006).

[10] W. Nam, *Acc. Chem. Res.*, **40**, 465 (2007).

[11] J. M. Bollinger Jr., C. Krebs, *Curr. Opin. Chem. Biol.*, **11**, 151 (2007).

[12] M. Rolff, F. Tuczek, *Angew. Chem. Int. Ed.*, **47**, 2344 (2008).

[13] E. I. Solomon, J. W. Ginsbach, D. E. Heppner, M. T. Kieber-Emmons, C. H. Kjaergaard, P. J. Smeets, L. Tian, J. S. Woertink, *Faraday Discuss.*, **148**, 11 (2011).

[14] J. Hohenberger, K. Ray, K. Meyer, *Nat. Commun.*, **3**, 720 (2012).

[15] P. C. A. Bruijnincx, G. van Koten, R. J. M. Klein Gebbink, *Chem. Soc. Rev.*, **37**, 2716 (2008).

[16] C. E. Tinberg, S. J. Lippard, *Acc. Chem. Res.*, **44**, 280 (2011).

[17] F.-H. Li, G.-H. Zhao, H.-X. Wu, H. Lin, X.-X. Wu, S.-R. Zhu, H.-K. Lin, *J. Inorg. Biochem.*, **100**, 36 (2006).

[18] C. Jung, *Biochim. Biophys. Acta*, **1814**, 46 (2011).

[19] C. Krebs, J. C. Price, J. Baldwin, L. Saleh, M. T. Green, J. M. Bollinger Jr., *Inorg. Chem.*, **44**, 742 (2005).

[20] S. Shaik, S. Cohen, Y. Wang, H. Chen, D. Kumar, W. Thiel, *Chem. Rev.*, **110**, 949 (2010).

[21] E. I. Solomon, S. D. Wong, L. V. Liu, A. Decker, M. S. Chow, *Curr. Opin. Chem. Biol.*, **13**, 99 (2009).

[22] E. I. Solomon, D. E. Heppner, E. M. Johnston, J. W. Ginsbach, J. Cirera, M. Qayyum, M. T. Kieber-Emmons, C. H. Kjaergaard, R. G. Hadt, L. Tian, *Chem. Rev.*, **114**, 3659 (2014).

[23] T. L. Poulos, *Chem. Rev.*, **114**, 3919 (2014).

[24] Z. Halime, K. D. Karlin, in Copper-Oxygen Chemistry; K. D. Karlin, S.Itoh (Eds.), *Wiley Series of Reactive Intermediates in Chemistry and Biology*, John Wiley & Sons: New York, 283 (2011).

[25] M. Sono, M. P. Roach, E. D. Coulter, J. H. Dawson, *Chem. Rev.*, **96**, 2841 (1996).

[26] J. T. Groves, *Proc. Natl. Acad. Sci.* U. S. A., **100**, 3569 (2003).

[27] P. R. Ortiz de Montellano (Ed.), *Cytochrome P450: Structure, Mechanism and Biochemistry*, 3rd ed., Kluwer Academic/Plenum Publishers, New York, (2004).

[28] B. Meunier, S. P. de Visser, S. Shaik, *Chem. Rev.*, **104**, 3947 (2004).

[29] A. W. Munro, H. M. Girvan, K. J. McLean, *Nat. Prod. Rep.*, **24**, 585 (2007).

[30] K. M. Kadish, K. M. Smith, R. Guilard (Eds.), *Handbook of Porphyrin Science*, World Scientific Publishing Co., New Jersey, (2010).

[31] P. R. Ortiz de Montellano, *Chem. Rev.*, **104**, 932 (2010).

[32] S. P. de Visser, D. Kumar (Eds.), *Iron-containing enzymes: Versatile catalysts of hydroxylation reaction in nature*, RSC Publishing, Cambridge (UK), (2011).

[33] T. D. H. Bugg, *Curr. Opin. Chem. Biol.*, **5**, 550 (2001).

[34] M. J. Ryle, R. P.Hausinger, *Curr. Opin. Chem. Biol.*, **6**, 193 (2002).

[35] S. V. Kryatov, E. V.Rybak-Akimova, S. Schindler, *Chem. Rev.*, **105**, 2175 (2005).

[36] M. M. Abu-Omar, A. Loaiza, N. Hontzeas, *Chem. Rev.*, **105**, 2227 (2005).

[37] A. R. McDonald, L. Que Jr., *Coord. Chem. Rev.*, **257**, 414 (2013).

[38] D. Buongiorno, G. D. Straganz, *Coord. Chem. Rev.*, **257**, 541 (2013).

[39] S. Al-Attar, S. de Vries, *Coord. Chem. Rev.*, **257**, 64 (2013).

[40] L. Quintanar, L. Rivillas-Acevedo, R. Grande-Aztatzi, C. Z. Gómez-Castro, T. Arcos-Lo´pez, A. Vela, *Coord. Chem. Rev.*, **257**, 42 (2013).

[41] S. Fukuzumi, K. D. Karlin, *Coord. Chem. Rev.*, **257**, 187 (2013).

[42] L. Rulíšek, U. Ryde, *Coord. Chem. Rev.*, **257**, 445 (2013).

[43] V. Conte, A. Coletti, B. Floris, G. Licini, C. Zonta, *Coord. Chem. Rev.*, **255**, 2165 (2011).

[44] G. Licini, V. Conte, A. Coletti, M. Mba, C. Zonta, *Coord. Chem. Rev.*, **255**, 2345 (2011).

[45] P. J. Gonzalez, M. G. Rivas, C. S. Mota, C. D. Brondino, I. Moura, J. J. G. Moura, *Coord. Chem. Rev.*, **257**, 315 (2013).

[46] H. Broda, S. Hinrichsen, F. Tuczek, *Coord. Chem. Rev.*, **257**, 587 (2013).

[47] A. B. Tomter, G. Zoppellaro, N. H. Andersen, H.-P. Hersleth, M. Hammerstad, Å. K. Røhr, G. K. Sandvik, K. R. Strand, G. E. Nilsson, C. B. Bell III, A.L. Barra, E. Blasco, L. Le Pape, E. I. Solomon, K. K. Andersson, *Coord. Chem. Rev.*, **257**, 3 (2013).

[48] P. Nordlund, P. Reichard, *Annu. Rev. Biochem.*, **75**, 681 (2006).

[49] J. Herrick, B. Sclavi, *Mol. Microbiol.*, **63**, 22 (2007).

[50] N. Nelson, C. F. Yokum, *Annu. Rev. Biochem.*, **57**, 521 (2006).

[51] C. W. Cady, R. H. Crabtree, G. W. Brudvig, *Coord. Chem. Rev.*, **252**, 444 (2008).

[52] D. J. Vinyard, G. M. Ananyev, G. C. Dismukes, *Annu. Rev. Biochem.*, **82**, 577 (2013).

[53] P. E.M. Siegbahn, *Chem. Eur. J.*, **14**, 8290 (2008).

[54] N. M. DeVore, E. E. Scott, *J. Biol. Chem.*, **287**, 26576 (2012).

[55] J. R. O'Brien, D. J. Schuller, V. S. Yang, B. D. Dillard, W. N. Lanzilotta, *Biochemistry*, **42**, 5547 (2003).

[56] J. H. Dawson, R. H. Holm, J. R. Trudell, G. Barth, R. E. Linder, E. Bunnenberg, C. Djerassi, S. C. Tang, *J. Am. Chem. Soc.*, **98**, 3707 (1976).

[57] P. Nicholls, I. Fita, P. C. Loewen, *Adv. Inorg. Chem.*, **51**, 51 (2000).

[58] N. G. Veitch, A. T. Smith, *Adv. Inorg. Chem.*, **51**, 107 (2000).

[59] H.-P. Hersleth, U. Ryde, P. Rydberg, C. H. Görbitz, K. K. Andersson, *J. Inorg. Biochem.*, **100**, 460 (2006).

[60] A. D. Becke, *J. Chem. Phys.*, **98**, 5648 (1993).

[61] C. W., BauschlicherJr, A. Ricca, H.Partridge, S. R. Langhoff, In Recent Advances in Density Functional Methods, Part II*;* Chong, D. P., Ed.;World Scientific Publishing Co.: Singapore, pp. 165 (1997)

[62] P. E. M. Siegbahn, Electronic Structure Calculations for Molecules Containing Transition Metals. In Advances in Chemical Physics; Prigogine, I., Rice, S. A., Eds.; J. Wiley: New York, Vol. XCIII,pp. 333 (1996).

[63] P. E. M. Siegbahn, R. H. Crabtree, *J. Am. Chem. Soc.*, **119,** 3103 (1997*).*

[64 A. Warshel, M. Levitt, *J. Mol. Biol.*, **103**, 227(1976*).*

[65] A. J. Mulholland, G. H. Grant, W. G. Richards, *Protein Eng.*, **6**, 133 (1993).

[66] M. R. A. Blomberg,T. Borowski, F. Himo, R. Z. Liao, P. E. M. Siegbahn,

Chem. Rev., **114**, 7, 3601 (2014).

[67] F. Ogliaro, S. P. de Visser, S. Shaik, *J. Inorg. Biochem.*, **91**, 554 (2002).

[68] P. Rydberg, E. Sigfridsson, U. Ryde, *J. Biol. Inorg. Chem.*, **9**, 203 (2004).

[69] D. Kumar, B. Karamzadeh, G. N. Sastry, S. P. de Visser, *J. Am. Chem. Soc.*, **132**, 7656 (2010).

[70] D. Kumar, R. Latifi, S. Kumar, E. V. Rybak-Akimova, M. A. Sainna, S. P. de Visser, *Inorg. Chem.*, **52**, 7968 (2013).

[71] M. T. Green, *J. Am. Chem. Soc.*, **121**, 7939 (1999).

[72] S. P. de Visser, S. Shaik, P. K. Sharma, D. Kumar, W. Thiel, *J. Am. Chem. Soc.*, **125**, 15779 (2003).

[73] K. Yoshizawa, Y. Shiota, T. Yamabe, *J. Am. Chem. Soc.*, **121**, 147 (1999).

[74] J. Rittle, M. T. Green, *Science*, **330**, 933 (2010).

[75] S. P. de Visser, *Angew. Chem. Int. Ed.*, **45**, 1790 (2006).

[76] S. P. de Visser, *J. Am. Chem. Soc.*, **128**, 9813 (2006).

[77] A. Decker, M. D. Clay, E. I. Solomon, *J. Inorg. Biochem.*, **100**, 697 (2006).

[78] R. Latifi, M. Bagherzadeh, S. P. de Visser, *Chem. Eur. J.*, **15**, 6651 (2009).

[79] S. P. de Visser, J.-U. Rohde, Y.-M. Lee, J. Cho, W. Nam, *Coord. Chem. Rev.*, **257**, 381 (2013).

[80] K. P. Jensen, P. Rydberg, J. Heimdal, U. Ryde, A comparison of the tetrapyrrole cofactors in nature and their tuning by axial ligands, in *Computational modeling for homogeneous and enzymatic catalysis*, K. Morokuma and J. Musaev (Eds.), Wiley-VCH, Weinheim, **27** (2008).

[81] R. van Eldik, *Coord. Chem. Rev.*, **251**, 1649 (2007).

[82] A.R. McDonald, L. Que Jr., *Nat. Chem.*, **3**, 761 (2011).

[83] J.M. Bollinger, C. Krebs, *J. Inorg. Biochem.*, **200**, 586 (2006).

[84] E.G. Hrycay, S.M. Bandiera, *Arch. Biochem. Biophys.*, **522**, 71 (2012).

[85] P. R. Ortiz de Montellano, J. J. De Voss, in *Cytochrome P450: Structure, Mechanism, and Biochemistry*, P. R. Ortiz de Montellano (ed.), 3rd ed., Kluwer Academic/Plenum Publishers, New York, 183 (2005).

[86] D. F. V. Lewis, *Guide to Cytochromes P450: Structure and Function*, Taylor and Francis, London, UK, (2001).

[87] I.G. Denisov, T.M. Makris, S.G. Sligar, I. Schlichting, *Chem. Rev.*, **105**, 2253 (2005).

[88] C. Krebs, D. Galonicǐ Fujimori, C. T. Walsh, J. M. Bollinger Jr., *Acc. Chem. Res.*, **40**, 484 (2007).

[89] C. E. Tinberg, S. Lippard, *Acc. Chem. Res.*, **44**, 280 (2011).

[90] M. Yagi, M. Kaneko, *Chem. Rev.*, **101**, 21 (2001).

[91] C. S. Mullins, V. L. Pecoraro, *Coord. Chem. Rev.*, **252**, 416 (2008).

[92] Y. Umena, K. Kawakami, J.-R. Shen, N. Kamiya, *Nature*, **473**, 55 (2011).

[93] J. P. McEvoy, G.W. Brudvig, *Chem. Rev.*, **106**, 4455 (2006).

[94] S. P. de Visser, *Coord. Chem. Rev.*, **253**, 754 (2009).

[95] O. Weinreb, T. Amit, S. Mandel, L. Kupershmidt, M.B.H. Youdim, *Antioxid. Redox Signal.*, **13**, 919 (2010).

[96] C. Wong, D.G. Fujimori, C.T. Walsh, C.L. Drennan, *J. Am. Chem. Soc.*, **131**, 4872 (2009).

[97] F. H. Vaillancourt, E. Yeh, D. A. Vosburg, S. Garneau-Tsodikova, C.T.

Walsh, *Chem. Rev.*, **106**, 3364 (2006).

[98] A. Butler, M. Sandy, *Nature*, **460**, 848 (2009).

[99] Y. Watanabe, H. Fujii, *Struct. Bond.*, **97**, 61 (2000).

[100] S. Shaik, W. Lai, H. Chen, Y. Wang, *Acc. Chem. Res.*, **43**, 1154 (2010).

[101] R. Zhang, M. Newcomb, *Acc. Chem. Res.*, **41**, 468 (2008).

[102] W. Nam, *Acc. Chem. Res.*, **40**, 522 (2007).

[103] M. M. Abu-Omar, A. Loaiza, N. Hontzeas, *Chem. Rev.*, **105**, 2227 (2005).

[104] L. Que Jr., *Acc. Chem. Res.*, **40**, 493 (2007).

[105] X. Shan, L. Que Jr., *J. Inorg. Biochem.*, **100**, 421 (2006).

[106] J. Cho, R. Sarangi, W. Nam, *Acc. Chem. Res.*, **45**, 1321 (2012).

[107] D. Goldberg, *Acc. Chem. Res.*, **40**, 626 (2007).

[108] Z. Gross, *J. Biol. Inorg. Chem.*, **6**, 733 (2001).

[109] F. Neese, W. Ames, G. Christian, M. Kampa, D. G. Liakos, D.A. Pantazis, M. Roemelt, P. Surawatanawong, S. Ye, *Adv. Inorg. Chem.*, **62**, 301 (2010).

[110] J. U. Rohde, J. H. In, M. H. Lim, W. W. Brennessel, M. R. Bukowski, A. Stubna, E. Münck, W. Nam, L. Que Jr., *Science*, **299**, 1037 (2003).

[111] T. L. Poulos, *Nat. Prod. Rep.*, **24**, 504 (2007).

[112] I. G. Denisov, T. M. Makris, S. G. Sligar, I. Schlichting, *Chem. Rev.*, **105**, 2253(2005).

[113] T. L. Poulos, *Chem. Rev.*, **7**, 3919 (2014).

[114] I. G. Denisov, D. T. Frank, S. G. Sligar, *Chem. Rev.*, **124**, 151, (2009).

[115] J. Xu, X., Wang, W. Guo, *J. Integr. Agr.*,**14,** 1673 (2015).

[116] T. Omura, and R. Sato, *J. Bio. Chem..*, **239,** 2370 (1964).

[117] A. W. Munro, H. M. Girvan, K. J. McLean, *Biochim. Biophys. Acta,***1770,** 345 (2007).

[118] E. G. Hrycay, S.M. Bandiera, *Archives of Biochem. Biophys.*,**522,** 71 (2012).

[119] X. Wang, S. Peter, M. Kinne, M. Hofrichter, J.T. Groves, *J. Amer. Chem. Soc.*, **134,** 12897 (2012).

[120] M., Zamocky, S., Hofbauer, I., Schaffner, B., Gasselhuber, A., Nicolussi, M., Soudi, K.F., Pirker, P.G., Furtmüller, C. Obinger, *Archives of Biochem. Biophys.*, **574,** 108 (2015).

[121] J. T. Groves, K., Shalyaev, J. Lee, Oxometalloporphyrins in oxidative catalysis, in: K.M. Kadish, K.M. Smith, R. Guilard, (Eds.), The Porphyrin Handbook, Academic Press, Elsevier Science (USA), **4**, 17 (2000).

[122] T. M. Makris, K.V. Koenig, I. Schlichting, S.G. Sligar, *J. Inor. Biochem.*,**100,** 507 (2006).

[123] B. Meunier, S.P. de Visser, S. Shaik, *Chem. Rev.*, **104,** 3947 (2004).

[124] H. Setzu, G. Goff, R. Feyereisen,*Philos. Trans. R. Soc. Lond. B. Biol. Sci.*,368, 20248 (2013)

[125] F. Ogliaro, S. P. de Visser, S. Cohen, P. K. Sharma, S. Shaik, *J. Am. Chem. Soc.*, **124**, 2806 (2002).

[126] T. Kamachi, Y. Shiota, T. Ohta, K. Yoshizawa, *Bulletin of the Chemical Society Japan,***76**, 721 (2003).

[127] M. J. Park, J. Lee, Y. Suh, J. Kim, W. Nam, *J. Am.Chem. Soc.*, **128**, 2630 (2006).

[128] P. K. Sharma, S. P. de Visser, S. Shaik, *J. Am. Chem. Soc.*, **125**, 8698 (2003).

[129] D. Kumar, S. P. de Visser, P. K. Sharma, H. Hirao, S. Shaik, *Biochem.*,**44**, 8148 (2005).

[130] C. Li, L. Zhang, C. Zhang, H. Hirao, W. Wu, S. Shaik, *Angew. Chem. Int. Ed.*, **46**, 8168 (2007).

[131] C. S. Porro, M. J. Sutcliffe, S. P. de Visser, *J. Am. Chem. Soc.*, **113**, 11635 (2009).

[132] P. Rydberg, U. Ryde, L. Olsen, *J. Chem. Theo. Comp.*, **4,** 1369 (2008).

[133] J. T. Groves, G. A. McClusky, *J. Am. Chem. Soc.*, **98**, 859 (1976).

[134] K. Auclaire, Z. Hu, D. M. Little, P. R. Ortiz de Montellano, J. T. Groves, *J. Am. Chem. Soc.*, **124**, 6020 (2002).

[135] A. Sorokin, A. Robert, B. Meunier, *J. Am. Chem. Soc.*, **115**, 7393 (1993).

[136] M. H. Gelb, D. C. Heimbrook, P. Malkonen, S. G. Sligar, *Biochem.*,**21**, 370 (1982).

[137] M. Sono, M. P. Roach, E. D. Coulter, J. H. Dawson, *Chem. Rev.*, **96**, 2841 (1996).

[138] W. D. Woggon, *Top. Curr. Chem.*, **184**, 39 (1996).

[139] B. Meunier, J. Bernadou, *Top. Catal.*,**21**, 47 (2002).

[140] H. Fretz, W.D. Woggon, R. Voges, *Helv. Chim. Acta.*, **72**, 391 (1989).

[141] C. Audergon, K. R. Iyer, J. P. Jones, J. F. Darbyshire, W. T. Trager, *J. Am. Chem. Soc.*, **121**, 41 (1999).

[142] M. Newcomb, R. Shen, S.-Y. Choi, P. H. Toy, P. F. Hollenberg, A. D.N. Vaz, M. J. Coon, *J. Am. Chem. Soc.*,**122**, 2677 (2000).

[143] M. Newcomb,P. H Toy,*Acc. Chem. Res.*,**33**, 449 (2000).

[144] S. P. de Visser, F. Ogliaro, N. Harris, S. Shaik, *J. Am. Chem. Soc.*, **123**, 3037 (2001).

[145] S. Shaik, S. P. de Visser, F. Ogliaro, H. Schwarz, D. Schroder, *Curr.Opin.Chem. Biol.*, **6**, 556 (2002).

[146] F. Ogliaro, N. Harris, S. Cohen, M. Filatov, S. P. de Visser, S. Shaik, *J. Am. Chem. Soc.*,**122**, 8977 (2000).

[147] S. Shaik, D. Kumar, S. P. de Visser, A. Altun, W. Thiel, *Chem. Rev.*,**105**, 2279 (2005).

[148] M. T. Green, *J. Am. Chem. Soc.*, **123**, 9218 (2001).

[149] J. C. Schöneboom, H. Lin, N. Reuter, W. Thiel, S. Cohen, F. Ogliaro, S. Shaik, *J. Am. Chem. Soc.*, **124**, 8142 (2002).

[150] R. Latifi, M. A. Sainna, E. V. Rybak-Akimova, S. P. de Visser, *Chem. Eur. J.* 4058 (2013).

[151] S.; Shaik, S. P. de Visser, Computational Approaches to Cytochrome P450 Function. *InCytochrome P450: structure, mechanism and biochemistry*, **2**, 45 (2004).

[152] S.P. de Visser, C.S. Porro, M.G. Quesne, M.A. Sainna, A.M. Munro, *Curr. Top. Med. Chem.*, **13**, 2218 (2013).

[153] S. Shaik, S. Cohen, S. P. de Visser, P. K. Sharma, D. Kumar, S. Kozuch, F. Ogliaro, and D. Danovic, *Eur. J. Inorg. Chem.*, 207 (2004).

[154] K.G., Welinder,*Curr. Opin. Chem. Biol.* **2**, 388 (1992).

[155] N. C. Veitch, *Phytochemistry*, **65**, 249 (2004).

[156] M. K. F. Wikstrom, *Nature*, **266**, 271 (1977).

[157] E. I. Solomon, T. C. Brunold, M. I. Davis, J. N. Kemsley, S.-K. Lee, N. Lehnert, F. Neese, A. J. Skulan, Y. S. Yang, J. Zhou, *Chem. Revs.*, **100**, 235 (2000).

[158] M. Merkx, D. A. Kopp, M. H. Sazinsky, J. L. Blazyk, J. Müller, S. J. Lippard, *Angew. Chem., Int. Ed.*, **40**, 2782 (2001).

[160] K. D. Koehntop, J. P. Emerson, L. Que Jr., *J. Biol. Inorg. Chem.*, **10**, 87 (2005).

[161] E. De Carolis, V. De Luca, *Phytochemistry*, **36**, 1093 (1994).

[162] P. Hedden, *Biochem. Soc. Trans.*, **20**, 373 (1992).

[163] A. G. Prescott, *J. Exp. Bot.*, **44**, 849 (1993).

[164] K. I. Kivirikko, R. Myllylä, in *The Enzymology of Posttranslational Modification of Proteins*, R. B. Freedman, H. C. Hawkins, (Eds.), Academic: London, **1**, 53 (1980).

[165] M. J. Chrispeels, *Methods Enzymol.*, **107**, 361 (1984).

[166] L. Tuderman, R. Myllyla¨, K. I. Kivirikko, *Eur. J. Biochem.*, **80**, 341 (1977).

[167] U. Puistola, T. M. Turpeenniemi-Hujanen, R. Myllyla, K. I. Kivirikko, *Biochim. Biophys. Acta*, **611**, 40 (1980).

[168] E. Holme, S. Lindstedt, I. Nordin, *Biochem. Biophys. Res. Commun.*, **107**, 518 (1982).

[169] R. S. Wehbie, N. S. Punekar, H. A. Lardy, *Biochem.*, **27**, 2222 (1988).

[170] C.-A. Hsu, M. D. Saewert, L. F. Polsinelli Jr., M. T. Abbott, *J. Biol. Chem.*, **256**, 6098 (1981).

[171] K. Valegard, A. C. T. Vanscheltinga, M. D. Lloyd, T. Hara, S. Ramaswamy, A. Perrakis, A. Thompson, H. J. Lee, J. E. Baldwin, C. J. Schofield, J. Hajdu, I. Andersson, *Nature*, **394**, 805 (1998).

[172] T. A. Link, in *Adv. Inorg. Chem.*, Academic: New York, Vol. 47, pp 83 (1999).

[173] I. Bertini, M. A. Cermonini, S. Ferretti, I. Lozzi, C. Luchinat, M. S. Viezzoli, *Coord. Chem. Rev.*, **151**, 145 (1996).

[174] D. Ballou, C. Batie, *Prog. Clin. Biol. Res.*, **274**, 211 (1988).

[175] S. E. Crutcher, P. J. Geary, *Biochem. J.*, **177**, 393 (1979).

[176] C. J. Batie, E. LaHaie, D. P. Ballou, *J. Biol. Chem.*, **262**, 1510 (1987).

[177] D. T. Gibson, W.-K. Yeh, T.-N.Liu, V. Subramanian, in *Oxygenases and Oxygen Metabolism*, M. Nozaki, S. Yamamoto, Y. Ishimura, M. J. Coon, L. Ernster, R W. Estabrook, (Eds.), Academic: New York, 51 (1982).

[178] B. D. Ensley, D. T. Gibson, *J. Bacteriol.*, **155**, 505 (1983).

[179] B. M. Bundy, A. L. Campbell, E. L. Neidle, *J. Bacteriol.*, **180**, 4466 (1998).

[180] A. Markus, D. Krekel, F. Lingens, *J. Biol. Chem.*, **261**, 12883 (1986).

[181] B. J. Wallar, J. D. Lipscomb, *Chem. Rev.*, **96**, 2625 (1996).

[182] H. Dalton, *Adv. Appl. Microbiol.*, **26**, 71 (1980).

[183] A. M. Valentine, S. J. Lippard, *J. Chem. Soc., Dalton Trans.*, 3925 (1997).

[184] C. Anthony, *The Biochemistry of Methylotrophs*, Academic: London, (1982).

[185] J. D. Lipscomb, *Annu. Rev. Microbiol.*, **48**, 371 (1994).

[186] J. J. R. Frausto da Silva, R. J. P. Williams, *The Biological Chemistry of the Elements*, Clarendon Press, Oxford, (1991).

[187] Y. Lindqvist, W. J. Huang, G. Schneider, J. Shanklin,*EMBO J.*, **15**, 4081 (1996).

[188] S. Numa, *Fatty Acid Metabolism and Its Regulation*, Elsevier: New York, (1984).

[189] F. D. Gunstone, *Fatty Acid and Lipid Chemistry*, 1st ed., Blackie: London, (1996).

[190] J. Shanklin, E. B. Cahoon, *Annu. Rev. Plant Physiol. Plant Mol. Biol.*, **49**, 611 (1998)

CHAPTER 2

METHODOLOGY

CHAPTER-2

METHODOLOGY

2.1: Quantum Mechanical calculations of atomic orbitals

To study the reaction mechanism qualitatively and quantitatively at electronic level with accuracy, fundamental physics of sub-atomic-particles must be procured that is governed through principles of quantum mechanics. In studying many body electronic systems computational methods that operate on "first principles" are referred as electronic structure methods. By definition, "first principles" methods dose not utilize any adjustable parameters; the simplistic description of the system under investigation will be enough to perform calculations. These methods proved to be highly reliable with great accuracy through experimental values [1]. Most of the electronic structure methods devise time-independent Schrödinger Equation in solving complex problems. Modern day science is indebted to the Schrodinger for this wave equation [2].

$$H\psi = E\psi \tag{2.1}$$

Here, H is the total Hamiltonian of the system and comprises of two terms Kinetic Energy and Potential Energy of the system, E is the energy eigen value when H is operated on ψ (wave function). ψ is a well behaved mathematical functions and inner product with its conjugate i.e. $\psi^*\psi$ represents probability density [3]. This equation in easily solvable for hydrogen and hydrogen like atoms but becomes insolvable for other

atomic numbers. Howsoever this equation is simple or easy to write and capable of fully describing any molecular system but the only problem lies in solving this equation. A very strong and beautiful equation that is capable of completely describing any system just by solving it yet, the basic problem lies with method of solving it. This will be clearer below.

Let us expand the Hamiltonian for the simplest system i.e. hydrogen atom. The potential and kinetic energy for motion of constituent system; electron and nucleus and thus eigen function is the total wavefunction with electronic as well as nuclear wave function. The Hamiltonian is expanded as:

$$H = -\sum_i \frac{\hbar^2}{2m_e}\nabla^2 - \sum_A \frac{\hbar^2}{2m_A}\nabla^2 - \sum_i \sum_A \frac{Z_A e^2}{r_{iA}} + \sum_{i<j} \frac{e^2}{r_{ij}} + \sum_{A<B} \frac{Z_A Z_B e^2}{r_{AB}} \quad (2.2)$$

Where i, j represent summation over electrons while A, B stand for nucleus. First two terms represents kinetic energy of electrons and nucleus, third term represents electron-nucleus potential energy, whereas third and fourth term represents inter-electron and inter-nucleon interaction energy. Born-Oppenheimer's gave an approximation that electrons motion are dependent on the nucleus, so electrons instantaneously change their position with any changes in the nucleus, thus Schrodinger equation became soluble by variable separable method [4, 6].

Changing nuclear positions necessitates addition of nuclear repulsion term to electronic term to the get correct total energy of new configuration. Although variation in nuclear position may be dealt with easily in atoms, scenario complicates in energy levels of even the simplest molecule (eg. diatomic or linear multi-atomic etc.). As discussed earlier that Hamiltonian compromises of a (a) kinetic energy (b) potential energy term which is then sub-divided into (i) nucleus-nucleus interactions (ignored due to Born-Oppenheimer

approximation), (ii) electron-nucleus potential energy and (ii) inter-electron interaction energy; it is this last that creates whole complexity. Hamiltonian with only electronic term comprises of:

$$H_e = -\sum_i \frac{1}{2}\nabla_i^2 - \sum_A \sum_i \frac{Z_A}{r_{iA}} + \sum_{i<j} \frac{1}{r_{ij}} \qquad (2.3)$$

Where first term is kinetic energy, second term is potential energy that arises due to nucleus-electron electrostatic attraction and the third term is electron-electron interaction energy. With this, H_e in hand, one gets E_e, and ψ_e as solution. Modified Schrodinger wave equation for n electron system is written as: [7]

$$H_e(1,2,...,n)\psi_e(1,2,...,n) = E_e\psi_e(1,2,...,n) \qquad (2.4)$$

It should be noted that there is only electronic part and not the nuclear part. The results are used to get total energy and total wavefunction of the system. Although nuclear interactions do not hold importance in atomic systems and but becomes significantly important in the molecular wave function (also generally referred as molecular orbitals). Multi-electron systems can only be solved using approximate methods and numerous methods have been proposed by many workers. Earliest attempt was made by D.R. Hartree in 1928 by considering wavefunction to be product of individual electrons present in the given systems (assuming Z-electron atom): [8]

$$\psi_e(r_1,\theta_1,\phi_1;r_2,\theta_2,\phi_2;...;r_z,\theta_z,\phi_z) = \psi_1(r_1,\theta_1,\phi_1)\psi_2(r_2,\theta_2,\phi_2)...\psi_z(r_z,\theta_z,\phi_z) \quad (2.5)$$

It is well known that Schrodinger equation involves potential energy operator which if known provides wavefunction and eigen value. But this term is not fully known for many electron systems and coordinates of the all the Z-electrons must be carried inside the wavefunction. Variable separable method is the best way that can provide Z-independent

linear differential equations from a single Schrodinger equation for Z-electron system (ignoring electron-electron potential term). The potential energy term can be solved afterwards by using approximate trial solution and later solving for the field that will converge to certain value after finite number of iterations, also commonly known as self consistent field. Alternatively, variational principle may be used to get desired solutions. But soon application of trial wavefunction was discarded because it violated Pauli's exclusion principle. After Fermi-Dirac statistics, [9] electrons were believed to possess spatial as well as spin functions:

$$\Psi_{tot} = \psi(\vec{r}) \times \xi(s) \tag{2.6}$$

Here $\psi(\vec{r})$represents spatial wave function while $\xi(\vec{s})$ stands for spin wave function (commonly represented by α or β) [10]. The electronic wavefunctions need to be anti-symmetric to obey Pauli Exclusion Principle. Slater devised a way with help of determinant to help in obtaining total electron wave functions anti-symmetric) [11] from spatial and spin coordinates. This determinant was known as Slater determinant: [12]

$$\psi = \frac{1}{\sqrt{N!}} \begin{vmatrix} \phi_1(r_1)\alpha(s_1) & \phi_2(r_1)\beta(s_1) & \dots & \dots & \dots & \phi_n(r_1)\beta(s_1) \\ \phi_1(r_2)\alpha(s_2) & \phi_2(r_2)\beta(s_2) & \dots & \dots & \dots & \phi_n(r_2)\beta(s_2) \\ \dots & \dots & \dots & & & \dots \\ \dots & \dots & & \dots & & \dots \\ \dots & \dots & & & \dots & \dots \\ \phi_1(r_n)\alpha(s_n) & \phi_2(r_n)\beta(s_n) & & & & \phi_n(r_n)\beta(s_n) \end{vmatrix} \tag{2.7}$$

Alternatively,

$$\psi = \frac{1}{\sqrt{N!}} \begin{vmatrix} \chi_1(1) & \chi_2(1) & \cdots & \cdots & \cdots & \chi_N(1) \\ \chi_1(2) & \chi_2(2) & \cdots & \cdots & \cdots & \chi_N(2) \\ \cdots & \cdots & \cdots & & & \cdots \\ \cdots & \cdots & & \cdots & & \cdots \\ \cdots & \cdots & & & \cdots & \cdots \\ \chi_1(N) & \chi_2(N) & & & & \chi_N(N) \end{vmatrix} \tag{2.8}$$

Using Slater determinant method Hartree and Fock were able to improvise Self-consistent field theory, whereby each electron was thought to move in the effective fixed field of the rest of the electrons and nucleus.

This method proved to be a great success as the electron-electron interaction term posed a severe hindrance in variable separation method. The energy of the atom or molecule is given by:

$$E = \frac{\int \psi^* H \psi d\tau}{\int \psi^* \psi d\tau} \tag{2.9}$$

or, in Dirac Notation,[13-15]

$$E = \frac{\langle \psi \mid H \mid \psi \rangle}{\langle \psi \mid \psi \rangle} \tag{2.10}$$

Besides being anti-symmetric, the wave functions need to be orthonormal. Below is the condition of ortho-normality of the wavefunctions.

$$\int \psi_m^* \psi_n d\tau = \delta_{mn} \qquad \text{OR} \qquad \langle \psi_m \mid \psi_n \rangle = \delta_{mn} \tag{2.11}$$

2.2: Hartree Self-Consistence Field

As discussed above and stated by Born-Oppenheimer approximation, nucleus is ~1840 times heavier than the electrons so instantaneous position of electrons is due to nuclear motion itself, hence one can assert that nuclear contribution to the Hamiltonian are not of

much worth. Though in molecules, nuclear configuration within atoms adds to nuclear potential. But, Born-Oppenheimer approximation resolved the problem by considering the potential due to nucleus in given geometry as constant. This value of the field must be added in the Hamiltonian for obtaining total wave function and energy of the molecule [16, 17].

N-electronic system Hamiltonian can be re-written as:

$$H_e = \sum_i h_i + \sum_i \sum_{j>i} g_{ij} + V_{nn} \tag{2.12}$$

Here,

$$h_i = -\frac{1}{2}\nabla^2 - \sum_A \frac{Z_A}{|R_A - r_i|} \tag{2.13}$$

and

$$g_{ij} = \frac{1}{|r_i - r_j|} \tag{2.14}$$

Where, h_i is the operator which represents the i^{th} electron motion under the field of all the nuclei of the given molecule; also it must be the only operator in absence of any internuclear and interelectronic interactions, g_{ij} operator represents the mutual repulsion between two electrons and V_{nn} is the interaction energy between two nucleus. According to the Dirac notation of energy,

$$E = \sum_i \langle \chi_i \mid h_i \mid \chi_i \rangle + \frac{1}{2} \sum_{i,j} \left(\langle \chi_i \chi_j \mid g_{ij} \mid \chi_i \chi_j \rangle - \langle \chi_i \chi_j \mid g_{ij} \mid \chi_j \chi_i \rangle \right) + V_{nn} \tag{2.15}$$

Or, it could be written as

$$E = \sum_i \langle \chi_i \mid h_i \mid \chi_i \rangle + \sum_{i<j} \left(J_{ij} - K_{ij} \right) + V_{nn} \tag{2.16}$$

Above equation first term is indicative of core Hamiltonian operator energy in the absence of any interaction, second term J_{ij} is Coulomb operator and the last term represents exchange operator [18]. Hydrogen atom is a two body problem and there exists exact solution to it unlike this many-body problem which does not have 'exact' solution. There is only a possibility of one solution being 'better' than the other. Variational principle is used to find stable configuration of Molecular Orbital (MO). Hence, out of two wave functions the 'better' one will be with minimum energy or less energy than the 'less' correct one. The basic criteria behind such optimization are that the MOs should remain normalized and orthogonal. To achieve this Lagranges's method of undetermined multiplier is used [16, 19].

$$S_{ij} = \int \chi_i \chi_j d\tau = \langle \chi_i \mid \chi_j \rangle = \delta_{ij} \tag{2.17}$$

With respect to variations in orbitals Lagrange function remains stationary:

$$L = E - \sum_{i,j} \lambda_{ij} \left(\langle \chi_i \mid \chi_j \rangle - \delta_{ij} \right) \tag{2.18}$$

Extremum equation of Lagrange function is:

$$\delta L = \delta E - \delta \sum_{i,j} \lambda_{ij} \left(\langle \chi_i \mid \chi_j \rangle - \delta_{ij} \right) = 0 \tag{2.19}$$

Where, λ_{ij} is the energy and is related to the molecular orbital energies. This formalism forces to consider simultaneous motion of all the electrons. These electron motion are interconnected with each other and coordinate change (spatial or spin) of one causes affect on remaining electrons. Such difficulty can be avoided by considering the motion of single electron under influence of field of nuclei and remaining electron in their fixed orbitals χ_j. The resulting equation then becomes: [16, 20]

$$F_i \chi_i = \sum_j \varepsilon_{ij} \chi_j \tag{2.20}$$

where F_i is called Fock operator :

$$F_i(1) = h_i(1) + \sum_j \left(J_j(1) - K_j(1) \right) \tag{2.21}$$

Here, 1 within parenthesis indicates operator of one particular electron, J represents electron repulsion (Coulomb operator) and K is the spin correlation term (exchange operator). Choosing Lagrangian multipliers zero exempting *i=j* we get standard Hartree Fock equation:

$$F_i \chi_i = \varepsilon_i \chi_i \tag{2.22}$$

solutions to the above equations are not unique as determinant remains unaffected by row/column transformations. As Fock operator is evaluable only if orbitals of remaining electrons are known. To contract this vicioius cycle, iterative method is employed which assumes trial solutions to get Fock operator (via Coulomb and Exchange operators) till solutions are 'self-consistent'. The Hartree Fock method is also known as mean field approximation method in which average electron-electron repulsion is taken into account [21].

2.3: Roothaan Hall Equation

Extension of Hartree SCF procedure was given by Fock by utilizing Slaters Determinant for wave function generation (which obeys Pauli's exclusion principle). Although obtaining solution from Hartree Fock equation was impractical for molecules. Approximations were incorporated by Roothan and Hall independently in HF equation. For this, MOs are expressed in form of basis functions which are basically called atomic

orbitals. These are at par with other method in easy interpretation of results, as chemical problems usually deal with molecules and its constituent atoms. Linear combination of basis function can be written as:

$$\phi_i = \sum c_{\mu i}\theta_\mu \tag{2.23}$$

Coefficient $c_{\mu i}$ are calculated with the concept of energy minimization. Set of self-consistent LCAO MOs ϕ_i are generated after this. These orbitals will be well suited for any set of particular basis function. We get Roothan-Hall equation by applying variational technique [22]:

$$\sum_\nu \left(F_{\nu\mu} - \varepsilon_i S_{\nu\mu}\right)C_{\nu i} = 0 \tag{2.24}$$

where $F_{\nu\mu}$ is the Fock operator and $S_{\nu\mu}$ is the overlap integral:

$$F_{\nu\mu} = \left\langle \theta_\nu \mid h \mid \theta_\mu \right\rangle + \sum_\gamma^{AO}\sum_\delta^{AO} D_{\gamma\delta}\left(\left\langle \theta_\nu\theta_\gamma \mid g \mid \theta_\mu\theta_\delta \right\rangle - \left\langle \theta_\nu\theta_\gamma \mid g \mid \theta_\delta\theta_\mu \right\rangle\right) \tag{2.25}$$

$$S_{\nu\mu} = \left\langle \theta_\nu \mid \theta_\mu \right\rangle \tag{2.26}$$

The density matrix is defined as

$$D_{\gamma\delta} = \sum_j^{occ.MO} C_{\gamma j}C_{\delta j} \tag{2.27}$$

Above equations are developed by Roothan [22] and Hall [23] independently. These equations are algebraic equations conveniently written in form of matrix equation:

$$FC = SCE \tag{2.28}$$

The elements of the Fock matrix are dependent upon coefficients $c_{\mu i}$, which appears on both sides of the equation and hence iterative procedure is adopted to solve them.

2.4: Computational scheme for solving Roothaan Hall equation

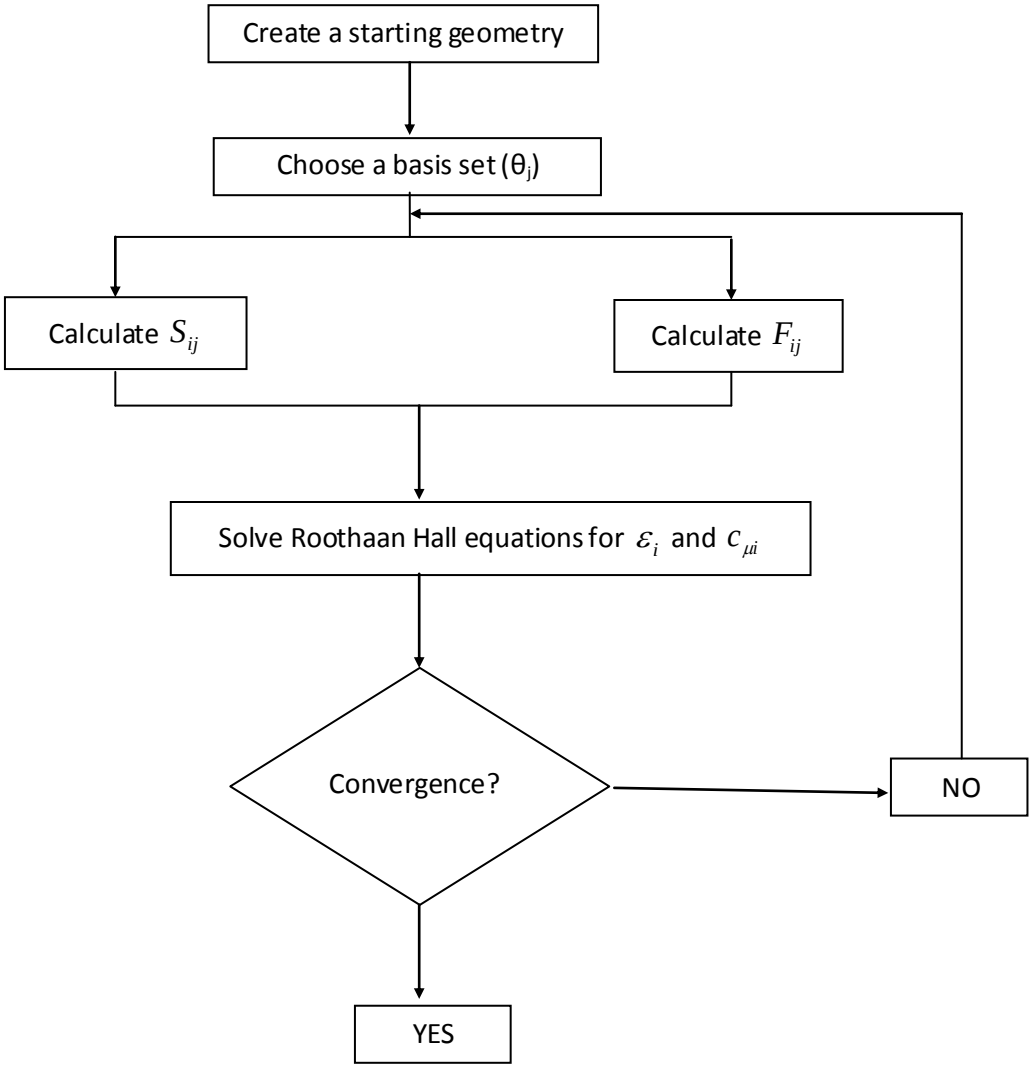

Figure 2.1: Algorithm for solving Roothaan Hall equation.

Hartree-Fock method is being utilized for solving Schrodinger equation by making an equation to solve all the individual one-electron wave functions:

$$F_i(1)\phi_i(1) = \varepsilon_i\phi_i(1) \qquad (2.31)$$

Here 1 inside parenthesis is indicative of one-electron equation. Choosing a certain basis set, trail wave functions are formulated which eventually generates overlap matrix S_{ji} and

Fock matrix F_{ij}. These matrix or integrals are then utilized for solving energy and coefficients c_{vi} of the given system. Iterative method is adopted till desired convergence is achieved. Since the effect of the correlated motion of electron is included in HF equations [24], it does not provide good accuracy. Few of the methods which includes electron correlations are Moller-Plesset [25] and Configuartion-interaction (CI) [26, 27].

2.5: Basis set

A basis set is a mathematical set of functions that are used to define or build atomic orbitals (molecular orbitals) of a molecule. An infinite number of basis set would be required to completely represent a basis set. This is not possible to compute due to truncation error. Hence there was a need to develop lesser basis functions set that would lower down the computational cost by choosing simpler integrals, also minimizing the error at the same time. Most obvious choice was using atomic orbitals as basis functions. For diatomic molecules, some atomic orbitals were centered on one atom and others on the second atom. This approach is known as Linear Combination of Atomic Orbitals (LCAO) [28]. Here, each atomic orbital is a combination of one or more Slater-type Orbitals (STOs) [29, 30]. The combination of such set generates molecular wave functions. Also set of virtual orbital is also defined other than filled orbitals:

$$\phi_i = \sum_r c_{ri} \chi_r \qquad (2.32)$$

Clearly, the number of active and virtual orbitals taken decides the quality of molecular orbitals thus obtained. This choice is crucial so that calculated energy gets converged within the basis set limit.

There are mainly two types of basis sets Slater type and Gaussian type. The STOs mathematical form for an s-type orbital has form:

$$S(r) = N_s e^{-\zeta r} \tag{2.33}$$

N_S is the normalization constant, r is the radial distance from the nucleus, and ζ is orbital exponent constant and it governs the width of the atomic orbital, whereas the GTO's [16, 31] form for the s-type orbital is:

$$g(r) = N_g e^{-\zeta r^2} \tag{2.34}$$

In order to generate higher order basis functions like p-type, d-type or higher functions, the STO or GTO are multiplied by an appropriate exponents of coordinates. GTO basis function in Cartesian system has following general form:

$$g(r) = N_g x^a y^b z^c e^{-\zeta r^2} \tag{2.35}$$

where, a, b and c constant values are chosen according to the type of the orbital. In SCF convergence the given molecular structure, its atomic orbitals combine or mix to generate molecular orbitals. The STO basis set has a direct physical interpretation and regarded as good basis set for molecular orbitals. But they are not preferred for molecular orbitals, as SCF calculations involve solving some required integrals which are computationally expensive. These required integrals are quite easy to solve in GTO basis set, although it underestimates the values near or far away from the nucleus. This problem can be solved by using linear combination of Gaussian functions. Gaussian function comprises of two components: coefficient and exponent. Calculations in which both the parameters are allowed to vary, such calculations are called as uncontracted or primitive Gaussians. If these terms are already defined and remain constant and numbers of terms in the expansion are contracted, this is called contracted Gaussian function.

A minimal basis set is a one of the type of the basis set where just the minimum or required number of functions are used to accommodate all filled orbitals in the shell [32]. Hence it uses only one basis function for each atomic orbital. Also, as stated above, Gaussian functions are not reliable for results, so to mimic STOs a combination of few GTOs is used. Three Gaussian functions are required to generate one STO closely. STO-3G is a most common minimal basis set. This notion simply means single contraction of three Gaussian type orbitals will generate approximate shape of STO type basis set. STO-nG is a general representation of basis set which simply means n Gaussian functions are clubbed to represent each orbital (in general n=2-6). Minimal basis set are however not helpful for compounds at the end of the period in the periodic table and also are not effective for non-spherical electronic distributions. If more than one basis function is chosen for atomic orbitals, then this problem can be solved. This increase in the number of basis functions is eventually helpful in getting energy closer to the actual energy value. Hence, it thus led to construct such basis set that contains more than one basis functions for each atomic orbitals. There are various types of such basis sets that are nowadays available in various computational chemistry softwares. Double zeta (DZ) basis set uses two basis functions for each type of minimal basis functions for two atoms with a variation of orbital exponent ζ. Double Zeta type basis set are usually sufficient in geometry optimization [33]. The various hybrid density functional used in present work are previously benchmarked by various scientific groups for such systems. The calculations for coefficient of hybrid density functional are benchmarked by experimental values using calculations that utilize double-ζ basis functions. Split valence double-ζ basis set is a slight variation above discussed method and is useful in non-isotropic

calculations. This method utilizes double basis functions for valence electrons and single basis functions for core electrons. Other basis set of such type are triple-ζ, quadrupole-ζ etc. which necessarily may not hold great variations in results.

Charge around atom of a molecule is slightly perturbed than isolated atom itself. To account the perturbation of electronic charges in a molecule polarization functions are used in basis sets. They use higher angular momentum orbitals and are indicated by the sign '*'. They enhance the wave function flexibility to change shape. Those molecular systems which have an electronic density situated far away from the nucleus like (anions, lone pairs, highly electronegative atoms etc.) diffuse basis functions are used in the basis set and these are represented by symbol '+' in the basis set representation. They basically involve small orbital exponent that results in larger spread of Gaussian functions. The effect of addition of diffuse functions to the basis set results in the change of relative energies of these molecular systems. These basis functions are also called as augmented basis sets. [34, 35]

Like minimal basis set, another basis set is Pople basis set [34, 36], denoted by 6-31G and usually popular for organic molecules. It indicates that each core orbital is described by a single contraction of six GTO primitives which describe each core orbital and two contractions, of which one with three primitives and another with one primitive describe each valence shell orbital. It is modified by the addition of single asterisk and double asterisks sign. Single asterisk (*) means addition of d primitives to the atoms excluding hydrogen whereas two asterisks (**) means addition of p primitives to atoms including hydrogen. Pople basis set can also be modified with the addition of plus '+' and double '++' sings. The single (+) simply means addition of diffused functions to all atoms other

than hydrogen and double (++) indicates addition of diffuse functions to all atoms including hydrogen.

There are various special basis sets that are used in computational chemistry calculations for transition metals. They utilizes effective core potential (ECP) [37] for all the electrons. As core electrons do not take part in a chemical reaction the orbitals are replaced by the electric potential in Hamiltonian in the ECP treatment. Also relativistic effect can be incorporated to improve energies. For iron, typical ECP containing basis sets are from Los Alamos type, eg., LACVP or LANL2DZ [38]. In our work, triple-ζ basis set (LACV3P+) has also been used that employs diffuse and polarization functions on metal. Kumar *el al* [39] have used two different basis sets, namely BS1 (LACVP on iron and 6-31G on the rest of the atoms) and BS2 (LACV3P+ on iron and 6-311+G* on the rest of the atoms) in a test calculation on substrate hydroxylation potential energy profile by a Cpd I model of cytochrome P450. This resulted in very little changes in optimized geometries and virtually identical relative energies along a reaction profile. As such, geometries are usually optimized using double-ζ basis set followed by calculation by single point energy calculation with a triple-ζ basis set. A subsequent analytic frequency calculation characterized the structures as local minima (with real frequencies) and transition state presence was marked with large single imaginary frequency for the correct mode.

2.6: Density Functional Theory

The ab initio methods using HF approximations are excellent technique in molecular orbital calculations but rather computationally expensive due to involvement of larger basis sets. Kohn et al argued in obtaining eigen value and eigen functions from this

quantum mechanical methods. They hypothesized obtaining such results by using functional of electron density [40]. A functional enables a function to be mapped to number:

$$Q[f(r)] = \int f(r)dr \tag{2.36}$$

Key essence is that energy of the given electronic system can also be written in terms of electron probability density. All the other properties of the given system such as ground-state molecular energy, wave function and all other molecular electronic properties can be determined by the ground electron probability density. This method became extremely popular due to inexpensive computation and good accuracy of results with experimental values for relatively larger systems [41]. It is popular because it acts as an alternative to HF methods, takes care of electron correlation as well. Approximate model by Thomas and Fermi contributed in the major development in DFT when one-electron equations were derived from which electron density can be obtained. In these calculations, total energy is split into four terms (i) kinetic energy, (ii) electron-nucleus interaction energy, (iii) electron-electron Coulombic term and, (iv) exchange correlation term (E_{XC}) [41, 42]. The first three terms resemble terms in Hartree-Fock Hamiltonian:

$$H_e = -\sum_i \frac{1}{2}\nabla_i^2 - \sum_A \sum_i \frac{Z_A}{|R_A - r_i|} + \sum_{i<j} \frac{1}{|r_i - r_j|} + E_{XC} \tag{2.37}$$

$$E_{el} = \sum_{i=1}^{N} \int \psi_i(r)\left(-\frac{\nabla^2}{2}\right)\psi_i(r)dr - \sum_{A=1}^{M} \int \frac{Z_A}{|R_A - r|}\rho(r)dr + \frac{1}{2}\iint \frac{\rho(r_1)\rho(r_2)}{|r_1 - r_2|}dr_1 dr_2 + E_{XC}(\rho(r)) \tag{2.38}$$

Hohenberg and Kohn showed that when density is extremely slow varying with position $E_{XC}[\rho]$ is accurately given as:

$$E_{XC}^{LDA}[\rho] = \int_V \rho(r)\varepsilon_{XC}(\rho)d\tau \tag{2.39}$$

Here, LDA refers to Local-Density Approximation, $\varepsilon_{XC}(\rho)$ is the exchange plus correlation energy per electron in a homogeneous electron gas with electron density ρ. According to Kohn and Sham approximation density of the system is the sum of the square moduli of a set of one-electron orthonormal orbitals:

$$\rho(r) = \sum_i |\psi_i(r)|^2 \tag{2.40}$$

One-electron equation after using such electron density and application of variational field on them transforms as:

$$\left\{-\frac{1}{2}\nabla^2 - \left(\sum_{A=1}^{M}\frac{Z_A}{r_{1A}}\right) + \int \frac{\rho(r_2)}{r_{12}}dr_2 + V_{XC}[r_1]\right\}\psi_i(r_1) = \varepsilon_i\psi_i(r_1) \tag{2.41}$$

Where,

$$V_{XC}[r] = \left(\frac{\delta E_{XC}[\rho(r)]}{\delta\rho(r)}\right) \tag{2.42}$$

Self-consistent approach can be further adopted in the above discussed equation whereby trial electron density can be chosen to get set of orbitals. Furthermore, convergence of the electron density is tested and then total energy is evaluated.

Apriori electron-correlation term is not known, so approximate equations are set-up for the estimation of its contribution. It is divided into an exchange functional (E_X) and a correlation functional (E_C). Ex represents interactions of same spin electrons in different orbitals, whereas E_C denotes pairing energy of electrons in the same orbitals [43, 44].

These exchange energy is estimated from the Slater exchange function:

$$E_X^{Slater} = -\frac{9}{4\alpha_{ex}}\left(\frac{3}{4\pi}\right)^{1/3}\sum_{\gamma}\int\left[\rho_1^{\gamma}(r_1)\right]^{4/3}dr_1 \qquad (2.43)$$

Here, α_{ex} is an exchange scale factor, which has the value 2/3 for electron gas.

E_C^{VWN} is a commonly used correlation energy functional, attributed to works by Vosko, Wilk and Nusair. For a gas with spin densities and, it represents correlation energy per electron $\varepsilon_c\left[\rho_1^{\alpha},\rho_1^{\beta}\right]$:

$$E_C^{VWN} = \int \rho_1(r_1)\varepsilon_c\left[\rho_1^{\alpha}(r_1),\rho_1^{\beta}(r_1)\right]dr_1 \qquad (2.44)$$

Slater exchange and Vosko-Wilk-Nusair correlation combine to give Local Density Approximation. Both are derived directly from homogeneous electron gas equations. For correction of non-local terms, better exchange and correlation functions were required. Some the popular functions amongst others are Lee, Yang and Parr (LYP correlation functional), [44] Perdew and Wang (PW91 correlation functional) [45] and Becke (B96 correlational functional) each having their own merits and/or demerits.

Later Becke developed the hybrid density functional procedures [46]. This proved to a breakthrough in the field of the DFT development as he was able to benchmark DFT methods with the experimental known values of ionization energies, electron affinities and proton affinities with high accuracy.

Exchange and correlation functions contributions were estimated using a three parameter (hybrid) density functional method. These fit parameters (A, B and C) were optimized in the test set with experimental. After trying different combination of exchange and correlation functionals, B3LYP method has emerged as most popular one throughout the

years, although it does not mean that it is most accurate amongst all. Essentially the hybrid density functional method B3LYP has the following form:

$$E_{XC}^{B3LYP} = AE_X^{Slater} + (1-A)E_X^{HF} + B\Delta E_X^{Becke} + E_C^{VWN} + C\Delta E_C^{LYP} \qquad (2.45)$$

Thus, it is hybrid in sense that it takes the LDA functions of Slater and Vosko-Wilk-Nusair, the Hartree-Fock exchange, a correction term to the exchange due to Becke and Lee-Yang-Parr correction for non-local correlation factors. The coefficients A, B and C are essentially fit-parameters obtained through fitting the energies of B3LYP/6-31G* calculations in opposition to experimentally obtained electron affinities and ionization energies. Hence, B3LYP method is not truly an ab initio method. Precisely, the term "ab initio" means starting from scratch without prior knowledge of experiment. However, these fit-parameters have created an accurate and low-cost computational method and as a result B3LYP has emerged as one of the widest used techniques in science over the past decade. The hybrid as well as non-hybrid DFT methods have emerged extremely accurate and versatile in computational techniques. Although high level ab initio methods such as coupled cluster method (CC, CCD, CCSD), Moller Plesset perturbation theory (MBPT, MP, MP2) etc. promise good results than DFT calculations, their speed in combination with reasonable accuracy makes them a very popular and useful methodology.

This technique has developed over years that fitting parameters have improved considerably by enlarging the test set. In his original paper, Becke already published calculated energies within 2 kcal/mol compared to experimental values. Pople et al have defined ultimate accuracy goal of computational chemistry to 1 kcal/mol [7]. Hence DFT has become one of the most extensively used methods in Chemistry which combines reasonable accuracy with speed. In fact, B3LYP methodology presents a considerable

improvement over HF as well as MP2 calculations [47]. In some cases DFT is capable of reproducing results obtained with much more computationally demanding G2 methodology of Pople et al. Clearly DFT provides a low-cost alternative to quantum mechanical procedures and is highly suitable candidate for performing calculations on biochemical systems [48].

2.7: Geometry Optimizations using DFT

Two dimensional potential energy surface (PES) has been shown in Figure 2.2. The arrows in the figure bring together reactant and the product geometry through the reaction coordinate. Reactants, intermediates and products are local minima structures whereas the points that connect them are transition state, or first order saddle point, which is the lowest possible path that connects these minima structures. In reaction mechanism studies based on the DFT modeling, particularly in catalysis that is based upon transition state theory, the key objective is characterization and prediction of all these structures. This is usually attained through geometry optimization algorithms which are inbuilt in software employed (Gaussian, jaguar etc). Various algorithms for finding these structures have been developed. They can be broadly classified into two categories i.e. first-order methods or second-order methods. The first-order involves only an analytical first-order derivative and the second-order method employ Hessian matrix and first-order derivatives to build a quadratic model for optimization [49].

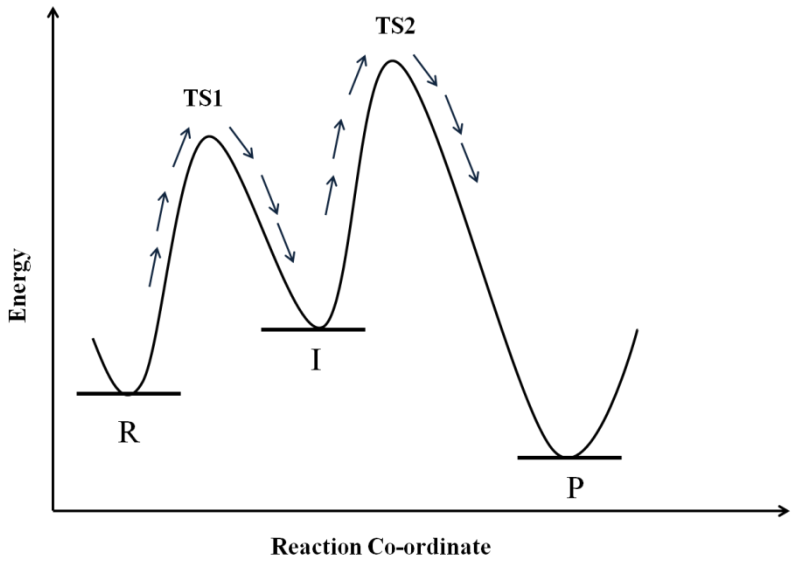

Figure 2.2: Potential energy surface representation of the reaction landscape.

2.8: Solvent effects

The quantum mechanical calculations generally refer to isolated molecule or for gas-phase. However reactions in a laboratory are performed in solutions. There are possibilities of induced polarization in solvent molecules by the solute (molecule under study) which are in its vicinity. This could generate an electric field which can distort the solute's molecular electronic wave. Thus molecular properties in solution will tend to differ to some extent from those in gas-phase.

Solvent effect can be counted by doing rigorous calculations on the molecular properties of the system, this system comprises of solute molecule surrounded by solvent molecules completely and then re-optimization of resulting structure [50]. To mimic the effect of solvent many methods were proposed like Continuum solvent model, Quantum-Onsager self consistent reaction field method, multiple expansion method etc. but they were time consuming and computationally extensive. Hence instead of adding solvent molecule directly, it is deemed better to add solvent corrections to energetics using implicit solvent

model. This can be done at single point level (energy is recalculated with a solvent model on gas-phase optimized geometry) or by re-optimizing structure using a solvent model. Software packages like Gaussian and Jaguar include solvent models like Polarizable Continuum Model (PCM), Conducting Polarizable Continuum Model (CPCM) [51] wherein calculations are done by assuming solvent as a perturbation of the molecule with a dielectric constant. The molecular structure of the solvent is ignored and the solvent is modeled as a continuous dielectric of infinite extent that surrounds a cavity containing the solute molecule. The molecule is assumed to be placed in a cavity surrounded by dielectric continuum. The cavity is described as the area around the molecule that contains less than pre-defined amount of electron density of the molecule and is often based on Van der Waals radii of atoms. The classical Poisson equations are then used to calculate the electronic potential arising from the molecule-solvent interactions using a defined dielectric constant.

References:

[1] J. E. Klepeisa, J. Mater. Res., **21,**12, (2006)

.[2] E. Schroedinger, *Ann. Physik*, **79**, 361 (1926).

[3] L. Pauling, E. B. Wilson, *Introduction to Quantum Mechanics*, McGraw-Hill, New York (1935).

[4] M. Born, J. R. Oppenheimer, *Ann. Physik.*, **84**, 457 (1927).

[5] W. Kolos, L.Wolniewicz, *J. Chem. Phys.*, **41**, 3663 (1964).

[6] B. T. Sutsliffe, *Adv. Quantum. Chem.*, **28**, 65 (1997).

[7] J. A. Pople, D. L. Beveridge, *Approximate Molecular Orbital Theory*, McGraw-Hill Book Co., New York (1970).

[8] D. R. Hartree, *Proc. Cambridge Phil. Soc.*, **24:89**, 111, 426 (1928).

[9] G. Uhlenbeck, S. Goudsmit, *Nature wissenschaften*, **13**, 953 (1925).

[10] J. A. Pople, D. L. Beveridge, P. A. Dobosh, *J. Chem. Phys.*, **47**, 2026 (1967).

[11] W. Pauli, *Z. Physik.*, **31**, 765 (1925).

[12] J. C. Slater, *Phys. Rev.*, **35**, 509 (1930) and **34**, 1239 (1959).

[13] P. A. M. Dirac, *The Principle of Quantum Mechanics*, Oxford University Press, London (1958).

[14] J. K. L. McDonald, *Phys. Rev.*, **43**, 830 (1933).

[15] R. H. Young, *Int. J. Quant. Chem.*, **6**, 596 (1972).

[16] F. Jenson, *Introduction to Computational Chemistry*, 2nd edition, John Wiley & Sons Ltd., Chichester (2007).

[17] I. N. Levine, *Quantum Chemistry*; Chapter-11, "*The Hartree Fock Self-Consistent Method*", Pearson, Fifth edition (2000).

[18] I. N. Levine, *Quantum Chemistry.*, Chapter-8, "Perturbation Theory", Pearson, Fifth edition (2000).

[19] J. A. Pople, D. L Beveridge, *Z. Physik*., **61**, 126 (1930).

[20] J. E. Lennard-Jones, *Proc. Roy. Soc. (London),* **A198,** 14 (1949).

[21] C. Edimiston, K. Ruedenberg, *Rev. Mol. Phys.,* **34**, 457 (1963); J. *Chem. Phys.,* **43**, 597 (1965).

[22] C. C. Roothan, *J. Rev. Mod. Phys.,* **23**, 69 (1951).

[23] G. G. Hall, *Proc. Roy. Soc., (London),* **205,** 541 (1951).

[24] W .J. Hehre, L. Radom, J. A. Pople, P.v.R. Schleyer, *Ab Initio Molecular Orbital Theory.*, Wiley (1986).

[25] B. O. Roos, (eds.) *Lecture Notes in Quantum Chemistry,* Springer -Verleg (1992)

[26] J. Olsen, O. Christiansen, H. Koch, P. Jorgensen, *J. Chem. Phys. Lett.*, **261**, 369 (1996).

[27] C. Moller, M. S. Plesset, *Phys. Rev*., **46**, 618 (1934).

[28] E. Hückel, *Z. Physik*., **70**, 204 (1931).

[29] D. Feller, E. R. Davidson, *Rev. Comp. Chem.*, 1 (1990).

[30] T. Helgaker, P. R. Taylor, "*Modern Electronic Structure Theory*", Part II (D. Yarkony ed.), World Scientific, 727 (1995).

[31] S. F. Boys, *Proc. Roy. Soc.*, (London), **A 200**, 542 (1950).

[32] W. J. Hehre, R. F. Stewart, J. A. Pople, *J. Chem. Phys.*, **51**, 2657 (1969).

[33] J. S. Binkley, J. A. Pople, *J. Am. Chem. Soc.*, **102**, 939 (1980).

[34] M. J. Frisch, J. A. Pople, Binkley, *J. Chem. Phys.*, **80**, 3265 (1984).

[35] W. J. Hehre, R. Ditchfield, J. A. Pople, *J. Chem. Phys.*, **56**, 2257 (1972).

[36] T. H. Dunning Jr. and P. J. Hay, *Modern Theoretical Chemistry*, Ed. H. F. Schaefer III, Vol. 3, pp. 1, Plenum, New York (1977).

[37] H. Hellmann, *J. Chem. Phys.*, **3**, 61 (1935).

[38] P. J. Hay, W. R. Wadt, *J. Chem. Phys.*, **82**, 270 (1985).

[39] D. Kumar, B. Karamzadeh, G. N. Sastry and S. P. de Visser, *J. Am. Chem. Soc.*, **132**, 7656 (2010).

[40] T. Ziegler, *Chem. Rev.*, **91**, 651 (1991).

[41] W. Khon, L. Sham, *J. Phys. Rev.*, **140**, 1133 (1965).

[42] P. Hohenberg, W. Khon, *Phys. Rev.*, **136**, 864 (1964).

[43] S. H. Vosko, L. Wilk, M. Nusair, *Can. J. Phys.*, **58**, 1200 (1980).

[44] C. Lee, W. Yang, R. G. Parr, *Phys. Rev.*, **B37**, 785 (1988).

[45] J. P. Perdew, Y. Wang, *Phys. Rev.*, **B45**, 13244 (1992).

[46] A. D. Becke, *J. Chem. Phys.*, **98**, 5648 (1993).

[47] R. G. Parr, W. Yang, *Density Functional Theory*, Oxford University Press (1989).

[48] P. E. M. Siegbahn, *Quaet. Rev. Biophys.*, **36**, 91 (2003).

[49] X. Li, *J. Chem. Theory. Comput.*, **2**, 835 (2006).

[50] J. H. Jensen, *Molecular Modeling Basics*, CRC Press, Boca Raton (2010).

[51] J. Tomasi, B. Mennucci and R. Cammi, *Chem. Rev.*, **105**, 2999 (2005).

CHAPTER 3

MODELING THE HYDROXYLATION OF ESTRAGOLE VIA HUMAN LIVER CYTOCHROME P450

CHAPTER-3

MODELING THE HYDROXYLATION OF ESTRAGOLE VIA HUMAN LIVER CYTOCHROME P450

3.1: Introduction

Estragole (1-allyl-4-methoxybenzene) is a common component of spice plants like star anise, fennel and basil oil. Additionally estragole is used in flavorings, as essential oils that are added in many food, detergents and cosmetic products. It is regarded as a genotoxic hepatocarcinogen in rats and its potential toxicity in humans is still under prime debate. *Foeniculum vulgare* Mill (fennel) is a major source responsible for the human exposure to this phytochemical [1]. Its toxicity gets activated with the hydroxylation at benzylic position (C1') position [2] by P450s present in human liver 1A2, 2A6, 2C9, 2D6 and 2E1. The major P450s that are involved in catalysis of estragole are 1A2 and 2A6. Other enzymes play their role in catalysis of estragole at relatively higher concentration. The metabolite obtained upon hydroxylation at C1 position is not toxic in itself, however its conjugation with sulphate by a sulfotransferase to produce 3´-sulfoxyestragole is genotoxic [2]. Figure 3.1 shown below marks the general reaction scheme that was studied computationally.

Cytochrome P450s are versatile biological catalyst found in nature in all living forms such as bacteria, mammals, fungi and plants [3, 4]. P450s are key players responsible for metabolic conversion of chemical compounds to reactive metabolites which later binds macromolecules.

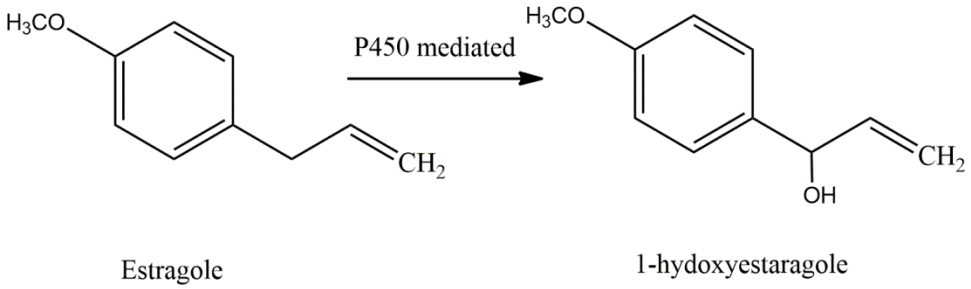

Figure 3.1: Activation reaction of estragole to produce 1-hydroxyestragole by Cpd I of P450 enzymes, a precursor for the formation of genotoxic 3' – sulfoxyestragole.

It activate and oxidize fairly large variety of substrates [5, 6]. Due to their broad chemical functions they are well studied with potential application in field of biotechnology and medicine. P450s are monooxygenases class of heme enzymes. Their common reaction mechanism with substrates occurs through single oxygen atom transfer [7-9]. Initially, in the resting state, the heme iron (III) is hexacoordinated. At distal side it is connected to water molecule and is axially ligated to the thiolate of cysteinate residue which eventually connects it to rest of the protein. The catalytic cycle of P450 gets initiated with the entry of substrate inside the binding pocket. As the substrate approaches the heme, it transpires the release of water molecule ligated to iron and changes the spin-state, which triggers electron transfer from the reduction partner of P450. Later, the molecular oxygen binds itself to the iron and gets reduced and protonated to form ferric- hydroperoxo species also known as compound 0 (Cpd 0). Subsequent protonation leads to the formation of ultimate oxidant iron (IV) oxo porphyrin cation radical species compound I (Cpd I). The structure of CpdI is depicted in Scheme 3.2 (a), along with short

representation used to show porphyrin ring. CpdI reacts with the substrate to form oxidized product through various reactions like desaturation/ring closure and oxygen atom transfer reactions like aliphatic and aromatic hydroxylation, sulphoxidation, epoxidation etc.

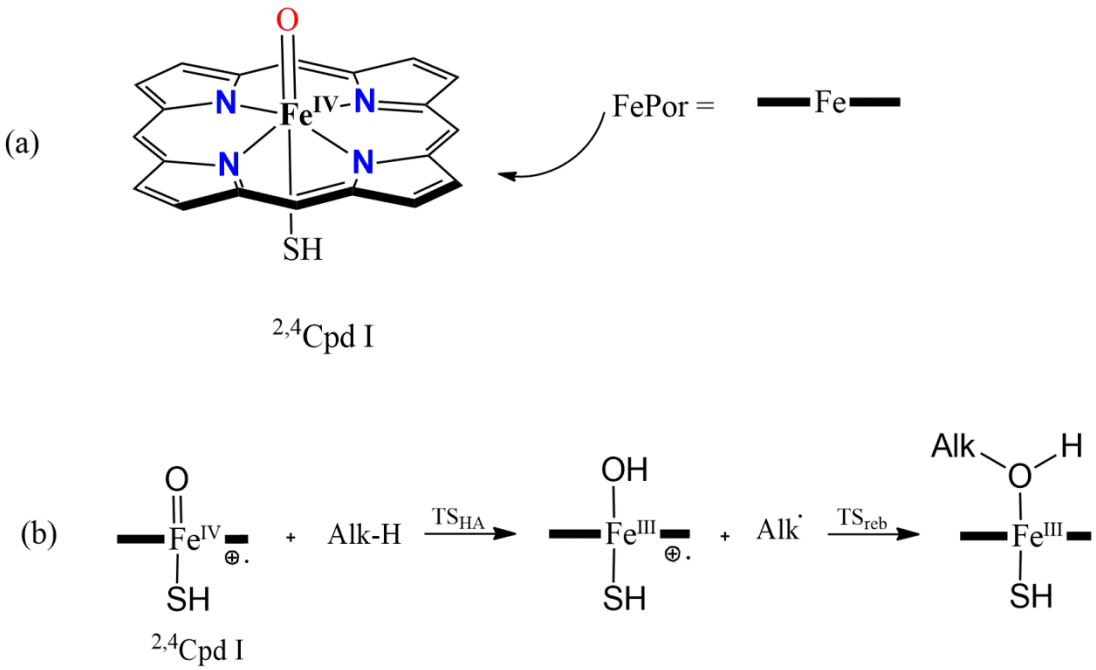

Scheme 3.2: (a) Schematic Structure of Compound 1 (Cpd I) along with porphyrin ring representation in right (b) Schematic Two-state rebound mechanism used by P450 for aliphatic hydroxylation.

It is well studied through many experimental and theoretical [10-13] studies that alkane (C-H) hydroxylation is stepwise and proceeds through rebound mechanism [14], this is shown in Scheme 3.2 (b). The first step is associated with the removal of hydrogen atom from the carbon to be hydroxylated to form ferric hydroperoxo intermediate via transition state (TS_{HA}), while the later step involves the rebound of radical carbon to produce hydroxylated product complex via rebound transition state (TS_{reb}).

Quantum mechanical calculations (QM) are valuable methods that provide us a tool to deeply penetrate and understand the formation of toxic metabolites from drugs and chemical compounds followed by analysis of their reaction energy profiles. In the present work, density functional theory (DFT) based QM calculations were employed to explore the cytochrome P450 catalyzed reaction mechanism for aliphatic hydroxylation of estragole at benzylic carbon C1 position to explore the overall reaction energy profile and to understand the formation of involved intermediates and transition states. The mechanism was modeled on two spin surfaces for Cpd I-estragole complex viz., quartet (high spin (HS)) and doublet (low spin (LS)). Furthermore, this study was helpful in gaining substantial insights into the electronic arrangement and 3D structural features of intermediates, transition states and product complexes formed during the progress of the reaction along with their free energies.

3.2 Methodology

The calculations provided in the present study were computed using Gaussian 09 [15] software and implemented DFT method. To support our results from previous studies [11, 16-18], B3LYP hybrid density functional method has been chosen, using LACVP (Los Almos) type basis set on iron that uses double ζ- core potential along with 6-31 G basis set on the rest of the atoms (Basis set BS1) [19]. Optimization of geometry and scans were performed at B3LYP/BS1 level of the theory. Geometry scan maxima is used for the transition state searches along with frequency calculations that confirm structures to be first order saddle point depicting single imaginary frequency for the correct mode. Full geometry optimization at same level of the theory has been performed, followed with frequency calculations that confirmed structures to be local minima and transition states

to be first order saddle point. Cpd I used in present investigation was modeled as iron embedded in protoporphyrin IX, side chains were removed to make calculations less extensive, also replacement of side chain will not greatly affect the energies of high-lying occupied and low lying virtual orbitals of chemical system. Similary, for simplification of the substrate structure 3-4 methoxyestragole is replaced by 4-methoxy substituent to reduce computation cost.

3.3: Result and Discussions

3.3.1: Electronic structure of Cpd I

Cpd I possess a dense manifold of orbitals [20-22] and therefore it has multiple closely lying spin states and electromeric states. An understanding of its orbital picture is necessary to understand the trends and pattern during the course of the reaction. Figure 3.3 shows all the high-lying occupied and low-lying virtual orbitals of heme system that are key orbitals involved in catalyst mechanism. In the extreme left of the Figure 3.3, we have porphyrin ring orbitals which are π –type high-lying non-bonding orbitals and under D_4^{th} symmetry their labels are assigned as a_{1u} and a_{2u}. The a_{2u} orbital is a bit higher in energy than a_{1u} due to its mixing with the axial thiolate ligand. Other than these porphyrin ring orbitals, there are five metal 3d orbitals that mix with axial ligand oxygen. Uppermost orbital in Figure 3.3, is $\sigma^*_z{}^2$ anti-bonding orbital, this arises due to the mixing of $3d_z^2$ orbital of iron and $2p_z$ orbital of oxygen along S-Fe-O bond axis. Right below in the Figure 33 lies σ^*_{xy} is a planar orbital formed due to the mixing of $3d_{xy}$ orbital of iron and $2p_{xy}$ orbital of porphyrin nitrogen along Fe-N bond axis. With the combination of $3d_{xz}/3d_{yz}$ metal orbital and oxygen $2p_x/2p_y$ orbital arises formation of low-lying π_{xz}/π_{yz}

orbital. These are found to be always filled and their anti-bonding pairs π^*_{xz}/π^*_{yz} orbital along Fe-O axis. $\delta_{x^2-y^2}$ orbital is lone pair porphyrin ring.

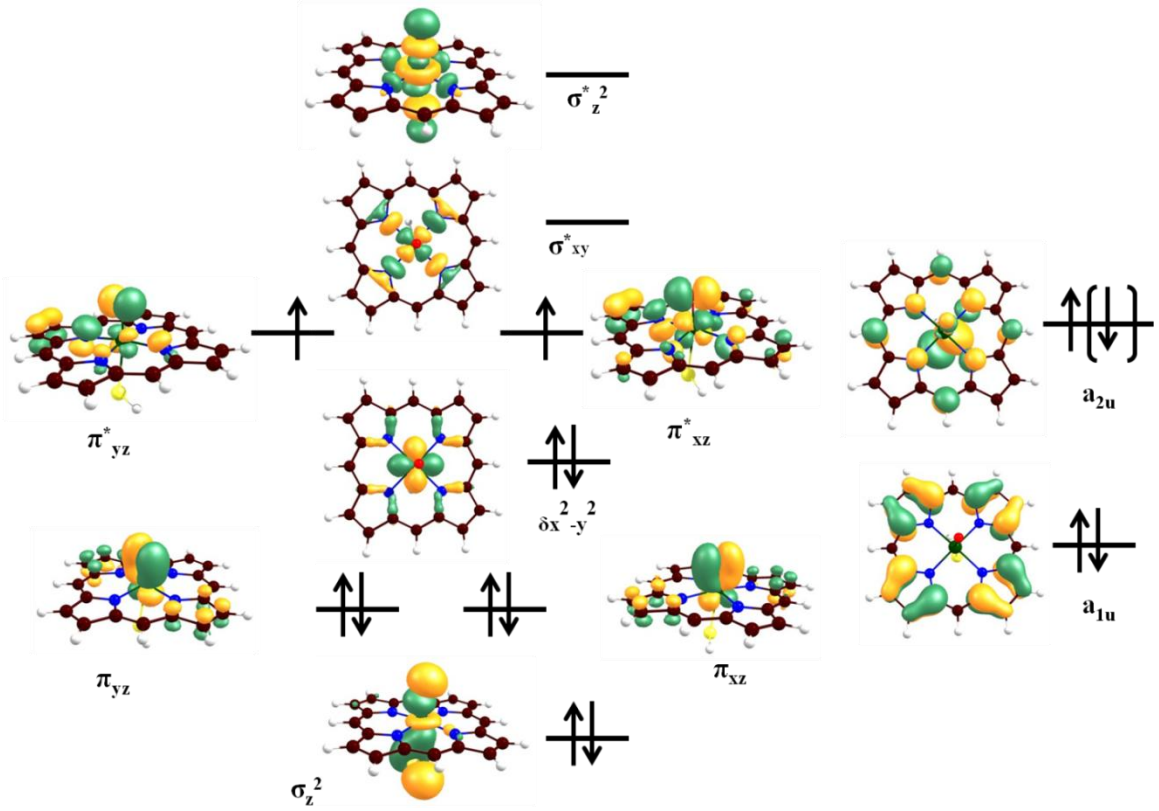

Figure 3.3: Molecular orbitals of Cpd I involved in the reaction[5].

3.3.2: Aliphatic Hydroxylation

In accordance with previously calculated and benchmarked studies, we investigated our reaction mechanism with modeled active site complex of cytochrome P450 i.e. Cpd I with substrate [16, 20, 23].We are focused at C1 position aliphatic hydroxylation of estragole and it starts with hydrogen abstraction step via transition state TS_H to generate a radical intermediate INT. This radical intermediate rebounds to generate product complex PC crossing rebound transition state (TS_{reb}). The potential energy surface of the reaction mechanism is shown in Figure 3.4.

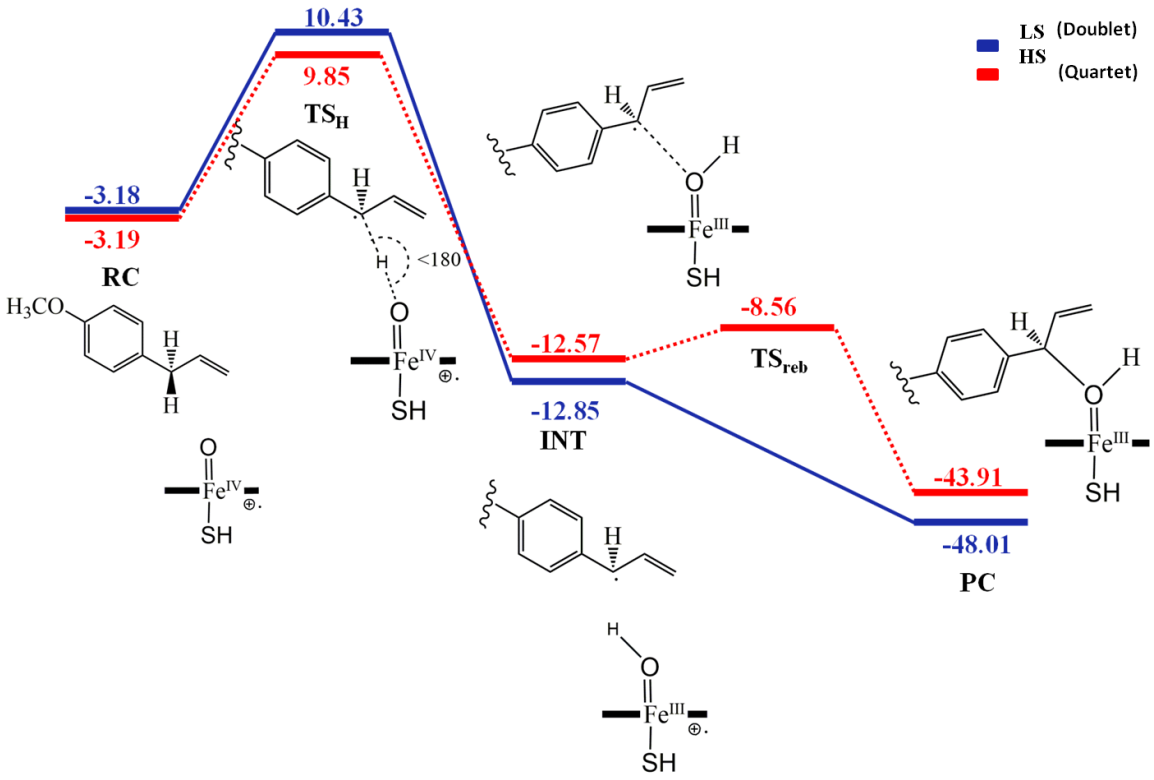

Figure 3.4: Potential energy profile for aliphatic hydroxylation at benzylic position of estragole calculated using DFT methodology at B3LYP/BS1 level of the theory, all energies here are reported in kcal/mol, the bond lengths in angstrom (Å), bond angles in degree (°) and frequencies in wavenumber (cm^{-1}).

The reaction analogous to previously reported studies is stepwise and is highly exothermic after radical intermediate to product formation. The reaction follows two state reaction (TSR) mechanism and results are in good agreement with previous studied reactions following TSR mechanism. Hydrogen atom abstraction is the rate determining step of the reaction, barrier heights for doublet and quartet are observed to be 10.43 and 9.85 kcal/mol respectively. Frequency calculations showed single large imaginary frequencies for both spin states i1508.20 cm^{-1} (doublet) and i1455.38 cm^{-1} (quartet) [24-

26], these results are reminiscent of typical H-abstraction barrier and simply means that large Kinetic Isotopes Effect (KIE) will be observed after replacement of deuterium with hydrogen [27].

Optimized three dimensional structures of transition states $^{2,4}TS_H$ showed transferring hydrogen atom is close to the carbon atom and this kind of transition state shows less barrier height in comparison to the late transition state. Subsequent formation of radical intermediate occurs and their formation is exothermic with energy values -12.85 and -12.57 kcal/mol for doublet and quartet respectively. Typically of TSR mechanism reactant complex for both spin surfaces are close in energy and virtually degenerate till H-abstraction barrier [5, 10-13, 28]. With the formation of radical intermediates ^{2,4}INT both spin surfaces bifurcate, rebound transition state is observed for high spin (HS) state with barrier height of -8.56 kcal/mol to form product complex whereas the reaction was barrier-less on low spin surface (LS) and concerted product formation is observed. The last reaction step for product formation was highly exothermic for both spin surfaces showing energy value below -40.00 kcal/mol.

Table 3.1: Spin densities and Mulliken atomic charges

The abbreviations are: SH= thiolate group, Sub = substrate (estragole), Por = Porphyrin

(a) Reactant Complex (RC)

	Spin Densities					Charges				
	ρ_{Fe}	ρ_{O}	ρ_{Por}	ρ_{SH}	ρ_{Sub}	Q_{Fe}	Q_{O}	Q_{Por}	Q_{SH}	Q_{Sub}
LS	1.20	0.89	-0.51	-0.58	0.00	0.51	-0.35	-0.10	-0.04	-0.01
HS	1.07	0.94	0.44	0.53	0.00	0.50	-0.34	-0.09	-0.04	-0.01

(b) Transition State (TS_H)

	Spin Densities					Charges				
	ρ_{Fe}	ρ_{O}	ρ_{Por}	ρ_{SH}	ρ_{Sub}	Q_{Fe}	Q_{O}	Q_{Por}	Q_{SH}	Q_{Sub}
LS	1.62	0.39	-0.32	-0.32	-0.37	0.49	-0.49	-0.21	-0.06	0.28
HS	1.20	0.77	0.19	0.40	0.43	0.46	-0.47	-0.26	0.00	0.27

(c) Intermediate Complex (INT)

	Spin Densities					Charges				
	ρ_{Fe}	ρ_{O}	ρ_{Por}	ρ_{SH}	ρ_{Sub}	Q_{Fe}	Q_{O}	Q_{Por}	Q_{SH}	Q_{Sub}
LS	1.81	0.25	-0.12	0.28	-0.98	0.44	-0.59	-0.28	0.03	0.38
HS	1.81	0.28	-0.12	0.03	0.99	0.44	-0.59	-0.30	0.03	0.42

(d) Rebound Transition State (TS_{reb})

	Spin Densities					Charges				
	ρ_{Fe}	ρ_{O}	ρ_{Por}	ρ_{SH}	ρ_{Sub}	Q_{Fe}	Q_{O}	Q_{Por}	Q_{SH}	Q_{Sub}
HS	2.27	0.04	-0.12	0.10	0.70	0.52	-0.61	-0.40	-0.09	0.58

(e) Product Complex (PC)

	Spin Densities					Charges				
	ρ_{Fe}	ρ_{O}	ρ_{Por}	ρ_{SH}	ρ_{Sub}	Q_{Fe}	Q_{O}	Q_{Por}	Q_{SH}	Q_{Sub}
LS	1.09	-0.00	-0.08	-0.00	0.00	0.33	-0.59	-0.54	0.02	0.76
HS	2.53	0.01	-0.00	0.46	-0.00	0.52	-0.58	-0.45	-0.16	0.68

The reaction between Cpd I and substrate is modeled. The reactant complex electronic configuration was investigated and found to be $\delta^{*2}_{x2-y2}\ \pi^{*1}_{xz}\ \ \pi^{*1}_{yz}\ a^{1}_{2u}$. The RC was followed with the formation of transition state $^{2,4}TS_H$ having electronic configuration $\delta^{*2}_{x2-y2}\ \pi^{*1}_{xz}\ \ \pi^{*1}_{yz}\ a^{2}_{2u}\ \varphi^{1}_{c}$ to form intermediate complex ^{2,4}INT. Validity of spin and electron densities was further confirmed by mulliken analysis and charge analysis Table 3.1. The spin density showed transition states to be radical in nature. The intermediate spin densities along with electronic configuration depicted one electron transfer from substrate to porphyrin a_{2u} orbital. The nature of both the intermediates was found to be radical and electron density accumulates at C1 position of the substrate with spin density (ρ_{sub} -0.98 and 0.99) doublet and quartet respectively. Intercrossing of spin is also observed in energy profile Figure 3.4, this is indicative of spin-crossover in the catalytic cycle. Throughout the reaction process the orbital occupancy changes for a_{2u}, π^{*}_{xz} /π^{*}_{yz} , $\sigma^{*}{}_{z}{}^{2}$ and substrate orbital φ_c to conserve the overall spin during the entire reaction and also for electron sharing in making and breaking of bonds. First electron transfer for the formation of bond between oxo group and H atom is achieved by electron transfer from substrate to the Cpd I, one of the electron is transferred to heme a_{2u} orbital making it fully occupied leaving substrate to be singly occupied φ^1. Last step of the reaction that is radical rebound occurs to generate product complex PC with electronic configuration $\delta^{*2}_{x2-y2}\ \pi^{*1}_{xz}\ \ \pi^{*1}_{yz}\ \sigma^{*1}_{z^2}\ \sigma^{*0}_{xy}\ a^{2}_{2u}\ \varphi^{0}_{c}$ for quartet spin and $\delta^{*2}_{x2-y2}\ \pi^{*2}_{xz}\ \ \pi^{*1}_{yz}\ \sigma^{*0}_{z^2}\ \sigma^{*0}_{xy}\ a^{2}_{2u}\ \varphi^{0}_{c}$ for doublet spin state. The rebound transition state $^4TS_{reb}$ is observed only on high spin (HS) with electronic configuration $\delta^{*2}_{x2-y2}\ \pi^{*1}_{xz}\ \pi^{*1}_{yz}\ \sigma^{*1}_{z^2}\ \sigma^{*0}_{xy}\ a^{2}_{2u}\ \varphi^{0}_{c}$.

In case of low spin (LS) the rebound barrier required is usually ~1kcal/mol and hence the potential energy surface is flat. The value for rebound transition state (TS_{reb}) was observed to be -8.56 kcal/mol and its adequacy is confirmed by single imaginary frequency of i231.43 cm^{-1} for the correct mode of vibrations. The discrepancies in potential surface in rebound step for both spins can be understood from the transfer of electron to the respective orbitals. In LS the second electron from φ_c gets transferred to low-lying π^*_{xz} orbital to generate ^{2}P (III) whereas more energy is required to transfer an electron to high-lying virtual orbital $\sigma^*_{z^2}$ to form ^{4}P (III).

There must be some changes in three dimensional geometries in structure from RC to PC (Figure 3.5) which helped in easy transfer of electron in making and breaking of bonds. The geometric features of the H-atom abstraction are similar to that of direct H atom abstraction from methane via bare FeO^+ [29] and diiron model complexes [30]. The transition state TS_H for H abstraction at C1 position is shown in Figure 3.5, O-H bond and C-H bond 1.25Å (1.27Å) and 1.34Å (1.31Å) respectively for doublet (quartet). The bond angle for C-H-O is linear with value 170.65° (174.53°) which is a genuine pattern for H-abstraction process by various FeO species. As discussed above smaller C-H bond distances compared with O-H bond is regarded as earlier transition state and barrier heights associated with such geometrical features is lower to that of late TS. Intermediate cluster formation occurs after crossing the transition state (TS_H), C1 radical centre is oriented towards the hydoxy group this can be seen from Figure 3.5. The second half of the reaction is the oxygen rebound mechanism where carbon radical and iron-hydroxo species combine to form product complex and essential part of this process is the formation of the C-O bond. For the formation of C-O bond carbon radical needs to rotate

to attack on iron-hydroxo species, this step requires energy barrier to cross. On quartet spin surface rebound transition state TS_{reb} is observed. During geometric scan we see sharp changes in bond lengths, C-O bond decreases and Fe-O bond increases coupled with decrease in Fe-S bond length at same time. This effect is known as "push-effect" [5] shown in Figure 3.5 and is observed in hydroxylation reaction catalyzed by P450s. Whereas on doublet spin surface our calculations predicted no direct transition state and it could be regarded as virtually barrier-less to produce product. This step is highly exothermic in nature and proceeds at very low cost of energy. The driving force is a direct consequence of large product stability.

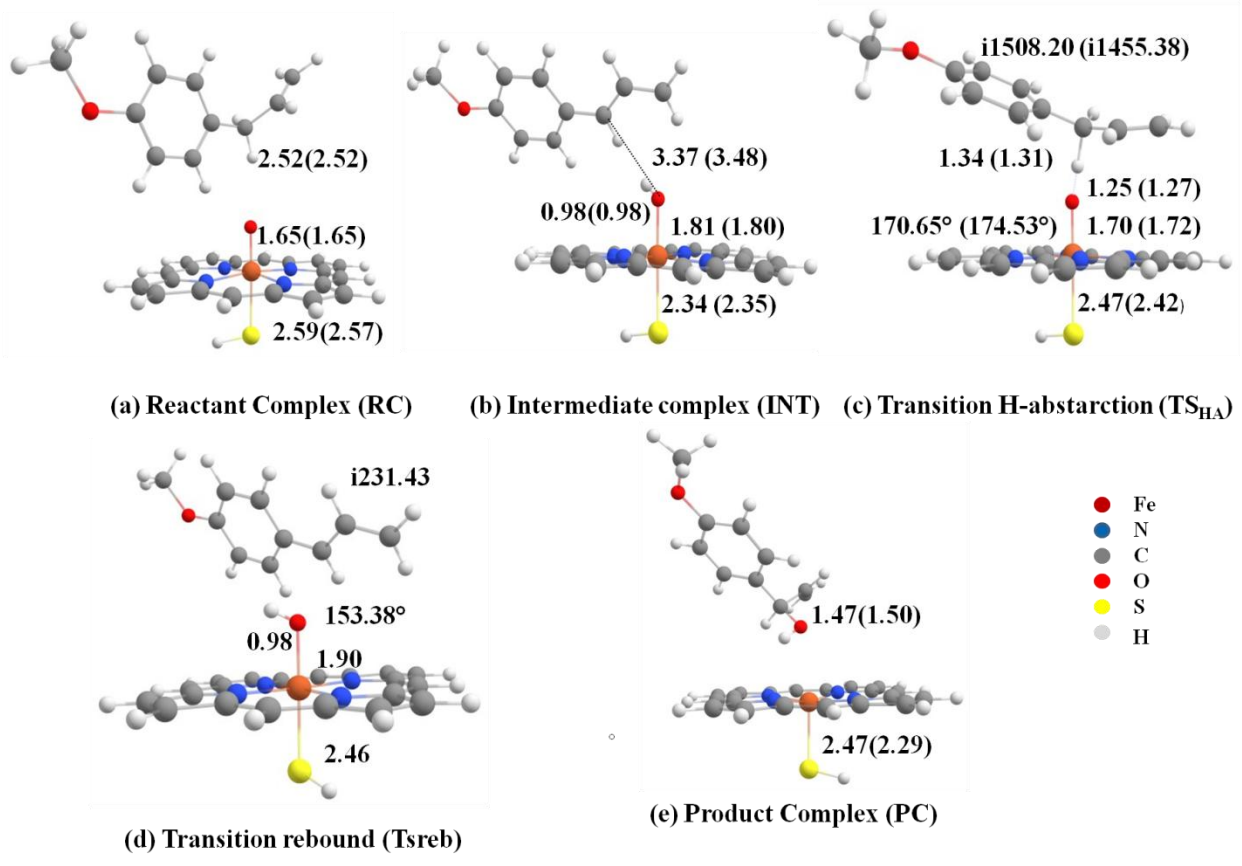

Figure 3.5: Optimized 3-D geometries of (a) Reactant Complex (RC), (b) Intermediates (INT) (c) H-abstraction Transition state (TS_H) (d) Rebound Transition State

(TS_{reb}) and (e) Product Complexes (PC) for doublet (quartet) spin states, along with the necessary bond lengths in Å and imaginary frequency of TS in cm^{-1}. In Figure without and within parenthesis are indicative of LS (HS)-doublet and quartet. All geometries were optimized at B3LYP/BS1 level of theory.

3.4 Conclusions

Present studies on cytochrome P450 monooxygenases found in human liver utilizing DFT based QM calculations to completely elucidate reaction energy profile of C-H hydroxylation of estragole. The hydroxylated product is a precursor in the activation of toxic metabolite by sulfotransferase to produce 3´-sulfoxyestragole. The theoretical investigation revealed that a Two State Reactivity (TSR) mechanism is followed for both HS and LS. The reaction is throughout exothermic and the LS surface offers easier pathway for the product formation. The rate limiting step was found to be H-abstraction step with 9.85 kcal/mol and 10.43 kcal/mol for quartet and doublet spin state respectively. It can be asserted from above discussed results that C1 position hydroxylation of estragole with Cpd I of P450 is rebound mechanism for HS surface and concerted for LS surface. The intermediates are highly short-lived and product formation directly occurs from intermediate on LS surface, although possibility of stereochemical scrambling is present on HS.

References:

[1] S. Levorato, L. Dominici, C. Fatigoni, C. Zadra, R. Pagiotti, M. Moretti, M. Villarini, *Food Chem. Toxicol.*, **111,** 616 (2018).

[2] B. H. Monien, B. Sachse, B. Niederwieser, K. Abraham, *Chem. Res. Toxicol.*, **32,** 2260 (2019).

[3] S. Shaik, S. Cohen, Y. Wang, H. Chen, D. Kumar, W. Thiel, *Chem. Rev.*, **110,** 949 (2010).

[4] S. Shaik, S. P. De Visser, 3rd ed., edited by P. R. O. de Montellano, Ed. New York: Kluwer Academic / Plenum Publishers, (2005).

[5] S.P. De Visser, A. Altun, W. Thiel, *Chem. Rev.*, **105,** 2279 (2005).

[6] M. R. A. Blomberg, T. Borowski, F. Himo, R. Liao, P. E. M. Siegbahn, *Chem. Rev.*, **114,** 3601 (2014).

[7] B. Meunier, S. P. de Visser, S. Shaik, *Chem. Rev.*, **104,** 9, 3947, (2004).

[8] J. T. Groves, *Proc. Natl. Acad. Sci.*, **100,** 3569 (2003).

[9] Y. Watanabe, H. Nakajima, T. Ueno, *Acc. Chem. Res.*, **40,** 554 (2007).

[10] F. Ogliaro, N. Harris, S. Cohen, M. Filatov, S. P. deVisser, S. Shaik, *J. Am. Chem. Soc.*, **122**, 8977 (2000).

[11] T. Kamachi, K. Yoshizawa, *J. Am. Chem. Soc.*, **125,** 4652 (2003).

[12] S. P. De Visser, D. Kumar, S. Cohen, R. Shacham, S. Shaik, *J. Am. Chem. Soc.*, **126,** 8362 (2004).

[13] Xi. Li, V. Postils, W. Sun, M. Sola, Y. Wang, W. Nam, S. P. de Visser, *J. Chem. Eur.*, **23,** 6406 (2017).

[14] S. Shaik, S. Cohen, S. P. deVisser, P. K. Sharna, D. Kumar, S. Kozuch, F. Ogliaro,

D. Danovich, *Eur. J. Inorg. Chem.*, **2004**, 207 (2004).

[15] D. J. Frisch, M. J. Trucks, G. W. Schlegel, H. B. Scuseria, G. E. Robb, M. A. Cheeseman, J. R. Scalmani, G. Barone, V. Mennucci, B. Petersson, G. A. Nakatsuji, H. Caricato, M. Li, X. Hratchian, H. P. Izmaylov, A. F. Bloino, J. Zheng, G. Sonnenb, *Official Gaussian 09 Literature Citation*. (2009).

[16] F. G. C. Reinhard, S. P. De Visser, *J. Chem. Eur.*, **23,** 2935 (2017).

[17] D. Kumar, S. De Visser, S. Shaik, *J. Am. Chem. Soc.*, **125,** 13024 (2003).

[18] Y. A. R. Hussain, R. Yadav, M. Ahmed, T. A. Khan, D. Kumar, *J. Comput. Chem.*, **41**, 330 (2020).

[19] P. J. Hay, W. R. Wadt, *J. Chem. Phys.*, **82,** 299 (1985).

[20] F. Ogliaro , S.P. deVisser , S. Cohen, J. Kaneti, S. Shaik*, Chem. Bio. Chem.*, **11,** 848 (2001).

[21] M. A. Sainna, S. Kumar, D. Kumar, S. Fornarini, M. E. Crestoni, S. P. deVisser *Chem. Sci.*, **6,** 1516 (2015).

[22] S. P. de Visser, F. Ogliaro, P. K. Sharma, S. Shaik, *J. Am. Chem. Soc.*, **124,** 11809 (2002).

[23] S. P. De Visser, S. Shaik, P. K. Sharma, D. Kumar, W. Theil, *J. Am. Chem. Soc.*, **125**, 15779 (2003).

[24] P. Barman, P. Upadhyay, A. S. Faponle, J. Kumar, S. S. Nag, D. Kumar, C. V. Sastri, S. P. deVisser, *Angew.Chem. Int.Ed*, **55,** 11091 (2016).

[25] A. Timmins, M. Saint-André, S. P. de Visser, *J. Am. Chem. Soc.*, **139,** 9855 (2017).

[26] S. P. de Visser, *Inorg. Chem.*, **45,** 9551 (2006).

[27] S. P. De Visser, *J. Chem. Eur.*, **12,** 8168 (2006).

[28] P. K. Sharma, S. P. de Visser, F. Ogliaro, S. Shaik, *J. Am. Chem. Soc.*, **125,** 2291 (2003).

[29] K. Yoshizawa, Y. Shiota, T. Yamabe, *Organometallics*, **17,** 2825 (1998).

[30] H. Basch, K. Mogi, D. G. Musaev, K. Morokuma, *J. Am. Chem. Soc.*, **121,** 7249 (1999).

CHAPTER 4

BIOTRANSFORMATION OF BISPHENOL AND THEIR ANALOGUES BY CYTOCHROME P450 USING DFT

CHAPTER-4

BIOTRANSFORMATION OF BISPHENOL AND THEIR ANALOGUES BY CYTOCHROME P450 USING DFT

4.1: Introduction

Innumerable chemical compounds are synthesized at large scales to support our comfortable life. Though, many such compounds later show adverse effects on environment and human health. Some of these chemicals are regarded as "endocrine-disrupting chemicals (EDCs)", as they are responsible for hormonal dysfunction in animals and humans. Bisphenol A (BPA, 2, 2-bis (4-hydroxyphenyl) propane) is universally used in industry as monomer in the synthesis of polycarbonate and epoxy plastics. It is well known that it behaves as weak estrogen and thus regarded as one of the endocrine disrupting chemicals (EDCs) [1, 2]. BPA is ever-present in environment and humans are exposed to this chemical from dietary and non-dietary sources [3, 4].Various studies carried out so far reported extensive occurrence of BPA in human serum, placental tissue, umbilical cord blood, urine and breast milk posing serious threat [3-5]. Other than being EDC in humans; BPA showed prominent developmental, reproductive, immune, cardiovascular and metabolic effects [5]. Owing to its hazardous effects in 2017, it has been listed in the substances of very high concern by the European Chemical Agency (ECHA) [6-8]. Constant efforts are being made in exploring new substitutes of BPA by food packing companies and various analogs of BPA are used to fulfill the purpose [9]. These analogues such as (BPF, BPZ, BPAF, BPS etc.) share the basic

structure which has two benzene rings (substituted or un-substituted) separated by small carbon or chemical chain.

Metabolism largely affects the toxicity of bisphenols, Kitamura et al. summarized and discussed the effects of metabolic modification on the estrogenic and antiandrogenic activities of BPA [10]. Metabolism and excretion pathways of bisphenol analogues may also resemble with that of BPA [10]. P450 present in human liver can become a dominating metabolizing enzyme under certain circumstances like in rat and human fetal liver which show little or no glucuronidation [14, 15]. BPAs undergo large number of metabolite formation after interacting with P450 viz hydroxylated BPA (o-OH BPA) through aromatic hydroxylation [16], further oxidation of hydroxylated metabolite may lead to the formation of quinone and through ipso-substitution can form hydroxycumyl alcohol (HCP), isopropyl alcohol (IPP), and hydroquinone (HQ) [17], or can undergo dimerization 4-methyl-2,4-bis(4-hydroxyphenyl)pent-1-ene (MBP) [18-19], and through epoxidation step to form arene epoxide intermediate [20]. Metabolic modification of bisphenol and bisphenol analogues possess greater toxicity with estrogenic and antiandrogenic activities [15]. Hence, understanding the biotransformation mechanism of BPA in humans is important in its toxicity assessment.

Present work focuses on investigating aromatic hydroxylation reaction mechanism mediated by P450 to produce catechol (o-OH BPA or 3-OH-BPA) and two of the substitutes of BPA which are used in industry viz BPF and BPZ (Scheme 4.1) along with the epoxidation of BPA mediated by P450 has also been thoroughly explored. Hydroxylation of BPA through P450 results in the formation of catechol (3-OH-BPA), this shows weakly endrogenic and weakly antiandrogenic activities. Further oxidation of

3-OH-BPA produces ortho quinone i.e. BPA 3-4-quinone, it is found to from adducts with DNA [16]. Likewise epoxides are highly unstable and hence reactive; they have potency to readily react with the DNA bases and amino acids of protein to form adducts that are comparably stable. Hence, epoxidation reactions have raised serious concern owing to their toxicological effects [21].

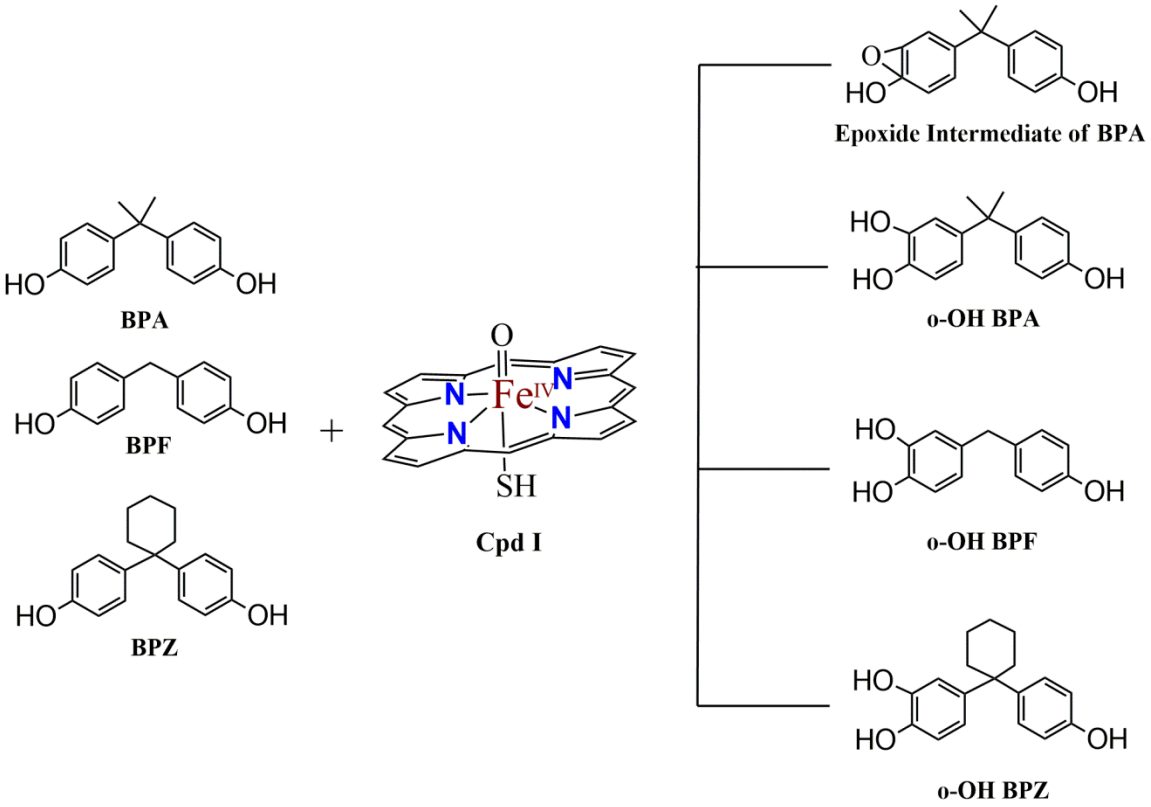

Scheme 4.1: Proposed metabolic biotransformation of BPA, BPZ and BPZ by human liver P450.

In preceding years quantum mechanical calculations have been employed extensively to unravel the mechanistic details of P450 catalyzed oxidation of an array of xenobiotics [22, 23, 24-28]. Density Functional Theory (DFT) based quantum mechanical calculations were employed to thoroughly understand the energy profile, intrinsic electronic structure and its contribution to the selectivity and reactivity in activation of

BPA and their analogues. QM calculation-based studies are an effective tool that allows us to understand reaction mechanism associated with typical biocatalytic processes and helps in answering above questions. At the same time they allow the inspection of alternative pathways which can be energetically and mechanistically more preferred.

4.2: Computational Method

4.2.1: Model system

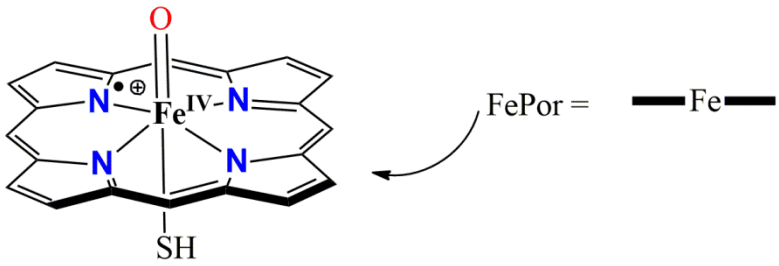

^{2,4}Cpd I

Scheme 4.2: Active site model of the Fe (IV)=O species of P450 used in the study of epoxidation of BPA.

The most simplistic model of Cpd I, $Fe^{4+}O^{2-}$ $(C20N4H12)^{1-}$ $(SH)^{1-}$ shown in Scheme 4.2 was utilized in modeling the active site of P450 in epoxidation mechanism of BPA. It is noteworthy here that being simplistic and ignoring the actual side chain of porphyrin ring system, active site residues involved during substrate binding and its conversion; there will be some imprecision in energy calculated but previously done investigation utilizing the same model have proven its reliability to competently reproduce its atomistic and electronic features of P450 that governs its reactivity [22, 25-27, 29-31]. Furthermore,

Cpd I involves two energetically close spin surfaces quartet high-spin (HS) and doublet low-spin (LS) [23, 30] the epoxidation was evaluated for both HS and LS.

4.2.2: DFT calculations

Quantum mechanical approach utilizing DFT was implemented using Gaussian 09 [32] software. Optimization of structures was performed in gas phase using B3LYP functional. Split basis sets were utilized for better results. Iron atom was subjected to LANL2DZ basis set along with double zeta effective core potential (ECP) and, for remaining of the atoms 6-31G basis set was used (referred to as BS1) [33]. Reliability of B3LYP functional in modeling the P450 mediated biotransformation and relevant kinetics has been well established through numerous studies. To search transition state, potential energy scans (PES) were conducted. Validation of transition state structure was done using geometry optimization followed with analytic frequency calculations at the same level of the theory. Single imaginary frequency involving correct vibrational mode confirmed the structure to be a TS and real frequencies for other structures viz reactant, intermediate and product confirmed their aptness. Further to check the results at higher basis set single point energy calculations were put in consideration that showed minor difference in the energy values and hence confirmed the barrier heights to be true. Higher basis set was referred as (BS2 in short), for iron LACV3P basis set and triple zeta core potential and 6-31G* basis set for the other atoms [34].

4.3: Results and Discussions

4.3.1: Aromatic hydroxylation of BPA

Aliphatic hydroxylation reaction mechanism catalyzed by P450, has been extensively studied. The mechanism initially begins with the abstraction of hydrogen via two-state reactivity (TSR) on competing doublet (LS) and quartet (HS) spin surfaces. The H-abstraction results in the formation of radical intermediate, followed with rebound transition state to produce alcohol product on the HS spin surface and mostly concerted product formation on the LS surface [35-38]. Unlike the case, in aromatic hydroxylation the process is thermodynamically more demanding due to immoderate strength of the C-H bond to be broken. Analogous to previously reported and calculated aromatic hydroxylation mediated by oxy-ferryl cation radical species (Cpd I) on the variety of substrates [39-41], the bond activation steps starts from electrophilic attack (or π attack) of Cpd I on benzene ring resulting in the formation of Meisenheimer complex which is either cation type intermediate (I_{cat}) or radical intermediate (I_{rad}), after crossing the barrier (TS1) needed for initial C-O bond formation. Radical intermediate formation transpires single electron transfer from substrate to oxidant to generate Fe(IV) type complex with electronic occupation of kind $\delta_{x2-y2}^{*2}\ \pi_{xz}^{*1}\ \ \pi_{yz}^{*1}\ a_{2u}^{2}\ \varphi_{c}^{1}$, meanwhile in cationic intermediate double electron transfer occurs to give rise to Fe(III) type complex with electronic occupancy $\delta_{x2-y2}^{*2}\ \pi_{xz}^{*1}\ \pi_{yz}^{*2}\ a_{1u}^{2}\ \varphi_{c}^{0}$ for doublet and $\delta_{x2-y2}^{*2}\ \pi_{xz}^{*1}\ \pi_{yz}^{*1}\ \sigma_{z^2}^{*1}\ \sigma_{xy}^{*0}\ a_{2u}^{2}\ \varphi_{c}^{1}$ for quartet. Further from this intermediate complex step, transfer of hydrogen from the *ipso* carbon to the nearest pyrole nitrogen occurs crossing the TS2 ($H \rightarrow N$) barrier to form protonated porphyrin intermediate. The proton shuttle to the nitrogen of

the porphyrin ring occurs due to the basic nature of nitrogen. The intermediate formed reprotonates the oxo group of the substrate and results in the hydroxylated product, with negligible or no barrier TS3 (H → O). Moreover, transfer of hydrogen to the *ortho* carbon can lead to produce ketone, seen in benzene hydroxylation studies by de. Visser et. al. But, before we move further in details and discussion we must understand the electronic configuration of the Cpd I, suggested by early DFT based QM [42, 43] studies and also QM/MM studies [44, 45].

Figure 4.3 contains the orbital shapes of high-lying occupied and low-lying virtual 3d metal orbitals and π^* heme orbitals involved in reaction. The z-axis here is considered along Fe-O-S bond axis which is perpendicular to the plane of the porphyrin ring, x and y axes along Fe-N bonds of porphyrin. These orbitals are result of 3d metal orbitals contributions; the lowest of all orbitals involved is non-bonding doubly occupied $\delta^2_{x^2-y^2}$ orbital which lies in heme plane. Slightly above in energy with non-bonding δ lies two sets of orthogonal π^*_{xz} and π^*_{yz} orbitals originated due to the combination of 3d metal orbital and 2p orbital of oxo group. Out of five metal combining orbitals two lowest virtual orbitals are σ^*_{xy} orbital, resulted due to the non-bonding interaction of metal and porphyrin nitrogen atoms. Second is $\sigma^*_{z^2}$ orbital formed due to the non-bonding interactions along S-Fe-O bond axis with overlap of distal and axial ligands orbitals.

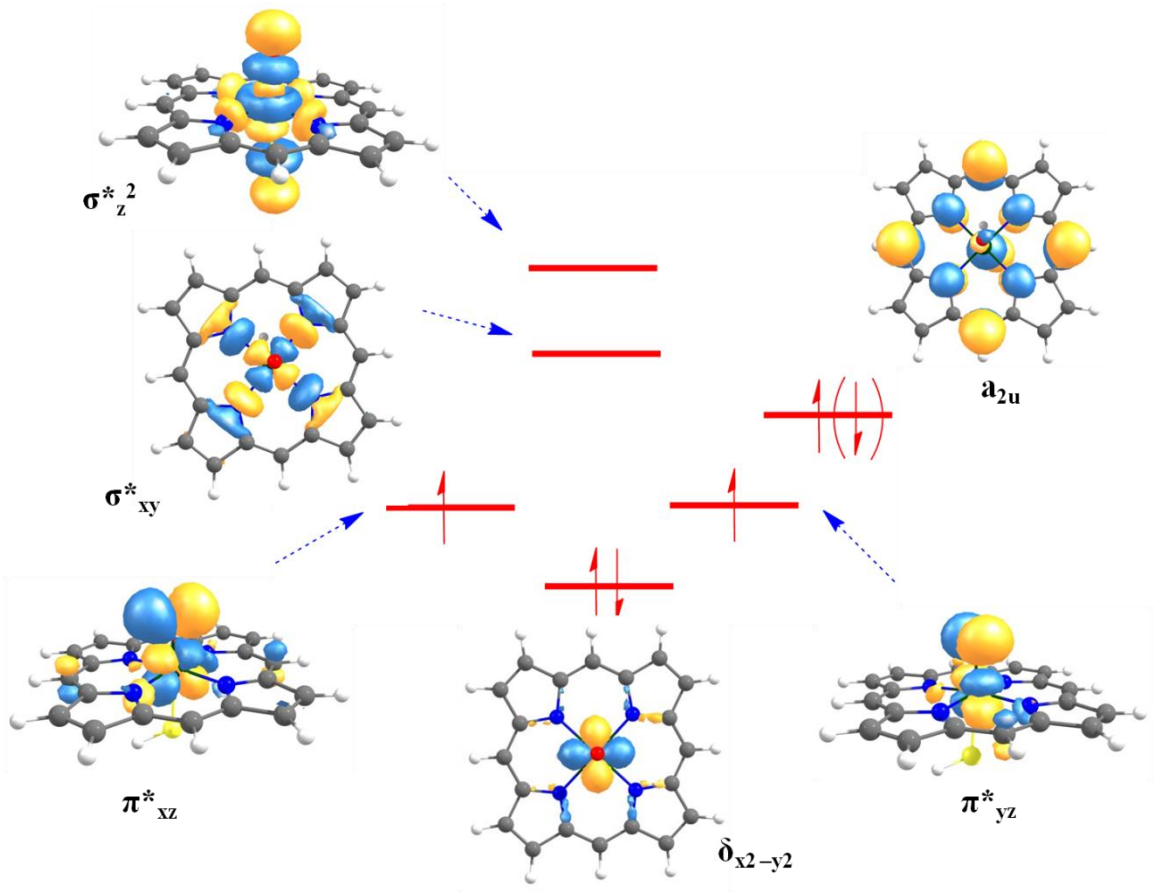

Figure 4.3: Prime molecular orbital diagrams of Cpd I in order of increasing energy.

Also singly occupied orbital of porphyrin is involved in molecular mechanism of P450 and it is labeled as a_{2u} in D_4^{th} symmetry. Due to the small interaction encountered between a_{2u} and two π^* orbitals, both the high spin (HS) and low spin (LS) are close in energy and this is the reason behind origination of two spin states surfaces with distinct reaction barriers [44].

We investigated the reaction mechanism of aromatic hydroxylation of BPA at *ortho* position to investigate full reaction potential energy profile Figure 4.4. After the formation of reactant complex on both spin surfaces doublet and quartet virtual degeneracy can be observed. The reaction is stepwise with electrophilic attack of oxo

group of Cpd I to the *ortho* carbon atom of the BPA to form tetrahedral Meisenheimer intermediate complex **I 1** as the first step, by crossing the C-O bond formation barrier TS1. The π- activation barrier ^{4,2}**TS1** is observed as 15.69 and 12.92 kcal mol^{-1} for high spin (HS)/ low spin (LS) respectively and aromaticity of the ring gets distorted with the formation of C-O bond. The difference of HS over LS is nearly 3 kcal mol^{-1} and hence we can see the preference of aromatic activation to LS surface.

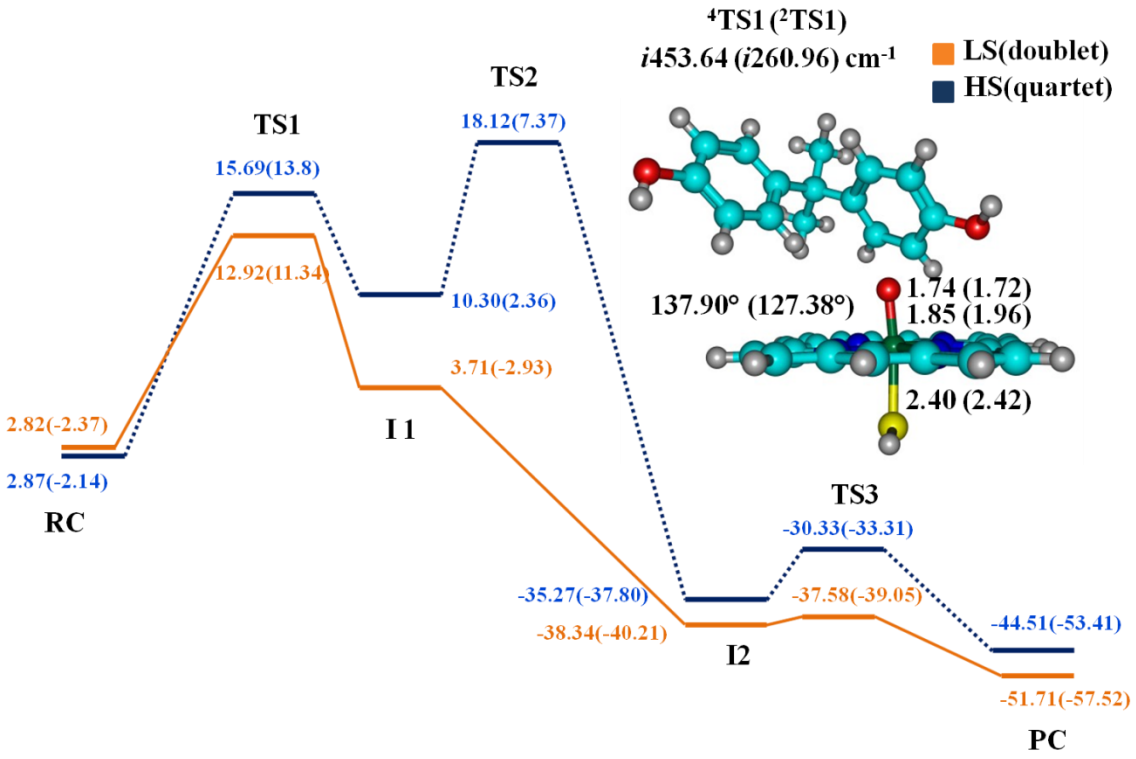

Figure 4.4: Potential energy landscape for the hydroxylation of BPA by active oxidant of P450 (Cpd I), for the HS and the LS, all energies are expressed in kcal/mol and imaginary frequencies in cm^{-1}. The bond lengths in units (Å), and bond angles in unit (°) . The free energies are obtained by optimization at BS1//BS2 level of the theory for the reactant, transition states, intermediates and product.

Spin density analysis and charge distribution indicated ^{4,2}**TS1** to be radical type (ρ_{sub} = 0.53/-0.32 in ^{4,2}**TS1**). The tetrahedral intermediate **I1** is endothermic on both surfaces but quartet ^{4}**I1** energy is high by 7 kcal/mol to corresponding doublet state. The nature of intermediate **I 1** is radical type for HS spin state; substrate here has donated one electron to a2u orbital of porphyrin maintaining the overall quartet spin with electronic occupation $\delta_{x2-y2}^{*2}\ \pi_{xz}^{*1}\ \ \pi_{yz}^{*1}\ a_{2u}^{2}\ \varphi_{c}^{1}$. Whereas on LS spin surface the intermediate nature is cationic and substrate here has donated both its electrons, one to a2u and another to π_{yz}^{*} conserving doublet spin state with configuration $\delta_{x2-y2}^{*2}\ \pi_{xz}^{*1}\ \pi_{yz}^{*2}\ a_{1u}^{2}\ \varphi_{c}^{0}$. Whereas on LS spin surface the intermediate nature is cationic and substrate here has donated both its electrons, one to a_{2u} and another to π_{yz}^{*} conserving doublet spin state with configuration $\delta_{x2-y2}^{*2}\ \ \pi_{xz}^{*1}\ \ \pi_{yz}^{*2}\ a_{1u}^{2}\ \varphi_{c}^{0}$. Several attempts have been made by us via swapping of molecular orbitals to find radical intermediate on doublet but all our attempts failed as the wave function converged back to the cationic form.

Table 4.1: Mulliken charges and spin densities of BPA optimized at (B3LYP/BS1) level of the theory.

RC

	Spin densities					Charges				
	Fe	O	Por	SH	Sub	Fe	O	Por	SH	Sub
M2	1.19	0.90	-0.51	-0.57	0.00	0.28	-0.24	0.08	-0.13	-0.00
M4	1.06	0.90	-0.51	-0.57	0.00	0.20	-0.21	0.13	-0.12	-0.00

TS1

	Spin densities					Charges				
	Fe	O	Por	SH	Sub	Fe	O	Por	SH	Sub
M2	1.54	0.19	-0.22	-0.20	-0.32	0.21	0.13	-0.04	-0.08	-0.22
M4	1.40	0.72	0.02	0.31	0.53	0.46	-0.41	-0.36	-0.01	0.35

INT1

	Spin densities					Charges				
	Fe	O	Por	SH	Sub	Fe	O	Por	SH	Sub
M2	1.05	0.03	-0.14	-0.02	0.07	0.36	-0.50	-0.48	-0.04	0.66
M4	1.96	0.31	-0.12	0.00	0.83	0.50	-0.51	-0.36	0.00	0.37

TS2

	Spin densities					Charges				
	Fe	O	Por	SH	Sub	Fe	O	Por	SH	Sub
M4	2.60	0.18	-0.04	0.45	-0.19	-0.60	0.21	0.20	-0.03	0.20

INT2

	Spin densities					Charges				
	Fe	O	Por	SH	Sub	Fe	O	Por	SH	Sub
M2	1.00	0.02	-0.07	0.03	0.00	0.33	-0.69	-0.34	-0.05	0.74
M4	2.84	0.06	0.06	0.02	0.01	0.95	-0.96	-0.25	-0.36	0.65

TS3

	Spin densities					Charges				
	Fe	O	Por	SH	Sub	Fe	O	Por	SH	Sub
M2	1.03	0.01	-0.07	0.02	0.00	0.34	-0.72	-0.39	-0.03	0.80
M4	2.74	0.03	0.04	0.16	0.00	0.52	-0.72	-0.45	-0.13	0.77

PC

	Spin densities					Charges				
	Fe	O	Por	SH	Sub	Fe	O	Por	SH	Sub
M2	1.14	-0.00	-0.09	-0.05	0.00	0.76	-0.80	-0.45	-0.24	0.74
M4	2.51	0.00	0.02	0.47	-0.00	0.64	-0.77	-0.35	-0.30	0.78

Experimental results of Asaka and Fujii gave evidence of C-O bond formation by fast electron transfer and thus supported the formation of cationic intermediate [46]. Also, large change in Fe-O bond length from 1.65 to 1.93 is observed for ^{2}**I1** which is further validating double electron transfer, and this can be seen from Figure 4.5. The huge

differences in energy of intermediate **I1**, thus can be ascertained to differences in the nature of intermediate. Formation of the radical intermediates is energetically costly and is overall endothermic [47]. The driving force is clearly greater for LS profile; thus, reaction follows single state reactivity (SSR) not TSR type mechanism as seen in aliphatic hydroxylation. Further after **I1,** transfer of ipso position hydrogen occurs crossing **^{4}TS2** with large activation energy of 18.12 kcal/mol to generate **I2** on quartet spin state. This barrier is missing and the step is concerted on LS profile to produce **^{2}I2** with large exothermicity. The proton-shuttled intermediate **I2** transfers the proton back to the phenolate group of substrate to finally give product **^{4,2}P** -44.51/-51.71 kcal/mol via **^{4,2}TS3** on HS/LS profile, here also the LS barrier height is negligible and is comparable to **^{2}I2**. This is depicted in Figure 4.4. Aromatic hydroxylation reaction proceeds mostly on LS surface [48] hence the rate limiting step is C-O bond activation barrier step **^{2}TS1**, here we see an elongation of Fe-O bond from 1.66 Å to 1.72 Å, the substrate approach is side-on as observed in case of benzene hydroxylation [41]. **^{2}TS1** is earlier with C….O bond distance of 1.96 Å compared with ^{4}TS1 1.85 Å. Generally earlier transition states correspond to lower barrier heights on the potential energy surface compared with late transition states.

Spin density (ρ) establishes transition state TS1 as a radical type with value on FeO, Por, and Sub as 1.73, -0.22 and -0.3 respectively. Reactant complex electronic occupancy is $\delta_{x2-y2}^{*2}\ \pi_{xz}^{*1}\ \pi_{yz}^{*2}\ a_{2u}^{1}$ which is descriptive of nearly 2 on FeO unit and 1 on porphyrin ring, this shows that the radical character of porphyrin in RC is lost in the transition state. The overall electronic configuration of doublet is $\delta_{x2-y2}^{*2}\ \pi_{xz}^{*1}\ \pi_{yz}^{*1}\ a_{2u}^{2}\ \varphi_{sub}^{1}$, here transfer of electron from Sub (BPA) to a_{2u} orbital of porphyrin has occurred. The angle <FeOC is

also small for doublet compared to quarter 127.38° (137.90°), which leads to stable TS energy for doublet. As we move from **TS1** to **I1** we see a lengthening in Fe-O bond length from 1.72Å to 1.93Å and shortening of C-O bond from 1.96Å to 1.48Å. Subsequently after the formation of cationic intermediate **I1**, the transfer of proton to one of the nitrogen of porphyrin ring occurs, the transition state barrier is missing in calculations due to highly short-lived nature. From **I2**, proton transfer to the phenolate group occurs crossing small barrier ^{2}**TS3** >1 kcal mol^{-1}, the imaginary frequency is large (i829.92 cm^{-1}) corresponding to translational vibration of O…..H bond.

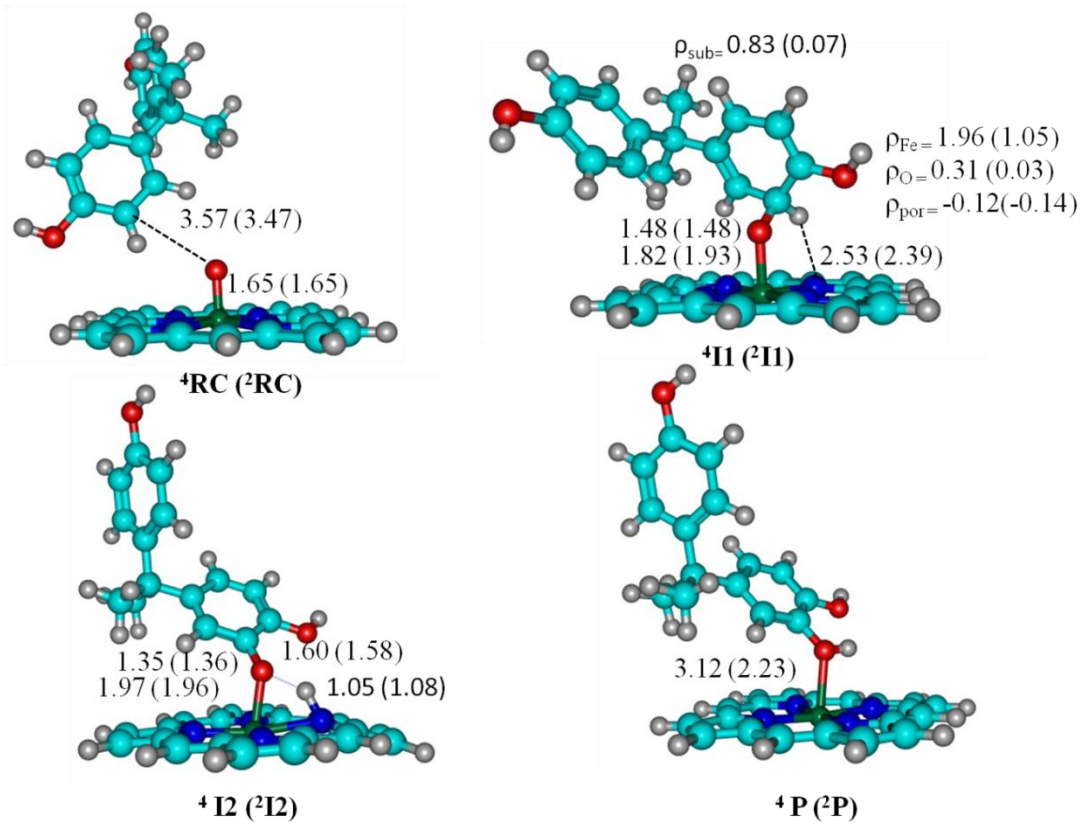

Figure 4.5: Optimized structures of reactant complex (**RC**), Intermediate 1 (**I1**), Intermediate 2 (**I2**) and Product (**P**) of BPA with Cpd I along with spin density of I1 in (ρ) atomic units and all bond lengths in angstroms (Å).

Overall aromatic hydroxylation reaction of BPA with Cpd I of P450 is stepwise and occurs on the doublet spin state with electrophilic attack as the rate determining step with value of 12.92 kcal mol^{-1}. The values are in accord with the previously reported studies of aliphatic and aromatic hydroxylation by iron (IV)-oxo porphyrin cation radical complexes [40, 47, 49].

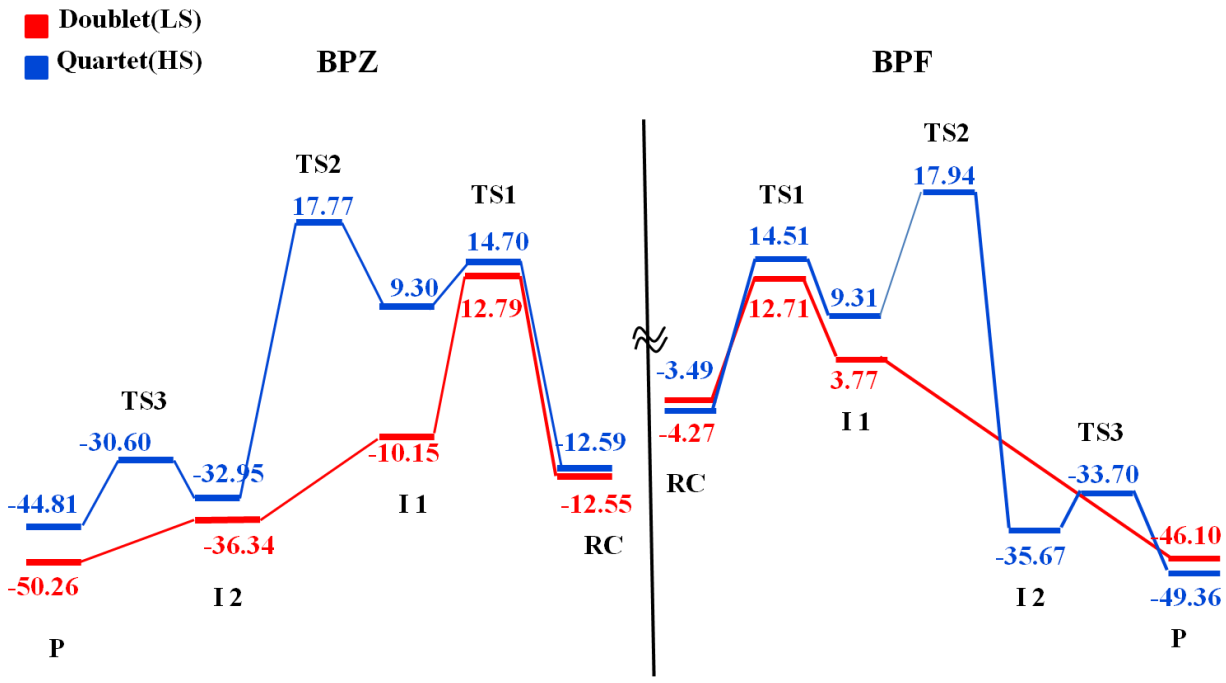

Figure 4.6: Above Figure represents schematic energy landscape of BPZ and BPF for two spin states (doublet and quartet) optimized at BS1 level of the theory. All energies reported above are in kcal/mol.

Thereafter, we calculated the full reaction profile for BPA analogs Bisphenol F (BPF) and Bisphenol (BPZ), shown in Figure 4.6. The landscape of BPZ shows similar patterns and energies of activation were in same range. Similar to the BPA data reported above the ^{2}**TS1** was below ^{4}**TS1** and rate determining step was π activation. The second transition state ^{4}**TS2** offered large value for proton transfer step just like previous

calculation. But, no barrier has been observed for both proton transfer steps on LS profile i.e initially from substrate (BPZ) to porphyrin nitrogen and secondly to oxygen for product formation. The reaction occurs in concerted manner after cationic intermediate **I1**. The reaction is feasible on doublet spin surface just like the above mentioned results. Similar to above reported results the energy profile of BPF data also proceeds on LS spin state with rate determining electrophilic addition barrier **TS1** leading to the formation of cationic intermediate **I1**. Although for BPF substrate intermediate **I2** (i.e. ipso proton attached to ring nitrogen) has not been observed and reaction is rather direct to produce product. We did try to optimize **I2** structure but wave function consistently converged back to product for this step. So, from these entire results one can clearly see preference of doublet surface for all three substrates metabolized by P450, the rate determining barrier heights are comparable, only in the case of BPF reaction is barrierless after the formation of **I1** and at **I2** position optimization of the structure collapses to direct product. This shows BPF has highly short-lived intermediates and consecutive transition states that are not trapped during scan calcualtions. The BPA and BPZ energy profile is more or less same despite structural changes whereas BPF metabolism is highly exothermic. The spin densities, bond length, angles during the entire reaction for all three substrate were more or less same. All energies are mentioned in Table 4.2 and 4.3, for BPF and BPZ respectively.

Table 4.2: Relative internal energies, zero-point energies and free energies of all the complexes of BPF calculated theory (data in kcal/mol).

Compound	ΔE [kcal/mol, BS1]	ΔE+ZPE [kcal/mol, BS1]	ΔG [kcal/mol, BS1]	ΔE [kcal/mol, BS2]
^{2}Cpd I+BPF	0.10	0.01	0.33	0.00
^{4}Cpd I+BPF	0.00	0.00	0.00	0.07
^{2}RC	-3.49	-5.30	4.43	-2.80
^{4}RC	-4.27	-4.01	3.79	-3.80
^{2}TS1	12.70	12.86	25.16	11.70
^{4}TS2	14.51	14.64	26.67	12.53
^{2}I1	3.77	4.72	17.32	-2.77
^{4}I1	9.31	9.80	-21.50	1.87
^{4}TS2	17.94	16.31	27.50	-
^{4}I2	-35.67	-34.83	-23.41	-38.52
^{4}TS3	-33.70	-35.56	-23.96	-35.96
^{2}P	-46.10	-44.54	-33.94	-53.96
^{4}P	-49.36	-48.65	-38.94	-57.13

Table 4.3: Relative internal energies, zero-point energies and free energies of all the complexes of BPZ calculated theory (data in kcal/mol).

Compound	ΔE [kcal/mol, BS1]	ΔE+ZPE [kcal/mol, BS1]	ΔG [kcal/mol, BS1]	ΔE [kcal/mol, BS2]
^{2}Cpd I+BPZ	0.10	0.01	0.33	0.00
^{4}Cpd I+BPZ	0.00	0.00	0.00	0.05
^{2}RC	-12.79	-11.81	-0.79	-10.63
^{4}RC	-12.50	-11.86	-0.44	-10.49
^{2}TS1	12.79	12.82	25.69	11.20
^{4}TS1	14.70	14.80	28.00	12.83
^{2}I1	-10.15	-9.56	5.16	-17.89
^{4}I1	9.30	9.72	22.8	2.01
^{4}TS2	17.77	16.13	28.65	6.83
^{2}I2	-36.34	-35.26	-21.03	-38.10
^{4}I2	-32.95	-32.04	-19.26	-35.99
^{4}TS3	-30.60	-32.51	-19.27	-33.49
^{2}P	-50.26	-48.51	-35.47	-56.46
^{4}P	-44.81	-43.98	-33.87	-52.03

Below we have tried to show the investigated bond activation transition state structures of remaining two of the analogs of BPA viz BPF and BPZ which are shown in Figure 4.7. All the transition state structures depicted same electronic structure with the subsequent electron transfer from substrate moieties to a_{2u} orbital of the heme and spin density on the substrates depicted radical character. We can further confirm from the Figure 4.7, the orientation of substrates is sidewise, geometrically alike BPA transition state structure TS1. The electrophilic addition transition states shown in Figure 4.7, resembles in the barrier height with those reported above for BPA Figure 4.4. The barrier height for BPF was found to be 14.51 kcal/mol and 12.71 kcal/mol for quartet and doublet respectively. Similarly values for ^{2,4}TS1 for BPZ were found to be 14.70 kcal/mol and 12.79 kcal/mol for HS (LS). Above investigation suggests that substitutes of BPA which are used in the industry could show similar activation barrier heights in the formation of toxic metabolite catechol. The results give affirmation that similar biotransformation mechanism is used by P450s for analogues of BPA in the monohydroxylated metabolite formation for BPF and BPZ. Additionally, it was investigated from one of studies that hydroxycumyl alcohol (HCA) type structures were also formed from BPF and BPZ and they utilize same biotransformation mechanism like BPA (i.e. *ipso*-substitution reaction) [50]. Clearly from present investigations elucidation of the metabolic pathways and products should be emphasized during risk assessment of bisphenol analogues as they show similar reaction mechanism pattern and energies.

To further find rationale on obtained rate constants and the properties of the catalyst/oxidant which determines the reaction processes, we tried to find correlation of rate constants with the physicochemical properties of the substrate. Similar correlation

were previously done for the rate determining step of the hydrogen atom abstraction barrier by Cpd I, it is found that it correlates with the bond dissociation energy i.e. stronger the C-H bond, larger [47-52] will be the H-abstraction barrier height.

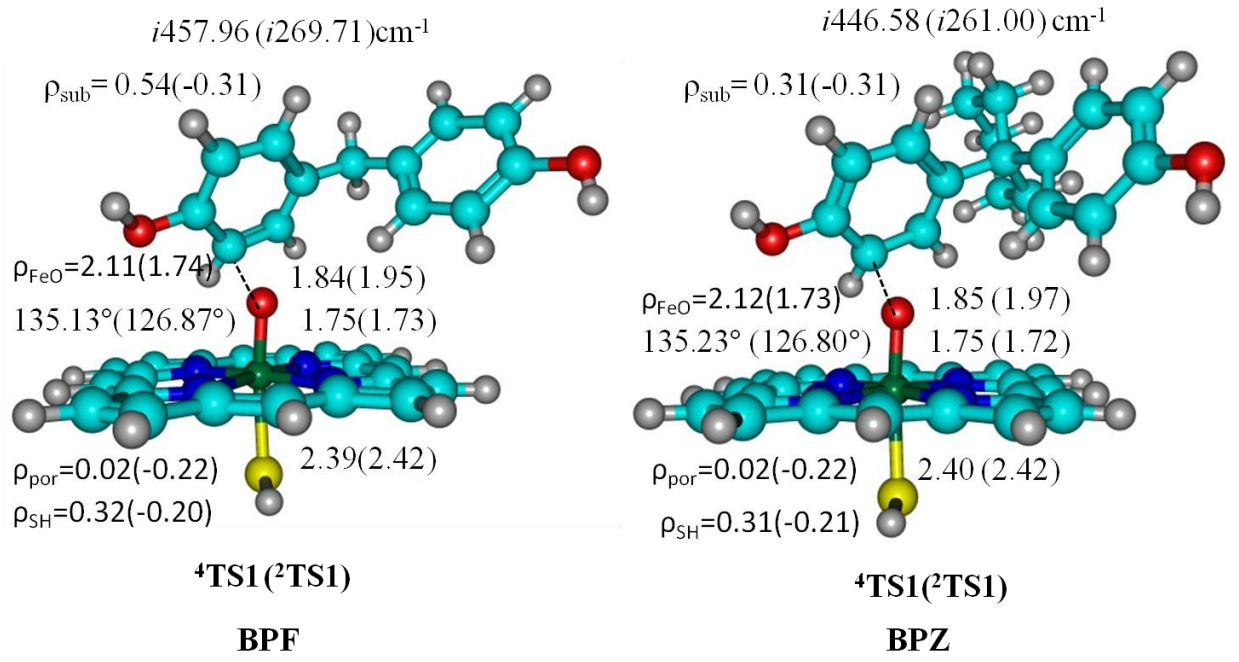

Figure 4.7: Optimized 3-D structures of bond activation transition state (i.e. C-O bond TS) at BS1 level of the theory of BPF and BPZ, the bond lengths are in Å, angle in degrees (°) and imaginary frequencies in wavenumber (cm^{-1}).

Whereas in case of aromatic hydroxylations mediated by iron oxo complexes barrier height correlates with the ionization energy (IE) of substrates [47,51]. Dependence of rate determining barrier on the IE of substrate is also observed for double bond epoxidation, just like aromatic hydroxylation. This implies that a substrate containing both arene and double bond group will preferentially activate aromatic hydroxylation rather than epoxide formation by double bond epoxidation. Table 4.4 displays the values of computationally calculated IE of different analogs of BPA with the activation energy of electrophilic

attack TS1 for doublet and quartet spin states respectively for various analogues. The value of activation are comparable as these are analogues of same base structure and so is our barrier heights which range within 1 kcal/mol difference for both HS and LS for all three compounds (BPA, BPF and BPZ) and is in accord to the rationale.

Table 4.4: Ionization energies of substrates (BPA, BPF, and BPZ) and rate determining barrier heights for two spin states doublet and quartet. All energy values reported in the Table are in kcal/mol.

Substrate	Ionization energies (IE)	Barrier height ($^2TS_1$)	Barrier height ($^4TS_1$)
BPA	163.15	12.92/11.34	15.69/13.48
BPF	169.42	12.71/11.70	14.51/12.53
BPZ	163.15	12.79/11.20	14.70/12.83

This correlation confirms our barrier heights to be true and justifies the values of ^{4,2}TS1 for BPA, BPF and BPZ which are coming comparable from our DFT calculations. As results were crosschecked at higher level of theory we clearly see a trend for doublet spin state. The values of ionization energies are not covering broad range so values of activation energy barrier are overlapping but direct dependence of them on the IE cannot be ruled out. These findings further allow us to predict the barrier heights for two remaining analogs of BPA.

4.3.2: Epoxidation of BPA

The energy profile for epoxidation mechanism of BPA with modeled Cpd I (SH) of P450 is illustrated in Figure 4.8. After the formation of reactant complex **(^{2,4}RC)**, the reaction

proceeds with the attack of Cpd I Fe=O moiety on the π system of the BPA to give O-addition radical intermediate (**^{2,4}Int)** via transition state TS_{CO}. Intermediated formation is further accompanied by ring-closure barrier **(^{2,4}TSrc)** to generate epoxide product **(^{2,4}P)**. Mostly the LS surface offers lower or no ring-closure barrier whereas HS surface provide substantial barrier [27]. The mechanism is stepwise just like aliphatic hydroxylation which offers initial rate determining H abstraction barrier [53-55]. Similarities in epoxidation and aliphatic hydroxylation mechanism are also seen in ring-closure barrier of epoxidation and rebound step of hydroxylation. Both these mechanism steps are much more feasible on LS surfaces and significant barrier is encountered on HS profile [56].

The reactant for HS/LS profile are close in energy with energy difference within 1kcal/mol with values 2.87/2.82 respectively, typical of TSR [57]. Fe=O group of BPA attacks the C5 position of benzene ring to yield intermediate (**^{2,4} Int**) with energy of 9.75/3.70 kcal/mol respectively via transition state for C-O bond formation step. The corresponding barriers heights for HS/LS were found to be 14.82/12.91 kcal/mol. This step is the highest energy step encountered in the entire reaction energy profile hence it is the rate-determining step of the reaction, The nature of intermediate was found to be radical type for HS (quartet) and cationic type for LS (doublet).

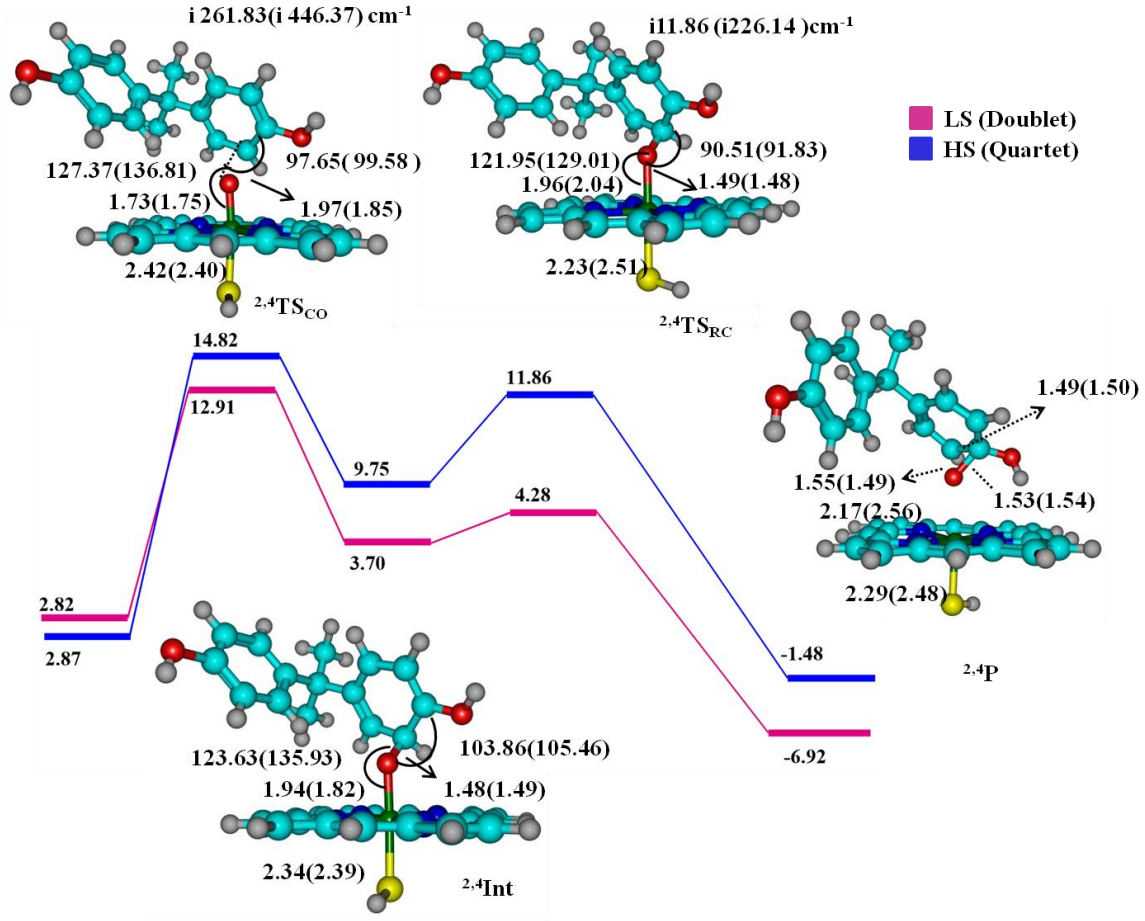

Figure 4.8: Free energy landscape of epoxidation mediated by P450 all energies reported are in kcal/mol, bond lengths in Å, bond angles in degree (°), and frequencies in wavenumber units. The energies depicted in Figure reported as LS (doublet)/HS (quartet) respectively. The energy is calculated using B3LYP/BS1 level of the theory.

Intermediate formation is followed by ring closure that takes place towards hydroxyl group containing carbon i.e. C4 carbon with barrier of 11.86/4.28 kcal/mol for HS/LS respectively. The ring closure barrier offered negligible barrier of >1kcal/mol on LS profile whereas large barrier is encountered on HS surface, homologous to previously

reported results on epoxidation. The product formed was exothermic in nature with respective energy values of -1.48/-6.92 kcal/mol for HS/LS. The results are in unison with previously reported results on C=C epoxidation [58-61].

In general quartet and doublet rate determining transition state structures are found to be within 2 kcal/mol, this could be ascertained to the same electron transfer processes, in accordance with the transfer of electron from substrate into a_{2u} orbital to generate radical type transition state with iron in oxidation state (IV). Two types of electron transfer processes are seen on different spin surfaces in intermediate formation. On HS (quartet) surface substrate donates one of its electrons to the porphyrin ring system with electronic reorganization $\delta_{x2-y2}^{*2}\ \pi_{xz}^{*1}\ \pi_{yz}^{*1}\ a_{2u}^{2}\ \varphi_{c}^{1}$ producing radical type character. On the other hand LS (doublet) surface was accompanied with two electron transfer, first to the a_{2u} orbital of ring to result closed porphyrin ring system and second electron of substrate is transferred to one of the Fe-O non-bonding orbital pairs $\pi_{xz}^{*}\ /\pi_{yz}^{*}$ with electronic configuration $\delta_{x2-y2}^{*2}\ \pi_{xz}^{*1}\ \pi_{yz}^{*2}\ a_{1u}^{2}\ \varphi_{c}^{0}$. Later type of electronic configuration observed is like electronic organization seen in product, hence intermediate on LS surface is like product. This could be the reason behind the large differences in energy of intermediates of HS and LS respectively. Since LS spin surface has acquired product configuration, the ring closure step of the reaction is nearly concerted analogous to previously reported studies on epoxidation. In contrast to LS, the ring-closure on HS suffers large ring-closure barrier due to migration of electron from substrate to the high energy anti-bonding orbital resulting in spin organization $\delta_{x2-y2}^{*2}\ \pi_{xz}^{*1}\ \pi_{yz}^{*1}\ \sigma_{z^2}^{*1}\ \sigma_{xy}^{*0}\ a_{2u}^{2}\ \varphi_{c}^{0}$. Electron transfer processes and their authenticity are also being investigated through spin densities and atomic charges depicted in Table 4.5.

Table 4.5: Mulliken charges and spin densities of BPA optimized at (B3LYP/BS1) level of the theory.

RC

	Spin densities					Charges				
	Fe	O	Por	SH	Sub	Fe	O	Por	SH	Sub
M2	1.19	0.90	-0.51	-0.57	0.00	0.28	-0.24	0.08	-0.13	-0.00
M4	1.06	0.90	-0.51	0.57	0.00	0.20	-0.21	0.13	-0.12	-0.00

TS1

	Spin densities					Charges				
	Fe	O	Por	SH	Sub	Fe	O	Por	SH	Sub
M2	1.54	0.19	-0.22	-0.20	-0.31	1.41	0.71	0.02	0.31	0.54
M4	0.45	-0.41	-0.34	-0.04	0.34	0.47	-0.41	-0.37	-0.01	0.31

INT1

	Spin densities					Charges				
	Fe	O	Por	SH	Sub	Fe	O	Por	SH	Sub
M2	1.04	0.03	-0.14	-0.02	0.07	0.36	-0.50	-0.48	-0.04	0.66
M4	1.98	0.31	-0.12	0.01	0.81	0.51	-0.51	-0.37	0.00	0.37

TS2

	Spin densities					Charges				
	Fe	O	Por	SH	Sub	Fe	O	Por	SH	Sub
M2	1.06	0.01	-0.11	-0.02	0.05	0.37	-0.49	-0.52	-0.03	0.67
M4	2.47	-0.01	-0.07	0.33	0.29	0.56	-0.50	-0.47	-0.17	0.58

PC

	Spin densities					Charges				
	Fe	O	Por	SH	Sub	Fe	O	Por	SH	Sub
M2	1.12	-0.00	-0.09	-0.03	0.00	0.34	-0.44	-0.52	0.02	0.59
M4	2.55	0.00	-0.01	0.45	0.00	0.56	-0.42	-0.48	-0.16	0.51

Initially for the reactant complex FeO moiety bears spin density nearly equal to 2, this depicts single occupation of electron in π^*_{xz} and π^*_{yz} anti-bonding orbitals, rest of the density is distributed on porphyrin and axial ligand, substarte φ_c is filled so it shows zero spin density value. These spin density values represent total three unpaired electrons

which couples in ferromagnetic or anti-ferromagnetic manner to form doublet and quartet. As we move towards C-O bond formation transition state and see in Table 1 the spin density on porphyrin and axial ligand decreases and substrate develops spin density depicting radical character of substrate in transition state for both LS/HS. At intermediate quartet spin, density clearly shows all three unpaired electron are distributed on FeO moiety and substrate, but in doublet state (LS), densities on oxygen (O), porphyrin and substrate disappears indicating single unpaired electron and hence confirms product like electronic configuration at intermediate itself. Spin densities of the second transition state involved in the reaction i.e. ring-closure barrier step shows value of nearly 3 on FeO moiety and decline of density on substrate. Product reduction can be ascertained with changes in the oxidation state of iron from Fe (IV) to Fe (III), same can be inferred from the values. The quartet and doublet spin surfaces are associated with barrier heights that are genuine transition states (TS) with single imaginary frequency (i261.83 cm^{-1} and i446.37 cm^{-1}) for doublet (11.91 kcal/mol) and quartet (12.82 kcal/mol) spin states, respectively. This step of the reaction mechanism is rate determining step, followed by a radical intermediate (IM) on quartet and cationic intermediate on doublet. Successive to intermediate complex barrier in ring-closure step on quartet surface suffers large barrier with ^{4}TSrc imaginary frequency (i226.14 cm^{-1}) and nearly barrier-less formation of product on doublet surface. In the profile we see energy >1 kcal/mol is required for crossing the ring-closure barrier on LS having a very small imaginary frequency (i11.86 cm^{-1}) suggesting flat TS. These results are reminiscent to preceding studies on epoxidation whereby LS surface offers barrierless product formation from both radical type and cationic intermediate [59, 62]. After having had depicted the electronic

organization of the reaction on both spin states, let us further investigate into the geometrical features of the complexes encountered in the reaction pathway. Geometries of the complexes shown in Figure 4.8 depicts that the transition state of the C-O bond formation are early with C….O bond distances of 1.97 (1.85) Å for LS and HS surfaces respectively. The bond length of C-O bond reduces to 1.48 (1.49) Å for LS (HS) in intermediate complex. Decrease in bond angle both <FeOC and <CCO is accompanied in the ring closure transition state ^{2,4}TSrc on both spin states. The FeOC bond angle decreases to 121.95° (129.01°) from 123.63° (135.93°) for doublet (quartet) respectively, along with decrease in CCO bond angle to 90.51° (91.83°) from 103.86° (105.46°) moving along intermediate to ring-closure TS.

Table 4.6: Relative internal energies, zero-point energies and free energies of all the complexes obtained during epoxidation of BPA, calculated theory (data in kcal/mol).

Compound	**ΔE [kcal/mol, BS1]**	**ΔE+ZPE [kcal/mol, BS1]**	**ΔG [kcal/mol, BS1]**	**ΔE [kcal/mol, BS2]**
^{2}Cpd I+BPA	0.10	0.01	0.33	0.00
^{4}Cpd I+BPA	0.00	0.00	0.00	0.06
^{2}RC	-2.82	-2.76	6.20	-2.37
^{4}RC	-2.87	-2.66	6.44	-2.14
^{2}TS1	12.81	13.04	26.45	11.34
^{4}TS1	14.72	14.96	28.23	12.96
^{2}I1	3.60	4.61	18.45	-2.92
^{4}I1	9.65	10.16	23.06	2.42
^{2}TS2	4.18	5.03	19.80	-3.07
^{4}TS2	11.76	11.44	24.24	3.80
^{2}PC	-7.02	-5.71	8.027	-17.08
^{4}PC	-1.58	-1.70	9.103	-14.08

To determine that results are not dependent on the choice of basis set single point energy calculations were performed for all complexes on higher basis set LACV3P/6-31G* (BS2). Also to test the effect of protein environment on the barrier heights and energy values of intermediates solvent corrections were performed in dielectric constant ϵ=5.7 mimicking chlorobenzene. All energy values reciprocated the energy profile, with step-wise mechanism; these results are tabulated in Table 4.6. The HS surfaces undergo two transition states with the formation of epoxide product while the LS surface experiences single transition state. The C-O bond formation is the rate determining step of the reaction in both BS2 calculated results and also in solvent phase. Also it can be clearly seen that cationic intermediate on LS profile acquires stable energy in solvent than BS1, this behavior is in agreement with previous findings [59].

4.4: Conclusions

Quantum mechanical calculation performed on monohydroxylation reactions of Bisphenol (BPA) and it analogues (BPF and BPZ) catalyzed by cytochrome P450 revealed similar barrier heights and potential energy landscape. Results were found adequate and trends were confirmed when subjected to the higher level of the theory for each set of compound. The theoretical investigation of the aromatic hydroxylation mechanism mediated by P450 reveals that LS surface is more facile over HS. The rate-determining step of the reaction was found to be the electrophilic addition step for all compounds subjected to investigation. Also, the approach of the substrates was found sidewise to oxidant in all transition states ^{4,2}TS1. Bond activation transition states were found to be dependent on the ionization energies of the substrates; clearly this can be used as a parameter to find the barrier heights of other analogues of bisphenols.

Epoxidation via P450 is a two-step process with O addition as first and ring-closure as second step, subsequently leading to the formation of the epoxide product. The rate-determining step of the reaction i.e., C-O bond formation step (or O-addition step) on LS surface experiences lower energy barrier in comparison to HS surface. While moving towards second step of the reaction, LS state offers negligible barrier to product formation whereas large barrier is encountered on HS state, this is suggestive that LS state is mainly responsible for epoxidation of BPA. Also, the values of energies of the reaction mechanism were found adequate at higher basis set and subsequent solvent corrections. Epoxides being highly unstable species are difficult to be directly detected in experiments. DFT based calculations provide an alternative in intriguing the epoxidation reaction mechanism of BPA. The results have given fruitful insights in understanding the epoxidation of BPA and its toxicity prediction; these results will be further helpful in exploring the reactivity and toxicological effects of BPA.

References:

[1] J.H. Kang, F. Kondo, Y. Katayama, *Toxicology*, **226,** 79 (2006).

[2] J. I. Cacho, N. Campillo, P. Viñas, M. Hernández-Córdoba, *J. Chromatogr. A*, **1247,** 146 (2012).

[3] L. N. Vandenberg, R. Hauser, M. Marcus, N. Olea, W. V Welshons, *Reprod. Toxicol.*, **24,** 139 (2007).

[4] T. Geens, *et al.*, *Food Chem. Toxicol.*, **50,** 3725 (2012).

[5] J. R. Rochester, *Reprod. Toxicol.*, **42,** 132 (2013).

[6] J. M. Barroso, *Off. J. Eur. Union*, **26,** 11 (2011).

[7] "European Commission. Commission Regulation (EU) 2018/213 on the use of bisphenol A in varnishes and coatings intended to come into contact with food and amending Regulation No 10/2011 as regards the use of that substance in plastic food.," (2018).

[8] "Food and Drug Administration (FDA). Indirect Food Additives: Polymers," **77,** 41899 (2012).

[9] M. T. García-Corcoles, M. Cipa, R. R. Gomaze, A. Rivas, F.O. Serran, J. L. Vilchez, A.Z. Gomaze, *Talanta*, **178,** 441 (2018).

[10] S. Kitamura, T. Suzuki, S. Sanoh, R. Kohta, N. Jinno, K. Sugihara, *Toxicol. Sci.*, **84,** 249 (2005).

[11] G. Ginsberg, D. C. Rice, *Environ. Health Perspect.*, **117,** 1639 (2009).

[12] G. M. Pacifici, M. Kubrich, L. Giuliani, M. de Vries, A. Rane, *Eur. J. Clin. Pharmacol.*, **44,** 259 (1993).

[13] N. Quesnot, S. Bucher, B. Fromenty, M. A. Robin, *Chem. Res., Toxicol*, **27**, 1463 (2014).

[14] S. Nakamura, Y. Tezuka, A. Ushiyama, C. Kawashima, Y. Kitagawara, K. Takahashi, S. Ohta, T. Mashino, *Toxicol. Lett.*, **203**, 92 (2011).

[15] S.Yoshihara, T. Mizutare, M. Makishima, N. Suzuki, N. Fujimoto, K. Igarashi, S. Ohta, *Toxicol Sci.*, **78**, 50 (2004).

[16] D. Gramec Skledar, and L. Peterlin Masic, *Environ. Toxicol. Pharmacol.*, **47**, 182 (2016).

[17] J. Schmidt, P. Kotnik, J. Trontelj, Z. Knez, and L. P. Masic, *Toxicology in Vitro*, **27**, 1267 (2013).

[18] J. S. Edmonds, M. Nomachi, M. Terasaki, and M. Morita, *Biochem. Biophys. Res. Commun.*, **319**, 556 (2004).

[19] J. Hu, Y. Cai, W. Li, G. Liu, Y. Tang, *Mol. Inf.*, **2020**, 39, 1900178.

[20] F. P. Guengerich, *Chem. Res. Toxicol.*, **14,** 6, (2001).

[21] P. F. Fitzpatrick, *Biochemistry*, **42,** 14083 (2003).

[22] P. R. Oritz de Montellano, *In Cytochrome P450: Structure, Mechanism, and Biochemistry*, 2nd ed. New York: Plenum Press, (1995).

[23] R. Ullrich, M. Hofrichter, *Cell. Mol. Life Sci.*, **64**, 3, 271 (2007).

[24] S. Shaik, S. Cohen, Y. Wang, H. Chen, D. Kumar, W. Thiel, *Chem. Rev.*, **110**, 949 (2010).

[25] V. Postils, M. Saint-Andre, A. Timmins, X.X. Li, Y. Wang, J.M. Luis, M. Sola, S.P. de Visser, *Int. J. Mol. Sci.*, 19, 1974 (2018).

[26] Z. Fu, Y. Wang, J. Chen, Z. Wang, X. Wang, *Environ. Sci. Technol.*, **50**, 8155 (2016).

[27] L. Ji, *Chem. Res. Toxicol.*, **33**, 1539 (2020).

[28] G. Ma, H. Yu, T. Xu, X. Wei, J. Chen, H. Lin, G. Schuurmann, *Environ. Sci. Technol.* ,**52**, 11838 (2018).

[29] S. Shaik, D. Kumar, S. P. de Visser, A. Altun, W. Thiel, *Chem. Rev.*, **105**, 2279 (2005).

[30] L. Ji, S. Ji, C. Wang, K. P. Kepp, *Environ. Sci.Technol.*, **52**, 4422 (2018).

[31] D. Kumar, P. De Visser, S. Shaik, *J. Am. Chem. Soc.*, **125**,13024 (2003).

[32] Y. A. R. Hussain, R. Yadav, M. Ahmed, T. A. Khan, D. Kumar, *J. Comput. Chem.*, **41**, 330, (2020).

[33] D. J. Frisch, M. J. Trucks, G. W. Schlegel, H. B. Scuseria, G. E. Robb, M. A. Cheeseman, J. R. Scalmani, G. Barone, V. Mennucci, B. Petersson, G. A. Nakatsuji, H. Caricato, M. Li, X. Hratchian, H. P. Izmaylov, A. F. Bloino, J. Zheng, G. Sonnenb, Official Gaussian 09 Literature Citation, (2009).

[34] P. J. Hay, W. R. Wadt, P. J. Hay, W. R. Wadt, J. Chem. Phys., **82**, 270 (1985).

[35] D. Kumar, B. Karamzadeh, G. N. Sastry, S. P. de Visser, J. Am. Chem. Soc., **132**, 7656 (2010).

[36] S. P. de Visser, D. Kumar, S. Cohen, R. Shacham, S. Shaik, *J. Am. Chem. Soc.*,

126, 8362 (2004).

[37] F. Ogliaro, N. Harris, S. Cohen, M. Filatov, S. P. de Visser, S. Shaik, *J. Am. Chem. Soc.*, **122,** 8977 (2000).

[38] T. Kamachi, K. Yoshizawa, *J. Am. Chem. Soc.*, **125,** 4652 (2003).

[39] S. Shaik, S. Cohen, S. P. deVisser, P. K. Sharna, D. Kuamr, S. Kozuch, F. Ogliaro, D. Danovich, *Eur. J. Inorg. Chem.*, **2004**, 207 (2004).

[40] C. Hazan, D. Kumar, S. P. De Visser, S. Shaik, *Eur. J. Inorg. Chem.*, 2966 (2007).

[41] S. P. de Visser, S. Shaik, *J. Am. Chem. Soc.*, **125,** 7413 (2003).

[42] C. M. Bathelt, L. Ridder, J. Mulholland, J. N. Harvey, *Org. Biomol . Chem.*, **2**, 2998 (2004).

[43] M. T. Green, *J. Am. Chem. Soc.*, **121,** 7939 (1999).

[44] S. P. de Visser, S. Shaik, P. K. Sharma, D. Kumar, W. Thiel, *J. Am. Chem. Soc.*, **125,** 15779 (2003).

[45] C. M. Bathelt, A. J. Mulholland, J. N. Harvey, *J. Phys. Chem. A*, **112,** 13149 (2008).

[46] J. C. Schöneboom, H. Lin, N. Reuter, W. Thiel, S. Cohen, F. Ogliaro, S. Shaik, *J. Am. Chem. Soc.*, **124,** 8142 (2002).

[47] S. Shaik, S. P. deVisser, F. Ogliaro, H. Schwarz, D. Schro¨der, *Curr. Opin. Chem. Biol.*, **6**, 556 (2002).

[48] M. Asaka, H. Fujii, *J. Am. Chem. Soc.*, **138,** 26, 8048 (2016).

[49] D. Kumar, G. N. Sastry, S. P. De Visser, *J. Phys. Chem. B*, **116,** 718 (2012).

[50] S. P. deVisser, D. Kumar, Ed., *Iron-containing enzymes: versatile catalysts of hydroxylation reactions in nature*. RSC Publishing, (2011).

[51] F.G. Cantu-Reinharrd, M.A. Sainna, P. Upadhayay, A. Balan, D. Kumar, S. Fornarini, M.E. Crestoni, S.P De Visser, *Chem. Eur. J.*, **22,** 18608 (2016).

[52] J. Schmidt, P. Kotnik, J. Trontelj, Z. Knez, L. P. Masic, *Toxicol. In Vitro*, **27,** 1267 (2013)

[53] S. Shaik, P. Milko, P. Schyman, D. Usharani, *J. Chem. Theory Comput.*, **7,** 327 (2011).

[54] J. M. Mayer, *Annu. Rev. Phys. Chem.*, **55,** 363 (2004).)

[55] B. Meunier, S. P. deVisser, S. Shaik, *Chem. Rev*. **104**, 3947 (2004).

[56] J. Zhang, L. Ji, W. Liu, *Chem. Res. Toxicol*, **28**, 1522 (2015).

[57] S. P. de Visser, F. Ogliaro, N. Harris, S. Shaik, *J. Am. Chem. Soc.*, **123**, 3037 (2001).

[58] S. P. de Visser, F. Ogliaro, S. Shaik, Angew. Chem. Int. Ed., **40**, 2871 (2001).

[59] S. P. de Visser, F. Ogliaro P. K. Sharma, S. Shaik, *J. Am. Chem. Soc.*, **124**, 11809 (2002).

[60] S. P. de Visser, D. Kumar, S. Shaik, *J. Inorg. Biochem.*, **98**,1183 (2004).

CHAPTER-5

EQUATORIAL LIGAND EFFECTS ON THE RATE OF HYDROGEN ABSTRACTION BARRIERS BY IRON (IV)=OXO SPECIES OF N4PY

CHAPTER-5

EQUATORIAL LIGAND EFFECTS ON THE RATE OF HYDROGEN ABSTRACTION BARRIERS BY IRON (IV)=OXO SPECIES OF N4PY

5.1: Introduction

Metal containing enzymes are responsible in the biosynthesis of life sustaining compounds and also in the metabolism and biodegradation of harmful compounds [1-6, 7-11]. Short lived intermediate species makes the studies of enzyme catalyzed reaction mechanism a challenging endeavor. Therefore, recognition of the active species involved in the biotransformation and also the features of the active site that governs and affects the rate-determining step is sometimes unclear. In order to completely understand functional properties of these metal containing enzymes (active sites), synthetic models that mimic the actual enzyme (known as biomimetic models) are developed. These models comprise of metal centre embedded inside coordination environment which resembles with actual enzyme and are dissolved in organic solvents [12-14]. These biomimetic models provide vital information regarding the catalytic cycle and operational mode of the biological systems. Diverse reports are present in the literature for fine tuning the properties of high valent metal oxo intermediates through primary coordination sphere and affects it subjects on the reactivity, spin-state ordering of the metal atom etc [15-19]. Changes in the primary coordination sphere are quite dramatic,

hence a notion is put forward that modifications in the secondary coordination sphere should be subtle [20-22].

Mostly biomimetic models consist of mononuclear metal centre embedded inside ligand scaffolds and pentadentate ligands have turned to be popular because they usually generate few isomeric structures. One such N5 based pentadentate ligand that has been extensively studied is N4PY [23-26] {N, N-bis (2-pyridylmethyl)-N bis (2-pyridyl) methylamine}. In its iron (IV)-oxo form, i.e. $[FeIV(O)(N4Py)]^{2+}$ complex have four nitrogen donar atoms (N_{eq}) which are perpendicular to the iron(IV)-oxo axis and axially ligated nitrogen atom of amine which is trans to the oxo group. This ligand framework offers bowl like cavity for the iron atom as well as to the substrates involved in the reaction mechanism. In successive years, Fe (IV)-oxo complex of N4PY (1b) have been successfully characterized and well studied which makes it a suitable candidate to study the effect of ligand substitution on the electronic properties and its reactivity. It was synthesized by Feringa and Que [27] and it was one of the first iron(IV)-oxo biomimetic species that was characterized by UV-vis, Mossbauer, resonance Raman, electron paramagnetic resonance, nuclear magnetic resonance (NMR) and also through X-ray crystallography [25]. In addition to this, different reactivity studies with varying substrates have also been done which concluded that it reacts via oxygen tom transfer [29].

Particularly ortho-substitution of the pyridine rings is a well practiced strategy that can significantly affect the iron (IV)-oxo core as it makes equatorial Fe-N bond weak. Hence to get more insights into the effect of equatorial ligand perturbations on the non-heme biomimetic model system iron (IV)-oxo species, several models are designed and

computed in the present work. The ortho-position of frontal and backward pyridine rings here are substituted with the light methyl groups viz 2b and 3b. The reactivity of the models with the substrate ethybenzene was explored using computational techniques.

5.2: Methodology

5.2.1: Models

All the complexes (biomimetic catalyst) used in the present study are discussed below and are shown in the Scheme 5.1. The unsubstituted ligand N4PY is **[**N, N-bis (2-pyridylmethyl)-N bis (2-pyridyl) methylamine], its active intermediate responsible for the hydrogen atom abstraction (HAA) and oxygen atom transfer (OAT) reactions is $[FeIV(O)(N4Py)]^{2+}$, this catalyst is referred in present investigation as **1b**. Substitution changes are performed on the 6^{th} position of the pyridine ring systems of the N4PY ligand framework. The two pyridine rings which are connected through the methylene carbon are substituted by the methyl group, this ligand framework is named as 2(6-^{Me}Py)N_{ax}2Py or MeN4Py. The active oxidant is $[FeIV(O)(^{Me}N4Py)]^{2+}$, this is referred as **2b**. The **3b** complex consists of substitution on the two other pyridine rings which are connected with the two methine carbon, this sort of engineering is rarely reported in the literature. This ligand framework is named as 2PyN_{ax}2(6-^{Me}Py) or N4Py^{Me}, its active intermediate is $[FeIV(O)(N4Py^{Me})]^{2+}$.

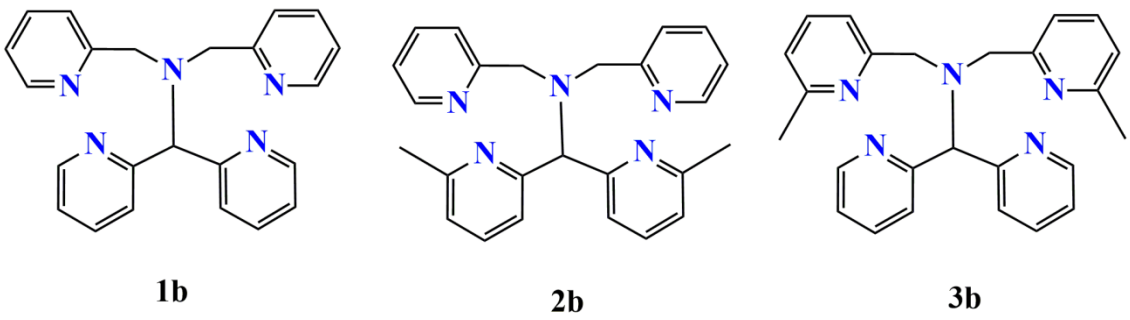

Scheme 5.1 Schematic models of 1b, 2b and 3b oxidants that are used in the present study

5.2.2: Computational Methods

Quantum mechanical calculations were computed using Gaussian 09 [30] software implementing Density Functional Theory (DFT). The above discussed models of N4PY that are basically Fe (IV)=O species are used for the investigation. Two of the lowest energy spin states are taken into consideration while performing calculations, low-lying triplet with S=1 and high-lying quartet state having spin S=2. The calculations were performed using DFT functional B3LYP along with split basis set. For iron atom LANL2DZ basis set with double zeta effective core potential was used and for the remaining of the atoms (C, H, N,O and S) 6-31 G basis set was used i.e. (BS1) [31]. All the structures were optimized in gas phase and relaxed potential energy scans (PES) were set for finding hydrogen abstraction rates for three models viz **1b**, **2b** and **3b**. To ascertain structures as minima and saddle point, analytic frequency calculations were also subjected. Corresponding to transition state, single imaginary frequency with correct mode was obtained and real frequencies were found for reactants and intermediates for all models with ethylbenzene as substrate.

In order to analyze the effect of solvent on the reaction rate of the models, all the calculations performed in the gas phase were repeated in solvent with geometry optimization, PES and frequency calculations. Solvent calculations were performed using polarizable continuum model (PCM) with dielectric constant (ϵ = 35.688) mimicking acetonitrile solvent.

5.3: Results and Discussions

5.3.1: Orbital occupation

To completely understand the rate-enhancement of 2b and 3b over 1b in hydrogen atom abstraction from the C-H bond of substrate, Density Functional Theory (DFT) calculations were used that are previously benchmarked from the experimental rate constants of $[FeIV(O)(N4Py)]^{2+}$ [32-34]. The methods and procedures that are utilized in the present study reproduce the experimentally found free energies of activation within 3 kcal/mol [35, 36]. Over 50 different methods and basis sets validated the accuracy of the basis set B3LYP/BS1 both in gas phase and solvent is one of the best methods for such systems [34]. Furthermore, for bifurcation pathways that leads to the multiple products, correct product distributions of reactivities was found for the of non-heme iron(IV)-oxo complexes and hence accurate transition state ordering was predicted by the methods used [37,38].

We should first attain familiarity with electronic and structural configuration of **1b** i.e. $[N4Py][Fe(IV)=O^{2+}$ for the triplet and quintet spin states. The ground state was found to be the triplet spin state and quintet spin state lies 13.25 kcal/mol above it. The orbital diagram of $[N4Py][Fe(IV)=O^{2+}$ is shown in Figure 5.1. The d block of metal splits into

the three below two pattern which is reminiscent of distorted octahedron. Group of three orbitals consists of lowest lying δ orbital and two antibonding pairs of π^* orbitals formed with interaction of Fe ($d\pi$)-O ($p\pi$). Coming to group of two orbitals; it consists of σ^* antibonding orbitals arising due to combination of lone pairs of equatorial nitrogen and other due to interaction of the two axial ligands. Iron atom remain in oxidation state of IV, the d block comprise four electrons.

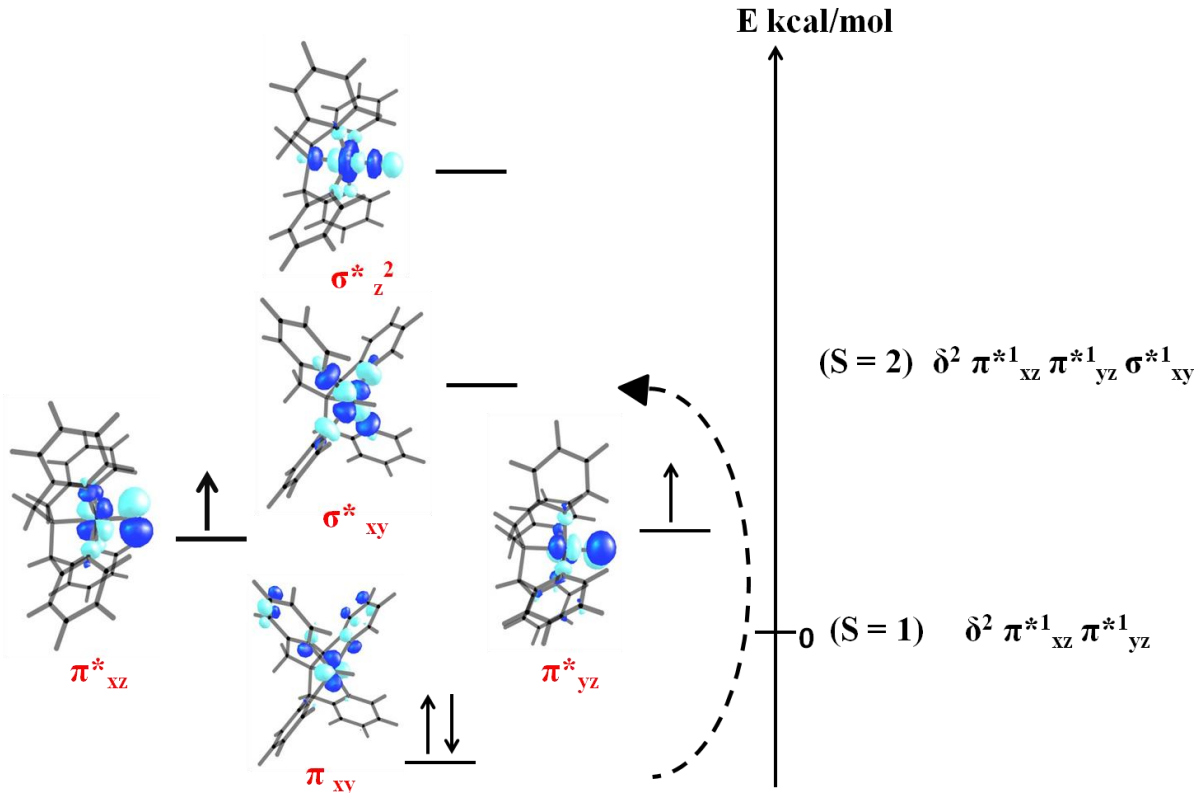

Figure 5.2: Key orbitals of [N4Py][Fe(IV)=O^{2+} complex with two low-lying spin states, arranged in increasing order of energy.

The ground state is triplet with spin quantum number S=1 having electronic configuration $\delta^2_{x2-y2}\ \pi^{*1}_{xz}\ \pi^{*1}_{yz}$ and second low-lying state above triplet is quintet with spin quantum number S=2 and electronic configuration $\delta^1_{x2-y2}\ \pi^{*1}_{xz}\ \pi^{*1}_{yz}\ \sigma^{*1}_{z^2}$ The energy

of quintet relative to triplet is a balance between larger orbital energy gap of δ to σ^*_{xy} that is determined by N-Fe bond strength favoring S=1, and five d-d interaction favors S=2. This leads to the small energy gap between two and hence makes the way for TSR reaction mechanism.

5.3.2: H-abstraction barrier rate of 1b

Investigation of rate of hydrogen abstraction with **1b** with ethyl benzene as substrate was performed, the reaction energy profile is shown in Figure 5.3 along with the structures of the species involved. As per the previously reported results the ground state of the complex was triplet and quintet state lies well separated from the ground state. The relative energy of reactant complex formation with that of isolated oxidant complex [N4Py][Fe(IV)=O^{2+} [39,40] was found to be -5.75 kcal/mol for the triplet spin and 7.46 kcal/mol for the quintet spin state. As the reaction proceeds towards the hydrogen abstraction step spin crossover was observed. Now the quintet state lies lower than triplet state at the transition state geometry. The barrier heights were found to be 9.36 kcal/mol on the low spin (LS) triplet surface and 8.02 kcal/mol for the high-spin (HS) quintet surface.

The intermediate complex formation has energy value of -4.57 and -5.85 kcal/mol for the triplet and quintet spin state respectively. A frequency calculation reveals reactant and intermediate complex as minima with real frequencies. Whereas in case of transition state structures single imaginary frequency for correct mode is observed. The frequencies were found to be i1449.74 cm^{-1} and i245.99 cm^{-1} for the LS and HS respectively. These results are reminiscent of the previously reported findings with N4PY as oxidant on the range of substrates [40,41]. Thereafter, all the calculations were further performed in solvent, here

acetonitrile with dielectric constant (ϵ = 35.688). The values can be seen from the reaction profile, addition of solvent has increased the energies.

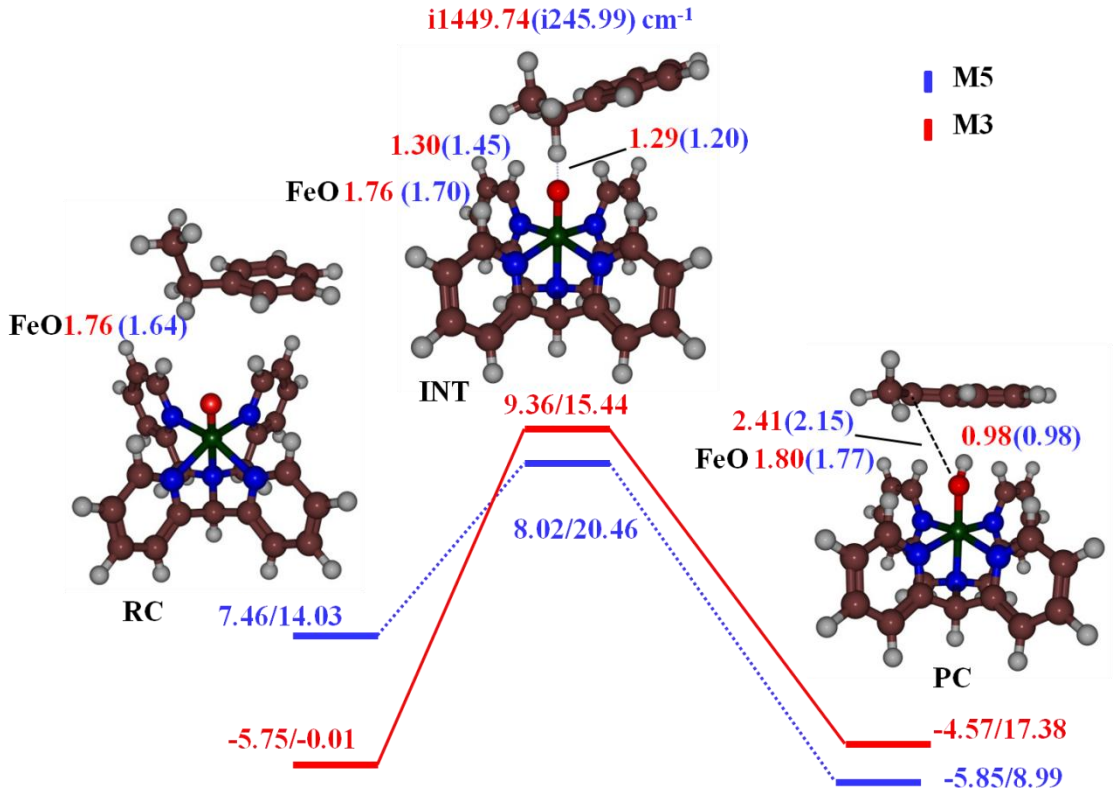

Figure 5.3: Potential energy landscape of H-abstraction barrier heights from ethyl benzene by **1b** for triplet/quintet spin states. The energy are calculated at the B3LYP/BS1//B3LYP/BS1(solv) level of the theory. All energy values are reported are in kcal/mol, frequencies in wavenumber (cm^{-1}), and bond lengths in Å.

5.3.3: H-abstraction barrier rate of 2b

Electronic structure of the 2b was found to similar as that of 1b. Here also, the ground state was found to be the triplet spin state and quintet spin state lies 7.65 kcal/mol above

it. Although, this difference has been decreased, compared to **1b**. Rate of hydrogen abstraction for **2b** was also performed on same substrate ethylbenzene, energy profile is shown in Figure 5.4. A change done in ligand environment by light methyl groups has not perturbed the spin state ordering. Triplet is the ground state and quintet lies above it with substantial difference, similar to the unsubstituted N4PY system **1b**. Gas phase barrier on the triplet spin surface is 12.56 kcal/mol and for the quintet surface is 7.02 kcal/mol. The imaginary frequency was found to be i1576.84 and i90.08 cm^{-1}. With the inclusion of solvent the barrier rises to 19.10 kcal/mol, for the triplet and 17.67 kcal/mol. With the inclusion of solvent the barrier rises to 19.10 kcal/mol, for the triplet and 17.67 kcal/mol for the quintet. Hence, from the values obtained for both gas phase and solvent phase, calculations depict spin cross-over. With the formation of the intermediate complex, the energy gets lower with the values for triplet/quintet state respectively.

Decreased energy gap between ground state triplet and the quintet could possibly enhance the reactivity of the system dramatically. This can also be inferred from the data obtained after calculations. The barrier height has been reduced by 1 kcal/mol on the quintet spin state.

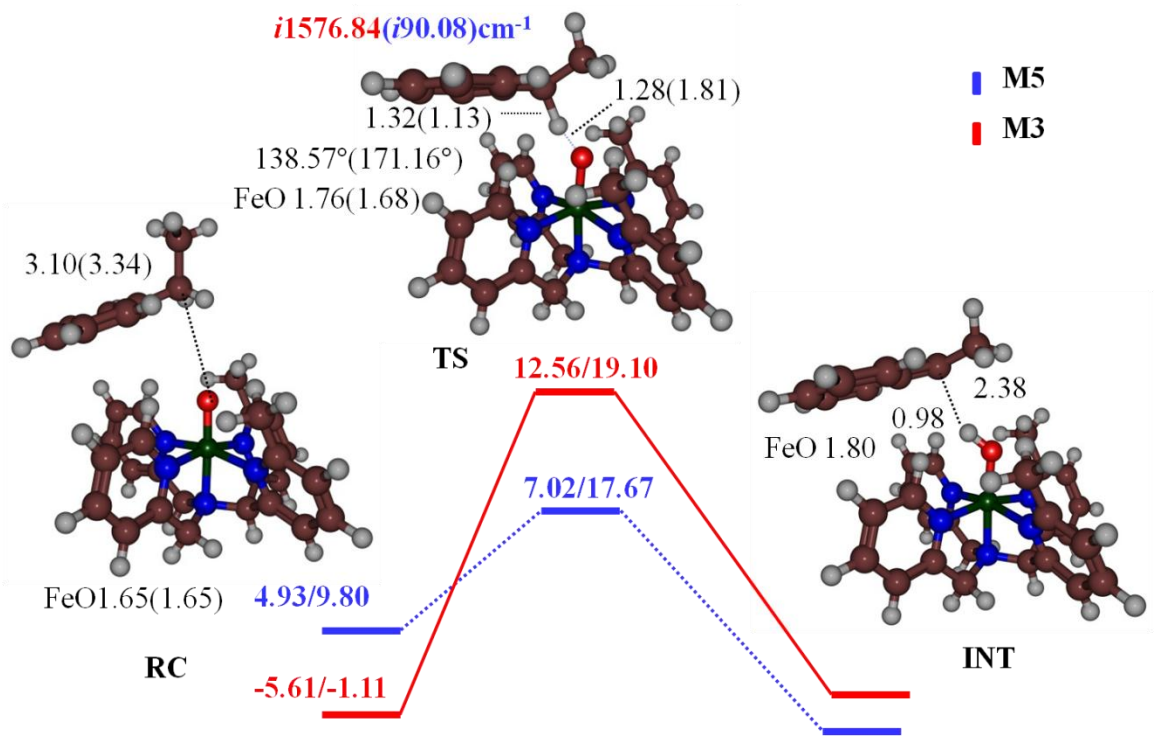

Figure 5.4: Potential energy landscape of H-abstraction barrier heights from ethyl benzene by **2b** for triplet/quintet spin states. The energy are calculated at the B3LYP/BS1//B3LYP/BS1(solv) level of the theory. All energy values are reported are in kcal/mol, frequencies in wavenumber (cm^{-1}), and bond lengths in Å.

5.3.4: H-abstraction barrier rate of 3b

The ground state of the biomimetic complex remains to be the triplet and quintet lies 16.93 kcal/mol higher. The H-abstraction barrier heights in gas phase were found to be 9.68 kcal/mol on the triplet spin surface and 4.57 kcal/mol on the quintet spin surface. The **3b** complex shows least H-abstraction barrier on the quintet spin surface compared to both **1b** and **2b**. The transition states show large single imaginary frequency for the correct mode with values *i*94.51 cm^{-1}. The intermediate complex stabilizes the energy to

lower values of energy -4.10 kcal/mol and -5.11 kcal/mol for triplet/quintet respectively. Further on the addition of solvent the barrier rises to 16.64 kcal/mol and 14.40 kcal/mol for triplet and quintet spin surface. However the spin-crossover and spin state ordering remains conserved with the incorporation of solvent

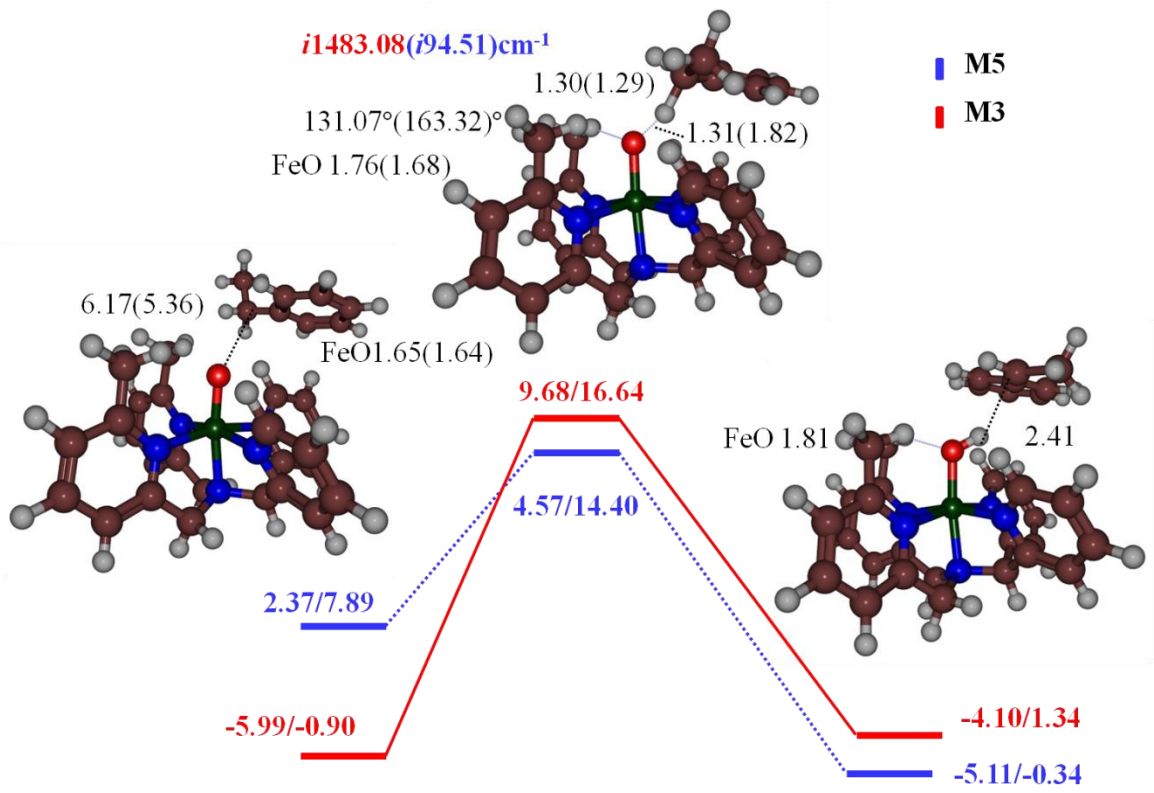

Figure 5.5: Potential energy landscape of H-abstraction barrier heights from ethyl benzene by **3b** for triplet/quintet spin states. The energy are calculated at the B3LYP/BS1//B3LYP/BS1(solv) level of the theory. All energy values are reported are in kcal/mol, frequencies in wavenumber (cm^{-1}), and bond lengths in Å.

The optimized geometry of all the complexes viz **1b**, **2b** and **3b** in the triplet and quintet spin state is shown in Figure 5.5. For all the complexes triplet spin state is the ground state and the quintet is well above separated from the ground state triplet. Experimental Mössbauer and EPR studies depict, **1b** as a triplet Fe (IV) oxo species, which is the case

with the rest of the substituted system. Clearly, there is a change in the triplet-quintet energy-gaps but spin state ordering remains the same. Previously done DFT studies on the $[FeIV(O)(N4Py)]^{2+}$ system report LS-HS energy gap more than 4 kcal/mol, this matches well with our studies [32,42]. Analysis of the geometrical features of the system for all complexes reveals that the Fe-O distances in **2b** and **3b** complexes are precisely same with the **1b** complex. These distances are in analogy with the previously reported bond lengths and vibrations from theoretical calculations and also crystal structure distances of iron(IV)-oxo complexes [44-46,47,48]. No major differences in the average Fe-N_{eq} are seen upon the substitution of methyl groups onto pyridine rings. Similarly Fe-N_{ax} bond lengths are also similar. However, we see a modest bend in the O-Fe-N_{ax} bond angle of ^{3,5}**3b** for triplet 172° and for quintet 174°. Weak interactions between the methyl hydrogen atoms and the oxo group are also observed for a distance 2.0 Å - 2.4 Å in ^{3,5}**2b** and ^{3,5}**3b** complexes.

Investigation of the HAA step from ethyl benzene as a substrate for all three complexes **1b**, **2b** and **3b** depicts that the **3b** complex is the better oxidant of all and offers fast hydrogen transfer with a lower energy barrier. Substrate approach towards iron(IV)-oxo species is changed in both the substituted systems. In case of ^{3,5}2b the substrate tries to access the oxo group from left whereas in ^{3,5}3b substrate enters from right hand side.

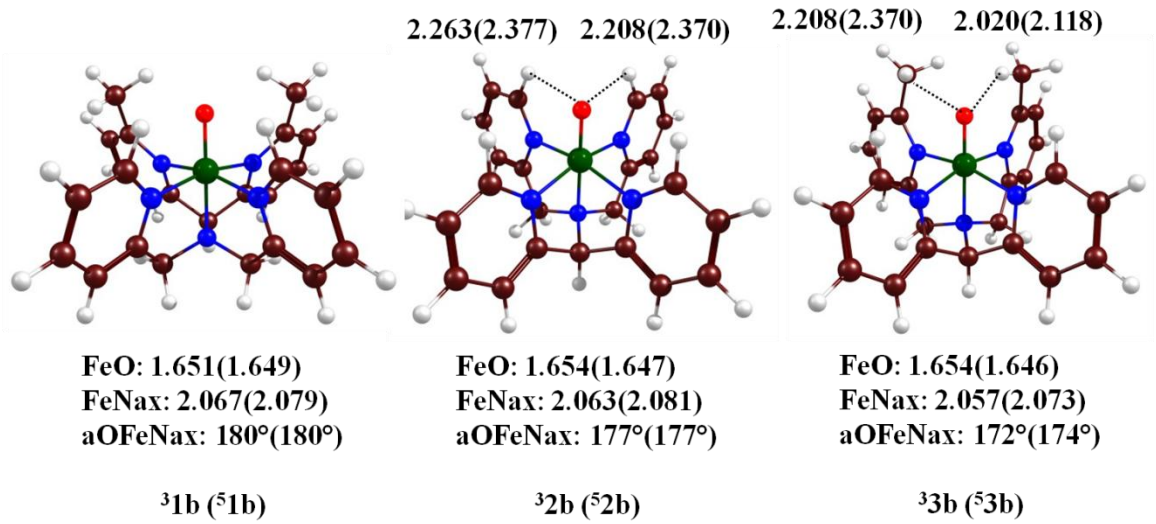

Figure 5.6: Optimized geometry of 1b, 2b and 3b complex for the triplet (quintet) respectively. The geometries are optimized at B3LYP/BS1 level of the theory. All the bond lengths are reported in (Å) and angle in (°).

Due to the substitution on the 6th position of the pyridine rings the entry from the side of substitution gets blocked, this entry effect is a direct outcome of the substitution. Apart from the substrate preference in entry for the two substituted complex, we do not see any drastic changes in the transition state C-H and O…H bond lengths for all three complexes. The triplet spins state shows C-H bond length of 1.30 (1.32) [1.30] Å and O-H bond length of 1.29 (1.28) [1.31] Å for $^{3}TS_{1b}$ ($^{3}TS_{2b}$) [$^{3}TS_{3b}$] respectively. Similar pattern were observed on quintet spin surface transition state. The C-H and O-H bond lengths were different from the triplet spin surface but remained constant throughout for all the complexes. The transition state occurred at O-H bond distance of 1.20 (1.81) [1.82] Å for $^{5}TS_{1b}$ ($^{5}TS_{2b}$) [$^{5}TS_{3b}$] respectively. The reaction is feasible on the quintet spin state for all the oxidant studied in the present investigation. Despite having similar bond

lengths 3b H-abstraction barrier on the quintet spin surface is lower by 3kcal/mol from the 2b oxidant.

So, we tried to explore the electronic properties in order to understand the reactivity differences arising in 1b, 2b and 3b complexes. Mulliken spin density analysis confirms the electronic configuration of the reactant in triplet state to be $\delta^{2}_{x2-y2}\ \pi^{*1}_{xz}\ \pi^{*1}_{yz}$ by group spin density of nearly 2 on the FeO moiety for all the oxidants. For the transition state the spin density on FeO moiety decreases and half spin density is observed on the ethylbenzene substrate, which suggests the electronic organization as $\delta^{2}_{x2-y2}\ \pi^{*1}_{xz}\ \pi^{*2}_{yz}\ \varphi^{1}_{c}$. At intermediate geometry, the spin of 1 is observed on both Fe and substrate that makes the electronic configuration $\delta^{2}_{x2-y2}\ \pi^{*1}_{xz}\ \pi^{*2}_{yz}\ \varphi^{1}_{c}$ and shows full transfer of elecron. Coming to the quintet spin state the reactant complex spin density shows value of 3 on FeO and nearly half on N4PY suggesting configuration $\delta^{1}_{x2-y2}\ \pi^{*1}_{xz}\ \pi^{*1}_{yz}\ \sigma^{*1}_{z^2}$. Whilst in transition state for H- abstraction the spin density changes to 4 on FeO group and is tending to attain half spin density (-0.27) indicating downward spin electron on the substrate. These spin density values show that transition state is like intermediate complex, ferric hydroxo i.e. [Fe(III)-OH N4PY], hence electronic configuration of the system changes to $\delta^{1}_{x2-y2}\ \pi^{*1}_{xz}\ \pi^{*1}_{yz}\ \sigma^{*1}_{z^2}\ \varphi^{1}_{c}$. These results are obtained for all 1b, 2b and 3b oxidants for both triplet/quintet. The data of respective spin density and charges for the (RC, TS, and INT) are complied in Table 5.1, 5.2 and 5.3 shown below.

Table 5.1: Mulliken charges and spin densities of 1b (RC, TS, and INT) optimized at (B3LYP/BS1) level of the theory.

Reactant Complex								
	Spin Densities (ρ)				Charges (Q)			
	Fe	O	N4PY	Sub	Fe	O	N4PY	Sub
Triplet	1.05	0.98	0.04	0.00	0.66	-0.32	0.95	0.05
Quintet	2.93	0.75	0.31	0.00	0.83	-0.32	0.78	0.06
Transition State								
	Spin Densities (ρ)				Charges (Q)			
	Fe	O	N4PY	Sub	Fe	O	N4PY	Sub
Triplet	0.85	0.68	-0.04	0.51	0.71	-0.53	1.42	0.39
Quintet	3.72	0.38	0.37	-0.49	0.94	-0.56	1.07	0.43
Intermediate								
	Spin Densities (ρ)				Charges (Q)			
	Fe	O	N4PY	Sub	Fe	O	N4PY	Sub
Triplet	0.88	0.19	-0.05	0.97	0.69	-0.64	1.47	0.46
Quintet	3.99	0.47	0.48	-0.95	1.02	-0.76	1.18	0.54

Table 5.2: Mulliken charges and spin densities of 2b (RC, TS, and INT) optimized at (B3LYP/BS1) level of the theory.

Reactant Complex								
	Spin Densities (ρ)				Charges (Q)			
	Fe	O	N4PY	Sub	Fe	O	N4PY	Sub
Triplet	1.03	0.99	-0.03	0.00	0.67	-0.34	1.60	0.06
Quintet	2.92	0.76	0.31	0.00	0.81	-0.33	0.79	0.05
Transition State								
	Spin Densities (ρ)				Charges (Q)			
	Fe	O	N4PY	Sub	Fe	O	N4PY	Sub
Triplet	0.83	0.68	-0.05	0.52	0.73	-0.54	1.31	0.39
Quintet	3.46	0.46	0.34	-0.27	0.88	-0.47	1.31	0.27

Intermediate								
	Spin Densities (ρ)				Charges (Q)			
	Fe	O	N4PY	Sub	Fe	O	N4PY	Sub
Triplet	0.86	0.21	-0.05	0.97	0.72	-0.65	1.45	0.46
Quintet	3.92	0.44	0.49	-0.96	1.03	-0.76	1.16	0.52

Table 5.3: Mulliken charges and spin densities of 3b (RC, TS, and INT) optimized at (B3LYP/BS1) level of the theory.

Reactant Complex								
	Spin Densities (ρ)				Charges (Q)			
	Fe	O	N4PY	Sub	Fe	O	N4PY	Sub
Triplet	1.02	1.00	-0.03	0.00	0.67	-0.33	1.60	0.05
Quintet	2.90	0.78	0.28	0.00	0.80	-0.32	1.46	0.05
Transition State								
	Spin Densities (ρ)				Charges (Q)			
	Fe	O	N4PY	Sub	Fe	O	N4PY	Sub
Triplet	0.83	0.67	-0.05	0.52	0.71	-0.54	1.42	0.39
Quintet	3.41	0.50	0.33	-0.25	0.85	-0.44	1.32	0.26
Intermediate								
	Spin Densities (ρ)				Charges (Q)			
	Fe	O	N4PY	Sub	Fe	O	N4PY	Sub
Triplet	0.89	0.18	-0.06	0.97	0.69	-0.65	1.48	0.46
Quintet	3.94	0.43	0.47	-0.97	1.05	-0.78	1.16	0.52

From the above set of spin density analysis and data it is clear that all the complexes spin density are in range and no drastic changes in any complex are being observed. So, neither there are major structural differences in the bond lengths nor in spin densities of all the associated structures. Despite substitution being performed on the same ligand framework, with same substituent group (here methy group), the changes in the reactivity of 3b are drastic compared with the 2b oxidant.

The only change noticeable enough between 1b, 2b and 3b stucture is the angle between OFeNax. There is a substantial bend in the angle for 3b complexes shown in Figure 5.5 from 180° to 172°for triplet and 180° to 174° for the quintet. This bend in the angle is providing better overlap between substrate orbital and $\sigma^*_{z^2}$ orbital along OFeNax axis and hence easy transfer of electron is possible at a lower energy cost. This implies that the changes in the reactivity of complexes arise due the stericc effects which substitution incorporates. The steric hindrance causes the better substrate-oxidant positing which leads to the better orbital overlap and hence easy electron transfer.

5.4 Conclusions

The optimization of the substituted scaffolds is very tricky as they are susceptible to the slight changes in the backbone structure. But the benchmarking from the previous and existing systems of iron (IV)-oxo complexes in different oxidation state reactions have made the methods to be accurate. The theoretical calculations on the N4PY and its substituted scaffolds allowed thorough understanding of the intricate behavior raised due to steric and electronic effects in details. With the substitution of methyl groups on the mononuclear nonheme iron(IV)-oxo model systems in an octahedral environment, changes in the reactivity are prominent from the above investigation. Engineered oxidant

3b shows lower HAA barrier compared from 2b and 1b complexes. Detailed investigation of the electronic organization points out that the enhanced reactivity is not an outcome of electronic features in all the complexes. Rather geometrical features which occur due to the substitution could be the cause for the possible reactivity. The substitution causes steric factors on the forefront and which brings better positing of the substrate with respect of the oxidant. In real enzymatic systems residues help in the positing of the substrate and easy electron flow. The present investigation suggests that substitutional effects can also channelize the approach of the substrate which can thereby enhance the reactivity and selectivity of the reaction.

References:

[1] M. Costas, M. P. Mehn, M. P. Jensen, L. Que Jr., *Chem. Rev*., **104**, 939, (2004).

[2] M. M. Abu-Omar, A. Loaiza, N. Hontzeas, *Chem. Rev*. **105**, 2227, (2005).

[3] C. Krebs, D. G. Fujimori, C. T. Walsh, J. M. Bollinger Jr., *Acc. Chem. Res*.,**40**, 484 (2007).

[4] P. C. A. Bruijnincx, G.V. Koten, R. J. M. Klein Gebbink, *Chem. Soc. Rev*., **37**, 2716 (2008).

[5] B. Meunier, S. P. de Visser, S. Shaik, *Chem. Rev*., **104**, 3947 (2004)

[6] I. G. Denisov, T. M. Makris, S. G. Sligar, I. Schlichting, *Chem. Rev*., **105**, 2253 (2005).

[7] P. R. Ortiz de Montellano, *Chem. Rev*., **110**, 932 (2010).

[8] D. Li, Y. Wang, K. Han, *Coord. Chem. Rev*. **256**, 1137 (2012).

[9] M. R. A. Blomberg, T. Borowski, F. Himo, R. Z. Liao, P. E. M. Siegbahn, *Chem. Rev*., **114**, 3601 (2014).

[11] S. P. de Visser, D. Kumar, (Eds., *Iron-containing enzymes: Versatile catalysts of hydroxylation reaction in nature*), RSC Publishing, Cambridge (UK), (2011).

[12] E. I. Solomon, T. C. Brunold, M. I. Davis, J. N. Kemsley, S. K. Lee, N. Lehnert, F. Neese, A. J. Skulan, Y. S. Yang, J. Zhou, *Chem. Rev*., **100**, 235 (2000).

[13] J. U. Rohde, J. H. In, M. H. Lim, W. W. Brennessel, M. R. Bukowski, A. Stubna, E. Munck, W. Nam, L. Que Jr, *Science*, **299**, 1037 (2003).

[14] C. V. Sastri, J. Lee, K. Oh, Y. J. Lee, T. A. Jackson, K. Ray, H. Hirao, W. Shin, J. A. Halfen, J. Kim, L. Que Jr, S. Shaik, W. Nam, *Proc. Natl. Acad. Sci. USA*, **104**, 1918 (2007).

[15] I. Prat, L. Gomez, M. Canta, X. Ribas, M.Costas, *Chem. Eur. J.*, **19**, 1908 (2013).

[16] M. G. Quesne, D. Senthilnathan, D. Singh, D. Kumar, P. Maldivi, A. B. Sorokin, S. P. de Visser, *ACS Catal.*, **6**, 2230 (2016).

[17] P. Barman, A. S. Faponle, A. K. Vardhaman, D. Angelone, A. M. Lohr, W. R. Browne, P. Comba, C. V. Sastri and S. P. de Visser, *Inorg. Chem.*, **55**, 10170 (2016).

[18] S. P. de Visser, L. Tahsini and W. Nam, *Chem. Eur. J.*, **15**, 5577 (2009).

[19] J. Annaraj, J. Cho, Y. M. Lee, S. Y. Kim, R. Latifi, S. P. de Visser, W. Nam, *Angew. Chem. Int. Ed.*, **48**, 4150 (2009).

[20] S. Sahu, L. R. Widger, M. G. Quesne, S. P. de Visser, H. Matsumura, P. M. Loccoz, M. A. Siegler, D. P. Goldberg, *J. Am. Chem. Soc.*, **135**, 10590 (2013).

[21] D. C. Lacy,R. Gupta, K. L. Stone, J. Greaves, J. W. Ziller, M. P. Hendrich, A. S. Borovik, *J. Am. Chem. Soc.* , **132**, 12188 (2010).

[22] U. Isci, A. S. Faponle, P. Afanasiev, F. Albrieux, V. Briois, V. Ahsen, F. Dumoulin, A. B. Sorokin, S. P. de Visser, *Chem.Sci.*, **6**, 5063 (2015).

[23] M. Lubben, A. Meetsma, E. C. Wilkinson, B. Feringa, L. Que Jr., *Angew. Chem. Int. Ed.*, **34**, 1512 (1995).

[24] J. Kaizer, E. J. Klinker, N. Y. Oh, J. U. Rohde, W. J. Song, A. Stubna, J. Kim, E. Munck, W. Nam, L. Que Jr., *J. Am. Chem. Soc.* **126**, 472 (2004).

[25] E. J. Klinker, T. A. Jackson, M. P. Jensen, A. Stubna, G. Juhász, E. L. Bominaar, E. Munck, L. Que Jr., *Angew. Chem. Int. Ed.*, **45**, 7394 (2006).

[26] D. Wang, K. Ray, M. J. Collins, E. R. Farquhar, J. R. Frisch, L. Gomez, T. A. Jackson, M. Kerscher, A. Waleska, P. Comba, M. Costas, L. Que Jr., *Chem. Sci.*, **4**, 282 (2013).

[27] M. Lubben, A. Meetsma, E. C. Wilkinson, B. Feringa, L. Que Jr., *Angew. Chem. Int. Ed.*, **34**, 1512 (1995).

[28] L. Bogath, R. Csonka, G. Speier, M. Reglier, A. J. Simaan, J. V. Naubron, M. Giorgi, K. Lazar, J. Kaizer, *Inorg. Chem*., **55**, 10090 (2016).

[29] S. K. Padamati, A. Draksharapu, D. Unjaroen, W. R. Browne, *Inorg. Chem*., **55**, 4211 (2016).

[30] D. J. Frisch, M. J. Trucks, G. W. Schlegel, H. B. Scuseria, G. E. Robb, M. A. Cheeseman, J. R. Scalmani, G. Barone, V. Mennucci, B. Petersson, G. A. Nakatsuji, H. Caricato, M. Li, X. Hratchian, H. P. Izmaylov, A. F. Bloino, J. Zheng, G. Sonnenb, Official Gaussian 09 Literature Citation, (2009).

[31] P. J. Hay, W. R. Wadt, P. J. Hay, W. R. Wadt, J. Chem. Phys., **82**, 270 (1985).

[32] S. Kumar, A. S. Faponle, P. Barman, A. K. Vardhaman, C. V. Sastri, D. Kumar and S. P. de Visser, *J. Am. Chem. Soc*.,**136**, 17102 (2014).

[33] A. K. Vardhaman, C. V. Sastri, D. Kumar, S. P. de Visser, *Chem. Commun*., **47**, 11044 (2011).

[34] F. G. Cantu Reinhard, A. S. Faponle, S. P. de Visser, *J. Phys. Chem. A*, **120**, 9805 (2016).

[35] M. A. Sainna, S. Kumar, D. Kumar, S. Fornarini, M. E.Crestoni, S. P. de Visser, *Chem. Sci*., **6**, 1516 (2015).

[36] F.G. Cantu Reinhard, M. A. Sainna, P. Upadhyay, G. A. Balan, D. Kumar, S. Fornarini, M. E. Crestoni, S. P. de Visser, *Chem. Eur. J.*, **22**, 18608 (2016).

[37] L. Ji, A. S. Faponle, M. G. Quesne, M. A. Sainna, J. Zhang, A. Franke, D. Kumar, R. van Eldik, W. Liu, S. P. de Visser, *Chem. Eur. J.*, **21**, 9083 (2015).

[38] B. Karamzadeh, D. Kumar, G. N. Sastry, S. P. de Visser, *J. Phys. Chem. A*, **114**, 13234 (2010).

[39] J. Kaizer, E. J. Klinker, N. Y. Oh, J. U. Rohde, W. J. Song, A. Stubna, J. Kim, E. Munck, W. Nam, L. Que Jr., *J. Am. Chem. Soc.*, **126**, 472 (2004).

[40] D. Kumar, H. Hirao, L. Que, Jr., S. Shaik, *J. Am. Chem. Soc.* **127**, 8026 (2005).

[41] E. J. Klinker, S. Shaik, H. Hirao, L. Que, Jr. *Angew. Chem. Int. Ed.,* **48**, 1291 (2009).

[42] A. K. Vardhaman, P. Barman, S. Kumar, C. V. Sastri, D. Kumar, S. P. de Visser, *Angew. Chem. Int. Ed.*, **52**, 12288 (2013).

[43] D. Kumar, H. Hirao, L. Que Jr., S. Shaik, *J. Am. Chem. Soc.*,**127**, 8026 (2005).

[44] S. P. de Visser, *J. Am. Chem. Soc.*, **128**, 9813 (2006).

[45] L. Bernasconi, E.J. Baerends, *Eur. J. Inorg. Chem.*, **12**, 672 (2008).

[46] S. D. Wong, C. B. Bell III, L. V. Liu, Y. Kwak, J. England, E. E. Alp, J. Zhao, L. Que Jr., E. I. Solomon, *Angew. Chem. Int. Ed.*, **50**, 3215 (2011).

[47] M. Martinho, F. Banse, J.F. Bartoli, T. A. Mattioli, P. Battioni, O. Horner, S. Bourcier, J. J. Girerd, *Inorg. Chem.*, **44**, 9592 (2005).

[48] A. S. Borovik, *Acc. Chem. Res.*, **38**, 54 (2005).

CHAPTER 6

CONCLUSIONS

CHAPTER- 6

CONCLUSIONS

The present thesis highlights following points as general conclusions:

- Theoretical model calculations are now regarded equally important in determining mechanism of metalloenzymes. Experimental methods have the advantage that they are studied on the actual (real) system, but spectroscopically guarding of short-lived species, electron transfer and interpretation of results is quite troublesome. Theoretical modeling can easily assist experimental studies with good accuracy due to both the development of the theory and the decades of experience in this area. The accuracy of the system depends on the choice of the method and the real system under consideration.

- The present thesis work helped in exploring the reactions mechanism of various oxygen atom transfer (OAT) reactions which includes reactions like, aromatic and aliphatic hydroxylation, olefin epoxidation, of transition metal containing complexes. The research characterized the active oxidant in the reaction processes and the rate determining step in the mechanism. Moreover, in several cases models were devised that rationalize reaction processes and barrier heights that can be used to predict rate constants of processes.

- Present work also devised models for non-heme iron(IV)-oxo species of N4PY that investigated in lowering the reaction barrier of hydrogen transfer by equatorial substitution of ligands. The theoretical calculations revealed lower activation barrier in H-atom transfer from the substituted systems.

- The studies present in this thesis work are expected to bridge the computational and experimental work being carried out in biomimetic/enzymatic reactions. Also they are expected to meet challenges of drug synthesis (pharmaceutical reactions), hydroxylation and oxidation of common toxic compounds both natural and artificial.

LIST OF PUBLICATION

Published papers in the refereed journals

1. **Rolly Yadav,** Nidhi Awasthi, Anamika Shukla, Devesh Kumar, Modelling of Hydroxylation of Estragole via Human Liver Cytochrome P450, Journal of Molecular Modeling, **27**, 199, (2021).
2. Razak Hussain, **Rolly Yadav**, Mushtaq, Tabreiz Ahmad Khan, Devesh Kumar, Yusuf Akhter, Interplay Between Two Spin States Determines the Hydroxylation Catalyzed by P450 Monooxygenase from Trichoderma Brevicompactum, ***Journal of Computational Chemistry***, **41**, 14, (2020).
3. **Rolly Yadav,** Anwesh Pandey, Nidhi Awasthi, and Anamika Shukla, Molecular Docking Studies of Enzyme Binding Drugs on Family of Cytochrome P450 Enzymes, ***Advanced Science, Engineering and Medicine***, **11,** 5, (2019).
4. Nidhi Awasthi, **Rolly Yadav,** Anamika Shukla, Devesh Kumar, Interplay Between Two Degenerate Spin State Determines the Hydroxylation of 4-Nitrophenol Catalyzed via Cytochrome P450, ***Inorganic Chemistry Communications***, **132**, 7, 108857, (2021).
5. Nidhi Awasthi, **Rolly Yadav,** Anamika Shukla, Devesh Kumar, Metabolism of 8-Aminoquinoline (8AQ) Primaquine via Aromatic Hydroxylation Step Mediated by Cytochrome P450 Enzyme using Density Functional Theory, ***Journal of Organometallic Chemistry* , 122154**, 2021.

6. Anamika Shukla, Ruchi Mishra, **Rolly Yadav**, Nidhi Awasthi, Devesh Kumar, Computational Investigations on Interactions between DNA and Flavonols, ***Journal of Biointerface Research in Applied Chemistry,*** **12,** 6, (2021).

7. Alok Shukla, A.K. Dwivedi, Nidhi Awasthi, **Rolly Yadav**, Interaction of Carbazoles and their Analogs with Human Cytochrome, ***Compliance Engineering Journal***, **11,** 10, (2020).

8. A. K. Dwivedi, Nidhi Awasthi, **Rolly Yadav**, Shivani Chaudhary, Anamika Shukla, Narinder Kumar*, Spectroscopic Analysis of Porphyrin (C20H12N4) Ring Studiedby DFT Methodology, ***Journal of Information and Computational Science***, **9**, 8, (2019).

9. A.K. Dwivedi, **Rolly Yadav**, Ruchi Mishra, Asheesh Kumar, , Nidhi Awasthi, Anamika Shukla, Computational Molecular Characterization of Important Flavonoids: An In silico study, ***Compliance Engineering Journal***, **10**, 8, (2019).

Communicated Paper

1. **Rolly Yadav**, Sam de Visser, Chivikula V. Sastri, Devesh Kumar*, Biotransformation of Bis Phenols and their Analogs by P450 using DFT, ***Chem European Journal***.
2. **Rolly Yadav,** Nidhi Awasthi, Devesh Kumar*, Biotransformation of BPA via Epoxidation Catalyzed by Cytochrome P450, ***Journal of Inorganic Chemistry Communications,*** INOCHE-D-21-01456, (2021).

LIST OF CONFERENCES/SEMINARS/WORKSHOPS

1. **International Conference On Nanoscience & Nanotechnology (ICNN-2017)** on 22nd - 24th sept. at Babasaheb Bhimrao Ambedkar University, Lucknow. (Participation)

2. **North Indian Science Congress (NISC-2018) & International Conference On Science and Technology for Sustainable Future** on 10th & 11th at Babasaheb Bhimrao Ambedkar University, Lucknow. (Participation)

3. **National Symposium on Advanced Materials Science**, Department of Physics Deen Dyal Upadhyay Gorakhpur University, Gorakhpur, 7th -8th December, 2018. (Poster)

4. **International Confrence on Chemical Sciences : National and Global Perspective**, Department of Chemistry, Christian Degree Collage, Uttar Pradesh, Lucknow, 29th-31st,October, 2018. (Poster)

5. **International Conference on Advanced Chemical and Structural Biology (ICACSB-2019)** during February 19th-21th, 2019 at Thanjavur, Chennai. (Poster)

6. **International Symposium on Advances in Functional and Biological Materials (ISAFBM-2019)** Feb. 28th, 2019 in Lucknow University, UP (Poster)

7. **National Conference on Smart Materials, Devices and Sustainable Technologies (SMDST-2019)** during March 15th-16th, 2019 in MMM University of Technology, Gorakhpur (UP).

8. **National Conference on Recent Advances in Chemical Sciences (NCRACS-2019)** during March 29-30, 2019 in MMM University of Technology, Gorakhpur (UP). (Oral)

9. **Workshop on Applications of Gaussian and GaussView Software** during July 18th-19th, 2019 in Lucknow University, UP. (Participation)

10. **International conference on Ultrasonics and Materials science for advanced technology (ICUMSAT-2019)**, November 16th-18th, Department of Physics, Veer Bahadur Singh Purvanchal University, Jaunpur. (Poster)

11. **Indo-Brazilian e-Symposium on Solid State Properties of Pharmaceuticals**, held from 29th -30th Apr 2020, organized by University of Lucknow. (e-poster)

12. Workshop on **Tools and Techniquies to perfrom molecular modeling and computer-aided drug design (MMTT-2021)** January 11th-17th, 2021 organized by NIPER-GUWAHATI. (e-poster)

Journal of Molecular Modeling (2021) 27:199
https://doi.org/10.1007/s00894-021-04815-z

ORIGINAL PAPER

Modeling the hydroxylation of estragole via human liver cytochrome P450

Rolly Yadav[1] · Nidhi Awasthi[1] · Anamika Shukla[1] · Devesh Kumar[1]

Received: 5 April 2021 / Accepted: 2 June 2021

Abstract

Natural compounds derived from plants are generally regarded safe and devoid of adverse effects. However, there are individual ingredients that possess toxic, genotoxic, and carcinogenic activities. These compounds when exposed at specific level become hazardous to health. Estragole (1-allyl-4-methoxybenzene) is a common component of spice plants. Its toxicity gets activated with the hydroxylation at benzylic carbon (C1') position by P450 enzymes present in the human liver. The present study grounds to explore the reaction mechanism of conversion of estragole to hydroxylated metabolite using computational methodology. Density functional theory (DFT)-based calculations were employed to explore the cytochrome P450–catalyzed mechanism at C1 position aliphatic hydroxylation of estragole. Overall reaction energy profile, electronic configuration, and 3D structure of all intermediates, transition states, and product complexes formed during the reaction along with their free energies were tried to be investigated.

Keywords Estragole · DFT · P450 · Hydroxylation · Genotoxic

Introduction

Estragole (1-allyl-4-methoxybenzene) is a common component of spice plants like star anise, fennel, and basil oil. Additionally, estragole is used in flavorings, as essential oils that are added in many food, detergents, and cosmetic products. It is regarded as a genotoxic hepatocarcinogen in rats, and its potential toxicity in humans is still under prime debate. *Foeniculum vulgare* Mill. (fennel) is a major source responsible for the human exposure to this phytochemical [1]. Its toxicity gets activated with the hydroxylation at benzylic (C1') position [2] by the following P450 enzymes present in the human liver: 1A2, 2A6, 2CI9, 2D6, and 2E1. The major P450 enzymes that are involved in the catalysis of estragole are 1A2 and 2A6. Other enzymes play their role in the catalysis of estragole at relatively higher concentration. The metabolite obtained upon hydroxylation at C1 position is not toxic within itself; however, its conjugation with sulfate by a sulfotransferase to produce 3′-sulfoxyestragole is genotoxic [2]. Figure 1 marks the general reaction scheme that was studied computationally.

Cytochrome P450 enzymes are versatile biological catalyst found in nature in all living forms such as bacteria, mammals, fungi, and plants [3, 4]. P450 enzymes are key players responsible for metabolic conversion of chemical compounds to reactive metabolites which later binds macromolecules.

They activate and oxidize a fairly large variety of substrates [5, 6]. Due to their broad chemical functions, they are well studied with potential application in the field of biotechnology and medicine. P450 enzymes are a monooxygenase class of heme enzymes. Their common reaction mechanism with substrates occurs through single-oxygen-atom transfer [7–9]. Initially, in resting state, the heme iron(III) is hexacoordinated. At the distal side, it is connected to water molecule and is axially ligated to the thiolate of cysteinate residue which eventually connects it to the rest of the protein. The catalytic cycle of P450 gets initiated with the entry of substrate inside the binding pocket. As the substrate approaches the heme, it transpires the release of water molecule ligated to iron and changes the spin state, which triggers electron transfer from the reduction partner of P450. Later, the molecular oxygen binds itself to the iron and gets reduced and protonated to form ferric hydroperoxo species also known as compound (Cpd) 0.

✉ Devesh Kumar
dkclcre@yahoo.com

[1] Molecular Modeling Lab, Department of Physics, School of Physical and Decision Sciences, Babasaheb Bhimrao Ambedkar University, Lucknow, UP 226025, India

Published online: 11 June 2021

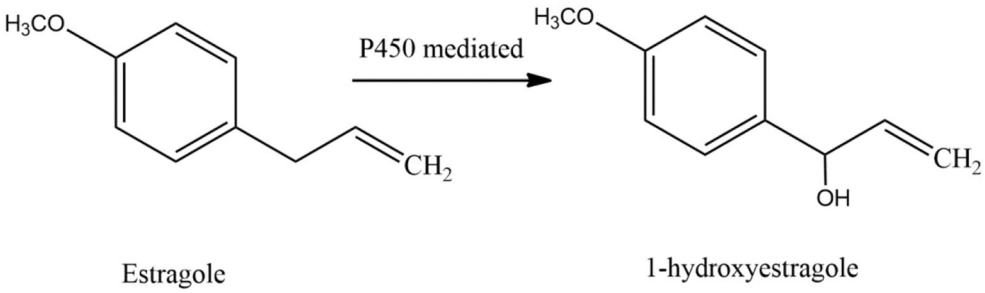

Fig. 1 Activation reaction of estragole to produce 1-hydroxyestragole by Cpd I of P450 enzymes, a precursor for the formation of genotoxic 3′-sulfoxyestragole

Subsequent protonation leads to the formation of ultimate oxidant iron(IV) oxo porphyrin cation radical species compound I (Cpd I). The structure of Cpd I is depicted in Scheme 1a, along with short representation used to show porphyrin ring. Cpd I reacts with the substrate to form oxidized product through various reactions like desaturation/ring closure and oxygen atom transfer reactions like aliphatic and aromatic hydroxylation, sulfoxidation, epoxidation etc. It is well studied through many experimental and theoretical [10–13] studies that alkane (C–H) hydroxylation is stepwise and proceeds through rebound mechanism [14], and this is shown in Scheme 1b. The first step is associated with the removal of hydrogen atom from the carbon to be hydroxylated to form ferric hydroperoxo intermediate via hydrogen abstraction transition state (TS_H), while the later step involves the rebound of radical carbon to produce hydroxylated product complex via rebound transition state (TS_{reb}).

Quantum mechanical (QM) calculations are valuable methods that provide us a tool to deeply penetrate and understand the formation of toxic metabolites from drugs and chemical compounds followed by analysis of their reaction energy profiles. In the present work, density functional theory (DFT)-based QM calculations were employed to explore the cytochrome P450–catalyzed reaction mechanism for aliphatic hydroxylation of estragole at benzylic carbon C1 position to explore the overall reaction energy profile and to understand the formation of involved intermediates and transition states. The mechanism was modeled on two spin surfaces for Cpd I-estragole complex, viz. quartet (high spin (HS)) and doublet (low spin (LS)). Furthermore, this study was helpful in gaining substantial insights into the electronic arrangement and 3D structural features of intermediates, transition states, and product complexes formed during the progress of the reaction along with their free energies.

Methodology

The calculations provided in this study were computed using Gaussian 09 [15] software and implemented DFT method. To support our results from previous studies [11, 16–18], B3LYP hybrid density functional method has been chosen, using LACVP (Los Almos)-type basis set on iron that uses double ζ-core potential along with 6–31 G basis set on the rest of the atoms (basis set (BS1) [19]. Optimization of geometry and scans were performed at the B3LYP/BS1 level of the theory. Geometry scan maxima are used for the transition state searches along with frequency calculations that confirm

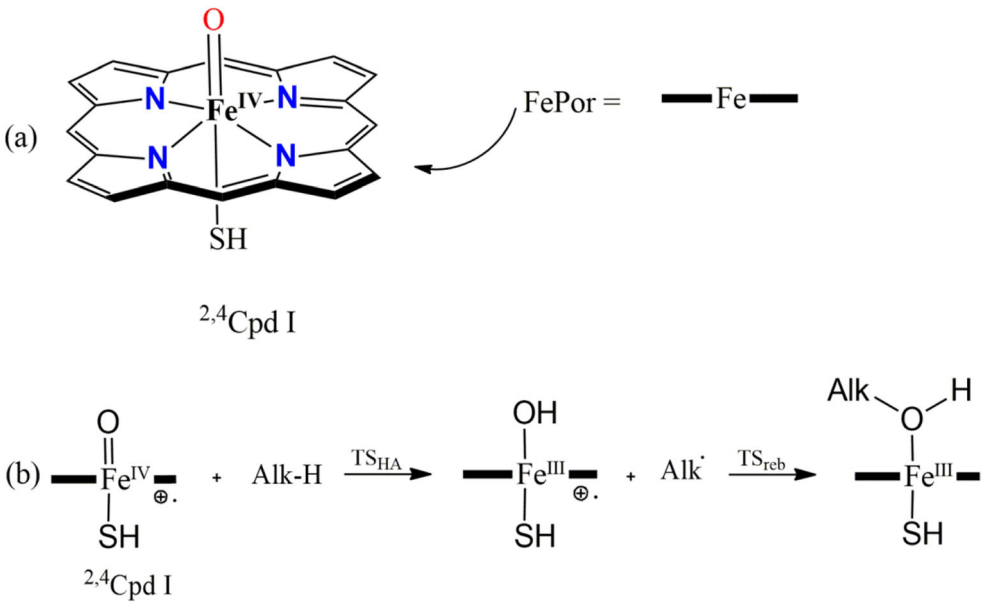

Scheme 1 **a** Structure of compound 1 (Cpd I) along with porphyrin ring representation in the right. **b** Two-state rebound mechanism used by P450 for aliphatic hydroxylation

structures to be a first-order saddle point depicting single imaginary frequency for the correct mode. Full geometry optimization at the same level of the theory has been performed, followed with frequency calculations that confirmed structures to be local minima and transition states to be the first-order saddle point. Cpd I used in present investigation was modeled as iron embedded in protoporphyrin IX, side chains were removed to make calculations less extensive, and also replacement of side chain will not greatly affect the energies of high-lying occupied and low-lying virtual orbitals of a chemical system. Similarly for simplification of the substrate, the structure 3-4-methoxyestragole is replaced by the 4-methoxy substituent to reduce computation cost.

Results and discussion

Electronic structure of Cpd I

Cpd I possess a dense manifold of orbitals [20–22], and therefore, it has multiple closely lying spin states and electromeric states. An understanding of its orbital picture is necessary to understand the trends and pattern during the course of the reaction. Figure 2 shows all the high-lying occupied and low-lying virtual orbitals of a heme system that are key orbitals involved in the catalyst mechanism. In the extreme left of the figure, we have porphyrin ring orbitals which are π-type high-lying non-bonding orbitals and, under D_{4th} symmetry, their labels are assigned as a_{1u} and a_{2u}. The a_{2u} orbital is bit higher in energy than a_{1u} due to its mixing with the axial thiolate ligand. Other than these porphyrin ring orbitals, there are five metal 3*d* orbitals that mix with axial ligand oxygen. The uppermost orbital in the figure is $\sigma^*_z{}^2$ anti-bonding orbital, and this arises due to the mixing of $3d_z{}^2$ orbital on iron and $2p_z$ orbital of oxygen along the S–Fe–O bond axis. Right below in the figure lies σ^*_{xy} which is a planar orbital formed due to the mixing of $3d_{xy}$ orbital of iron and $2p_{xy}$ orbital of porphyrin nitrogen along the Fe–N bond axis. With the combination of $3d_{xz}/3d_{yz}$ metal orbital and oxygen $2p_x/2p_y$ orbital arising the formation of low-lying π_{xz}/π_{yz} orbital, these are found to be always filled and their anti-bonding pairs of π^*_{xz}/π^*_{yz} orbital are along the Fe–O axis. The $\delta_{x^2-y^2}$ is a non-bonding doubly occupied orbital that resides into the heme plane.

Aliphatic hydroxylation

In accordance with previously calculated and benchmarked studies, we investigated our reaction mechanism with a modeled active site complex of cytochrome P450, i.e., Cpd I with substrate [16, 20, 23]. We are focused at the C1 position aliphatic hydroxylation of estragole, and it starts with hydrogen abstraction step via the transition state TS_H to generate a radical intermediate INT. This radical intermediate rebounds

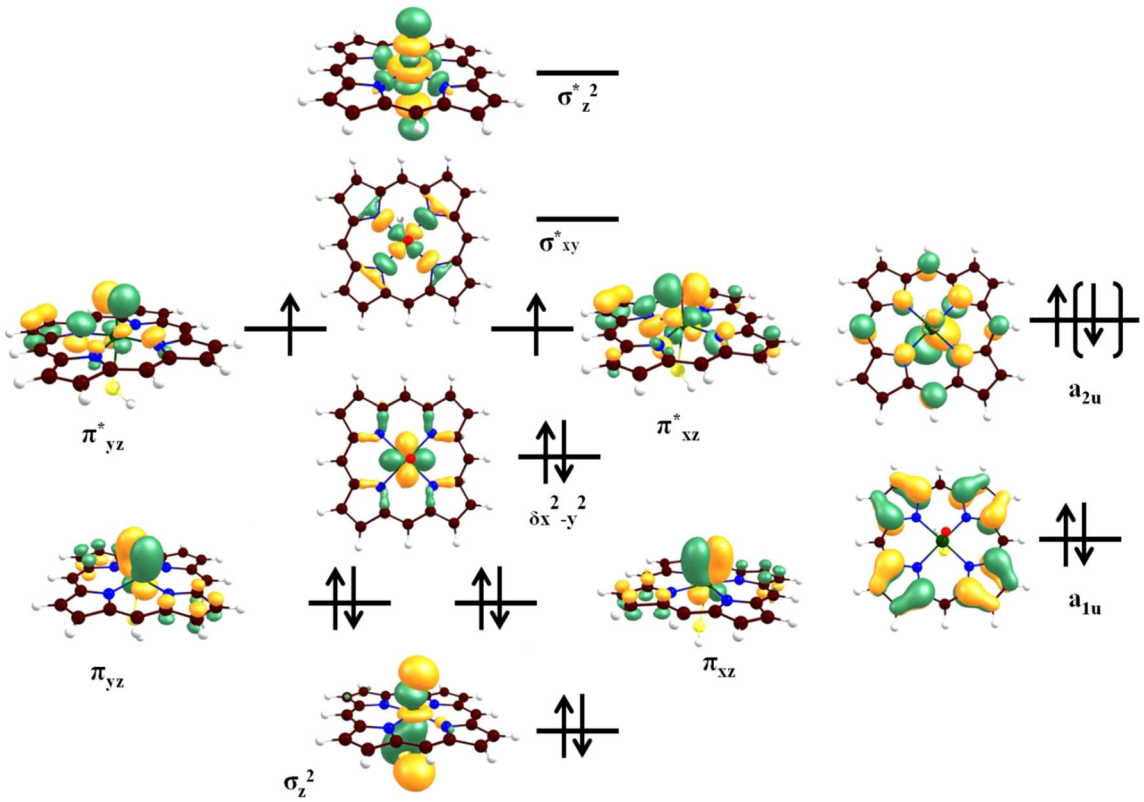

Fig. 2 Molecular orbitals of Cpd I involved in the reaction [5]

to generate product complex (PC) crossing a rebound transition state (TS_{reb}). The potential energy surface of the reaction mechanism is shown in Fig. 3. The reaction analogous to previously reported studies is stepwise and is highly exothermic after radical intermediate to product formation. The reaction follows a two-state reaction (TSR) mechanism, and results are in good agreement with previous studied reactions following TSR mechanism. Hydrogen atom abstraction is the rate-determining step of the reaction, and barrier heights for doublet and quartet are observed to be 10.43 kcal/mol and 9.85 kcal/mol, respectively. Frequency calculations showed single-large imaginary frequencies for both spin states: i1508.20 cm^{-1} (doublet) and i1455.38 cm^{-1} (quartet) [24–26], and these results are reminiscent of typical H-abstraction barrier which simply means that large kinetic isotope effect (KIE) will be observed after replacement of deuterium with hydrogen [27].

Optimized three-dimensional structures of the transition state $^{2,4}TS_H$ showed the transferring hydrogen atom is close to the carbon atom, and this kind of transition state shows less barrier height in comparison to the late transition state. Subsequent formation of radical intermediate occurs, and their formation is exothermic with energy values − 12.85 kcal/mol and − 12.57 kcal/mol for doublet and quartet, respectively. Typical TSR mechanism reactant complex for both spin surfaces is close in energy and virtually degenerates till the H-abstraction barrier [5, 10–13, 28]. With the formation of the radical intermediate ^{2,4}INT, both spin surfaces bifurcate, and rebound transition state is observed for HS state with the barrier height of − 8.56 kcal/mol to form product complex whereas the reaction was barrier-less on LS surface and concerted product formation is observed. The last reaction step for product formation was highly exothermic for both spin surfaces showing an energy value below − 40.00 kcal/mol.

The reaction between Cpd I and substrate is modeled. The reactant complex electronic configuration was investigated and found to be $\delta^{*2}_{x2-y2}\ \pi^{*1}_{xz}\ \pi^{*1}_{yz}\ a^{1}_{2u}$. The reactant complex (RC) was followed with the formation of the transition state $^{2,4}TS_H$ having the electronic configuration $\delta^{*2}_{x2-y2}\ \pi^{*1}_{xz}\ \pi^{*1}_{yz}\ a^{2}_{2u}\ \varphi^{1}_{c}$ to form the intermediate complex ^{2,4}INT. Validity of spin and electron densities was further confirmed by Mulliken analysis and charge analysis Table 1. The spin density showed transition states to be radical in nature. The intermediate spin densities along with electronic configuration depicted one electron transfer from the substrate to the porphyrin a_{2u} orbital. The nature of both the intermediates was found to be radical, and electron density accumulates at the C1 position of the substrate with spin density (ρ_{sub} − 0.98 and 0.99) doublet and quartet, respectively. Intercrossing of spin is also observed in energy profile Fig. 2, and this is indicative of spin crossover in the catalytic cycle. Throughout the reaction process, the orbital occupancy changes for a_{2u}, $\pi^{*}_{xz}/\pi^{*}_{yz}$, $\sigma^{*}_{z}{}^{2}$, and substrate orbital φ_c to conserve the overall spin during the entire reaction and also for electron sharing in the making and breaking of bonds. First electron transfer for the formation of the bond between oxo group and H atom is achieved by electron transfer from the substrate to the Cpd I, and one of the electrons is transferred to the heme a_{2u} orbital, making it fully occupied leaving substrate to be singly occupied φ^1. Last step of the reaction is radical rebound which occurs to generate a PC with the electronic configuration $\delta^{*2}_{x2-y2}\ \pi^{*1}_{xz}\ \pi^{*1}_{yz}\ \sigma^{*1}_{z^2}\ \sigma^{*0}_{xy}\ a^{2}_{2u}\ \varphi^{0}_{c}$ for quartet spin state and $\delta^{*2}_{x2-y2}\ \pi^{*2}_{xz}\ \pi^{*1}_{yz}\ \sigma^{*0}_{z^2}\ \sigma^{*0}_{xy}$

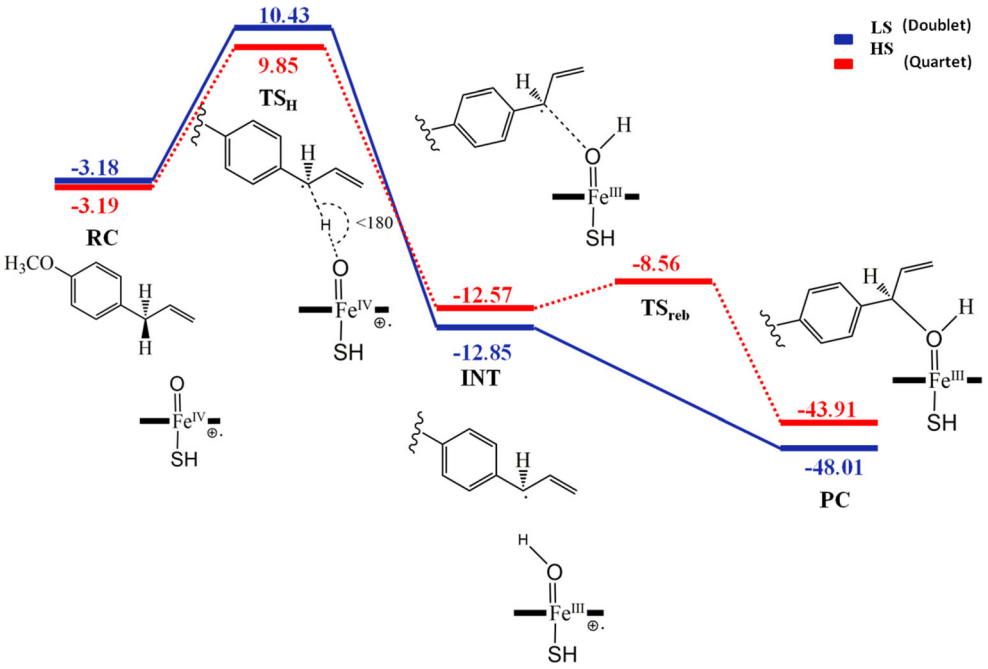

Fig. 3 Potential energy profile for aliphatic hydroxylation at the benzylic position of estragole calculated using DFT methodology at the B3LYP/BS1 level of the theory. All energies here are reported in kcal/mol, the bond lengths in angstrom (Å), the bond angles in degree (°), and the frequencies in wavenumber (cm^{-1})

Table 1 Spin densities and Mulliken atomic charges

	Spin densities					Charges				
	ρ_{Fe}	ρ_{O}	ρ_{Por}	ρ_{SH}	ρ_{Sub}	Q_{Fe}	Q_{O}	Q_{Por}	Q_{SH}	Q_{Sub}
Reactant complex (RC)										
LS	1.20	0.89	−0.51	−0.58	0.00	0.51	−0.35	−0.10	−0.04	−0.01
HS	1.07	0.94	0.44	0.53	0.00	0.50	−0.34	−0.09	−0.04	−0.01
Transition state (TS_H)										
LS	1.62	0.39	−0.32	−0.32	−0.37	0.49	−0.49	−0.21	−0.06	0.28
HS	1.20	0.77	0.19	0.40	0.43	0.46	−0.47	−0.26	0.00	0.27
Intermediate complex (INT)										
LS	1.81	0.25	−0.12	0.28	−0.98	0.44	−0.59	−0.28	0.03	0.38
HS	1.81	0.28	−0.12	0.03	0.99	0.44	−0.59	−0.30	0.03	0.42
Rebound transition state (TS_{reb})										
HS	2.27	0.04	−0.12	0.10	0.70	0.52	−0.61	−0.40	−0.09	0.58
Product complex (PC)										
LS	1.09	−0.00	−0.08	−0.00	0.00	0.33	−0.59	−0.54	0.02	0.76
HS	2.53	0.01	−0.00	0.46	−0.00	0.52	−0.58	−0.45	−0.16	0.68

SH thiolate group, *Sub* substrate (estragole), *Por* porphyrin

$a_{2u}^2\ \varphi_c^0$ for doublet spin state. The rebound transition state $^4TS_{reb}$ is observed only on HS with the electronic configuration $\delta_{x2-y2}^{*2}\ \pi_{xz}^{*1}\ \pi_{yz}^{*1}\ \sigma_{z^2}^{*1}\ \sigma_{xy}^{*0}\ a_{2u}^2\ \varphi_c^0$. In case of LS, the rebound barrier required is usually ~ 1 kcal/mol and hence the potential energy surface is flat. The value for rebound transition state (TS_{reb}) was observed to be − 8.56 kcal/mol, and its adequacy is confirmed by a single imaginary frequency of i231.43 cm^{-1} for the correct mode of vibrations. The discrepancies in the potential surface in rebound step for both spins can be understood from the transfer of electron to the respective orbitals. In LS, the second electron from φ_c gets transferred to the low-lying π_{xz}^* orbital to generate ^{2}P(III) whereas more energy is required to transfer an electron to the high-lying virtual orbital $\sigma_{z^2}^*$ to form ^{4}P(III).

There must be some changes in three-dimensional geometries in structure from RC to PC (Fig. 4) which helped in the easy transfer of electron in the making and breaking of bonds.

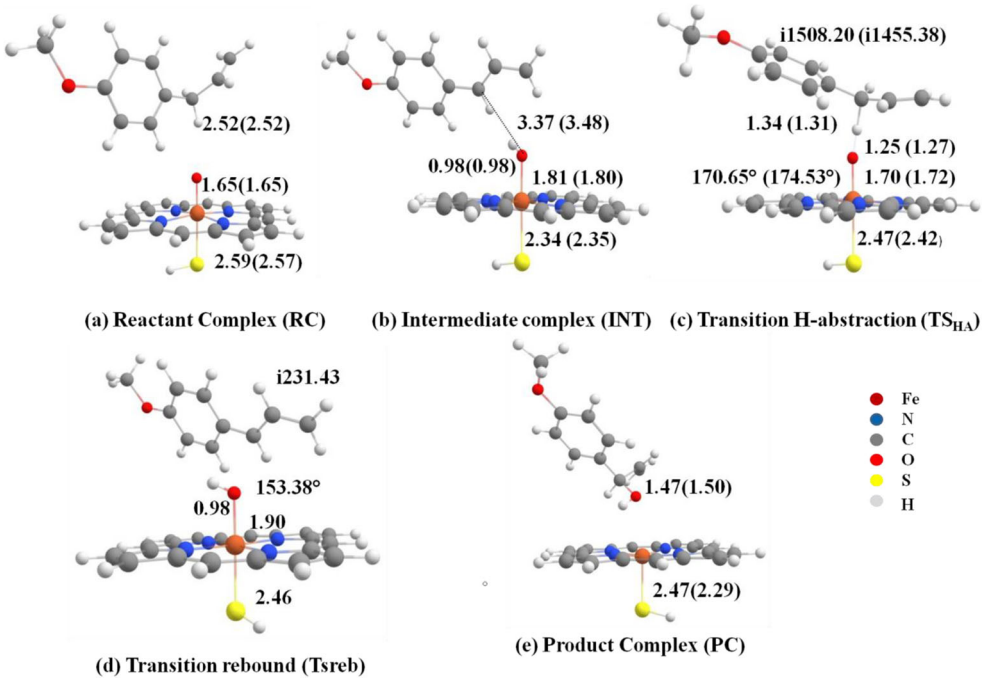

Fig. 4 Optimized 3-D geometries of **a** reactant complex (RC), **b** intermediate complex (INT), **c** H-abstraction transition state (TS_H), **d** rebound transition state (TS_{reb}), and **e** product complex (PC) for doublet (quartet) spin states, along with the necessary bond lengths in Å and the imaginary frequency of TS in cm^{-1}. In the figure, without and within parentheses are indicative of LS (HS) doublet and quartet. All geometries were optimized at the B3LYP/BS1 level of theory

The geometric features of the H-atom abstraction are similar to those of direct H-atom abstraction from methane via bare FeO^+ [29] and diiron model complexes [30]. The transition state TS_H for H abstraction at C1 position is shown in Fig. 4, with the O–H bond and C–H bond of 1.25 Å (1.27 Å) and 1.34 Å (1.31 Å), respectively, for doublet (quartet). The bond angle for C–H–O is linear with the value 170.65° (174.53°) which is a genuine pattern for the H-abstraction process by various FeO species. As previously discussed, smaller distances of the C–H bond compared with those of the O–H bond are regarded as earlier transition state and barrier heights associated with such geometrical features are lower than those of late TS. Intermediate cluster formation occurs after crossing the transition state (TS_H), and the C1 radical center is oriented towards the hydroxyl group, which can be seen from Fig. 4. The second half of the reaction is the oxygen rebound mechanism where carbon radical and iron-hydroxo species combine to form product complex, and the essential part of this process is the formation of the C–O bond. For the formation of the C–O bond, carbon radical needs to rotate to attack on iron-hydroxo species, and this step requires an energy barrier to cross. On the quartet spin surface where the rebound transition state TS_{reb} is observed during geometric scan, we see sharp changes in bond lengths, the C–O bond decreases, and the Fe–O bond increases, coupled with a decrease in the Fe–S bond length at the same time. This effect is known as "push-effect" [5], which is shown in Fig. 4, and is observed in the hydroxylation reaction catalyzed by P450 enzymes, whereas on the doublet spin surface, our calculations predicted no direct transition state and it could be regarded as virtually barrier-less to produce product. This step is highly exothermic in nature and proceeds at a very low cost of energy. The driving force is a direct consequence of large product stability.

Conclusions

Present studies on cytochrome P450 monooxygenases found in the human liver by utilizing DFT-based QM calculations completely elucidate the reaction energy profile of C–H hydroxylation of estragole. The hydroxylated product is a precursor in the activation of toxic metabolite by sulfotransferase to produce 3′-sulfoxyestragole. The theoretical investigation revealed that a two-state reactivity (TSR) mechanism is followed for both HS and LS. The reaction is exothermic throughout, and the LS surface offers an easier pathway for the product formation once the hydrogen abstraction barrier is overcomed. The rate-limiting step was found to be H-abstraction step with 9.85 kcal/mol and 10.43 kcal/mol for quartet and doublet spin states, respectively. It can be asserted from above-discussed results that the C1 position hydroxylation of estragole with Cpd I of P450 is a rebound mechanism for the HS surface and concerted for the LS surface. The intermediates are highly short-lived, and the product formation directly occurs from an intermediate on the LS surface, although the possibility of stereochemical scrambling is present on HS.

Acknowledgements RY is thankful to the Department of Science and Technology (DST), Government of India, for the INSPIRE fellowship (DST/INSPIRE FELLOWSHIP IF-170546). AS is also thankful for DST-INSPIRE fellowship. NA would like to acknowledge the UGC Non-NET fellowship.

Code availability Software programs used are already cited at appropriate places. No codes are used to perform the study.

Author contribution Rolly Yadav and Prof. (Dr.) Devesh Kumar conceived the presented idea. Rolly Yadav performed the computation and prepared the manuscript. Nidhi Awasthi and Anamika Shukla contributed in the analysis of the results. Dr. Devesh Kumar supervised the findings of the work. All authors approved the final draft of the manuscript.

Data availability Data can be made available upon request to corresponding author.

Declarations

Conflict of interest The authors declare no competing interests.

References

1. Levorato S et al (2018) In vitro toxicity evaluation of estragole-containing preparations derived from Foeniculum vulgare Mill. (fennel) on HepG2 cells. Food Chem Toxicol 111:616–622
2. Monien BH, Sachse B, Niederwieser B, Abraham K (2019) Detection of N-acetyl-S-[3′-(4-methoxyphenyl)allyl]-l-Cys (AMPAC) in human urine samples after controlled exposure to fennel tea: a new metabolite of estragole and *trans*-anethole. Chem Res Toxicol 32(11):2260–2267
3. Shaik S, Cohen S, Wang Y, Chen H, Kumar D, Thiel W (2010) P450 enzymes: their structure, reactivity, and selectivity—modeled by QM/MM calculations. Chem Rev 110(2):949–1017
4. Shaik S, De Visser SP (2005) Computational approaches to cytochrome P450 function3rd edn, edited by P. R. O. de Montellano. Kluwer Academic/Plenum, New York
5. De Visser P, Altun A, Thiel W (2005) Theoretical perspective on the structure and mechanism of cytochrome P450. Chem Rev 105: 2279–2328
6. Blomberg MRA, Borowski T, Himo F, Liao R, Siegbahn PEM (2014) Quantum chemical studies of mechanisms for metalloenzymes. Chem Rev 114:3601–3658
7. Meunier B, de Visser SP, Shaik S (2004) Mechanism of oxidation reactions catalyzed by cytochrome P450 enzymes. Chem Rev 104(9):3947–3980
8. Groves JT (2003) The bioinorganic chemistry of iron in oxygenases and supramolecular assemblies. Proc Natl Acad Sci 100(7):3569 LP–3563574
9. Watanabe Y, Nakajima H, Ueno T (2007) Reactivities of oxo and peroxo intermediates studied by hemoprotein mutants. Acc Chem Res 40(7):554–562
10. Ogliaro F, Harris N, Cohen S et al (2000) A model "rebound" mechanism of hydroxylation by cytochrome P450: stepwise and

effectively concerted pathways, and their reactivity patterns. J Am Chem Soc 122:8977–8989
11. Kamachi T, Yoshizawa K (2003) A theoretical study on the mechanism of camphor hydroxylation by compound I of cytochrome P450. J Am Chem Soc 125:4652–4661
12. De Visser SP, Kumar D, Cohen S, Shacham R, Shaik S (2004) A predictive pattern of computed barriers for C-H hydroxylation by compound I of cytochrome P450. J Am Chem Soc 126:8362–8363
13. De Visser AS et al (2017) Reactivity patterns of protonated compound II and compound I of cytochrome P450: what is the better oxidant? Chem Eur J 13:6406–6418
14. Shaik S, Cohen S, Danovich D (2004) The "rebound controversy": an overview and theoretical modeling of the rebound step in C–H hydroxylation by cytochrome P450. Eur J Inorg Chem:207–226
15. D. J. Frisch, M. J. Trucks, G. W. Schlegel, H. B. Scuseria, G. E. Robb, M. A. Cheeseman, J. R. Scalmani, G Barone, V. Mennucci, B. Petersson, G. A. Nakatsuji, H. Caricato, M. Li, X. Hratchian, H. P. Izmaylov, A. F. Bloino, J. Zheng, G. Sonnenb, Official Gaussian 09 Literature Citation. 2009
16. Reinhard FGC, De Visser SP (2017) Oxygen atom transfer using an iron(IV)-oxo embedded in a tetracyclic N-heterocyclic carbene system: how does the reactivity compare to cytochrome P450 compound I? Chem Eur J 23:2935–2944
17. Kumar D, De Visser P, Shaik S (2003) How does product isotope effect prove the operation of a two-state "rebound" mechanism in C–H hydroxylation by cytochrome P450? J Am Chem Soc 125: 13024–13025
18. Hussain YAR, Yadav R, Ahmed M, Khan TA, Kumar D (2020) Interplay between two spin states determines the hydroxylation catalyzed by P_{450} monooxygenase from *Trichoderma brevicompactum*. J Comput Chem:1–7
19. Hay PJ, Wadt WR, Hay PJ, Wadt WR (1985) Ab initio effective core potentials for molecular calculations. Potentials for K to Au including the outermost core orbitals. J Chem Phys 82:299
20. Perman B et al (2001) The experimentally elusive oxidant of cytochrome P450: a theoretical "trapping" defining more closely the "real" species. ChemBioChem 11:848–851
21. M. E. C. and S. P. de V. Mala A. Sainna, Suresh Kumar, Devesh Kumar, Simonetta Fornarini, A comprehensive test set of epoxidation rate constants for iron(IV) – oxo porphyrin cation radical. Chem Sci, vol. 6, pp. 1516–1529, 2015
22. de Visser SP, Ogliaro F, Sharma PK, Shaik S (2002) What factors affect the regioselectivity of oxidation by cytochrome P450? A DFT study of allylic hydroxylation and double bond epoxidation in a model reaction. J Am Chem Soc 124(39):11809–11826
23. De Visser SP, Shaik S, Sharma PK, Kumar D (2003) Active species of horseradish peroxidase (HRP) and cytochrome P450: two electronic chameleons. J Am Chem Soc 4:15779–15788
24. Barman P et al (2016) Communication: Deformylation reaction by a nonheme manganese(III)–peroxo complex via initial hydrogen-atom abstraction. Angew Chem Int Ed 55:11091–11095
25. Timmins A, Saint-André M, de Visser SP (2017) Understanding how prolyl-4-hydroxylase structure steers a ferryl oxidant toward scission of a strong C–H bond. J Am Chem Soc 139(29):9855–9866
26. de Visser SP (2006) What external perturbations influence the electronic properties of catalase compound I? Inorg Chem 45(23): 9551–9557
27. De Visser SP (2006) Substitution of hydrogen by deuterium changes the regioselectivity of ethylbenzene hydroxylation by an oxo–iron–porphyrin catalyst. Chem Eur J 12:8168–8177
28. Sharma PK, de Visser SP, Ogliaro F, Shaik S (2003) Is the ruthenium analogue of compound I of cytochrome P450 an efficient oxidant? A theoretical investigation of the methane hydroxylation reaction. J Am Chem Soc 125(8):2291–2300
29. Yoshizawa K, Shiota Y, Yamabe T (1998) Abstraction of the hydrogen atom of methane by iron-oxo species: the concerted reaction path is energetically more favorable. Organometallics 17:2825–2831
30. Basch H, Mogi K, Musaev DG, Morokuma K (1999) Mechanism of the methane → methanol conversion reaction catalyzed by methane monooxygenase: a density functional study. J Am Chem Soc 121(31):7249–7256

Received: 15 June 2019 | Revised: 30 January 2020 | Accepted: 10 February 2020

DOI: 10.1002/jcc.26177

FULL PAPER

Journal of COMPUTATIONAL CHEMISTRY WILEY

Interplay between two spin states determines the hydroxylation catalyzed by P_{450} monooxygenase from *Trichoderma brevicompactum*

Razak Hussain[1] | Rolly Yadav[2] | Mushtaq Ahmed[3] | Tabreiz A. Khan[1] | Devesh Kumar[2] | Yusuf Akhter[4]

[1]Department of Botany, Aligarh Muslim University, Aligarh, Uttar Pradesh, India

[2]Department of Applied Physics, School for Physical Sciences, Babasaheb Bhimrao Ambedkar University, Lucknow, Uttar Pradesh, India

[3]Centre for Molecular Biology, School of Life Sciences, Central University of Jammu, Bagla, Jammu and Kashmir, India

[4]Department of Biotechnology, Babasaheb Bhimrao Ambedkar University, Lucknow, Uttar Pradesh, India

Correspondence
Devesh Kumar, Department of Applied Physics, Babasaheb Bhimrao Ambedkar University, School for Physical Sciences, Vidya Vihar, Raebareli Road, Lucknow, Uttar Pradesh 226025, India.
Email: dkclcre@yahoo.com
Yusuf Akhter, Department of Biotechnology, Babasaheb Bhimrao Ambedkar University, Vidya Vihar, Raebareli Road,Lucknow, Uttar Pradesh 226025, India.
Email: yusuf@daad-alumni.de

Funding information
Department of Biotechnology, Ministry of Science & Technology, Government of India, Grant/Award Number: BT/PR14510/BID/07/334/2010; Department of Science and Technology, Ministry of Science & Technology, Govt. of India

Abstract

Tri11 (now renamed as *tri22*) encoded cytochrome P_{450} monooxygenase in *Trichoderma brevicompactum* catalyzes the C-4 C-H hydroxylation of 12, 13-epoxytrichothec-9-ene (EPT) to produce trichodermol in the biosynthetic pathway of trichodermin/harzianum A. The density functional theory (DFT)-quantum mechanics (QM) approach is applied to elucidate the hydroxylation of EPT by using a model active species of P_{450} (Cpd I). The QM calculations were performed on the active site complex, to find out transition-state structure, intermediate, and product complexes for the two spin states at different potential energy surfaces. The two state reactivity rebound-free product formation resulted from the interplay of two spin states (doublet and quartet).

KEYWORDS

cytochrome P_{450} monooxygenase, density functional theory, high spin state, low spin state, *Trichoderma brevicompactum*

1 | INTRODUCTION

Trichoderma spp. produce agriculturally important trichothecenes trichodermin and harzianum A.[1,2] The *tri22* encoded cytochrome P_{450} monooxygenase hydroxylates C-4 of 12,13-epoxytrichothec-9-ene (EPT) to produce trichodermol in trichodermin/harzianum A biosynthetic pathway in *Trichoderma* spp.[3,4] (Figure 1). Cytochrome P_{450s} are considered as the most versatile enzymes in nature, they catalyze a variety of stereospecific and regioselective monooxygenation reaction processes.[5,6] The structural and functional aspects of P_{450s} are very similar in different organisms.[7] The substrates of different shapes and sizes can be activated by binding to P_{450s} due to their broad chemical function.[8] Unactivated C—H bonds of organic molecules are hydroxylated by P_{450s}.[9] The hemoproteins-P_{450s} metabolize various compounds using a high-valent iron (IV)-oxo species complex known as Compound I (Cpd I) which is covalently

Razak Hussain and Rolly Yadav contributed equally to this study.

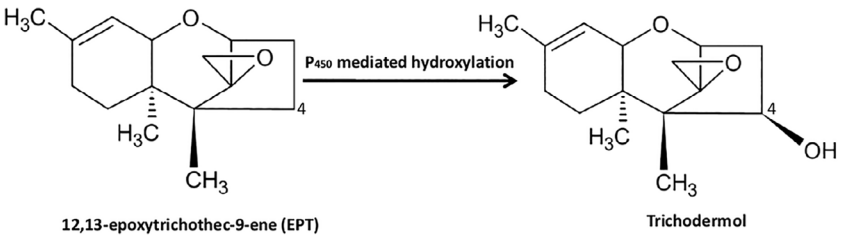

FIGURE 1 Conversion reaction of compound 12,13-epoxytrichothec-9-ene (EPT) to product Trichodermol

attached to the enzyme through a conserved cysteinate residue.[5,10–12] The molecular oxygen is bound on an iron (III)-heme group of P_{450s} and an oxygen atom is transferred to substrate either by a hydroxylation or an epoxidation reaction.[13] P_{450s} also catalyze a variety of monooxygenation biochemical reactions.[14] The generally accepted mechanism of P_{450s} for hydroxylation reaction involves hydrogen abstraction–oxygen rebound mechanism, which is characterized by a transition state formed from Cpd I.[7] The reaction can proceed in two spin states, high spin (HS) and low spin (LS) with corresponding rate-limiting barriers.[11,15,16] Cpd I is the key oxidant involved in the hydroxylation of a wide variety of aliphatic to aromatic substrate reactions.[17] Aromatic rings hydroxylations are the challenging reactions and have a great significance in biological and chemical processes and Cpd I is known for mediating the aromatic hydroxylations catalyzed by P_{450s}.[12,18] Various experimental and theoretical studies have shown the two state rebound mechanism of C—H hydroxylation, in this process, the first step is the abstraction of a hydrogen atom from the substrate that leads to the formation of reactant complex, which is connected to a hydroxo intermediate radical species by a transition state and the consequent C—O bond formation resulted into ferric-alcohol product complex.[19]

For instance, various molecular dynamics simulation studies have shown the catalytic mechanism of P_{450s} through protein–ligand and protein–protein interactions.[20–25] However, the more precise reaction mechanism of electron transfer and product formation of P_{450s} could only be explained by QM/MM calculations.[6,17,19,26,27] The electronically important part (active site) comprises QM region, whereas the largest portion including protein and solvent constitutes MM region, the practical approaches for P_{450s} and similar metalloenzymes applies DFT for QM region.[6,28] The QM-DFT methods are used in vast majority and considered as most reliable and accurate for P_{450s} and other metalloproteins, the hybrid DFT-B3LYP method is considered most suitable and used preferably for studying QM regions of metalloenzymes.[6] The two-state reactivity (TSR) is the most widely used mechanism for studying C—H hydroxylation where the reaction proceeds through two spin states with corresponding energy barriers.[5,19,29] The TSR is a useful mechanism of catalysis for low energy pathways.[30] In the present work, we have studied hydroxylation of EPT C-4 atom to produce trichodermol (Figure 1) catalyzed by cytochrome P_{450} monooxygenase, the reaction mechanism is modeled with Cpd I-EPT complex (RC) in two spin states, quartet (HS) and doublet (LS) with QM calculations.

2 | METHODS

This work uses DFT method contrivance by *Gaussian 09* software.[31] Calculations were performed for $Por^{+\cdot}Fe^{IV}$=O in two different spin states (doublet and quartet) using EPT as substrate. Initial calculations were done by hybrid density functional B3LYP using LANL2DZ basis set on iron and 6-31G basis set on rest of the atoms (BS1) abbreviated as B3LYP/BS1[32] for the optimization of geometry and analytic frequency. Here, geometry optimizations of reactants, intermediates, and products for HS and LS were performed and underlying reaction pathway was searched on full potential energy surface (PES) with subsequent transition states. Analytic frequency calculations confirmed the local minima (i.e., reactant, intermediate, and product) by showing real frequencies and first-order saddle point (i.e., transition state) with single imaginary frequency. Furthermore, results were crosschecked at B3LYP/BS2 level of theory which uses triple zeta effective core potential on iron and 6-31+G* basis set on rest of the atoms. Barrier heights were calculated with isolated reactant geometries (Figures 3 and 4).

3 | RESULTS AND DISCUSSION

The C—H hydroxylation reactions are considered as challenging perspective in the catalytic cycle of P_{450s}.[12,33,34] In the present work, we explained the C-4 hydroxylation of 12,13-epoxytrichothec-9-ene (EPT) that follows a rebound-free mechanism without a barrier with a complex radical intermediate (IM) characterized by a hydrogen atom abstraction transition state (TS).[33] To understand the reaction mechanism, the electronic configuration of active species-Cpd I must be understood. Figure 2 shows the optimized orbitals of Cpd I,[8,35,36] these orbitals are formed by the combination of 3*d* orbitals of iron, with 2*p* orbitals of porphyrin and axial ligand oxygen. The σ^*_z2 antibonding orbital is formed by interaction of $3d_z^2$ orbital on iron and $2p_z$ orbital on oxygen atom whereas the σ^*_{xy} antibonding orbital is formed by interaction between $3d_{xy}$ orbital of iron and $2p_{xy}$ orbital of nitrogen atoms of porphyrin (Fe–N orbitals). The interaction of $3d_{xz}/3d_{yz}$ orbital of iron with $2p_x/2p_y$ orbital of oxygen give rise to low lying bonding π_{xz}/π_{yz} that are found to be always filled and two sets of antibonding π^*_{xz}/π^*_{yz} orbitals (Fe–O orbitals). $\delta_{x^2-y^2}$ represents the lone pair of electrons on the porphyrin ring. Other than metal type orbitals, there are also two π-type high-lying nonbonding porphyrin orbitals which under D_{4th} symmetry have labels a_{1u} and a_{2u} (Figure 2). The

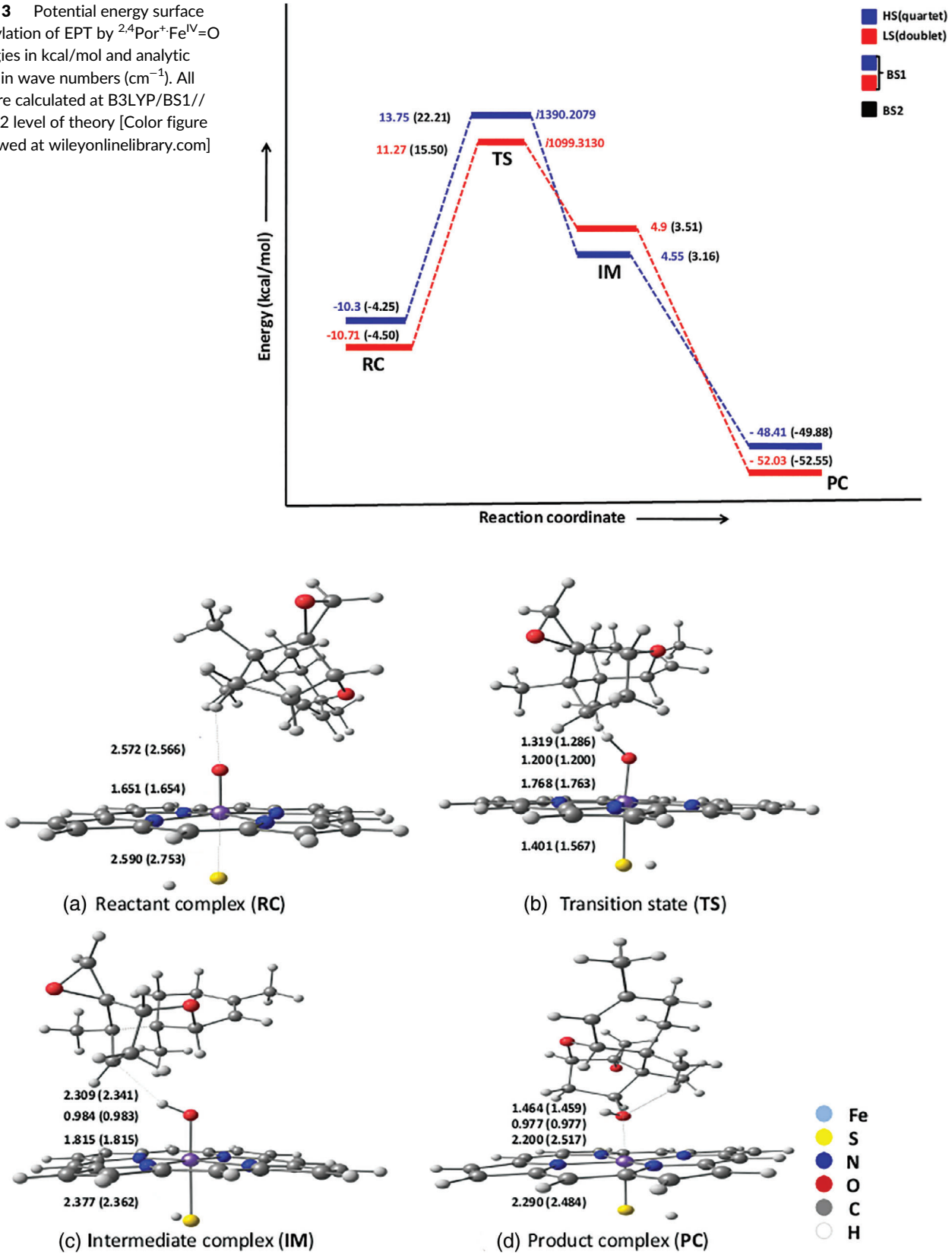

FIGURE 3 Potential energy surface of hydroxylation of EPT by $^{2,4}Por^{+\cdot}Fe^{IV}=O$ with energies in kcal/mol and analytic frequency in wave numbers (cm^{-1}). All energies are calculated at B3LYP/BS1//B3LYP/BS2 level of theory [Color figure can be viewed at wileyonlinelibrary.com]

FIGURE 4 Optimized geometries of (a) Reactant complex (RC), (b) Transition state (TS), (c) Intermediate complex (IM), and (d) Product complex (PC) with differences in the bond lengths for respective atoms without and within brackets indicating for LS (HS)-doublet and quartet state, respectively [Color figure can be viewed at wileyonlinelibrary.com]

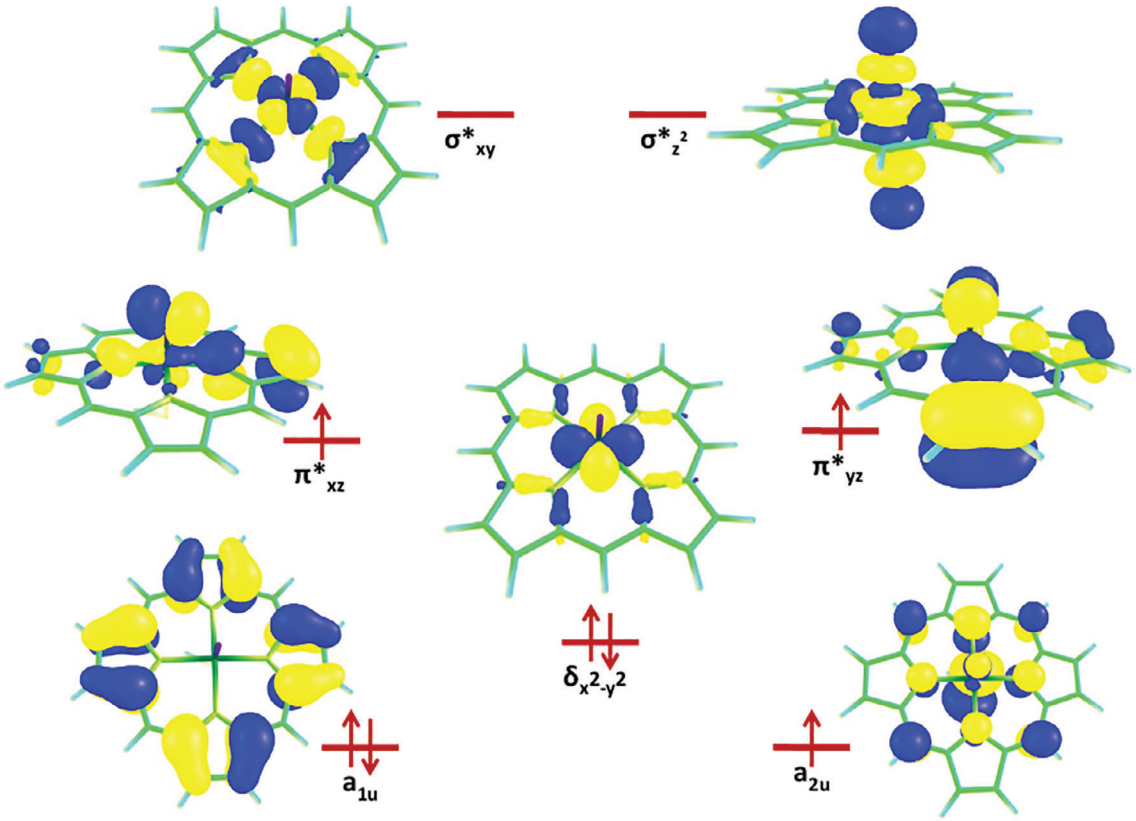

FIGURE 2 Key molecular orbitals of Cpd I with respective representation involved in catalytic mechanism [Color figure can be viewed at wileyonlinelibrary.com]

TABLE 1 Spin densities and atomic charges (Mulliken charges)

(a) Reactant complex (RC)										
	Spin density					Charges				
	ρ_{Fe}	ρ_{O}	ρ_{Por}	ρ_{Sub}	ρ_{SH}	Q_{Fe}	Q_{O}	Q_{Por}	Q_{Sub}	Q_{SH}
HS	1.08	0.93	0.46	0.00	0.53	0.22	−0.25	−1.14	−0.12	−0.12
LS	1.21	0.88	−0.51	0.00	−0.58	0.30	−0.28	−0.1	0.01	0.13
(b) Transition state (TS)										
	Spin density					Charges				
	ρ_{Fe}	ρ_{O}	ρ_{Por}	ρ_{Sub}	ρ_{SH}	Q_{Fe}	Q_{O}	Q_{Por}	Q_{Sub}	Q_{SH}
HS	0.91	0.71	1.33	−0.45	0.50	0.17	0.10	0.93	−0.47	−0.19
LS	1.86	−0.03	−0.19	0.49	−0.17	0.83	−0.46	−0.14	−0.11	−0.12
(c) Intermediate complex (IM)										
	Spin density					Charges				
	ρ_{Fe}	ρ_{OH}	ρ_{Por}	ρ_{Sub}	ρ_{SH}	Q_{Fe}	Q_{OH}	Q_{Por}	Q_{Sub}	Q_{SH}
HS	1.88	0.28	−0.12	0.97	−0.01	1.05	−0.52	−0.75	0.00	−0.28
LS	1.94	0.24	−0.11	−0.98	−0.09	1.04	−0.60	−0.21	−0.01	−0.22
(d) Product complex (PC)										
	Spin density					Charges				
	ρ_{Fe}	ρ_{O}	ρ_{Por}	ρ_{Sub}	ρ_{SH}	Q_{Fe}	Q_{O}	Q_{Por}	Q_{Sub}	Q_{SH}
HS	2.56	0.01	−0.03	0.01	0.45	0.82	−0.61	0.99	0.15	−0.35
LS	1.11	−0.00	−0.09	0.00	−0.02	0.77	−0.64	−0.02	0.14	−0.25

latter orbital (a_{2u}) strongly mixes with lone pair orbital of axial ligand, the mixing is strong in the presence of thiolate and reduction was found to be much more facile so-called "push effect."[34,37] The orbitals in Cpd I are filled in the form of following configuration π_{xz}^2 π_{yz}^2 $\delta_{x^2-y^2}^2$ $\pi^*_{xz}{}^1$ $\pi^*_{yz}{}^1$ $\sigma^*_z2^0$ $\sigma^*_{xy}{}^0$ $a_{1u}{}^2$ $a_{2u}{}^1$, this configuration may take the form of doublet or quartet spin state depending on electron spin if all three electrons are in up spin state (ferromagnetically coupled) then it will lead to quartet spin state and if two up one down (antiferromagnetically coupled) then it will result in doublet spin state.[8,38,39]

We modeled the reaction mechanism between reactant complex (Cpd I-EPT) in both quartet and doublet spin states, with an energy difference of 1.0 kcal/mol, so we can call both states as degenerate (Figure 3) with electronic configuration $\delta_{x2\text{-}y2}{}^2$ $\pi^*_{xz}{}^1$ $\pi^*_{yz}{}^1$ a_2u^1. The RC complex lead to the formation of an intermediate complex (IM) via a transition state with electronic configuration $\delta_{x^2-y^2}{}^2$ $\pi^*_{xz}{}^1$ $\pi^*_{yz}{}^1$ a_2u^2 $\phi_c{}^1$ as explained earlier.[40] The electronic configuration of IM showing that the substrate has donated one of its electrons during the formation of IM complex. Finally, the radical rebound (barrier-less) takes place that results in product formation (PC) with electronic configuration $\delta_{x^2-y^2}{}^2$ $\pi^*_{xz}{}^1$ $\pi^*_{yz}{}^1$ $\sigma^*_z2^1$ a_2u^2 $\phi_c{}^0$ (Quartet) and $\delta_{x^2-y^2}{}^2$ $\pi^*_{xz}{}^1$ $\pi^*_{yz}{}^2$ a_2u^2 $\phi_c{}^0$ (Doublet; Table 1). The orbitals occupancy must changes during the reaction process for electron transfer, this include the a_2u orbital of porphyrin, $\pi^*_{yz,}$ σ^*_z2 orbitals of iron and the substrate orbital for C—H hydroxylation, that is, ϕ_c. The reaction process involves the electron transfer event from substrate to the Cpd I, this purpose is achieved when the a_2u of porphyrin is fully occupied generating the intermediate complex (IM), leaving the ϕ_c of substrate singly occupied. During the second bond formation, an additional electron from substrate is transferred to either of two *d* orbitals to low lying π^*_{yz} orbital resulting in ferric alcohol complex in doublet state ^{2}P(III) or high lying σ^*_z2 orbital which will lead to the product complex in quartet state ^{4}P(III).[16] The second bond formation step was found barrier-less on both the spin surfaces, unlike general C—H hydroxylation processes, no rearrangement of alcohol product was found on high-spin surface that can lead to what we called "rebound barrier" (Figure 3).[39] As shown in the above results, the reactivity of Cpd I involves two closely lying spin sates process which are characterized by singly occupied σ^*_{xz}, σ^*_{yz}, and a_{2u} orbitals at ground state with separate reaction barriers, therefore, this reaction mechanism follows two state reactivity process (TSR). Moreover, our results are in perfect agreement with earlier reports of TSR process.[5,6,15,16,28–30,41–43]

With QM calculations, we proposed the complete reaction mechanism of EPT C-4 hydroxylation as shown in Figure 3. The proposed reaction mechanism involves various B3LYP calculations on Cpd I and the substrate EPT. The optimized RC complex of doublet and quartet spin states shows minor difference in energy gap, the slightly higher energy of quartet spin (−10.3 kal/mol) state indicates that the doublet (−10.71 kcal/mol) is the ground state as reported earlier by Wang et al.[44] Because of small energy gap between two spin states, the reaction mechanism was investigated at both spin states as shown in Figure 3. Our QM calculations revealed that the energy barriers at quartet spin states are very similar to those of the doublet spin state. The energy graph shows that the IM of quartet spin (4.55 kcal/mol) state is slightly more stable compared to doublet spin (4.9 kcal/mol) state with an energy gap of less than 1 kcal/mol.

We also observed an electron transfer and authenticity of electronic spins can also be seen from spin densities and atomic charges (Mulliken and NBO atomic charges) shown in Table 1 and Table S1. The FeO moiety bears charge of nearly 2 for IM indicating single occupancy of π^*_{xz} and π^*_{yz} orbitals and in product, there is spin density of nearly 3 which shows two electrons on either of π^*_{yz}/π^*_{xz} and one electron in other orbital and also reduction of iron from Fe(IV) to Fe(III) state can be inferred.[36] The occurrence of intercrossing in energy profiles between two spin states indicating the possibility of the presence of spin state cross over during the catalytic cycle and a complex catalytic process.[27,44,45] The quartet and doublet spin states involves a barrier with a genuine transition state (TS) having single imaginary frequency (*i*1390.2079 cm^{-1} and *i*1099.3130 cm^{-1}) for quartet (13.75 kcal/mol) and doublet (11.27 kcal/mol) spin states, respectively, and this step involved in reaction mechanism is rate determining step, followed by a radical intermediate (IM), and finally, the rebound-free product (PC) formation takes place. We have seen that during the hydrogen abstraction phase the two spin states are close to each other within a gap of 2.5 kcal/mol and during the intermediate complex formation process, the two spin states slightly overlap each other within an energy gap of 1 kcal/mol (Figure 3). However, as reported earlier that the rebound mechanism for quartet spin state involves a barrier and a second TS state, we did not find so, the rebound mechanism in both the spin states is barrier-free that lead to product formation without any second transition state.[5,16,29,33] The concerted reaction mechanism of hydroxylation for both HS and LS was reported for the first time by Kumar et al., and was subsequently confirmed by Wang et al.[16,33] The hydrogen abstraction barrier for HS state is slightly high in energy in comparison to LS due to more charge transfer to ferryl-oxo species from substrate (EPT) as shown in Figure 3 and Table 1. The concerted mechanism from intermediate to product for both the spin state can be asserted by few factors. First, LS spin state have been known to give rebound barrier free or (unscrambled product) due to the push effect of thiolate where Fe—O bond lengthening is the overall compensated by shortening of Fe—S bond. Second, the substrate-EPT is also a better electron donor, due to which C—O bond gets stronger and proximal ligand binding decreases and hence the good the radical becomes electron donor as shown in Figure 4 the rebound barrier decreases,[16,33,41] hence our HS spin surface also gives barrier free alcohol product. The product formation is more favorable in the LS-doublet because of the low-lying vacant orbitals that favors bonding formation and low barriers (−52.03 kcal/mol) whereas the HS-quartet

(–48.41 kcal/mol) favors repulsive interactions due to half-filled high-energy orbitals and hence disfavors bonding formation.[30]

4 | CONCLUSIONS

The present work on a cytochrome P_{450} monooxygenase from *Trichoderma brevicompactum* using DFT and QM calculations approach elucidated a complete reaction mechanism for a C—H hydroxylation reaction process and the results were further tested using BS2 basis set. QM calculations are considered as the most accurate process for studying the chemical reactions. This theoretical study reveals that the two state reactivity mechanism mediated by HS and LS is throughout exothermic as expected and is much more facile for LS state. The H-abstraction step is the rate-limiting step of reaction mechanism with activation energy of 13.75 and 11.27 kcal/mol for HS and LS, respectively. In conclusion, we can say that this hydroxylation process of EPT is a rebound-free reaction mechanism with a short-lived intermediate radical with no possibility for scrambling of structure and there is no process of regioselectivity, the product formation takes place directly from the IM. The present work carried out using DFT method, which complements the earlier results accurately and is a good approach which can be used in combination with experimental approaches.

ACKNOWLEDGMENTS

RH acknowledges National Fellowship for Higher Education from University Grants Commission, Govt. of India. RY acknowledges Department of Science and Technology (DST), Govt. of India for DST-Inspire Fellowship (DST/INSPIRE/IF170546). Research in YA lab is supported by extramural research funds from Department of Biotechnology (Ministry of Science & Technology, Govt. of India) (DBT) and Indian Council of Medical Research. DK acknowledges financial support from the DBT (BT/PR14510/BID/07/334/2010).

ORCID

Yusuf Akhter https://orcid.org/0000-0001-9564-9790

REFERENCES

[1] M. G. Malmierca, I. Izquierdo-Bueno, S. P. McCormick, R. E. Cardoza, N. J. Alexander, J. Barua, L. Lindo, P. A. Casquero, I. G. Collado, E. Monte, *Environ. Microbiol.* **2016**, *18*, 3991.
[2] P. K. Mukherjee, B. A. Horwitz, C. M. Kenerley, *Microbiology* **2012**, *158*, 35.
[3] R. E. Cardoza, M. G. Malmierca, M. R. Hermosa, N. J. Alexander, S. P. McCormick, R. H. Proctor, A. M. Tijerino, A. Rumbero, E. Monte, S. Gutiérrez, *Appl. Environ. Microbiol.* **2011**, *77*, 4867.
[4] M. G. Malmierca, R. E. Cardoza, N. J. Alexander, S. P. McCormick, R. Hermosa, E. Monte, S. Gutiérrez, *Appl. Environ. Microbiol.* **2012**, *78*, 4856.
[5] S. Shaik, S. P. De Visser, Computational approaches to cytochrome P450 function. in *Cytochrome P450: Structure, Mechanism, and Biochemistry*, 3rd ed. (Ed: P. R. O. de Montellano), Kluwer Academic/Plenum Publishers, New York **2005**, p. 45.
[6] S. Shaik, W. Lai, H. Chen, Y. Wang, *Acc. Chem. Res.* **2010**, *43*, 1154.
[7] R. Lai, H. Li, J. Phys, *Chem. B* **2016**, *120*, 12312.
[8] M. A. Sainna, S. Kumar, D. Kumar, S. Fornarini, M. E. Crestoni, S. P. de Visser, *Chem. Sci.* **2015**, *6*, 1516.
[9] J. Rittle, M. T. Green, *Science (80-.).* **2010**, *330*, 933.
[10] S. Shaik, S. Cohen, Y. Wang, H. Chen, D. Kumar, W. Thiel, *Chem. Rev.* **2009**, *110*, 949.
[11] D. Kumar, A. Altun, S. Shaik, W. Thiel, *Faraday Discuss.* **2011**, *148*, 373.
[12] F. G. Cantú Reinhard, M. A. Sainna, P. Upadhyay, G. A. Balan, D. Kumar, S. Fornarini, M. E. Crestoni, S. P. de Visser, *Chem. A Eur. J.* **2016**, *22*, 18608.
[13] V. Postils, M. Saint-André, A. Timmins, X.-X. Li, Y. Wang, J. Luis, M. Solà, S. de Visser, *Int. J. Mol. Sci.* **2018**, *19*, 1974.
[14] J. Shin, J.-E. Kim, Y.-W. Lee, H. Son, *Toxins (Basel).* **2018**, *10*, 112.
[15] S. Shaik, M. Filatov, D. Schröder, H. Schwarz, *Chem. A Eur. J.* **1998**, *4*, 193.
[16] Y. Wang, H. Wang, Y. Wang, C. Yang, L. Yang, K. Han, *J. Phys. Chem. B* **2006**, *110*, 6154.
[17] K. D. Dubey, B. Wang, S. Shaik, *J. Am. Chem. Soc.* **2016**, *138*, 837.
[18] M. Asaka, H. Fujii, *J. Am. Chem. Soc.* **2016**, *138*, 8048.
[19] A. Altun, S. Shaik, W. Thiel, *J. Am. Chem. Soc.* **2007**, *129*, 8978.
[20] R. Verma, U. Schwaneberg, D. Roccatano, *Biopolymers* **2014**, *101*, 197.
[21] P. Hlavica, *Adv. Exp. Med. Biol.* **2015**, *851*, 247.
[22] D. Batabyal, L. S. Richards, T. L. Poulos, *J. Am. Chem. Soc.* **2017**, *139*, 13193.
[23] S. A. Hollingsworth, B. D. Nguyen, G. Chreifi, A. P. Arce, T. L. Poulos, *J. Chem. Inf. Model.* **2017**, *57*, 2344.
[24] R. Hussain, I. Kumari, S. Sharma, M. Ahmed, T. A. Khan, Y. Akhter, *Biol. Inorg. Chem.* **2017**, *22*, 1197.
[25] R. Hussain, M. Ahmed, T. A. Khan, Y. Akhter, *Int. J. Biochem. Cell Biol.* **2018**, *103*, 74.
[26] A. Altun, V. Guallar, R. A. Friesner, S. Shaik, W. Thiel, *J. Am. Chem. Soc.* **2006**, *128*, 3924.
[27] A. K. Vardhaman, P. Barman, S. Kumar, C. V. Sastri, D. Kumar, S. P. de Visser, *Angew. Chem. Int. Ed.* **2013**, *52*, 12288.
[28] S. Shaik, D. Kumar, S. P. de Visser, A. Altun, W. Thiel, *Chem. Rev.* **2005**, *105*, 2279.
[29] S. Shaik, S. Cohen, S. P. de Visser, P. K. Sharma, D. Kumar, S. Kozuch, F. Ogliaro, D. Danovich, *Eur. J. Inorg. Chem.* **2004**, *2004*, 207.
[30] D. Schröder, S. Shaik, H. Schwarz, *Acc. Chem. Res.* **2000**, *33*, 139.
[31] M. J. Frisch, G. W. Trucks, H. B. Schlegel, G. E. Scuseria, M. A. Robb, J. R. Cheeseman, G. Scalmani, V. Barone, B. Mennucci, G. A. Petersson, *Gaussian 09*, Vol. 27, Gaussian Inc., Wallingford, CT **2009**, p. 34.
[32] P. J. Hay, W. R. Wadt, *J. Chem. Phys.* **1985**, *82*, 299.
[33] D. Kumar, S. P. de Visser, P. K. Sharma, S. Cohen, S. Shaik, *J. Am. Chem. Soc.* **2004**, *126*, 1907.
[34] J. T. Groves, *Nat. Chem.* **2014**, *6*, 89.
[35] F. Ogliaro, S. P. de Visser, S. Cohen, J. Kaneti, S. Shaik, *Chembiochem* **2001**, *2*, 848.
[36] F. Ogliaro, S. P. de Visser, S. Cohen, P. K. Sharma, S. Shaik, *J. Am. Chem. Soc.* **2002**, *124*, 2806.
[37] F. Ogliaro, S. P. de Visser, S. Shaik, *J. Inorg. Biochem.* **2002**, *91*, 554.
[38] G. H. Loew, D. L. Harris, *Chem. Rev.* **2000**, *100*, 407.
[39] K.-B. Cho, H. Hirao, S. Shaik, W. Nam, *Chem. Soc. Rev.* **2016**, *45*, 1197.
[40] L. Ji, J. Zhang, W. Liu, S. P. de Visser, *Chem. Asian J.* **2014**, *9*, 1175.
[41] F. Ogliaro, N. Harris, S. Cohen, M. Filatov, S. P. de Visser, S. Shaik, *J. Am. Chem. Soc.* **2000**, *122*, 8977.
[42] S. Shaik, S. P. de Visser, F. Ogliaro, H. Schwarz, D. Schröder, *Curr. Opin. Chem. Biol.* **2002**, *6*, 556.
[43] C. M. Bathelt, A. J. Mulholland, J. N. Harvey, *J. Phys. Chem. A* **2008**, *112*, 13149.

[44] X.-Y. Wang, H.-M. Yan, Y.-L. Han, Z.-X. Zhang, X.-Y. Zhang, W.-J. Yang, Z. Guo, Y.-R. Li, *RSC Adv.* **2018**, *8*, 15196.
[45] X. Wang, J. Shi, Y. Liu, *Inorg. Chem.* **2018**, *57*, 8933.

SUPPORTING INFORMATION

Additional supporting information may be found online in the Supporting Information section at the end of this article.

How to cite this article: Hussain R, Yadav R, Ahmed M, Khan TA, Kumar D, Akhter Y. Interplay between two spin states determines the hydroxylation catalyzed by P_{450} monooxygenase from *Trichoderma brevicompactum*. *J Comput Chem*. 2020;1–7. https://doi.org/10.1002/jcc.26177

Journal of Organometallic Chemistry 957 (2022) 122154

Contents lists available at ScienceDirect

Journal of Organometallic Chemistry

journal homepage: www.elsevier.com/locate/jorganchem

Metabolism of 8-aminoquinoline (8AQ) primaquine via aromatic hydroxylation step mediated by cytochrome P450 enzyme using density functional theory

Nidhi Awasthi[a], Rolly Yadav[a], Devesh Kumar[a,*]

[a] Department of Physics, School of Physical and Decision Sciences, Babasaheb Bhimrao Ambedkar University, Vidya Vihar, Raebareli Road, Lucknow, Uttar Pradesh 226025, India

ARTICLE INFO

Article history:
Received 11 September 2021
Revised 27 October 2021
Accepted 27 October 2021
Available online 29 October 2021

Keywords:
Cytochrome p450
Basis set
Density functional theory
Primaquine
Metabolism

ABSTRACT

The 8-aminoquinoline (8AQ) drug Primaquine (PQ) is a prime anti-malarial drug, used in the treatment of malaria due to plasmodium vivax and plasmodium ovale. The hydroxylated metabolite of Primaquine is also responsible for many essential sexual transmission stages of Plasmodium falciparum. Present work reported the hydroxylation of Primaquine at ortho (2PQ) and para (4PQ) position by Cytochrome P450 enzyme. Density functional theory (DFT) is used to investigate the underlying pathway for aromatic hydroxylation at ortho (2PQ) and para (4PQ) position to produce 2-hydroxylated and 4-hydroxylated Primaquine respectively. Truncated model of putative active oxidant i.e. ferryl oxo porphyrin cation radical [Fe^{IV}(O)(heme$^{+\cdot}$)], which is referred as Cpd I in Cytochrome P450 enzymes has been used to mimic the behavior of enzyme. Substrate was modelled and reaction mechanism for two degenerate spin states namely doublet and quartet were performed to dwell the overall potential energy landscape, along with electronic structure and properties of reactant complex (RC), transition states (TS), intermediates (IM) and product complex (PC). The reaction was stepwise with electrophillic addition as the rate determining step, spin selectivity product formation was observed for hydroxylated product formation on high spin (HS) surface. All calculations are done for isolated reaction coordinate.

1. Introduction

Cytochrome P450 is an important enzyme of nature, basically in biosystems. In humans, it is found in the liver [1]. But it is also highly expressed in areas of the central nervous system. These enzymes catalyze a variety of stereo-specific and regio-selective mono-oxygenation reaction processes. It is also used in detoxification processes and is a key drug-metabolizing enzyme involved in the metabolism of drugs [2]. It reacts as mono-oxygenase that transfer oxygen atom to the substrate. This oxygen can be transferred either by hydroxylation, epoxidation or sulfoxidation [3–6]. Due to its large versatility in the activation of the substrate, Cytochrome P450 is an essential enzyme, not only in biology but also, in biotechnological and pharmaceutical applications for investigations of drugs [7]. Moreover, its drug metabolism and involvement in brain chemistry make this enzyme a target for the drug industry and biomedical research [8–11].

Fundamentally, hydroxylation is of two types – one is (a) aliphatic, another is (b) aromatic. Both hydroxylations are important and their reaction pattern is different. Present research is focused on study of aromatic hydroxylation. In the modern synthesis chemistry, direct insertion of hydroxyl group into the aromatic compound is one of the most challenging fields, because of the strong bond of hydrogen and carbon (CH) atom of the benzene ring. But, despite this ambivalence, Cytochrome P450 catalyzes aromatic compound in relatively easy way. Hydroxylations of aromatic rings are important chemical reactions and are catalyzed by several metalloenzymes [8,9]. In biosystems, there are various essential processes of chemical reactions which lead to aromatic hydroxylation with Cytochrome P450 and convert several non-degradable compounds into biodegradable compounds [10–14]. Aromatic hydroxylation step via P450s is responsible for the breakdown of xenobiotics into water-soluble enzymes [3] . P450 catalyze estrogen hormone into 16–hydroxy-estrogen via aromatic hydroxylation step, which basically triggers breast cancer [15–17]. Moreover, plant P450 enzyme catalyze the isoliquiritigenin into the product, which has antitumor, antioxidant and phytoestrogenic activity [18]. Aromatic hydroxylation via P450 is also the center of research for

* Corresponding author.
E-mail address: dkclcre@yahoo.com (D. Kumar).

https://doi.org/10.1016/j.jorganchem.2021.122154
0022-328X/

drug metabolism including para-hydroxylation of Amphetamine and Tamoxifen [19–21] and several other substrates, like, β-blocker alprenolol [22] and the neurotoxin 1-methyl-4-phenyl-1,2,3,6-tetrahydropyridine which is a chemical inducer of Parkinson's disease [23,24]. So, in the field of bio-chemistry, aromatic hydroxylation via P450 is a crucial activity, but researchers are always fascinated by aromatic hydroxylation due to its unknown reaction mechanism with Cytochrome P450 [21,22]. The Cytochrome P450 is metabolize various compound using high-valent iron (iv) oxo species complex, generally known as Cpd1. This complex is formed during the catalytic cycle of Cytochrome P450 [26–29]. Initially, in catalytic cycle, Cytochrome P450 is at the resting state and the water molecule is ligated. The entry of the substrate expels the water molecule and tightly binds with the enzyme. Further, the oxidation step forms ferric peroxide species known as compound 0 (Cpd 0), and then after the protonation step Cpd 0 converts into active species of enzyme, iron (IV)-oxo complex, known as compound I (Cpd I). It is the primary oxidant involved in the oxidation reaction of all superfamily of P450s and here truncated model of Cpd I is used to explore the overall reaction.

For large number of atoms a more suitable method is used generally known as QM/MM (Quantum Mechanical/ Molecular Mechanical) method. The utility of this method is revealed by the first QM/MM study [30] of the active species. It was done by increasing molecules in all the species in the catalytic cycle of P450cam, [31] the active species of human isoforms, [26–32] and some of organic molecules [33,34] .

Moreover the QM/MM approach, is used for two- layer to three-layer of system, one can easily understand it by continuum solvation model which is used for third layer [35] or by ONIOM-type method in which system is divided in two layers two different layers one is inner QM layers and another is outer MM layer [36]. Such more involved QM/MM treatments have not yet been applied to P450 enzymes.

Present study addresses the aromatic hydroxylation of 8-aminoquinoline (8AQ), an anti-malarial drug Primaquine via Cpd I of P450. Primaquine is metabolized by CYP 2D6 enzyme [37]. CYP 2D6 is a member of the P450 enzyme, so their active site is similar for both enzymes. That's why P450 enzyme is used here for hydroxylation.

The 8-aminoquinoline (8AQ) drug Primaquine (PQ) is a prime anti-malarial drug, used in the treatment of malaria due to plasmodium vivax and plasmodium ovale [38]. It is also used in the treatment of pneumocystis pneumonia together with clindamycin, as an alternate treatment. It is one of the safest and most effective drugs and is placed in the list of essential drugs of World Health Organization (WHO) [39]. It was developed over 70 years ago. But, unfortunately, the reaction pathway was still blurred.

The hydroxylated metabolite of Primaquine is also responsible for many essential sexual transmission stages of Plasmodium falciparum [40]. There are six metabolites of 8AQ identified [37]. These metabolites are formed by the hydroxylation step, at each position of the benzene ring. Current study is investigating the hydroxylation step at ortho (2PQ) as well as para (4PQ) position of the benzene ring of Primaquine. DFT method is the most accurate and reliable for studying the reactivity pattern of Cpd I and also of several other essential metalloenzyme with hybrid function B3LYP of DFT [41,42]. The CH hydroxylation of the substrate with Cpd I is followed by two different spin surfaces, one is, high spin state (HS) and the other is, low spin state (LS). These two different spin state energy barriers lead to two-state reactivity (TSR) pattern [25,26]. In the present work, we have studied aromatic hydroxylation at the ortho position (2PQ) as well as at the para position of Primaquine (4PQ) (Fig. 1). The reaction patterns for reaction complex (RC), transition state (TS), intermediate state (IM) and product complex (PC) for both spin state, doublet (LS) as well as quartet

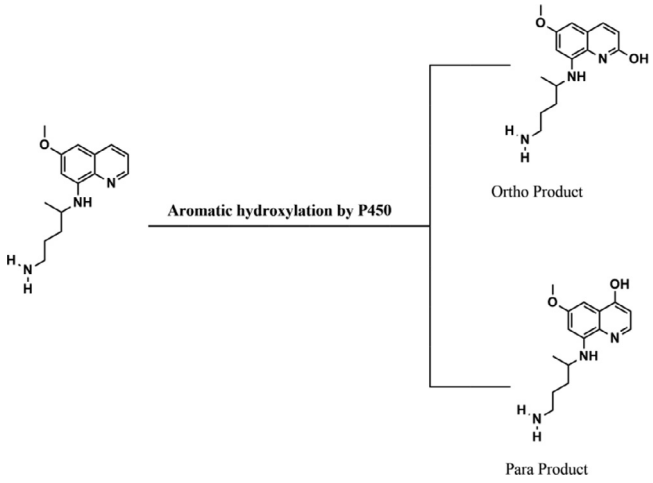

Fig. 1. Aromatic hydroxylation of Primaquine at ortho (2PQ) and para (4PQ) position by Cytochrome P450.

(HS), are shown in energy profiles as will discuss later. All calculations are done for isolated reaction coordinate. Further, we cross checked the results calculating single point energy using basis set LACVP, solvent effect with benzene, and in presence of two ammonium molecule, and results are overlapping to each other, which showed the reliability of results.

2. Methodology

Present study comprises an investigation of reaction energy profile by Quantum Mechanical (QM) method. Density functional theory (DFT) was involved using Gaussian 09 software [43]. In this work, all calculations were performed for porphyrin cation radical iron (IV) oxo species i.e. $Por^{+\cdot}Fe^{iv}=O$, which is commonly referred as (Cpd I), in two different spin states, doublet as well as quartet with Primaquine as a substrate. Optimization geometries of reactant, intermediate, product is performed and a genuine pathway for the reaction mechanism is found on potential energy surface (PES) with subsequent transition states. Initially, optimization of geometry was calculated by hybrid density functional B3LYP using LANL2DZ basis set on iron atom and 6–31 G basis set on the rest of the atom (BS1) abbreviated as B3LYP/BS1 [44]. Analytic frequency calculations performed after optimization confirmed the local minima of reactant, intermediate, product by showing the real frequencies and first-order saddle point i.e., transition state with single imaginary frequency. Moreover, results are crosschecked at B3LYP/BS2 theory by performing single-point calculations. This basis set involves triple zeta effective core potential on iron and 6–31+G^* basis rest on remaining atoms. Further, we calculated single point energy using basis set LACVP, solvent effect with Benzene and in presence of ammonia and results are overlapping to each other, which showed the reliability of results.

Barrier heights are calculated by isolated reactant geometries using 6–31 G, 6–31G^*, LACVP, solvent effect with benzene, and in presence of ammonia are shown in Figs. 2.

3. Results and discussion

3.1. Hydroxylation of primaquine at ortho position (2PQ)

The proposed work tried to explain aromatic hydroxylation of Primaquine at ortho position of the aromatic ring (C-2), to a complex intermediate (IM1) by attaching at the ortho position of carbon (C-2) with oxygen atom of Cpd I. In the next step, hydrogen atom (H-2) at ortho position gets attached with one of

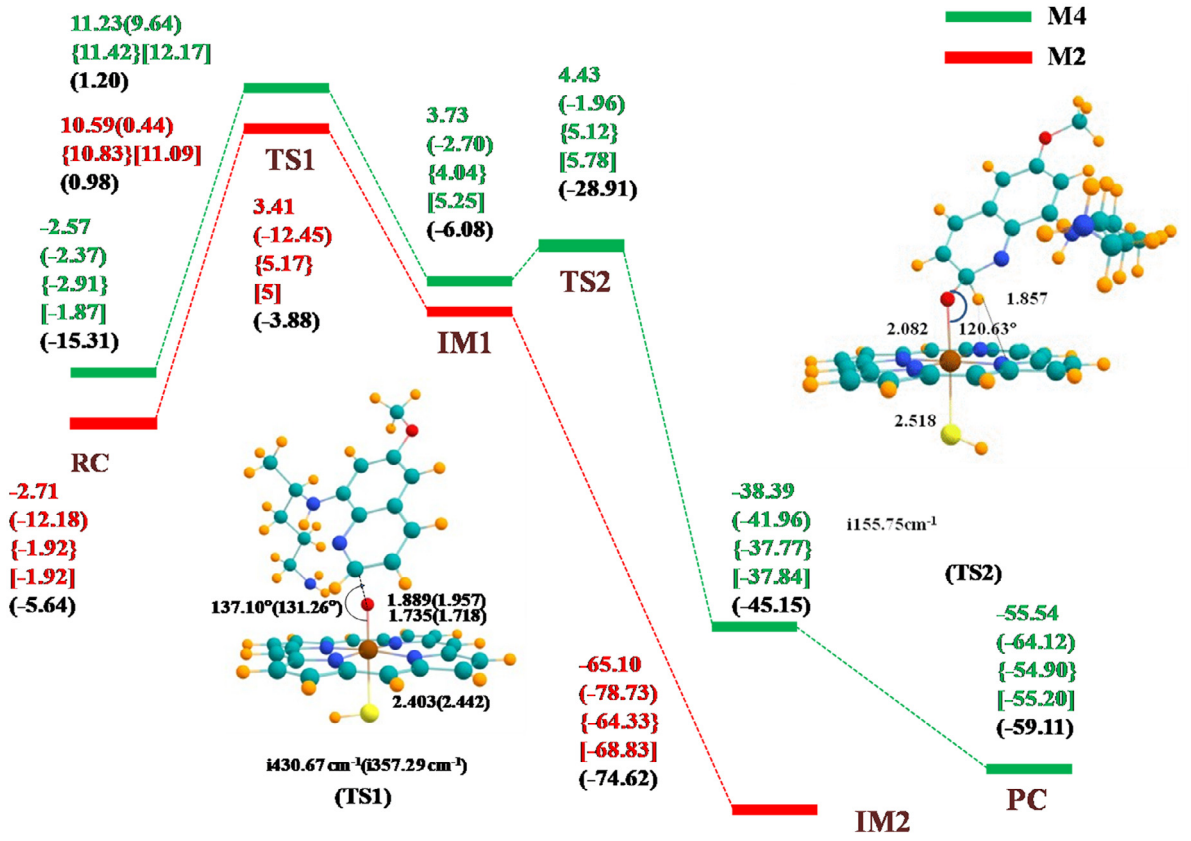

Fig. 2. Potential energy surface of hydroxylation of Primaquine (2PQ) by Cytochrome P450 with energies in kcal/mol. Bond length, bond angle and imaginary frequencies (in cm^{-1}) of quartet as well as doublet (in bracket) spin state is shown. Calculated energies of BS1 in red color without bracket, of LACVP in small bracket, of solvent effect with benzene in culy bracket, with ammonia molecule in large bracket and of 6-31G* basis set in black color, all are shown.

nitrogen atom of porphyrin ring forming a second intermediate state (IM2). Further, this hydrogen atom attaches to the abstracted oxygen atom of Cpd I, and form a product complex (PC).

The electronic configuration of CpdI must be clearly identified, for better understanding of its reaction pathway $3d_{z^2}$ orbital of iron and $2p_z$ orbital of oxygen of Cpd I together formed $\sigma^*_{z^2}$ antibonding orbital, whereas interaction of $3d_{xy}$ orbital of iron and $2p_{xy}$ orbital of nitrogen atoms of porphyrin together form antibonding orbital σ^*_{xy} . These orbitals are found to be unfilled initially due to their high energy state and filled in later part of reaction process. Further, $\delta_{x^2-y^2}$ is orbital of lone pair electron of porphyrin ring. The low-lying bonding orbital π_{xz} /π_{yz} as well as antibonding orbital π^*_{xz} / π^*_{yz} is formed by the interaction between $3d_{xz}$ /$3d_{yz}$ orbital of iron and $2p_x$ /$2p_y$ orbital of oxygen. These low-lying bonding π_{xz} /π_{yz} orbitals are always filled. Optimized orbitals are shown in Fig. 3.

Other than these five metal orbitals, two highlying orbitals of heterocyclic ring (a_{1u} and a_{2u}) are also involved. But, in enzymatic systems a_{2u} orbital is slightly high in energy due to mixing from sigma orbital of axial ligand thiolate. So, two spin states result with ferromagnetic and anti-ferromagnetic coupling between π^{*1}_{xz} π^{*1}_{yz} and a^2_{1u} respectively, whereas a_{1u} remains fully occupied. DFT calculations revealed nearly ~ 1 kcal/mol energy gap between quartet and doublet spin state as shown in Fig. 2

Substrate (Primaquine) and Cpd I together form reactant complex (RC) when put at interacting distance with each other. The electronic configuration of reactant complex (RC) for two spin states found to be δ^{*2}_{x2-y2} π^{*1}_{xz} π^{*1}_{yz} $\sigma^{*0}_{z^2}$ σ^{*0}_{xy} a^2_{1u} a^1_{2u}. The transfer of electron from ortho position of carbon (C-2) to oxygen atom of Cpd I, leads to the formation of first intermediate complex (IM1) with electronic configuration δ^{*2}_{x2-y2} π^{*1}_{xz} π^{*1}_{yz} $\sigma^{*0}_{z^2}$ σ^{*0}_{xy} a^2_{1u} a^2_{2u} φ^1_c , nature of electron in substrate φ^1_c (up and down) determines the spin state and also conserves the overall quartet and doublet spins (Fig. 2). The electronic configuration of first transition state (TS1) is same as configuration of first intermediate (IM1).

After this, in the high spin (HS) state, first intermediate leads to second intermediate (IM2) by transfer of charge from ortho carbon (C-2) to one of the nitrogen atom of porphyrin ring (NH) following the electronic configuration δ^{*2}_{x2-y2} π^{*1}_{xz} π^{*1}_{yz} $\sigma^{*1}_{z^2}$ σ^{*0}_{xy} a^2_{1u} a^2_{2u} φ^0_c, and the configuration of low spin state of second intermediate (IM2) state is δ^{*2}_{x2-y2} π^{*1}_{xz} π^{*2}_{yz} $\sigma^{*1}_{z^2}$ σ^{*0}_{xy} a^2_{1u} a^2_{2u} φ^0_c. Second transition state (TS2) of high spin state is observed as δ^{*2}_{x2-y2} π^{*1}_{xz} π^{*1}_{yz} $\sigma^{*1}_{z^2}$ σ^{*0}_{xy} a^2_{1u} a^2_{2u} φ^1_c. Further, product complex (PC) is formed by transfer of the hydrogen atom from nitrogen, and bind to the oxygen which has already been transferred at ortho position in second intermediate. The overall configuration of product is δ^{*2}_{x2-y2} π^{*1}_{xz} π^{*1}_{yz} $\sigma^{*1}_{z^2}$ σ^{*0}_{xy} a^2_{1u} a^2_{2u} φ^2_c, product formation is not observed in case of doublet spin state, due to formation of suicidal complex.

The electronic configurations must change due to transfer of charge, so that occupancy of orbital a_{2u} ,π^*, σ^* and φ_c is also changed. As we discussed earlier, all three electrons of orbital π^*_{xz}, π^*_{yz} and a_{2u} combine ferromagnetically or anti-ferromagnetically to form quartet or doublet spin state respectively. These type of reaction mechanism leads to the two state reactivity (TSR) pattern [45–50].

These calculations are done by quantum mechanical (QM) method using B3LYP basis set. There is a minor energy difference between doublet −2.71 kcal/mol and quartet spin state with energy −2.57 kcal/mol, of optimized reactant complex (RC) as

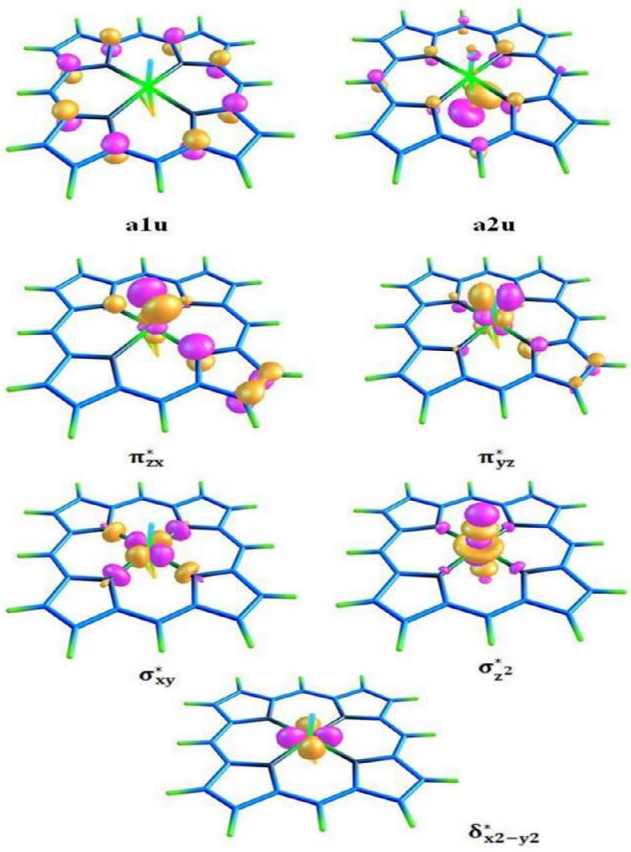

Fig. 3. Key orbitals of Cpd I in order of their energy.

shown in Fig. 3. The energy gap between these two states is very close, i.e., these are degenerate energy state as we have discussed above. Optimized structure of reactant complex (RC), transition state (TS), intermediate state (IM), and product complex (PC) for doublet and quartet spin state is shown in Figure S1 and Figure S2 respectively in supplementary information (SI). And their spin densities with mulliken charges are compiled in Table S1 in SI. Further, cross checked charge and spin densities using BS2 basis set for 2PQ are reported in Table S3 in supplementary information.

The energy of first transition state (TS1) of doublet spin state is 10.59 kcal/mol, it forms more stable state than quartet spin state having energy 11.23 kcal/mol. The energy of first intermediate (IM1) of doublet spin state is 3.41 kcal/mol, and it is comparable to quartet spin state 3.73 kcal/mol. Further, the energy of second transition state (TS2) of quartet spin state is 4.40 kcal/mol. These two degenerate states continuously maintain energy gap of (<1 kcal/mol) between them. The energy of second intermediate (IM2) of doublet spin state is −65.10 kcal/mol, and the energy of quartet spin state is −38.39 kcal/mol, this means it is more stable than quartet. LS surfaces offered formation of suicidal complexes, confirmed by reverse scan curves (shown in supporting information in S1). At the end, it forms product complex (PC) with energy −55.54 kcal/mol at high spin state. And the formed product is chemically named as 2-hydroxylated Primaquine (2-OH PQ).

With the frequency calculations, the reported imaginary frequencies of TS1 and TS2 of quartet spin state are 430.67i cm^{-1} and 155.75i cm^{-1} respectively. And imaginary frequency of TS1 of low spin state is 357.29i cm^{-1}. As shown in the energy profile Fig. 2, intercrossing of the energy states indicates the spin cross over during the catalytic cycle [33,34].

Moreover, the transfer of electron and spins of electron is also investigated by charges and spin densities (Mulliken and NBO atomic charges) using BS1 basis set and reported in Table S1 in SI.

3.2. Hydroxylation of primaquine at para position (4PQ)

Abstraction of hydrogen atom at para position of Primaquine is identified as 4PQ. All properties are also investigated for 4PQ by Quantum Mechanical (QM) methods. As we discussed earlier, in this reaction, hydrogen atom at the para position of substrate (Primaquine), is abstracted by Cpd I. The energy profile for both spin surfaces LS as well as HS is studied as shown in Fig. 4. Reactant complex of doublet and quartet spin state has same configuration as reactant complex of 2PQ. Before forming the product, both spin surfaces, high as well as low spin surfaces give two intermediate states IM1, IM2 with same electronic configuration as IM1, IM2 of 2PQ. Here one can clearly notice that the LS surfaces offered formation of suicidal complexes, which was further confirmed by running reverse scan curves (shown in supporting information in S2). Also, product 4-hydroxylated Primaquine (4-OH PQ) was found to offer more energy than intermediate 2 (IM2) which further justified the formation of dead product. Optimized structure of reactant complex (RC), transition state (TS), intermediate state (IM), and product complex (PC) for doublet or quartet spin state is shown in Figure S3 as well as in Figure S4 respectively in SI.

The reaction followed patterns of two state reactivity (TSR) mechanism and energy landscape for doublet and quartet was close and parallel with each other, but this pattern bifurcate at IM1. TSR behavior is transform to single state reactivity (SSR) and shows that the reaction is possible only for high spin surface (HS).

Also, electronic configuration of first transition states (TS1) of HS as well as LS is same as electronic configuration of TS1 of 2PQ. The electronic configuration of third transition state (TS3) of high spin surface is $\delta^{*2}_{x2-y2}\ \pi^{*1}_{xz}\ \pi^{*2}_{yz}\ \sigma^{*1}_{z^2}\ \sigma^{*0}_{xy}\ a^2_{1u}\ a^2_{2u}\ \varphi^0_c$ and product is $\delta^{*2}_{x2-y2}\ \pi^{*1}_{xz}\ \pi^{*1}_{yz}\ \sigma^{*1}_{z^2}\ \sigma^{*0}_{xy}\ a^2_{1u}\ a^2_{2u}$. The energy of reactant complex (RC) of doublet is −3.97 kcal/mol which is very close to quartet having the energy −2.64 kcal/mol. The first transition state (TS1) of doublet gives energy 12.86 kcal/mol and quartet gives the energy 11.72 kcal/mol. The energy of first intermediate (IM1) of doublet and quartet is 6.47 kcal/mol as well as 3.92 kcal/mol respectively. The energy profile of para position of aromatic hydroxylation is shown in Fig. 4. Both spin state continuously maintains 1 kcal/mol difference between them.

The energy of second intermediate (IM2) of doublet is −9.85 kcal/mol and quartet is −37.32 kcal/mol. The energy of third transition state of quartet (TS3) is −35.57 kcal/mol. Also, the energy of product of quartet spin state is −50.51 kcal/mol. The imaginary frequency of TS1 of doublet is −422.86 cm^{-1} and quartet is −439.29 cm^{-1}. And imaginary frequency of TS3 of quartet is −619.54 cm^{-1}. Imaginary frequencies of quartet and doublet spin state of transition states are shown in Figure S4 in SI. Optimized structure with corresponding bond length of all state of metabolic reaction for both surfaces is shown in Figure S3 & S4, respectively in SI. These two step reactions are exothermic as expected. The overall rate of a chemical reaction is often determined by the slowest step of reaction, known as rate limiting or rate determining step. C–O bond formation step is the rate limiting step.

Rate limiting step has activation energy 10.59 and 11.23 kcal/mol, for both LS as well as HS state, respectively. Further, the transfer of electron and spins of electron is also investigated by charges and spin densities (Mulliken atomic charges) using BS1 basis set for 4PQ reported in Table S2 in SI. Cross-checked charge and spin densities using BS2 basis set are reported as Table S4 in supplementary information.

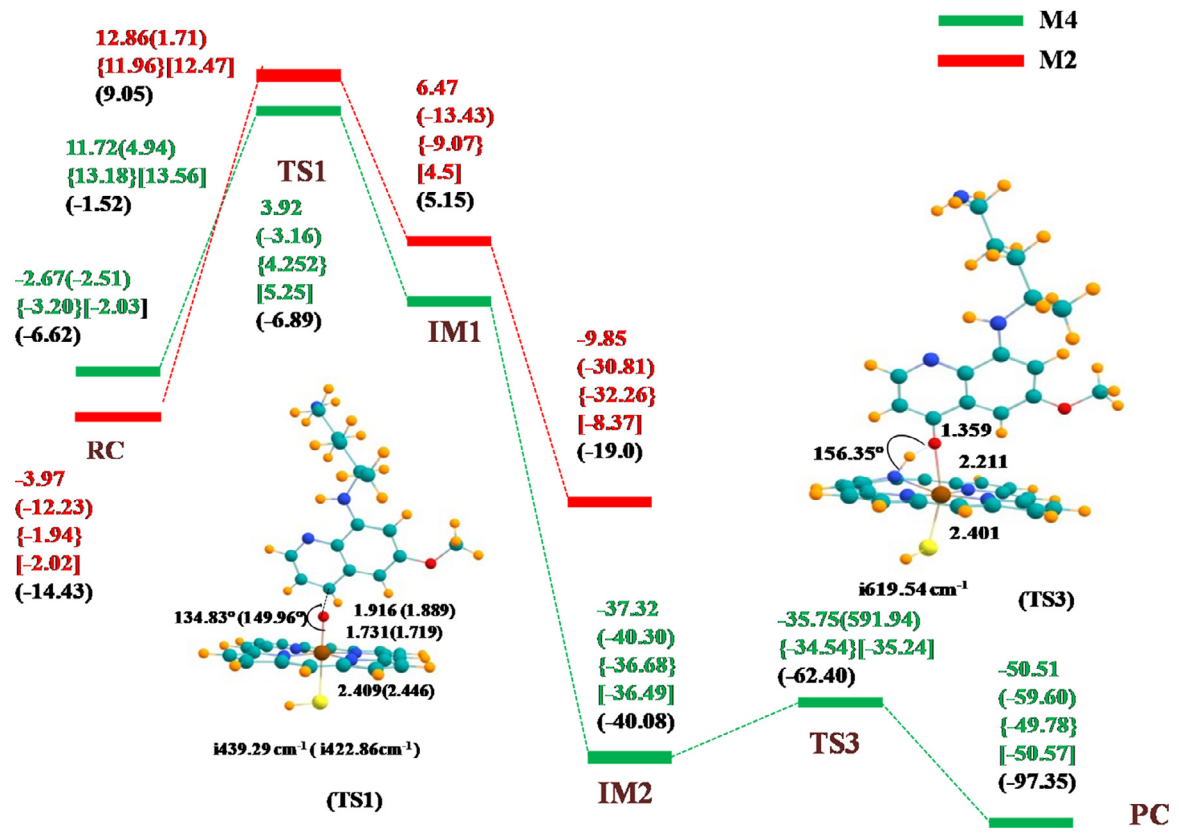

Fig. 4. Potential energy surface of hydroxylation of Primaquine (4PQ) by Cytochrome P450 4 with energies in kcal/mol. Bond length, bond angle and imaginary frequencies (in cm^{-1}) of quartet (in green color) as well as doublet (in bracket in red color) spin state is shown. Calculated energies of BS1 in red color without bracket, of LACVP in small bracket, of solvent effect with benzene in culy bracket, with ammonia molecule in large bracket and of 6-31G* basis set in black color, all are shown. . **Coordinate of third transition state (TS3) are not properly conversed for BS2*.. (For interpretation of the references to colour in this figure legend, the reader is referred to the web version of this article.)

4. Conclusion

The current work investigated the complete reaction pathway of aromatic hydroxylation of Primaquine with Cpd I by DFT using basis set 6–31 G (BS1) and the results were further cross checked using basis set 6–31*G** (BS2). Quantum mechanical calculations clearly depicted above hydroxylation reaction is rebound free process having more than one transition state with short lived intermediate state and (CO) – bond formation step to be rate determining step of the reaction. It can been seen from the energy profile for ortho (2PQ) and para (4PQ) position of Primaquine that quartet surface (HS) is responsible for the hydroxylated product whereas doublet spin surface profile is resulted in the formation of a *suicidal complex*. Finally, the product at high spin state surface (HS), is formed, the reaction followed patterns of two state reactivity (TSR) mechanism and energy landscape for doublet and quartet were close and parallel with each other, but this pattern bifurcate at IM1. TSR behavior is transformed to single state reactivity (SSR) showing that reaction is possible only for high spin surface (HS). In the energy profile it is clearly shown that H-abstraction step is rate determining step with activation energy 11.23 kcal/mol and 10.59 kcal/mol for HS and LS respectively for hydroxylation at ortho position while for the hydroxylation at para position the activation energy is 12.86 kcal/mol and 11.72 kcal/mol for HS and LS respectively. Here it is also concluded that this process is not regioselective and the product is formed directly from intermediate. So, the present work is expanded to a great extent about to the metabolism of Primaquine via P450 by giving a reaction pathway. Further, we calculated single point energy using basis set LACVP, solvent effect with Benzene and in presence of ammonia, and results are overlapping to each other, which showed the reliability of results. These formed products (metabolites) are further used for treatment of malaria. These quantum mechanical calculations are considered for good accuracy results. Present reactions mechanism is different from aliphatic hydroxylation reactions of Cytochrome P450 enzyme, due to formation of suicidal complex at the low spin surface. But further results give good accuracy as we expected and these results can be used for experimental researches and will give fruitful results. And there results have good accuracy for isolated reaction coordinates which shows the success of present work.

Declaration of Competing Interest

The authors declare that they have no known competing financial interests or personal relationships that could have appeared to influence the work reported in this paper.

Acknowledgement

NA is thankful to University Grant Commission (UGC) for non-net fellowship for higher education. RY acknowledge to Department of Science and Technology for DST-inspire fellowship (DST/INSPIRE). We would also like to thank Prof. C.V. Sastri IIT Guwahati for providing computational facilities.

Supplementary materials

Supplementary material associated with this article can be found, in the online version, at doi:10.1016/j.jorganchem.2021.122154.

References

[1] S. Shaik, S.P. De Visser, Computational approaches to cytochrome P450 function, Cytochrome P450 Struct. Mech. Biochem. Third Ed. (2005) 45–85, doi:10.1007/0-387-27447-2_2.

[2] S. Shaik, S. Cohen, Y. Wang, H. Chen, D. Kumar, W. Thiel, P450 enzymes: their structure, reactivity, and selectivity - Modeled by qm/mm calculations, Chem. Rev. 110 (2) (2010) 949–1017, doi:10.1021/cr900121s.

[3] M. Asaka, H. Fujii, Participation of electron transfer process in rate-limiting step of aromatic hydroxylation reactions by compound i models of heme enzymes, J. Am. Chem. Soc. 138 (26) (2016) 8048–8051, doi:10.1021/jacs.6b03223.

[4] N. Harris, S. Shaik, D. Schroder, H.H. Schwarz, Single- and Two-State reactivity in the gas-phase c-h bond activation of norbornane by "bare" feo+, Helv. Chim. Acta 82 (10) (1999) 1784–1797, doi:10.1002/(SICI)1522-2675(19991006)82:10⟨1784::AID-HLCA1784⟩3.0.CO;2-M.

[5] C.M. Link, A.D. Theoharides, J.C. Anders, H. Chung, C.J. Canfield, Structure-Activity relationships of putative primaquine metabolites causing methemoglobin formation in canine hemolysates, Toxicol. Appl. Pharmacol. 81 (2) (1985) 192–202, doi:10.1016/0041-008X(85)90155-3.

[6] L. Ji, A.S. Faponle, M.G. Quesne, M.A. Sainna, J. Zhang, A. Franke, D. Kumar, R. Van Eldik, W. Liu, S.P. De Visser, Drug metabolism by cytochrome P450 enzymes: what distinguishes the pathways leading to substrate hydroxylation over desaturation? Chem. - A Eur. J. 21 (25) (2015) 9083–9092, doi:10.1002/chem.201500329.

[7] E. O'Reilly, V. Köhler, S.L. Flitsch, Cytochromes P450 as useful biocatalysts: addressing the limitations, Chem. Commun. 47 (9) (2011) 2490–2501, doi:10.1039/c0cc03165h.

[8] F.P. Guengerich, Cytochrome P-450 3A4: regulation and role in drug metabolism, Annu. Rev. Pharmacol. Toxicol. 39 (1999) 1–17, doi:10.1146/annurev.pharmtox.39.1.1.

[9] U.M. Zanger, M. Schwab, Cytochrome P450 enzymes in drug metabolism: regulation of gene expression, enzyme activities, and impact of genetic variation, Pharmacol. Ther. 138 (1) (2013) 103–141, doi:10.1016/j.pharmthera.2012.12.007.

[10] S. Shaik, W. Lai, H. Chen, Y. Wang, The valence bond way: reactivity patterns of cytochrome P450 enzymes and synthetic analogs, Acc. Chem. Res. 43 (8) (2010) 1154–1165, doi:10.1021/ar100038u.

[11] M.S. Butler, Natural products to drugs: natural product derived compounds in clinical trials, Nat. Prod. Rep. 22 (2) (2005) 162–195, doi:10.1039/b402985m.

[12] R. Ullrich, M. Hofrichter, Enzymatic hydroxylation of aromatic compounds, Cell. Mol. Life Sci. 64 (3) (2007) 271–293, doi:10.1007/s00018-007-6362-1.

[13] D. Kumar, G.N. Sastry, S.P.De Visser, Axial ligand effect on the rate constant of aromatic hydroxylation, J. Phys. Chem. B 116 (Iv) (2012) 718–730.

[14] C.M. Bathelt, L. Ridder, A.J. Mulholland, J.N. Harvey, Aromatic hydroxylation by cytochrome P450: model calculations of mechanism and substituent effects, J. Am. Chem. Soc. 125 (49) (2003) 15004–15005, doi:10.1021/ja035590q.

[15] F. Zhang, J.L. Bolton, Synthesis of the equine estrogen metabolites 2-Hydroxyequilin and 2- Hydroxyequilenin, Chem. Res. Toxicol. 12 (2) (1999) 200–203, doi:10.1021/tx980189g.

[16] Z. Huang, F.P. Guengerich, L.S. Kaminsky, 16α-Hydroxylation of estrone by human cytochrome P4503A4/5, Carcinogenesis 19 (5) (1998) 867–872, doi:10.1093/carcin/19.5.867.

[17] A.J. Lee, M.X. Cai, P.E. Thomas, A.H. Conney, B.T. Zhu, Characterization of the oxidative metabolites of 17β-Estradiol and estrone formed by 15 selectively expressed human cytochrome P450 isoforms, Endocrinology 144 (8) (2003) 3382–3398, doi:10.1210/en.2003-0192.

[18] J. Guo, A. Liu, H. Cao, Y. Luo, J.M. Pezzuto, R.B. Van Breemen, Biotransformation of the chemopreventive agent 2',4',4-Trihydroxychalcone (Isoliquiritigenin) by UDP-Glucuronosyltransferases, Drug Metab. Dispos. 36 (10) (2008) 2104–2112, doi:10.1124/dmd.108.021857.

[19] J.L. Sessler, D. Seidel, Synthetic expanded porphyrin chemistry, Angewandte Chemie - International Edition (November 3, 2003) 5134–5175, doi:10.1002/anie.200200561.

[20] F. Carvalho, M.E. Soares, E. Fernandes, F. Remião, M. Carvalho, J.A. Duarte, R. Pires-das-Neves, M.D.L. Pereira, M.D.L. Bastos, Repeated administration of D-Amphetamine results in a time-dependent and dose-independent sustained increase in urinary excretion of p-Hydroxyamphetamine in mice, J. Heal. Sci. 53 (4) (2007) 371–377, doi:10.1248/jhs.53.371.

[21] S. Yoshioka, S. Takahashi, K. Ishimori, I. Morishima, Roles of the axial push effect in cytochrome P450cam studied with the site-directed mutagenesis at the heme proximal site, J. Inorg. Biochem. 81 (3) (2000) 141–151, doi:10.1016/S0162-0134(00)00097-0.

[22] S. NARIMATSU, M. TACHIBANA, Y. MASUBUCHI, S. IMAOKA, Y. FUNAE, T. SUZUKI, Cytochrome P450 isozymes involved in aromatic hydroxylation and side-chain N-Desisopropylation of alprenolol in rat liver microsomes, Biol. Pharm. Bull. 18 (8) (1995) 1060–1065, doi:10.1248/bpb.18.1060.

[23] P.R. Ortiz De Montellano, J.J. De Voss, Substrate oxidation by cytochrome P450 enzymes, Cytochrome P450 Struct. Mech. Biochem. Third Ed. (2005) 183–245, doi:10.1007/0-387-27447-2_6.

[24] T.D. Lash, Origin of aromatic character in porphyrinoid systems, J. Porphyr. Phthalocyanines 15 (11–12) (2011) 1093–1115, doi:10.1142/S1088424611004063.

[25] J. Wen, D. Chennamadhavuni, S.R. Morel, M.K. Hadden, Truncated itraconazole analogues exhibiting potent anti-hedgehog activity and improved drug-like properties, ACS Med. Chem. Lett. 10 (9) (2019) 1290–1295, doi:10.1021/acsmedchemlett.9b00188.

[26] S. Cohen, S. Kozuch, C. Hazan, S. Shaik, Does substrate oxidation determine the regioselectivity of cyclohexene and propene oxidation by cytochrome P450? J. Am. Chem. Soc. 128 (34) (2006) 11028–11029, doi:10.1021/ja063269c.

[27] P.R. Ortiz de Montellano, J.J. De Voss, Oxidizing species in the mechanism of cytochrome P450, Nat. Prod. Rep. 19 (4) (2002) 477–493, doi:10.1039/b101297p.

[28] Ortiz De Montellano, P.R.; De Voss, J.J. Substrate oxidation by cytochrome P450 enzymes. In *Cytochrome P450: Structure, Mechanism, and Biochemistry: Third edition*; Springer US, 2005; pp 183–245. https://doi.org/10.1007/0-387-27447-2_6.

[29] M. Torrent, D.G. Musaev, H. Basch, K. Morokuma, Computational studies of reaction mechanisms of methane monooxygenase and ribonucleotide reductase, J. Comput. Chem. 23 (1) (2002) 59–76, doi:10.1002/jcc.1157.

[30] J.C. Schöneboom, H. Lin, N. Reuter, W. Thiel, S. Cohen, F. Ogliaro, S. Shaik, The elusive oxidant species of cytochrome P450 enzymes: characterization by combined quantum mechanical/molecular mechanical (QM/MM) calculations, J. Am. Chem. Soc. 124 (27) (2002) 8142–8151, doi:10.1021/ja026279w.

[31] Shaik, S.; Cohen, S.; Wang, Y.; Chen, H.; Kumar, D.; Thiel, W.*P450 enzymes: their structure, reactivity, and selectivity - Modeled by qm/mm calculations*; 2010; Vol. 110. https://doi.org/10.1021/cr900121s.

[32] D. Fishelovitch, C. Hazan, H. Hirao, H.J. Wolfson, R. Nussinov, S. Shaik, QM/MM study of the active species of the human cytochrome P450 3A4, and the influence thereof of the multiple substrate binding, J. Phys. Chem. B 111 (49) (2007) 13822–13832, doi:10.1021/jp076401j.

[33] Y. Wang, H. Chen, M. Makino, Y. Shiro, S. Nagano, S. Asamizu, H. Onaka, S. Shaik, Theoretical and experimental studies of the conversion of chromopyrrolic acid to an antitumor derivative by cytochrome P450 stap: the catalytic role of water molecules, J. Am. Chem. Soc. 131 (19) (2009) 6748–6762, doi:10.1021/ja9003365.

[34] A. Altun, V. Guallar, R.A. Friesner, S. Shaik, W. Thiel, The effect of heme environment on the hydrogen abstraction reaction of camphor in P450cam catalysis: a qm/mm study, J. Am. Chem. Soc. 128 (12) (2006) 3924–3925, doi:10.1021/ja058196w.

[35] D. Riccardi, P. Schaefer, Q. Cui, PK a calculations in solution and proteins with qm/mm free energy perturbation simulations: a quantitative test of qm/mm protocols, J. Phys. Chem. B 109 (37) (2005) 17715–17733, doi:10.1021/jp0517192.

[36] T. Benighaus, W. Thiel, Efficiency and accuracy of the generalized solvent boundary potential for hybrid qm/mm simulations: implementation for semiempirical hamiltonians, J. Chem. Theory Comput. 4 (10) (2008) 1600–1609, doi:10.1021/ct800193a.

[37] B.S. Pybus, J.C. Sousa, X. Jin, J.A. Ferguson, R.E. Christian, R. Barnhart, C. Vuong, R.J. Sciotti, G.A. Reichard, M.P. Kozar, et al., CYP450 phenotyping and accurate mass identification of metabolites of the 8-Aminoquinoline, Anti-Malarial Drug Primaquine (2012) 1–9.

[38] D.R. Hill, J.K. Baird, M.E. Parise, L.S. Lewis, E.T. Ryan, A.J. Magill, Primaquine: report from cdc expert meeting on malaria chemoprophylaxis i, Am. J. Trop. Med. Hyg. 75 (3) (2006) 402–415, doi:10.4269/ajtmh.2006.75.402.

[39] K.A. Lee, W. Nam, Determination of reactive intermediates in iron porphyrin complex-catalyzed oxygenations of hydrocarbons using isotopically labeled water: mechanistic insights, J. Am. Chem. Soc. 119 (8) (1997) 1916–1922, doi:10.1021/ja9629118.

[40] G. Camarda, P. Jirawatcharadech, R.S. Priestley, A. Saif, S. March, M.H.L. Wong, S. Leung, A.B. Miller, D.A. Baker, P. Alano, et al., Antimalarial activity of primaquine operates via a two-step biochemical relay, Nat. Commun. 10 (1) (2019), doi:10.1038/s41467-019-11239-0.

[41] S. Shaik, H. Hirao, D. Kumar, Reactivity patterns of cytochrome P450 enzymes: multifunctionality of the active species, and the two states-two oxidants conundrum, Nat. Prod. Rep. 24 (3) (2007) 533–552, doi:10.1039/b604192m.

[42] H. Hirao, D. Kumar, L. Que, S. Shaik, Two-State reactivity in alkane hydroxylation by non-heme iron-oxo comolexes, J. Am. Chem. Soc. 128 (26) (2006) 8590–8606, doi:10.1021/ja061609o.

[43] M.J. Frisch, G.W. Trucks, H.B. Schlegel, G.E. Scuseria, M.A. Robb, J.R. Cheeseman, G. Scalmani, V. Barone, B. Mennucci, G.A. Petersson, et al., Gaussian 09, revision B.01, Gaussian 09, Revis. B.01, Gaussian, Inc., Wallingford CT (2009) 1–20.

[44] W.R. Wadt, P.J. Hay, Ab initio effective core potentials for molecular calculations. potentials for main group elements na to bi, J. Chem. Phys. 82 (1) (1985) 284–298, doi:10.1063/1.448800.

[45] S. Shaik, S. Cohen, S.P. De Visser, P.K. Sharma, D. Kumar, S. Kozuch, F. Ogliaro, D. Danovich, The "Rebound controversy": an overview and theoretical modeling of the rebound step in c-h hydroxylation by cytochrome P450, Eur. J. Inorg. Chem. (2) (2004) 207–226, doi:10.1002/ejic.200300448.

[46] R. Hussain, I. Kumari, S. Sharma, M. Ahmed, T.A. Khan, Y. Akhter, Catalytic diversity and homotropic allostery of two cytochrome P450 monooxygenase like proteins from trichoderma brevicompactum, J. Biol. Inorg. Chem. 22 (8) (2017) 1197–1209, doi:10.1007/s00775-017-1496-6.

[47] S.P. De Visser, S. Shaik, A proton-shuttle mechanism mediated by the porphyrin in benzene hydroxylation by cytochrome P450 enzymes, J. Am. Chem. Soc. 125 (24) (2003) 7413–7424, doi:10.1021/ja034142f.

[48] M. Albeck, S. Shaik, Publications of sason shaik, J. Phys. Chem. A 112 (50) (2008) 12741–12753, doi:10.1021/jp806628j.
[49] X.Y. Wang, H.M. Yan, Y.L. Han, Z.X. Zhang, X.Y. Zhang, W.J. Yang, Z. Guo, Y.R. Li, Do two oxidants (Ferric-Peroxo and ferryl-oxo species) act in the biosynthesis of estrogens? a dft calculation, RSC Adv. 8 (27) (2018) 15196–15201, doi:10.1039/c8ra01252k.
[50] S. Shang, Z. Lin, A. Yin, S. Yang, Y. Chi, Y. Wang, J. Dong, B. Liu, N. Zhen, C.L. Hill, et al., Self-Assembly of ln(iii)-containing tungstotellurates(vi): correlation of structure and photoluminescence, Inorg. Chem. 57 (15) (2018) 8831–8840, doi:10.1021/acs.inorgchem.8b00693.

Contents lists available at ScienceDirect

Inorganic Chemistry Communications

journal homepage: www.elsevier.com/locate/inoche

Interplay between two degenerate spin state determines the hydroxylation of 4-nitrophenol catalyzed via Cytochrome P450

Nidhi Awasthi, Rolly Yadav, Anamika Shukla, Devesh Kumar *

Department of Physics, School of Physical and Decision Sciences, Babasaheb Bhimrao Ambedkar University, Vidya Vihar, Raebareli Road, Lucknow, Uttar Pradesh 226025, India

ARTICLE INFO

Keywords:
Cytochrome P450
Density Functional Theory
Metalloenzyme
Basis set

ABSTRACT

4-Nitrophenol is formed during the synthesis of paracetamol. It is used in various xenobiotic metabolism processes and other essential biochemical processes. It is metabolized via cytochrome P450 enzyme. The present work reported the hydroxylations of 4-nitrophenol at the ortho position by Cytochrome P450 metalloenzyme. Truncated model of putative active oxidant i.e. ferryl oxo porphyrin cation radical [Fe^{IV}(O)(heme$^{+\bullet}$)], referred as Cpd I in cytochrome P450 enzymes has been used to mimic the behavior of enzyme. In the current investigations, 4-nitrophenol (Substrate) is modeled with Cpd I and reaction mechanism for two degenerate spin states named as doublet (LS) and quartet (HS) is performed to dwell the overall potential energy landscape, along with electronic structures and properties of reactant complex (RC), transition states (TS), intermediates (IM) and product complex (PC). The reaction is stepwise with electrophillic addition as the rate determining step, spin selectivity product formation is observed only at high spin (HS) surface. So, the present reaction pathway is single state reactivity (SSR) by forming the suicidal complex at low spin state (LS).

1. Introduction

The Cytochrome P450 is an essential enzyme found in nature [1]. It consists of number of enzymes with varying substrate selectivity, such as CYP1A2, 2A6, 2B6, 2C9, 2C19, 2D6, 2E1 and 3A etc. These enzymes are responsible for the metabolism of about 70% of therapeutic drugs [2]. In human, P450 is found in liver [3]. It contribute in the catalysis of variety of stereo and regio-selective mono-oxygenation reaction processes and also in detoxification processes [4]. Due to their wide range versatility in activation of several substrate, CYP is very important enzyme, in biology, biotechnological and pharmaceutical applications for investigations of new drugs [5]. Moreover, its involvement in drug metabolism make this enzyme a target for research in drug industry and biomedical field [6–9]. Despite of various member of P450 enzyme, CYP2E1 has been paid a considerable attention, because of its toxicological behavior. It is contributed in the metabolism of various organic solvents and environmental pollutants like, acetone, aniline, ethanol, or nitrosamines etc [10,11]. Metabolism by CYP2E1 might result in the formation of more reactive products, such as the toxic metabolite of acetaminophen (paracetamol) [11–13]. Formation of toxic product of acetaminophen (paracetamol) via CYP2E1, is its crucial behaviour. 4-nitrophenol hydroxylation may responsible for inhibition of toxic product of acetaminophen (paracetamol) via CYP2E1 enzyme.

4-nitrophenol is formed during the synthesis of paracetamol. Initially, it reduced to 4-aminophenol, after that acetylated via acetic anhydride [14]. It is also product of essential enzymatic reactions of several substrate like- 4-nitrophenyl phosphate, 4-nitrophenyl acetate, 4-nitrophenyl-β-D-glucopyranoside and more other derivatives. It plays a crucial role in xenobiotic metabolism process in both, human and mouse. In field of medicinal chemistry, it is used in manufacturing of drugs, insecticides, fungicides. Its structure has phenolic compound, in which nitro group is attached at the opposite of the hydroxyl group on benzene ring. It is also known as *p*-nitrophenol or 4-hydroxynitrobenzene due to presence phenol group. It is mostly used in detection of the presence of alkaline phosphatase activity [15].

The P450 enzyme metabolizes various compound using high-valent iron (IV) oxo species complex, generally known as Cpd I. This complex is formed during the catalytic cycle of Cytochrome P450. Initially, in catalytic cycle, P450 is in the resting state and a water molecule is ligated with it. Whenever, substrate enters, it tightly binds with porphyrin by expelling the water molecule. After the oxidation step a ferric peroxide species is formed, known as compound 0 (Cpd 0), and

* Corresponding author.
E-mail addresses: nidhimsc51@gmail.com (N. Awasthi), dkclcre@yahoo.com (D. Kumar).

https://doi.org/10.1016/j.inoche.2021.108857
Received 2 May 2021; Received in revised form 10 August 2021; Accepted 13 August 2021

Article

Advanced Science, Engineering and Medicine
Vol. 11, 1–5, 2019
www.aspbs.com/asem

Molecular Docking Studies of Enzyme Binding Drugs on Family of Cytochrome P450 Enzymes

Rolly Yadav, Anwesh Pandey, Nidhi Awasthi, and Anamika Shukla*

Department of Physics, School of Physical and Decision Sciences, Babasaheb Bhimrao Ambedkar University, Lucknow, UP, India

The combination of experimental and computational strategies has been of great value in the identification and development of metabolism of drugs. Nowadays modern drug design, molecular docking methods are helpful in exploring the ligand conformations adopted within the binding sites of macromolecular targets such as DNA, proteins, and enzymes, there by reducing cost, time and wayward efforts of chemist. Since the development of the algorithms in the 1980s, molecular docking became an important tool in drug discovery like investigation of crucial molecular events, including ligand binding modes and the corresponding intermolecular interactions that stabilize the ligand-receptor complex, can be conveniently performed. In present study we have tried to investigate the drug binding pocket of various cytochrome (CYP) enzymes found in humans. All structures of drugs are optimized at B3LYP/6-31** level of theory using Gaussian program suite. Docking of substrate-enzyme duo was done using AUTODOCK 4.0. Computational docking revealed that almost all drugs have same binding pocket with varied binding affinities due to change in interactions and interacting distance from heme prosthetic moiety with transition metal iron as chelating ion.

Keywords: CYP1A2, CYP2C9, CYP2D6, Docking, Enzyme.

1. INTRODUCTION

Enzymes are protein macromolecules which are present in cells of all living organisms ranging from simple micro-organisms to largest mammals. These protein structures act as a catalyst in various biological processes thereby making required product at faster rate without changing their original form after completion of reaction. Drug metabolism [1] is an extremely important area of research, as side effects of a particular drug can be known and resolved, designing of new and advanced drugs can be done etc. Cytochrome P450 (CYP450) is one of the most versatile enzymes in nature [2] usually found in abundance in liver cells of mammals and is involved in detoxification of xenobiotics [3, 4]. Primarily three families of P450s i.e., CYP1, CYP2, and CYP3 [1] are involved in human drug metabolism amongst them CYP1A2, CYP2A6, CYP2B6, CYP2C9, CYP2C19, CYP2D6, CYP2E1, and CYP3A4 appear to be the major contributors. In the present work CYP1A2, CYP2C9 and CYP2D6 are used. The CYP1A subfamily contains two members, CYP1A1 and CYP1A2 [5] which are involved in drug metabolism and have sparked considerable interest because they also seem to be associated with the metabolic activation of procarcinogens to mutagenic species, of the two members CYP1A2 is the major player. It is found in human liver and is responsible for metabolism of heterocyclic groups and aromatic rings. The enzyme CYP2C9 is another P450 monoxygenase enzyme which plays role in drug metabolism. It provides instructions for making enzymes found in liver microsomes. It is also responsible for the synthesis of steroids, cholesterol and other lipids. Among CYP enzymes CYP2D6 is known for its inability to be induced by xenobiotics [3, 4]. It can metabolize nearly 20% of drugs such as antidepressant, antiarrhythmics, beta blockers and opioid analgesics.

In the present study docking of drugs with enzyme is been analyzed the parameters that are put under consideration are binding free energies, the distance between the heme iron [6–8] and substrate reacting groups, interaction between the substrate and residue lining the active site [9]. The different values of binding free energies are a direct result of various interactions that takes place at microscopic level such as

*Author to whom correspondence should be addressed.

Biointerface Research in Applied Chemistry
Platinum Open Access Journal (ISSN: 2069-5837)

Article
Volume 12, Issue 6, 2022, 8117 - 8127
https://doi.org/10.33263/BRIAC126.81178127

Computational Investigations on Interactions Between DNA and Flavonols

Anamika Shukla [1,*], Ruchi Mishra [2], Rolly Yadav [1], Nidhi Awasthi [1], Devesh Kumar [1,*]

[1] Department of Physics, School of Physical and Decision Sciences, Babasaheb Bhimrao Ambedkar University, Lucknow, U.P., India; anamikashukla531@gmail.com (A.S.); rydapbbau@gmail.com (R.Y.); nidhimsc51@gmail.com (N.A.); dkclcre@yahoo.com (D.K.);
[2] Department of Applied Sciences and Humanities, Invertis University, Bareilly, U.P., India; ruchimishra242225@gmail.com (R.M.);
* Correspondence: dkclcre@yahoo.com;

Scopus Author ID 57212687797
Received: 4.10.2021; Revised: 15.11.2021; Accepted: 18.11.2021; Published: 9.12.2021

Abstract: Today, the main task of researchers is to study and develop drugs that are less toxic and have lesser side effects. The principal motive of this research is to study and analyze the interaction between naturally active compounds flavonoids with biomolecule DNA. Since the interaction between DNA and ligand is essential in drug designing, this study will provide a good base for further research and development of less toxic and more efficient drugs for various diseases. The selected compounds for this study are Kaempferide, Kaempferol, Morin, and Rutin. They all fall into the category 'flavonols' of flavonoids. Computational methods are implemented for theoretical drug designing. These are molecular optimization, molecular docking, and molecular dynamics. Computational results are compared with experimental data from previous studies. Molecular docking gives the most preferred orientation of ligands within DNA, and Molecular Dynamics provides the details about the DNA-ligand complex with respect to time. Free energy calculations were also performed by implementing MMPBSA and MMGBSA calculations.

Keywords: flavonoids; flavonols; DNA; molecular docking; molecular dynamics; MMPBSA/MMGBSA;

1. Introduction

The possible medication for cancer includes chemotherapy, radiation therapy, and surgery. But the main disadvantage of drugs used in treatment is that they are toxic [1-3]. Regular intake of these has various side effects [4]. It results in the starting of some other problem (disease). So, today the main task of researchers is to study and develop drugs that are less toxic and have lesser side effects. And here, the chosen compounds can be very beneficial. Flavonoids are natural compounds present in seeds, fruits, leaves of plants, and the bark of trees [5,6]. The human body takes them as daily nutrients. So, the main problem of toxicity is reduced a lot, using them as drugs for various diseases[7,8]. They will have minimum side effects. Flavonoids can prove a potent drug against cancer and other diseases [9-11].

Computational methods are beneficial and effective in predicting the nature and characteristics of various drugs as effective on diseases. Different research papers have predicted/concluded that computational methods are as predictive as experimental research [12]. We can rely on these systems for a good result. Theoretical research is essential because